

**A METHODOLOGY FOR TRACKING THE SCAPULA
UNDER DYNAMIC CONDITIONS**

A Thesis submitted to The University of Manchester for the degree of

Doctor of Philosophy

in the Faculty of Engineering and Physical Sciences

2015

Emmanuel Santiago Durazo-Romero

SCHOOL OF MECHANICAL, AEROSPACE AND CIVIL ENGINEERING

TABLE OF CONTENTS

LIST OF FIGURES	7
LIST OF TABLES	17
ABBREVIATIONS	18
NOMENCLATURE.....	20
ABSTRACT.....	21
DECLARATION	22
COPYRIGHT	22
ACKNOWLEDGMENTS	23
CHAPTER I: INTRODUCTION	24
1.1 Overview.....	24
1.2 Objectives and Methodology of the Research	27
CHAPTER II: SHOULDER INSTABILITY BACKGROUND	30
2.1 Introduction.....	30
2.2 Instability Classification Systems.....	30
2.3 Pathology of Shoulder Instability	32
2.4 Glenohumeral Instability classification	34
2.4.1 Muscle Patterning.....	36
2.4.2 Medical Diagnosis	38
2.4.3 Clinical Test	38
2.4.4 Clinical Diagnosis Supported by Technology.....	40
2.5 Shoulder Muscle Activity Assessment	41
2.6 Treatments of Shoulder Pathologies	43
2.7 Kinematics and Kinetics of the Unstable Shoulders.....	44
2.7.1 Research Approaches	45
2.7.2 Shoulder Instability Assessment due to Muscle Patterning of Four Major Muscles.....	48

2.8 Importance of the Quality and Accuracy of the Information	50
CHAPTER III: ANATOMY AND BIOMECHANICS OF THE SHOULDER.....	51
3.1 Introduction.....	51
3.2 Shoulder Anatomy	51
3.2.1 Shoulder Bones.....	51
3.2.2 Shoulder Joints	54
3.3 Biomechanics of the Shoulder	56
3.4 Human Planes	56
3.5 Shoulder Dynamics.....	58
3.5.1 Scapular Rotations.....	60
3.5.2 Glenohumeral Joint Orientations.....	61
3.6 Research Approaches for Glenohumeral Joint Tracking.....	64
3.6.1 Electromagnetic and Inertial Sensors	65
3.6.2 Locators and Clusters	67
3.6.3 Invasive Techniques to Track the Scapula	67
3.6.4 Glenohumeral Joint Tracking Quasi-static and Dynamic Conditions.....	67
3.7 Healthy Shoulder Kinematics	69
3.7.1 Glenohumeral Joint Range of motion	69
3.8 Shoulder Stabilizers	70
3.8.1 Important Shoulder Muscle Mechanics.....	73
CHAPTER IV: METHODOLOGY FOR TRACKING THE SCAPULA.....	77
4.1 Introduction.....	77
4.2 Methodology.....	77
4.2.1 Stage One: Quasi-static Motion	78
4.2.2 Stage two: Dynamic Motion.....	80
4.3 Methodology Validation	81
4.3.1 Materials and Methods	82

4.3.2 Calibration	83
4.3.3 Experimental Test Setup	85
4.3.4 Data Collection.....	88
4.3.5 Data Processing	88
4.3.6 Obtaining the Orientations	88
4.4 Results Scenario a): Stage One Quasi-static Orientations.....	91
4.5 Results Scenario a): Stage Two Dynamic Motion.....	94
4.6 Results Scenario b): Stage One Different Quasi-static Conditions	97
CHAPTER V: TRACKING THE SCAPULA: PORCINE STUDY	102
5.1 Introduction.....	102
5.2 Materials and Methods	102
5.2.1 Practice Dissection	103
5.2.2 Porcine Assessment.....	104
5.2.3 Stage One: Quasi-static Trials.....	111
5.2.4 Stage Two: Dynamic Trials.....	112
5.3 Data Processing	113
5.3.1 Orientation Calculation from IMUs	113
5.3.2 Stage One: Quasi-static	113
5.3.3 Stage Two: Dynamic Motions.....	115
5.4 Results.....	116
5.4.1 Stage One: Quasi-static Trials.....	116
5.4.2 Stage Two: Dynamic Trials.....	120
5.4.3 Comparison of Predicted and Measured Scapula Location in Dynamic Trials.....	122
5.4.4 Assessing the Dynamic Pattern	124
CHAPTER VI: GENERAL REPRESENTATIVE POLYNOMIAL FROM QUASI- STATIC MEASUREMENTS, HUMAN APPROACH.....	126

6.1 Introduction.....	126
6.2 Materials and Methods	126
6.2.1 Methodology Overview: Obtaining a Polynomial from Quasi-static Measurements.....	126
6.2.2 Subjects	129
6.2.3 Calibration	129
6.2.4 Experimental Set up	130
6.2.5 Data Collection.....	132
6.2.6 Data Processing	133
6.2.7 Obtaining the Orientations	133
6.3 Shoulder Results	133
6.3.1 Humeral Flexion-Extension	135
6.3.2 Humeral Abduction-Adduction.....	141
6.3.3 Control Group Results.....	147
CHAPTER VII: CASE STUDY	158
7.1 Introduction.....	158
7.2 Materials and Methods	158
7.2.2 Subjects	158
7.2.3 Calibration	159
7.2.4 Experimental Setup	159
7.2.5 Data Collection.....	160
7.2.6 Data Processing	161
7.3 Quasi-Static Results Part 1), Humeral Flexion-Extension	161
7.3.1 Part 1), Hyper Elastic Participant: Humeral Flexion-Extension	161
7.3.2 Part 1), Muscle Patterning Participant: Humeral Flexion-Extension.....	165
7.3.3 Quasi-static Results Comparison.....	168
7.4 Dynamic Results Part 2): Humeral Flexion-Extension	168

7.4.1 Part 2), Hyper Elastic Participant: Humeral Flexion-Extension	169
7.4.2 Part 2, Muscle Patterning Participant: Humeral Flexion-Extension	172
7.4.3 Dynamic Results Comparison for the Humeral Flexion-Extension.....	176
7.5 Quasi-Static Results Part 1), Humeral Abduction-Adduction.....	177
7.5.1 Part 1), Hyper Elastic Participant: Humeral Abduction-Adduction.....	177
7.5.2 Part 1), Muscle Patterning Participant: Humeral Abduction-Adduction	180
7.5.3 Quasi-static Results Comparison.....	182
7.6 Dynamic Results Part 2), Humeral Abduction-Adduction	183
7.6.1 Part 2), Hyper Elastic Participant: Humeral Abduction-Adduction.....	183
7.6.2 Part 2), Muscle Patterning Participant: Humeral Abduction-Adduction	187
7.6.3 Dynamic Results Comparison for Humeral Abduction-Adduction	191
CHAPTER VIII: DISCUSSIONS AND CONCLUSIONS	192
8.1 Methodology for Tracking the Scapula	192
8.2 Tracking the Scapula: Porcine Study.....	194
8.3 General Representative Polynomial from Quasi-static Measurements, Human Approach	195
8.4 Case Study	198
8.5 General Conclusions	203
8.6 Limitations of the Work.....	204
8.7 Future Work.....	205
REFERENCES	207
APPENDIX.....	222

Final word count 54753

LIST OF FIGURES

Figure 2.1. Stanmore classification of shoulder instability [25].	31
Figure 3.1. a) Shape and body of shoulder bones scapula, humerus and clavicle (anterior view). b) posterior view of the scapula.	52
Figure 3.2. Lateral view of the scapula, where the glenoid fossa is clearly visible.	53
Figure 3.3. Planes of reference and axes of movements.	57
Figure 3.4. Body position through the planes.	58
Figure 3.5. Classification of the shoulder joint movements.	60
Figure 3.6. The internal/external rotation of the scapula occurs in the longitudinal axis, the anterior/posterior titling of the scapula occurs in the mediolateral axis, while the upward/downward rotation occurs in the anterior/posterior axis.	61
Figure 3.7. 'x' unit vector components in a global reference frame generated by the origin (Or) and the global axis X,Y and Z.	63
Figure 3.8. Mass spring system before (a) and after (b) applying a force that generates a mass displacement.	65
Figure 3.9. Contraction and relaxation of a muscle, it is possible to compare the muscle contraction with a man pulling ropes.	73
Figure 4.1. General diagram for stage one. Quasi-static inputs from the humerus, scapula and scapula locator are recorded. Segments orientations are obtained and used to formulate the regression model (RM).	79
Figure 4.2. General diagram for stage two. Dynamic data from the humerus and the scapula IMUS are used as inputs to the regression model obtained in stage one to predict the orientation of the scapula as if the scapula is being tracked with the SL under dynamic conditions.	81
Figure 4.3. Flow diagram for scenario a) and b). Scenario a) aims to prove that the proposed methodology works. Scenario b) aims to understand the sensor behavior for different initial orientations.	83

Figure 4.4. Acrylic custom made scapula locator (SL) with plastic pins. Dimensions are in mm. The SL-IMU was placed on one of the arms of the SL. The arm is aligned with the lateral border of the scapula.....	84
Figure 4.5. IMU calibration on a flat surface, which aligned the global Z axis and the gravitational acceleration vector where X, Y and Z are the vector components of \vec{g} and local axes of the sensor are represented by x, y and z.	84
Figure 4.6. Wooden structure test used in scenario a) to simulate the humerus, the scapula and the SL. Quasi-static and dynamic measurements were performed on the wooden structure. Two extra pieces of wood were used to constrain the motion for the dynamic conditions and to help synchronise the dynamic motion.....	86
Figure 4.7. Scenario a), sensors placement over the wooden structure, with similar conditions to those in potential clinical trials. The local x-axes of the sensors simulating the scapula and humerus are close to vertical.....	87
Figure 4.8. Scenario b), SL and humeral sensors placed on the wooden structure, simulating conditions similar to those found in clinical conditions. The scapula-sensor was placed in different orientations on a curved surface simulating the effect that the shoulder muscles can have on the shoulder.	87
Figure 4.9. Local coordinate frame for a sensor. The orientations were obtained using direction cosines $(\theta_x, \theta_y, \theta_z)$, where \vec{g} represents the global Z-axis described in Figure 4.5.	88
Figure 4.10. Orientations in the global axes $(\theta_x, \theta_y$ and $\theta_z)$ for different quasi-static conditions, measured by the IMUs positioned on the humerus (H-IMU), scapula (S-IMU) and Scapular locator (SL-IMU).....	93
Figure 4.11. Change in orientations in the global axes $(\theta_x, \theta_y$ and $\theta_z)$ over the cycle for dynamic conditions, using the vertical or gravitational acceleration vector as a global reference frame.....	96
Figure 4.12. Wooden drawer test with random orientation for the virtual scapula sensor. θ_x represents the local yz plane orientation with respect to the	

vertical. θ_Y represents the local xy plane orientation with respect to the vertical and θ_Z represents the local xz plane orientation with respect to the vertical. Both $\theta_{X,Y,Z}$ and the virtual humerus are in degrees. 99

Figure 4.13. Schematic representation of the scapula and SL sensor orientation with respect to the vertical or gravitational acceleration vector in their initial conditions and the behaviour when their local yz plane of the sensor cross the ground or the perpendicular plane to the vertical. Figure a) and b) show the sensors initial conditions, while c) and d) represent the orientation after the sensors cross the vertical. e) represents the loocal coordinates of the scapula sensor and its components respect to the vertical and the ground. 100

Figure 4.14. Helmet test with random orientation for the virtual sacpula sensor. θ_X represents the local yz plane orientation with respect to the vertical. θ_Y represents the local xy plane orientation with respect to the vertical and θ_Z represents the local xz plane orientation with respect to the vertical. Both $\theta_{X,Y,Z}$ and the virtual humerus are in degrees. 101

Figure 5.1. Scenarios considered in the porcine study for skin artefact error investigation. 103

Figure 5.2. Disection test performed on a pig shoulder, before and after tissue removal. 104

Figure 5.3. Four inertial measurement units (IMUs) were used for the porcine test. ... 104

Figure 5.4. IMU calibration on a flat surface, which allows the global Z axis and the gravitational acceleration vector to remain vertical. Where X, Y and Z are the acceleration vector components of \vec{g} . x, y and z are the local axes of the sensor and X_H and Y_H are the global horizontal plane components of the Earth's magnetic field. 105

Figure 5.5. Acrylic custom made scapula locator (SL). Dimensions are in mm. 106

Figure 5.6. Frontal and lateral view of the wooden table used in the assessment. 106

Figure 5.7. Traingular wooden base, used to fix the humerus and ulna of the pig leg and support the humeral sensor. 107

Figure 5.8. Section view showing the support table, the assessment table inclined at an angle of 30° to the horizontal plane of the support table, the pig held in position by the body support and mechanical clamp and the upper forelimb of the pig resting on the H-shape jig screwed to the assessment table.....	107
Figure 5.9. Digital spirit level employed to balance the leg ‘H’ support and the triangular wooden base.....	108
Figure 5.10. a) A magnetic test was performed with the IMUs by locating the stainless steel screws close to them, Fig 5.10 a) also shows that there is not magnetic effect on the sensors, making their use suitable for the test. Fig 5.10 b).....	109
Figure 5.11. Side and plan views showing the position of the 4 IMUs, triangular shaped base (humeral base) used to tie the humerus and radio-ulnar joint, the non magnetic stainless steel screws fixed to the scapula bone, the scapula locator and porcine tissue and bone layers.....	110
Figure 5.12. Overlapping sensor test, to identify interference in the sensors signals and measurements due to its proximity.....	110
Figure 5.13. Some of the equipment used for the assessment. Including the precision drill (middle), double side tape (left) and a back u power plant (right).....	111
Figure 5.14. Top view of the assessment table indicating the different positions of the pig’s forelimb for the quasi-static measurements (1 to 7) and the initial and final position for the dynamic motion repetitions (A to B returning to A).....	112
Figure 5.15. PSD of the main axis of motion (Z) used to determine the cut-off frequency of the filter.....	115
Figure 5.16. Orientations in the global axes (θ_x , θ_y and θ_z) over the cycle for quasi-static conditions, measured by IMUs positioned on the Humerus (H-IMU) and is represented in the second (bottom) longitudinal axis, Scapula (S-IMU) and Scapular locator (SL-IMU) and the predictions obtained using the regression equation.	117

Figure 5.17. Orientations in the global axes (θ_x , θ_y and θ_z) over the cycle for dynamic conditions, measured by IMUs positioned on the skin (intact), bone, muscles and the screws (real orientation of the scapula). The second abscissa (bottom) represents the mean changes in angular orientation of the humeral sensor (H-IMU) in the three scenarios described with a maximum change of 28° and a standard deviation of $\pm 2.5^\circ$	121
Figure 5.18. Orientations in the global axes (θ_x , θ_y and θ_z) over the cycle for dynamic conditions, measured by the IMU positioned on the screws (SC-IMU-real orientation of the scapula) and the predictions obtained using the regression equation. The second abscissa (bottom) represents the mean changes in angular orientation of the humeral sensor (H-IMU) in the three scenarios described with a maximum change of 25° and a standard deviation of $\pm 1.5^\circ$	123
Figure 5.19. Dynamic correlation in the X axis for the direct measurements taken from the scapula sensor (different tissues) and the sensor placed over the screws.....	124
Figure 5.20. Dynamic correlation in the Y axis for the direct measurements taken from the scapula sensor (different tissues) and the sensor placed over the screws.....	125
Figure 5.21. Dynamic correlation in the Z axis for the direct measurements taken from the scapula sensor (different tissues) and the sensor placed over the screws.....	125
Figure 6.1. Stage one of the protocol to obtain a regression model (RM). The RM will be obtained using inputs from two quasi-static trials (T1 and T2), by obtaining the average of the best fit coefficient of each trial.....	127
Figure 6.2. a) The scapular IMU (S-IMU) was set on the intersection point of the perpendicular bisectors of the lines joining the acromion process (AP), the superior medial border of the scapula spine (SS) and the inferior scapular angle (AI), while the humerus sensor (H-IMU) was placed at the midpoint of the projected line of the AP and the lateral epicondyle (LE), between the triceps and biceps muscles. Figure 6.2 b) shows the	

position of the SL sensor (SL-IMU) and the pins of the SL placed over the bony landmarks.	128
Figure 6.3. Stage two assess es the level of agreement between the regression model (RM)and measured data, by using the humerus and scapula orinttation values from a third trial (T3) in the RM. The orientation predicted by the regression equation is compared with data from the SL recorded from the same third trial.	129
Figure 6.4. a) Heading reset was applied to all IMUs on a flat surface, which allowed both the global Z axis and the gravitational acceleration vector to remain vertical [16]. The local x, y and z orientation of a sensor (IMU) in the global X, Y and Z at the calibration moment are shown in Figure 6.4 a), where the gravitational acceleration vector (g) was used as a global reference to calculate the relative orientation between pairs of sensors (scapula-humerus-SL). Figure 6.4 b) Sensor aligment to apply the heading reset on a flat surface.	130
Figure 6.5. Participant in the fundamental position and SL placement with the three sensor used in the test.	131
Figure 6.6. Procedure used in the trials. Three trials were performed by each participant in flexion-extension and abduction-adduction recording the humerus, scapula, and the SL orientations.	132
Figure 6.7. a) represents the scapular upward and downward rotation, b) representsthe scapula anterior/posterior tilt, c) represents the scapula internal/external rotation, d) is showing the local plane alignment of the S-IMU, when the sensor is placed over the scapula.	134
Figure 6.8. Global X, Y and Z axes in relation to the GHJ components. Different humeral orientations in flexion.	135
Figure 6.9. Mean raw orientation in X, Y and Z of the first two trials (T1 and T2, in degrees) for humerus, scapula and SL, for one participant in humeral flexion-extension.	138

Figure 6.10. SL-Observed orientation from the third trial (T3) and predicted orientation for the SL in three axes for one participant in humeral flexion-extension.....	140
Figure 6.11. Global X, Y and Z axes in relation to the GHJ components. Different humeral orientations in abduction-adduction are shown: at rest position, one position around middle range of humeral abduction-adduction and one in an overhead position.....	141
Figure 6.12. Mean raw orientation in X, Y and Z of the first two trials (T1 and T2, in degrees) for humerus, scapula and SL, for one participant in humeral abduction-adduction.	144
Figure 6.13. Observed and predicted orientation for the SL in three axes for one participant in humeral flexion-extension.....	146
Figure 6.14. Observed and predicted orientation for the SL in three axes for nine participants in humeral flexion-extension for the X axis. Level of agreement between the observed and predicted values for nine subjects. .	149
Figure 6.15. Observed and predicted orientation for the SL in three axes for nine participants in humeral flexion-extension for the Y axis. Level of agreement between the observed and predicted values for nine subjects. .	150
Figure 6.16. Observed and predicted orientation for the SL in three axes for nine participants in humeral flexion-extension for the Z axis. Level of agreement between the observed and predicted values for nine subjects. .	151
Figure 6.17. Observed and predicted orientation for the SL in three axes for nine participants in humeral abduction-adduction for the X axis. Level of agreement between the observed and predicted values for nine subjects. .	154
Figure 6.18. Observed and predicted orientation for the SL in three axes for nine participants in humeral abduction-adduction for the Y axis. Level of agreement between the observed and predicted values for nine subjects. .	155
Figure 6.19. Observed and predicted orientation for the SL in three axes for nine participants in humeral abduction-adduction for the Z axis. Level of agreement between the observed and predicted values for nine subjects. .	156

Figure 7.1. The scapula IMU (S-IMU) was set on the intersection point of the perpendicular bisectors of the lines joining the acromion inferior angle (AA), superior medial border of the scapula spine (SS) and the inferior scapular angle (AI), while the humerus sensor (H-IMU) was placed at the midpoint of the projected line of the AA and the lateral epicondyle (EL), pointing posteriorly.....	160
Figure 7.2. Left shoulder component measurements under quasi-static orientations (deg) used to obtain the representative equation of each shoulder of the volunteer, where HE represents the hyper elastic participant, S the scapula and SL the scapula locator. Orientations are presented in the global axes (θ_x , θ_y and θ_z) over the cycle for quasi-static conditions in humeral flexion-extension.....	163
Figure 7.3. Left shoulder component measurements under quasi-static orientations (deg) used to obtain the representative equation of each volunteer, where MP represents the muscle patterning and different surgery process of participants, S the scapula and SL the scapula locator. Orientations are presented in the global axes (θ_x , θ_y and θ_z) over the cycle for quasi-static conditions in humeral flexion-extension.....	166
Figure 7.4. Left scapula Omega measurements before (Raw) and after correction (Corrected) for the participant with hyper elasticity (HE), where ω_x , ω_y and ω_z represent the angular velocity in rad/s for the three global axes, in humeral flexion-extension. The total humeral elevation (green dotted line) is presented at the right side of the charts.	170
Figure 7.5. Left scapula orientation (deg) measurements before (Raw) and after correction (Corrected) for the participant with hyper elasticity (HE), where θ_x , θ_y and θ_z represent the orientation in degrees for the three global axes in humeral flexion-extension.....	171
Figure 7.6. Left scapula Omega measurements before (Raw) and after correction (Corrected) for the participant with muscle patterning instability (MP), where ω_x , ω_y and ω_z represent the angular velocity in rad/s for the three global axes, in humeral flexion-extension. The total humeral elevation (green dotted line) is presented at the right side of the charts. ...	173

Figure 7.7. Left scapula orientation (deg) measurements before (Raw) and after correction (Corrected) for the participant with muscle patterning instability (MP), where θ_x , θ_y and θ_z represent the orientation in degrees for the three global axes in humeral flexion-extension.....	175
Figure 7.8. Left shoulder component measurements under quasi-static orientations (deg) used to obtain the representative equation of each volunteer, where HE represents the hyper elastic participant. Orientations are presented in the global axes (θ_x , θ_y and θ_z) over the cycle for quasi-static conditions in humeral abduction-adduction.....	178
Figure 7.9. Left shoulder component measurements under quasi-static orientations (deg) used to obtain the representative equation of each volunteer, where MP is the muscle patterning and different surgery process participant, S the scapula and SL the scapula locator. Orientations are presented in the global axes (θ_x , θ_y and θ_z) over the cycle for quasi-static conditions in humeral abduction-adduction.....	181
Figure 7.10. Left scapula Omega measurements before (Raw) and after correction (Corrected) for the participant with hyper elasticity (HE), where ω_x , ω_y and ω_z represent the angular velocity in rad/s for the three global axes, in humeral abduction-adduction. The total humeral elevation (green dotted line) is presented at the right side of the charts.....	185
Figure 7.11. Left scapula orientation (deg) measurements before (Raw) and after correction (Corrected) for the participant with hyper elasticity (HE), where θ_x , θ_y and θ_z represent the orientation in for the three global axes, in humeral abduction-adduction.....	186
Figure 7.12. Left scapula Omega measurements before (Raw) and after correction (Corrected) for the participant with muscle patterning (MP), where ω_x , ω_y and ω_z represent the angular velocity in rad/s for the three global axes, in humeral abduction-adduction. The total humeral elevation (green dotted line) is presented at the right side of the charts.....	188
Figure 7.13. Left scapula orientation (deg) measurements before (Raw) and after correction (Corrected) for the participant with muscle patterning (MP),	

where θ_X , θ_Y and θ_Z represent the orientation in for the three global axes
in humeral abduction-adduction..... 190

LIST OF TABLES

Table 2.1. Common injuries related to type of instability [42].	35
Table 3.1. Shoulder Static and Dynamic stabilizers [13, 141].	70
Table 3.2. Muscle actions [37, 108-109, 144-145].	72
Table 3.3. Muscle contribution to the abduction torque, measured by Escamilla [51].	76
Table 4.1. Best fit coefficients for the three axes of the wood drawer test.	94
Table 5.1. Scapula, humerus and screw sensors' Range of Motion.	113
Table 5.2. Best fit coefficients for the three axes of the porcine assessment.	119
Table 6.1. Best fit coefficients for the three axes of one participant for humeral flexion-extension.	139
Table 6.2. Best fit coefficients for the three axes of one participant for humeral abduction-adduction.	145
Table 6.3. Mean values of the best fit coefficients for the three axes from the first two trials for the nine participants in humeral flexion-extension. The coefficient values are in radians.	147
Table 6.4. Mean values of the best fit coefficients for the three axes from the first two trials for the nine participants in humeral abduction-adduction. The coefficient values are in radians.	152
Table 6.5. Averaged results from nine participants for humeral flexion-extension and abduction-adduction.	157
Table 7.1. Best fit coefficients for the three axes for the hyper elastic participant in humeral flexion-extension.	164
Table 7.2. Best fit coefficients for the three axes for the muscle patterning participant in humeral flexion-extension.	167
Table 7.3. Best fit coefficients for the three axes for the hyper elastic participant in humeral abduction-adduction.	180
Table 7.4. Best fit coefficients for the three axes for the muscle patterning participant in humeral abduction-adduction.	182

ABBREVIATIONS

GHJ	Gleno humeral joint
RoM	Range of motion
SCT	Stanmore Classification Triangle
EMG	Electromyography
sEMG	Superficial Electromyography
iEMG	Intramuscular Electromyography
MRI	Magnetic Resonance Image
MRA	Magnetic Resonance Arthrography
CT	Computerised Tomography Scanning
MDI	Multidirectional instability
TUBS	Traumatic Unidirectional Bankart Lesion
AMBRI	Atraumatic Multidirectional Bilateral
FEDS	Frequency, Aetiology, Direction and Severity
RCT	Rotator Cuff Tears
WMSD	Work related to Musculoskeletal Disorders
ABIS	Abduction Inferior Stability
ISB	International Society of Biomechanics
IMU	Inertial Measurement Unit
NSAIDs	Non Steroidal Anti Inflammatory Drugs
PM	Pectoralis Major muscle
LD	Latissimus Dorsi muscle
DT	Deltoid muscle
TP	Trapezius muscle
UTP	Upper Trapezius muscle
MTP	Middle Trapezius muscle
STJ	Scapulothoracic Joint
ACJ	Acromioclavicular Joint
SCJ	Sternoclavicular Joint
SP	Sagittal Plane
FP	Frontal/coronal Plane
TP	Transverse Plane
MA	Mediolateral Axis

AA	Anterior/posterior Axis
LA	Longitudinal Axis
SL	Scapula Locator
S-IMU	Scapula- Inertial Measurement Unit
SC-IMU	Screws- Inertial Measurement Unit
H-IMU	Humerus- Inertial Measurement Unit
SL-IMU	Scapula Locator- Inertial Measurement Unit
PSD	Power Spectrum Density
RMS	Root Mean Square error
CNS	Central Nervous System
AP	Action Potentials
MU,MUP	Motor Units, Motor Unit Potentials
MUAP	Motor Unit Action Potential
SENIAM	Surface EMG for Non Invasive Assessment of Muscles
DCM	Direction cosine matrix
RM	Regression Model
HE	Hyper Elastic
MP	Muscle Patterning

NOMENCLATURE

S-IMU	Scapula- Inertial Measurement Unit
SC-IMU	Screws- Inertial Measurement Unit
H-IMU	Humerus- Inertial Measurement Unit
SL-IMU	Scapula Locator- Inertial Measurement Unit
A_x, A_y, A_z	Acceleration components
\bar{g}	Gravitational acceleration vector
xy, yz, xz	Local Planes
X_m, Y_m, Z_m	Magnetometer outputs in the local axes
X_G, Y_G, Z_G	Global axes
$X_\theta, Y_\theta, Z_\theta$	Pitch, roll and heading angles relative to the horizontal
X_H, Y_H	Components of the heading vector in the pitch and roll axes
q	Quaternion
q_0, q_1, q_2, q_3	Quaternion components
q^*	Complex conjugate of a quaternion
q _{GL}	Quaternion rotation from the local reference frame to the global reference frame
$\theta_x, \theta_y, \theta_z$	Angular orientations
$T_1, T_2 \dots T_n$	Trials
ω	Angular velocity
SJ_G	Relative angular velocity of the joint (rad/s)
M	Torque (N-m)
I	Inertial tensor
α	Angular acceleration
JP	Joint power
O_r	Origin
d	Distance
m	Mass
a	Acceleration
F	Force
k	Spring constant
j	Arbitrary vector

ABSTRACT

In the diagnosis and analysis of shoulder instability a precise determination of the location and orientation of the Glenohumeral joint is important. A better understanding of shoulder kinematics and kinetics will help clinicians and therapists in the diagnosis and treatment of shoulder pathologies. To-date, non-invasive skin-based methods are often either restricted to quasi-static measurements or are inaccurate during dynamic assessments at high humeral elevations as a result of soft skin artefact.

Tracking the orientation of the scapula is difficult because it is surrounded by soft tissues, is held mainly by muscles and has only one direct point of attachment to the thorax. Instability of the glenohumeral joint generates poor functionality of the shoulder labrum and capsule as well as in the muscle and connective tissue structures that surround the shoulder. As the clinical phenomenon of shoulder instability is extremely complex, one of the priorities for the specialist in avoiding a faulty diagnosis is to recognise, identify and classify shoulder pathologies such as muscle patterning instability in the early stages of the investigation.

A two stage methodology for non-invasive tracking of the scapula under dynamic conditions is presented in this work. The methodology provides scapula location by combining data from two surface mounted sensors using a regression-type equation formulated from quasi-static trials undertaken using a scapula locator and three IMUs (first stage). In the second stage, the least square fit is used to improve the scapular orientation by utilising data from only two IMUs (humerus and scapula) under dynamic conditions. Accuracy was assessed in an animal study by comparing results with those from a bone based method during quasi static and dynamic tests. Tests were also undertaken to investigate the errors induced by the soft tissue artefact in surface based scapula location measurement. In dynamic trials the methodology proved more accurate in determining scapula location than a standard skin-based approach, and showed that the greatest contribution to soft tissue artefact was from the epidermal, dermal and subcutaneous tissue layers as opposed to the muscle layer. We confirmed that, in cases where subjects have relatively small amounts of soft tissue surrounding the scapula, surface based methods could provide reasonable accuracy. Our methodology utilised subject-specific data to formulate a regression equation, and can be used to provide accurate, non-invasive tracking of the scapula under dynamic conditions in subjects regardless of individual body morphology. After the methodology validation, study tests were undertaken in a case study in order to estimate the scapula orientation under dynamic conditions in a human without symptoms of any shoulder pathologies and in one participant diagnosed with shoulder instability due to muscle patterning.

The two stage methodology is proven to work in a healthy human participant in dynamic tests, in a person with no suspicion of shoulder instability. This methodology allows the error reduction generated by the soft tissues surrounded the scapula. The work presented here can be used as a framework for developing diagnosis protocols by using modern technology.

DECLARATION

No portion of the work referred to in the thesis has been submitted in support of an application for another degree or qualification of this or any other university or other institute of learning.

COPYRIGHT

i. The author of this thesis (including any appendices and/or schedules to this thesis) owns certain copyright or related rights in it (the “Copyright”) and s/he has given The University of Manchester certain rights to use such Copyright, including for administrative purposes.

ii. Copies of this thesis, either in full or in extracts and whether in hard or electronic copy, may be made only in accordance with the Copyright, Designs and Patents Act 1988 (as amended) and regulations issued under it or, where appropriate, in accordance with licensing agreements which the University has from time to time. This page must form part of any such copies made.

iii. The ownership of certain Copyright, patents, designs, trade marks and other intellectual property (the “Intellectual Property”) and any reproductions of copyright works in the thesis, for example graphs and tables (“Reproductions”), which may be described in this thesis, may not be owned by the author and may be owned by third parties. Such Intellectual Property and Reproductions cannot and must not be made available for use without the prior written permission of the owner(s) of the relevant Intellectual Property and/or Reproductions.

iv. Further information on the conditions under which disclosure, publication and commercialisation of this thesis, the Copyright and any Intellectual Property and/or Reproductions described in it may take place is available in the University IP Policy (see <http://documents.manchester.ac.uk/DocuInfo.aspx?DocID=487>), in any relevant Thesis restriction declarations deposited in the University Library, The University Library’s regulations (see <http://www.manchester.ac.uk/library/aboutus/regulations>) and in The University’s policy on Presentation of Theses

ACKNOWLEDGMENTS

I want to gratefully acknowledge The National Council on Science and Technology of Mexico (CONACYT) and the Secretaría de Educación Pública del Gobierno Mexicano for supporting the postgraduate student involved in this work.

I want to express my gratitude to my supervisors: Prof Alonso, Prof Adam Watts, Dr David and Dr Jaya for their support, patience and for sharing their experience with me; without their help this work could not be done.

I would like to thank to Dr Alan Walmsley for his academic support and his infinite patience and guidance through this process NDWA, also I would like to give special thanks to Mr Puneet Monga, Consultant Orthopaedic Surgeon, and Miss Julia Walton, Shoulder Physiotherapist, for additional advice and help.

And last but not least, I want to express my gratitude to my parents (Lupita y Chuy), family, friends, especially to Gabo and Chilo, and finally to the bioengineering group for their support and help.

Special thanks to my sister for being the greatest ever.

CHAPTER I: INTRODUCTION

1.1 Overview

Instability in the glenohumeral joint as a result of muscle patterning is a problem that is not well understood. Unintentional and unbalanced muscle actions may result in the subluxation of the humerus from its counterpart the glenoid fossa, yet the definitive source of the instability is not clear [1-7]. Problems with shoulder instability, when the diagnosis is not made in the early stages, increase the risk of inappropriate surgery or poor rehabilitation in the future [3, 8-9].

The shoulder joint is a ball and socket union formed by the humerus and scapula, enveloped by muscles, ligaments and tendons. These musculoskeletal components work together to maintain stability in the shoulder joint, and to transfer power to and from the limbs. The shoulder complex comprises of around 30 muscles and 32 bones, including the whole arm [10-11], thus highlighting the complexity of the upper arm.

The shoulder joint has the advantage of providing the arm with the greatest range of movement in different areas, especially in overhead activities, where the control and restriction generated by the muscles is highly important. In overhead activities (e.g. those undertaken by baseball pitchers, swimmers and tool workers among others) problems with shoulder articulation can have a profound negative impact. As a result of the ball and socket geometry of the shoulder joint, coordination between the dynamic and static stabilizers is necessary for the functionality of the joint [12-13]. Understanding the muscles activity will indicate the behaviour expected from the bones.

The muscles of the shoulder complex are very important in the behaviour of the joint, while a mechanical task is being performed [14]. The fact is that the muscle moves the bones by changing the length of the shoulder muscle fibres to absorb or generate energy. Unbalanced muscle actions can generate what is known as muscle patterning instability and result in the partial or complete dislocation of the glenohumeral head from the glenoid fossa.

A better understanding of shoulder kinematics and kinetics will help clinicians and therapists in the diagnosis and treatment of shoulder pathologies related to muscle

patterning. Good diagnosis and treatment will help the patient resume their daily activities quickly by avoiding lengthy rehabilitation treatment, expensive surgical procedures, pain and reduced work productivity due to absences [15].

The recuperation time required by a patient depends on the type and severity of injury; for example, for minor muscular problems, where the injury is not too severe, recuperation time might typically vary between 3 to 8 weeks. However, in cases where damage is more severe requiring a surgical procedure, recuperation may take 6 to 7 months or more, including the rehabilitation and treatment time. Moreover, as with the recuperation time, the expense associated with these problems depends on the kind and severity of the injury and damage. In the UK, an arthroscopic rotator cuff repair in 2008 cost up to £ 2,651 [16]. It is necessary to note that in the UK, the price paid for an open procedure is the same as an arthroscopic procedure. But in reality, the open procedure is more expensive due to the cost of consumables; hence the hospitals incur economic losses [17].

The shoulder joint rotations are generated by the shoulder muscle forces and moments applied to the shoulder bones and so move the arm through a whole Range of Motion (RoM) [12-13]. The congruence between shoulder bones is maintained by dynamic and static stabilizers however abnormal muscle action pattern can result in shoulder pathology. Studies have demonstrated the relation between wear patterns of the glenohumeral joint and the motion of the scapula [18-19].

Shoulder problems related to muscle patterning

The problems related to muscle patterning instability at the shoulder joint occur as a result of unintentional and unbalanced muscle actions which may be generated by multiple factors: trauma (in a direct way), physiological (ligament laxity), congenital or other issues. It is not currently very well understood what gives rise to the abnormal muscle activation pattern, but there have been many theories. While several methods such as questionnaires and diagnostic tests have been developed to determine shoulder instability, none of these methods is 100 percent accurate, especially in instability due to abnormal muscle patterning, for example: more than 50% of the world's population has suffers at least one episode of shoulder pain during any one year. In 2007, the emergency department of the USA reported 1,326,000 cases related to shoulder and

upper arm problems. A Norwegian survey reported that 46% of the population had at least one episode of shoulder problems [20]. In addition, the emergency departments of the USA reported 1,684,000 cases related to adverse effects of medical treatment and the National Ambulatory Medical Care Survey reported, during 2007, a total of 84,567,000 musculoskeletal diseases and connective tissue treatments [21-22]. The third most common complaint of the musculoskeletal system, is problems of the shoulder. In the UK alone 15,534 cases were registered for shoulder problems in the 2000 and 9,215 of those cases were followed up for the next three years [23].

A study conducted in a cohort of 4,080 sportsmen and women population reported that, reports than 6% of the athletes presented with instability without having any physical contact and 5% of that population presented with instability with unknown causes [24]. However, the study makes the inference that poor neuromuscular control is a major factor; which could fit in the definition of muscle patterning, and agrees with the findings of Matias and Pascoal [2] who suggest that problems with the scapular kinematics in shoulders with instability could be related to non optimal muscular activity.

Muscular coordination problems have been identified as a factor in shoulder disorders such as muscle patterning instability. Despite the coordination problems in the muscles, muscle strength does not vary in a systematic way [6, 25] making the diagnosis of muscle patterning instability even more difficult. Jaggi [6] commented that the pathologies that generate shoulder instability can appear as a structural problem in the rotator cuff, especially in the contact areas of the surface of the capsulolabral complex, or as non structural problems that may be related to the central and peripheral nervous system [6, 26]. Similar results were proposed by Barden *et al.* [27] where abnormal activation time of the shoulder muscle was found in participants with multidirectional instability.

Muscular imbalance can generate the superior decentralization of the humeral head that may lead to degenerative rotator cuff tears [5]. Jan *et al.* [28] suggest that in cases where the source of traumatic instability is not well known and radiographic studies give negative results, the development of muscle imbalance could be a factor in developing a joint injury. Abnormal activation patterns in the shoulder muscles could be initiated by

uncontrolled mechanical, electrical and chemical stimuli [29]. The unwanted muscle contraction could be reflected in the glenohumeral joint orientation altering the normal balance of the joint.

Instability of the glenohumeral joint generates poor functionality of the shoulder labrum and capsule as well as in the muscle and connective tissue structures that surround the shoulder ball and socket joint. As the clinical phenomenon of shoulder instability is extremely complex, one of the priorities for the specialist in avoiding a faulty diagnosis, is to recognise, identify and classify shoulder pathologies such as muscle patterning instability in the early stages of the investigation.

Medical science has been looking for a classification method to describe the damage suffered at the shoulder joint. A review of the literature suggests two different types of classification method; one that relates to the skeletal system and the other that relates to the muscular system, and their interaction. For example traumatic injuries with structural damage, commonly require surgery. On the other hand, medication, physical therapy, rehabilitation treatment and sometimes surgery, are common procedures used to treat muscular problems. Three important causes of recurrent instability have been detected after surgical procedures: an inappropriate or inadequate operation, or a wrong diagnosis [25].

1.2 Objectives and Methodology of the Research

The research aim of this thesis was to develop a non invasive framework/methodology that will provide information on scapular orientation that can be used to understand shoulder pathologies, starting from quasi-static measurements and progressing to dynamic measurements using a regression type equation to reduce the soft tissue artefact. The information obtained has the potential to be used in shoulder pathology diagnosis, to select the most appropriate rehabilitation treatment, assess the shoulder behaviour before and after surgery and as a base for using inertial technologies in telemedicine for a distance/remote assessment or pre-diagnosis. The research project was undertaken in collaboration with clinicians from Wrightington Hospital, Wigan, UK, Wrightington, Wigan and Leigh NHS Foundation Trust, who provided the patient information as well as medical advice in terms of anatomy, physiology and diagnosis. Although the framework developed in this thesis was applied to two shoulder motions

only, the methodology can be applied to different types of motion and shoulder pathologies.

To accomplish the aim of the research, it was necessary to develop and test the methodology in controlled conditions to assess the functionality of the methodology. Once the methodology functionality was assessed the next step was to understand the major sources of error that can obscure the true motion of the scapula and then, validate the proposed methodology. Once the methodology was validated, a general mathematical model to describe the scapula orientation under dynamic conditions was obtained and used to correct for the effect of the soft tissues over the scapula orientation. Finally the methodology was assessed using a case of study.

This thesis is structured as follows:

A literature review regarding shoulder pathologies and the current diagnostic methods is presented in Chapter II. In addition, the different techniques and devices that have been used previously to track the scapula are identified and described. The objective of this chapter is to highlight the importance of tracking the scapula under dynamic conditions in order to be able to assess the different kinds of shoulder instability where dynamic assessment is required.

Chapter III describes the structure and function of the shoulder joint and discusses the medical terms used, the anatomy and biomechanics of the shoulder.

Chapter IV describes the methodology used to determine scapula orientation. This methodology utilises a combination of data from inertial sensors and a scapula locator, obtained during quasi-static tests. The data is used to develop a regression-type equation; thereafter the equation is used to track the scapula under dynamic conditions by using data from just the two inertial sensors. The methodology utilises both scapula and humeral orientation (recorded under dynamic conditions) as inputs to the equation, instead of one input as in other dynamic tracking techniques [30]. It was expected that use of equation would reduce the error generated by the tissue artefact under dynamic conditions and output orientation as if the scapula was tracked with the scapula locator. A secondary aim of this section was to understand sensor behaviour prior to use in a clinical setting. An extra advantage of the methodology is that a good understanding of

shoulder behaviour using accelerometry will, in future, allow the use of mobile devices to obtain data that can be sent to the clinical specialists before appointments.

Chapter V describes the validation of the methodology described in chapter IV for non-invasive dynamic measurement using experimental tests undertaken on a porcine cadaver. A pig model was chosen because of the numerous anatomic and physiologic characteristics they share with humans [31-33]. Pigs have been used in numerous biomedical and biomechanics research studies, including surgical models and procedures. Importantly, for this study, the skin of the pig is structurally similar to human skin in terms of epidermal thickness and dermal-epidermal thickness ratios [32-34]. In addition, pigs develop considerable subcutaneous fat and have dermal collagen and elastic content akin to humans. Dynamic and quasi-static trials were performed on a pig cadaver, involving passive movement of the forelimb of the specimen to change humeral orientation in a sagittal plane.

Chapter VI describes how scapular orientation was estimated by means of a mathematical model relating data from three IMU sensors, one IMU is placed directly over the scapula, the second one is located over the humerus and the third one is located over a scapula locator (SL) device. Those IMU sensors recorded data from different quasi-static humeral orientation: flexion-extension and abduction-adduction movements were assessed. The advantage of this method is that it will enable IMUs to be used in a reliable way to evaluate shoulder pathology under dynamic conditions through a whole range of motion as if the GHJ were assessed by the SL, taking advantage of the SL technique and the use of IMUs under dynamic conditions.

Chapter VII describes the application of the novel methodology in a case study. Finally the conclusions of this work are presented in Chapter VIII.

CHAPTER II: SHOULDER INSTABILITY BACKGROUND

2.1 Introduction

Instability of the glenohumeral joint occurs when the congruence in the motion between the humeral head and the glenoid fossa is altered. Shoulder instability symptoms can present as a simple feeling of the joint slipping out and grow into a more complex shoulder situation such as the complete dislocation of the humeral head from the glenoid fossa.

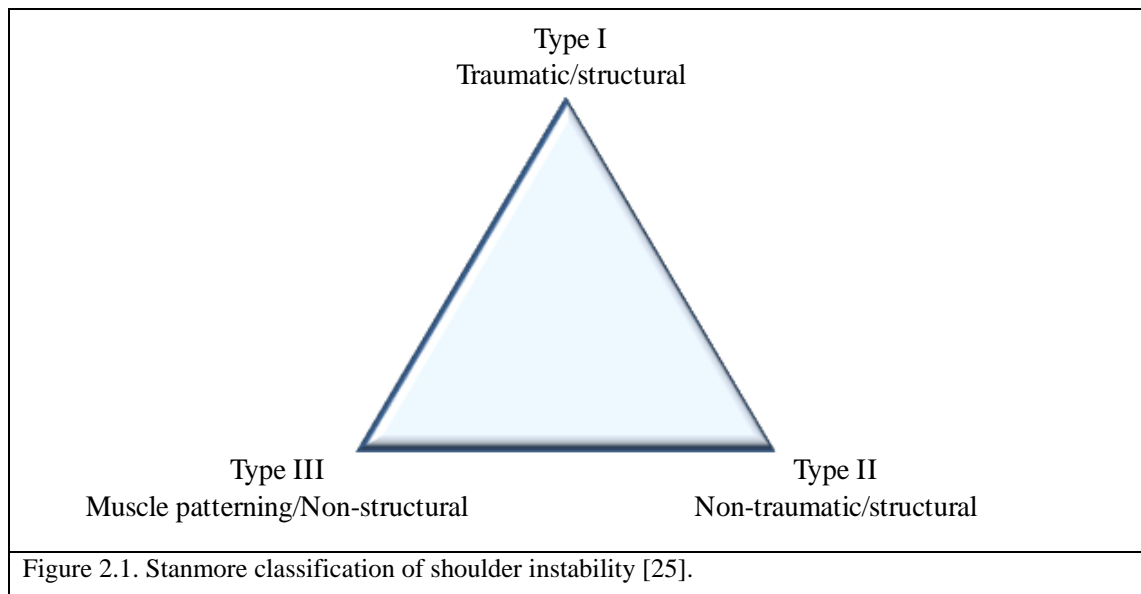
Shoulder instability due to muscle patterning has been associated with unbalanced and uncontrolled muscle forces that generate the partial or complete dislocation of the shoulder components [6-7, 35]. However, what causes the instability due to muscle patterning is not very well understood and it is commonly associated with other shoulder pathologies. Tyson [36] comments that glenohumeral instability can appear as a result of trauma, capsular laxity or glenoid hypoplasia [36]. Schachter *et al.* [37] suggest that any impingement or previous illness may increase the probability of suffering instability by shoulder pattern. They also comment that fatigue alters the glenohumeral and scapulothoracic kinematics [37]. Rowe *et al.* [35] reported poor success after a surgical procedure in patients with voluntary instability and psychological pathology.

Shoulder instability is a serious condition that affects the world's population, especially young people (e.g. swimmers [3]), under 30 years old [15, 36, 38]. A faulty diagnosis or poor rehabilitation process in this population can adversely affect the time taken for the resumption of daily activities, with serious instability problems at the shoulder joint taking up to 6 to 7 months for the rehabilitation and treatments process.

2.2 Instability Classification Systems

The Stanmore Classification Triangle (SCT) is one of the most common systems used to classify shoulder damage and pathology (Figure 2.1) [25]. The triangle has been a very useful tool to determine both the diagnosis and the type of rehabilitation required [6]. Any axis of the triangle can be used in an isolated way or in combination with another axis to describe damage. For example articular surface damage can fit in

traumatic/structural damage (Type I, SCT) and non traumatic/structural (Type II, SCT) without having any relation with muscle patterning (Type III, SCT) [25].



Detecting shoulder instability is a very difficult process because of inconsistencies between the methods used [4]. Diagnosis usually requires a physical examination (with or without anaesthetic) with the support of diagnosis modalities such as EMG, MRI, X rays and Ultrasound to help the specialist in the diagnosis. However, misdiagnosis can easily occur. Many of the classification methods have been developed to determine the instability present in the shoulder complex. Lewis *et al.* commented that failing to consider the likelihood of mixed pathologies is one of the most common problems with this class of methods since these pathologies can potentially change over time.

Some methods have been developed to approach and classify the instability problem [25, 39]:

The Rockwood Classification method (1979) [25] describes four types of instability:

- Traumatic subluxation, without previous dislocation.
- Traumatic subluxation, after previous dislocation.
- Atraumatic voluntary subluxation (with or without psychiatric problems).
- Atraumatic involuntary subluxation.

The Thomas and Matsen Classification method (1989) is an improved method based on the Rockwood system, but this method uses the initial letter as acronym [39]:

I. TUBS, Traumatic Unidirectional Bankart Lesion (treated with Surgery).

II. AMBRI, Atraumatic Multidirectional Bilateral, treated with rehabilitation (sometimes surgery is required).

Sometimes another “I” is added to the AMBRI + I, which means closure of the rotator Interval.

The Schneeberger and Gerber Classification method (1998) focuses on the absence of laxity in the joint. A traumatic event could result in unidirectional instability [25]. Gerber and Nyffeler improved the definition of instability by describing three types, dynamic, static and voluntary but they did not present a model [39].

Nyiri highlights that the International Classification of Disease (Ninth revision, ICD-9) is one of the most used methods to classify multidirectional instability (MDI), but it is not particularly reliable in classifying the shoulder instabilities [40]. Kuhn develops the FEDS (frequency, aetiology, direction and severity) method to classify the instability [1]. Other classification methods were also developed by Silliman and Hawkins [41].

The Stanmore Classification is based on triangle geometry as shown in Figure 2.1, where each vertex represents a group or a polar type, being the polar groups being II and III. These two groups have been the most difficult groups to decode and classify [25, 39].

2.3 Pathology of Shoulder Instability

Rotator Cuff Tears (RCT) - these injuries may be separated into partial or complete tears. Partial tears occur in the articular surface of the bursa and can be of different longitudes and depths, while a complete tear involves the total thickness of the rotator cuff. The complete tears permit direct contact between the subacromial bursa and the glenohumeral joint [20, 42]. One mechanical situation which influences the RCT is the “superior decentralization of the humeral head” which may be generated by muscular

imbalance (instability) by increasing shear and compressive forces in the tendons of the rotator cuff [5].

Impingement Syndrome - this syndrome presents with pain in the rotator cuff especially with forward elevation of the arm [36, 42]. When the upper limb is elevated the supraspinatus tendon is forced to move under the coracoacromial arch and the humeral head, catching the subacromial–subdeltoid bursa and bicep tendon, which generates inflammation (subacromial–subdeltoid bursa), tendon degeneration, and tears [20, 36].

Isolated Labral Tears - (functional instability, Tyson [36]), this problem can occur in people with no medically detectable instability (especially in overhead sports). These tears can occur in the anterior superior, superior, or posterior labrum. The isolated labral tears allow a slight instability and light subluxation of the humeral head [36].

Bicep tendon abnormalities may result in inflammation, degeneration, rupture, medial dislocation of the bicep tendon, and rotator cuff tears, permitting the upward displacement of the humeral head and increasing impingement of the bicep tendon [36]. Biceps tenosynovitis sometimes occurs as a result of trauma, or may be associated with chronic inflammatory disorder (rheumatoid arthritis) [42].

Trauma - it is common to see fractures in the shoulder. The most common fractures are fractures of the greater tuberosity, which are frequently associated with acute tears of the rotator cuff, [36]). Fracture dislocation usually ends in damage to the capsulolabral complex. One of the most common occurs in the anatomic neck of the humerus.

Masses - commonly known as tumours. Tumours can generate shoulder instability by altering the normal kinematics or by generating problems in neuromuscular control.

Arthritis - inflammatory arthritis may involve synovial proliferation, and cartilaginous or bony erosion. When it is in an advanced state (in musculotendinous structures), degenerative glenohumeral osteoarthritis results in osteophyte formation, sub-chondral sclerosis and loss of cartilage [36]. Osteoarthritis is associated with anterior shoulder dislocation and full thickness rotator cuff tears [20]. It is often thought that muscle patterning results in arthritis [43].

Adhesive Capsulitis - Tyson describes this illness as a “stiff painful shoulder joint with a limited range of motion”, [36]. It is generally known as frozen shoulder and is the result of a strong limitation in passive and active ranges of motion [20, 36].

Unnatural kinematics of the scapula, which contributes to shoulder pain and some pathologies such as frozen shoulder, instability [20].

2.4 Glenohumeral Instability classification

Instability of the glenohumeral joint can be classified by the direction of its occurrence, the trauma history, laxity, and the type of dislocation (total or partial dislocation).

The shoulder complex can present unidirectional, bidirectional and multidirectional forms of instability. On that basis it is possible to determine the planes where the instability can occur. Cordasco provides some help for determining the area of instability [8], Bohnsack classifies shoulder multidirectional stability based on the pathological laxity of the whole inferior glenohumeral ligament complex [44]:

- **Anterior instability** - soreness in the overhead, horizontal abduction (apprehension test) and external rotated position suggests this type of instability [8, 44-45].
- **Inferior instability** - indicated when the person experiences pain carrying heavy objects [44].
- **Posterior instability:** indicated by the sensation of feeling pain while patients are pushing heavy objects, flexing the arm forward or in internal rotation position.
- **Recurrent instability** is indicated when a weak external force generates repetitive dislocations or subluxation, [44].
- **Multidirectional instability (MDI):** A combination of directional instabilities. In the past multidirectional instability was also known as loose shoulder [46]. Reduction in the range of motion in patients with multidirectional instability has been attributed to a significant delay in the shoulder muscles' activation time as well as shortened periods of activation [27].

Table 2.1 illustrates some injuries related with glenohumeral instability are mentioned.

Table 2.1. Common injuries related to type of instability [42].		
Instability type	Background	Common lesion
Anterior instability	As result of previous dislocation	<p>Bankart's lesion (consists of the detachment of the inferior glenohumeral ligament / labral complex from the anteroinferior glenoid)</p> <p>Bony Bankart's lesion (consists in the rupture of the glenoid bone and the anterior labrum)</p> <p>Anterior labral ligamentous periosteal sleeve avulsion (consists in the rupture but not detachment of the labral ligamentous that rolls up in a sleeve, similar to the Bony Bankart's lesion)</p> <p>Hill- Sach fracture (consists of a posterosuperior humeral head impaction)</p> <p>Superior Labrum Anterior</p> <p>Posterior (SLAP) tears</p>
Posterior instability	Related to tears of the posterior labrum and posterior joint capsule	<p>Reverse Hill-Sach impaction fracture (anterior superior humeral head)</p> <p>Bennett lesion (is a crescentic, posterior, extra articular ossification, rising inferiorly from the glenoid posterior to the labrum)</p> <p>Bony Bankart's lesion on the posterior inferior margin of the glenoid rim</p>

Instability at the shoulder joint can be summarized as a non natural symptomatic motion of the glenohumeral components which is related to some degree of translation of the shoulder components (laxity), which can generate subluxation or dislocation of the shoulder and pain [25]. Subluxation is described as the symptomatic separation of the shoulder component surfaces without reaching the complete dislocation. On the other hand dislocation is the total separation of the glenohumeral joint components [25].

An unstable muscular attachment to the scapula can generate problems with force production, resulting in muscular instability that contributes to compound pathologies [47]. Glenohumeral stability can be affected by the presence of any structural injury, fatigue, or pain, in an isolated or mixed way [20]. The risk of instability is also increased by poor neuromuscular control [20].

2.4.1 Muscle Patterning

The dislocation of the humeral head is initiated by the failure of one of the ‘muscle force-couples’ that generate normal shoulder motion [35]. As a result of laxity of the ligaments in the middle range of the GHJ motion, the role played by the contracting muscles in generating the compression needed to keep the contact between the humeral head and the glenoid, becomes very important for the stability of the shoulder joint [48].

The work conducted by Hisao Endo [46] relating to multidirectional instability suggested that patients with loose shoulder present inferior subluxation of the glenohumeral joint bilaterally. The patients had no history of trauma or any abnormalities related to the glenohumeral bones and the surrounding muscles. The results from Endo also suggested that the range of motion of the shoulder was very close to the normal results obtained for a healthy control group. However, laxity was noted when the arm was in abduction, being pulled downwards, or holding a weight, but the differences decreased after 60° of arm elevation.

A severe case of instability in the shoulder area was presented by Stark [49]. This case presents a painless kinesio pathology in abduction motion. The examination of the patient showed muscle atrophy of the lower trapezius and weakness of the surrounding muscles. This was also associated with early lateral rotation of the scapula and dysrhythmia of the glenohumeral joint [49]. An interesting finding made during the

examination was a regular subluxation and relocation of the humeral head from the glenoid fossa, around 70° and 180° of abduction, and to a lesser degree during flexion. Another finding was the excessive internal rotation of the affected shoulder when compared with the non-affected shoulder [49].

The humeral head is held in a central position inside the glenoid fossa mainly by the rotator cuff muscles [50-51]. However, the stability of the shoulder can be altered by the large torques acting on the shoulder produced by the Latissimus dorsi, Serratus anterior, Pectoralis major and the Deltoids (major muscles). It is possible to explain the large torques by reference to the cross-sectional anatomy, which reveals the long distance of the muscle attachments from the rotation centre of the joint [13, 45]. Irregular activation patterns in the large shoulder muscles together with suppression of the rotator cuff muscles has been implicated in muscle patterning instability [52].

The following problems can be considered as possible causes of muscle patterning instability, by generating involuntary contraction in the shoulder muscles:

Myofascial Trigger Points are neuromuscular lesions free of pain. A Myofascial trigger point can modify the normal activation pattern of a shoulder muscle by generating a delay in the muscle fibres response.

Friction or drag inside the joint can generate an involuntary reaction of the shoulder components which generates involuntary muscle movements.

Stress or Fatigue - stress may modify the natural posture, consequently the shoulder kinematics can change, as well as the force angle, torque [37].

Many factors can alter the natural balance of the shoulder, not only a trauma, and if this happens several times, fatigue can occur. Another form of fatigue exists when a person over exercises his / her shoulder. One example of how the accumulation of several factors can affect the body was given by Yuk Szeto [53], who describes work related to musculoskeletal disorders (WMSD, usually affecting people who use computers). This disorder affects the neck and shoulder and is the sum of physiological, biomechanical, psychological and social factors [53]. Hypertonic muscles or muscles that are over exercised in the shoulder may initiate instability due to muscle patterning in the

glenohumeral joint, for example in the pectoralis major muscle and the deltoid muscle, because they can generate major forces under certain conditions (e.g. repeated overhead activities) that break the balance in the joint decreasing stability [7, 45]. For example Labriola *et al.* [45] founds that when the activity of the pectoralis major muscle increased, forces in the anterior direction increased or compressive forces suffered a reduction so the shoulder joint instability was compromised.

2.4.2 Medical Diagnosis

Choosing the right treatment for the instability is of great importance. The length of the procedure is determined by the type of instability and damage to the structures involving the muscles, bones, and tendons. Rouleau *et al.* [54] suggested different scores to measure the instability of the shoulder. While other researchers suggest that a combination of tests are needed such as an accurate history of the patients, physical examination and the use of image techniques [55].

Jaggi comments that the muscle patterning instability includes an abnormal action movement of the large muscles, and simultaneous suppression of the rotator cuff, commonly identified in people who are classified in group III of the Stanmore classification with a history of “party tricking” shoulder [6].

2.4.3 Clinical Test

There are several tests and questionnaires that are used to determine the instability, some of which need physical evaluation, while others are supported by the use of technology. The common tests performed by orthopaedic surgeons and therapists are presented in this section. The following list presents a wide variety of these tests [39, 55]:

The Laxity test shows the degree of translation suffered by the joint. There are 3 types of laxity tests:

The Load and Shift test the purpose of this test is to find the degree of translation the humeral head has on the glenoid fossa.

In order to evaluate the anterior/posterior laxity the **Drawer test** is a useful tool. Direct feedback can be obtained by the examiner when the anterior Drawer test is performed by the examiner. The **anterior Drawer** test is performed by extending the damaged arm at 80° to 120° of abduction, 0° to 20° of forward flexion and 0° to 30° of external rotation. The **posterior Drawer** test requires flexion of the elbow of around 120° while the shoulder is positioned in 80° to 120° of abduction, and between 20° to 30° of forward flexion [39].

The Sulcus sign test evaluates whether there are any signs of multidirectional stability. The focus of the test is to observe any depression and displacement between the acromion (lateral edge) and the humeral head, when a smooth downward traction of the humerus is undertaken [39].

The Provocation test assesses the capacity of the shoulder to resist challenges and to stabilise the shoulder in certain positions. The test also pays attention to the apprehension, loss of function, clicking or popping of the joint and pain.

The Relocation test consists in replacing the humerus head on the glenoid (natural position), as a result of applying a posterior force.

Other tests include the Release test and the Apprehension (augmentation) test. A particular test has been developed for the study of posterior instability. For example; **the Posterior Subluxation test**: for this tests the arm is required to be adducted and internally rotated at 70° to 90° of flexion. The **Jerk test**, this test is used for evaluation of the posterior capsular integrity. There are also other tests such as the **Flexion rotation pivot test** and the **Posterior apprehension test**.

Other unidirectional tests have been developed to determine the inferior laxity, such as the **Hyperabduction test**, **Inferior apprehension**, or the **Abduction Inferior Stability test (ABIS)**.

The tests that focus on the labral lesions are: the **Active compression test**, **Crank test**, **Biceps tension**, **compression rotation test**, **Speed's and clunk test**, and the **Anterior slide test**. Similarly, there are numerous tests for examining passive stability, such as **Yergason's test** and the **Biceps load test**.

Posterior shoulder instability is commonly diagnosed by the “**posterior stress test**”, which usually generates pain and instability [44]. For Subacromial pain evaluation, **Hawkins’ and Neers, Yergason’s and Speed’s test** are commonly used [56].

One of the simplest tests is the **Beighton score** which is a quick and very useful tool to determine the hyper mobility in the joints [57]. A score of up to four points indicates a generalized joint laxity [57-58].

2.4.4 Clinical Diagnosis Supported by Technology

With both the passage of time and the development of new technologies applied to medicine, general practitioners and surgeons have found new and useful tools for diagnosis. These include the use of X-Rays, Computerised Tomography Scanning (CT), Magnetic Resonance Imaging scanning (MRI), Electromyography (EMG), and ultrasound [36, 42, 59]. Technology has become a very important tool to avoid faulty diagnosis, especially when the symptoms of the pathology can be misunderstood, to identify the type and severity damage of the musculoskeletal components. Some examples of the available technology are:

- **X-Rays** - radiography is the most commonly used method to determine shoulder problems in terms of bone fracture or shoulder dislocation. X-rays can also reveal information regarding a Hill Sachs defect (humeral head), and sometimes muscle calcification problems if the X-ray is clean enough [36, 42]. Unfortunately X-rays do not give good information about the soft tissue structures around the shoulder (muscles and tendons).
- **Ultrasound** - Ultrasound is helpful in quantifying the changes in muscle length [14, 60], and to detect rotator cuff pathology. The ultrasound examination has the advantage that it can be done during a shoulder movement, but this evaluation requires a very experienced radiologist or technician.
- **Computed Tomography Scan** - CT scans provide a very good representation of the bony anatomy. The problem with this technique is the use of the ionising radiation, which does not give a good soft tissue contrast. But the clear CT scan helps in the diagnosis of the bony injuries, and to identify loose bodies through the shoulder joint. CT arthomography is used in the diagnosis of labral tears and intra articular loose bodies as well [59, 61].

- **Magnetic Resonance Imaging** - MRI brings the facility of showing multi planar images and greater soft tissue contrast. MRI helps in the diagnosis of rotator cuff degeneration, tears, and structural abnormalities (such as impingement syndrome, or biceps tendonitis) [59].
- **EMG** - The Electromyography is a technique used to evaluate the electric behaviour of the skeletal muscle or its coordination [62]. There are two types of EMG studies, surface studies and fine wires studies (the fine wires or intramuscular electrodes are commonly used to examine the rotator cuff muscles). EMG studies are very helpful in classifying instability in the shoulder and finding abnormal muscle patterns [52].

2.5 Shoulder Muscle Activity Assessment

The upper limb can achieve a wide range of motion and amplitudes generated by the sequential muscle activations. An Electromyography study is a way of assessing the muscles' contribution in each part of the motion.

Electromyography can be used to measure the differential in potential generated by the contraction of the muscles fibres thus enabling muscle activity to be assessed. Electromyography can be split into superficial or surface electromyography (sEMG) and intramuscular electromyography (iEMG) [27]. Intramuscular electromyography is invasive and consists of the insertion of a needle or wire through the muscle fibres to assess the muscle activity [62].

sEMG consists of the placement of electrodes that can adopt different shapes and has plates of a conductive material (for example Al/AgCl) [63]. Some electrodes used in the sEMG require a gel or paste to improve the conductivity. It is also required to clean the skin to remove dead skin cells, dirt and hair. sEMG has the advantage of being a non invasive method, but carries the risk of electrodes becoming loose (becoming unstuck from the skin) and high cross talk (activity of neighbouring muscles) [64]. In order to avoid cross talk, the location of the electrodes is highly important. As well as the location, the orientation of the electrodes is also significant. It is recommended to follow the fibre alignment of the muscles being studied.

The use of sEMG and motion analysis in different areas of medicine, sport, rehabilitation and bioengineering is rising [65]. The opportunity to analyse the non natural patterns and their relation to muscle behaviour provides a very helpful tool for the specialist.

The information that can be extracted by the use of the sEMG and motion analysis techniques is [65-66]:

- Muscle tendon system (non neural component) - the joint behaviour can be affected if the properties of the system change (joints moments, angles, and velocity).
- Paresis - bad muscle activation or incomplete activation, in other words a kind of incomplete paralysis.
- Spasticity - problems in controlling the muscles.
- Co - contraction - bad control activation of the antagonist muscles.

One clear example of using kinematic and electromyography techniques is the study of the upper limbs in children with hemiplegic cerebral palsy [67].

EMG has been used to determine the activation level and pattern of the muscles. Some authors have also tried to match the voltage of the EMG with the muscle force behaviour [68-70]. Some studies have been undertaken to describe and predict the muscle force and its relationship with the velocity, kinematic, muscle length change and muscle electric activation [68, 71-75]. These studies have been a very useful tool for understanding joint stability, in prosthesis design and muscle stiffness prediction.

Problems related to sEMG signals, which generate interpretation problems are [62]:

- Amplitude Cancellation, these phenomena occur when the positive and negative phases of MUAPs cancel each other out.
- Crosstalk, when the electrical activity of neighbouring muscles contaminates the EMG signal.
- Spatial variability, when there is unbalanced activity of the muscles.
- Variability of the EMG, adaptation to the process or tasks and problems related to the measurement process [62].

- Electromechanical Delay, any change in the activation time of a muscle generates bad coordination. This modification can occur without any modification in the force [62].
- Neuromuscular Fatigue, fatigue can generate an electromechanical delay. The increase of the EMG activity may not necessarily be related to fatigue, and could be originated by muscle compensation [62].

Another factor that can affect the quality of the electrical behaviour measurement according to Schachter *et al.* is muscular fatigue, which alters the glenohumeral and scapulothoracic kinematics [37]. A period of rest is suggested between each task. The period of relaxation depends on the routine performed [76], whether the exercises performed in the sets are light. It is important to highlight that the position of the patients affects the activation behaviour of the muscles [76].

2.6 Treatments of Shoulder Pathologies

The pain that shoulder instability can generate in the shoulder joint can be commonly confused with other shoulder pathologies such as impingement, acromioclavicular joint disease, or even cervical disc disease [42].

Some treatments are relatively simple such as ergonomics / adjustments at work or in daily life activities, as well as the classic superficial therapies of applying heat or ice [20]. However, other treatments may require training and qualified personnel, such as the use of corticosteroid, non steroidal anti inflammatory drugs (NSAIDs), exercise (movement and strengthening), acupuncture, ultrasound therapy, stretching and transcutaneous electrical nerve stimulation [20]. Lewis proposes three principles for treatment [25], following the Stanmore triangle classification:

- Surgical stabilization: recommended when structural instability exists.
- Non operative: recommended when muscle patterns exist, but there is no sign of structural instability.
- Non operative: when muscle pattern and structural instability exists.

It is also possible to divide the treatments as follows:

- **Open treatment** consists of an invasive procedure (surgery). This treatment can be split into open treatments for posterior and anterior instability. Anterior instability surgery is recommended for young and active patients, who participate in overhead activities [44]. Orthopaedic surgeons use the Arthroscopy method to determine structural damage at the shoulder joint. This process is very helpful for discerning the difference between the polar groups II and III of the Stanmore classification [25].
- **Conservative treatments** are recommended before two episodes of recurrent instability [44].

Takwale *et al.* developed a protocol for shoulder treatment which they divided into three phases [77]:

- **Orthopaedic surgeon examination** is where a visual analysis of the muscle presenting wears patterns.
- **Muscle identification** consists of recognising the group of muscles with abnormal patterns is undertaken.
- **Teaching the patient** means that the patient must recognize the involuntary pattern and restore normal stabilization.

2.7 Kinematics and Kinetics of the Unstable Shoulders

The stability of the Glenohumeral joint motion is affected by the motion of the scapula [78], which is supported and moved by the muscles. Evaluating scapula kinematics is difficult due to the surrounding soft tissues. For that reason it is common to find shoulder kinematic assessments with controlled motion usually in one plane, that do not take into account the full range of motion and rotations of the shoulder joint components through different planes [30, 79-81].

Large components of external rotation have been found when unstable shoulders have been assessed [61]. Most of the lesions in the shoulder area occur when the shoulder is abducted and rotated externally [59]. The work of Justus *et al.* [82] found that the increased external rotation is related with progressive anterior capsular lesions when the glenohumeral joint is elevated below of 60°. Their findings were based on cadaveric studies without the muscle complex.

In atraumatic multidirectional instability it is common for patients to feel uncomfortable with their arm elevated and they usually try to avoid high humeral positions according to Inui *et al.* [83]. In his work Inui found that the scapula would follow the glenohumeral motion. However he fails to explain why all the humeral heads displaced posteriorly, which highlights the possibility of poor neuromuscular imbalance and the way how the muscles pull the humeral head posteriorly [83].

The functionality of the glenohumeral joint may be achieved in daily life activities for patients with shoulder pathologies, including those activities where large amounts of rotation and wide ranges of motion are needed, even though the patient presents with a limited range of shoulder motion when affected and unaffected shoulders are being compared [84].

2.7.1 Research Approaches

To help in the diagnosis and rehabilitation of shoulder instability, determination of the location and orientation of the shoulder components and their behaviour in common activities is vital. In order to decode the shoulder behaviour different types of physical devices and methodologies have been developed by the researchers, such as bone pins, [30, 80], imaging techniques [85-86] and non-invasive techniques such as locators [87]. Unfortunately locators can only be used in quasi-static conditions, but they may reduce the error generated by the soft tissues. The non invasive techniques of measurements are commonly based on electromagnetic tracking devices [30, 79, 84, 88], optoelectronic tracking systems [81, 87, 89-90] and Inertial Measurement Units (IMU) [30, 88, 91-92], that are used under both dynamic and quasi-static conditions. However, these techniques and methods are affected by the soft tissue artefact when the orientation of the shoulder components must be determined using non-invasive methods [87, 90, 92-94]. Loss of accuracy has been reported with these techniques when used to track movements above humeral elevations of 90° [30, 93-94] mainly because of skin movement artefact. By knowing the location, orientation and relative motion of the shoulder bones, it is possible to infer what the shoulder muscles are doing.

Accurate determination of the location and orientation of the components of the glenohumeral joint is important for understanding how the shoulder behaves during daily activities [95-98] and can aid in the analysis and diagnosis of shoulder instability

[2, 19, 88, 91]. However, the soft tissue artefact generated by the motion of the shoulder components hinders the assessment of the scapula and humerus orientation with non-invasive tracking devices [87, 90, 92-94]. For example the belly formed by the deltoid muscle in overhead activities [87, 90]. In order to track the scapula orientation different techniques and methods have been used.

Currently, direct techniques, such as the use of bone pins, are considered the most accurate methods for tracking scapular position [30, 80]. However, the invasive nature of these methods severely limits their use in the clinical setting. The application of imaging techniques to track the scapula also suffers from a number of drawbacks and limitations including cost, availability and exposure of the patient to electromagnetic radiation [85-86].

The scapula locator (SL) technique is a non-invasive method for locating the scapula that may reduce the effect of soft tissue artefact when applied by a skilled and experienced operator. However, the SL is unsuitable for monitoring continuous motion because it must be relocated over the scapula bony landmarks for every movement [87].

IMUs can be used in dynamic trials over a wide range of motion, over 120° of humeral elevation in the case of arm motion [30]. Researchers have suggested that the use of IMUs attached directly to the skin over the humerus and scapula is sufficiently accurate for clinical purposes [30, 88, 91-92, 99-100].

Understanding how the shoulder works has been the focus of a number of studies. Research has focused on different shoulder loading conditions [96-97], or on describing the functional behaviour of the healthy glenohumeral joint in common activities [95, 98]. These studies have been performed using many of the devices and techniques described above, for example: Karduna *et al.* [30] assessed the accuracy of measuring three-dimensional dynamic scapular kinematics with a magnetic tracking device by comparing orientations from tracking devices attached to the skin with those from devices attached to bone pins. The Root-mean-square errors (RMSE) reported over the entire range of motion (RoM) ranged between 4.7° and 8.6° for scapular posterior tilt, between 2.0° and 4.2° (after a correction factor) for the scapular upward rotation and from 3.2° to 11.4° for external rotation of the scapula. They concluded that the non-

invasive approaches could provide reasonably accurate representations of scapular motion (limited to humeral elevation less than 120°).

Brochard *et al.* [93] and Lempereur *et al.* [94] compared scapular orientation, obtained using different optoelectronic tracking systems employing passive markers, with orientation from instruments that palpate the scapula (metal) or use marker clusters. The methods tested varied according to the action performed, indicating that certain methods were more suitable for some activities than for others. Even though the results obtained using the markers were similar overall to those obtained using the cluster or the instrument that palpated the scapula, it was noted that improvements were required around 90° and 120° of humeral elevation [30, 93-94] in order to reduce the artefact generated by the soft tissues.

Shoulder pathologies (glenohumeral subluxation and frozen shoulder) have been analysed using a SL and IMUs at the same time [88, 91] but the IMUs used in these studies were located over the SL with no sensor placed directly on the scapula. The results presented in the studies demonstrated that by using these methods it was possible to differentiate between, and compare the movement patterns of the affected and unaffected shoulders of a patient under quasi-static conditions. One disadvantage of using the SL in the assessment of shoulder pathology is that it prevents study of the effect of the muscles on the GHJ when the joint is in motion (the SL is restricted to quasi-static measurements). For a better understanding of the dynamic stabilizers in the shoulder joint a dynamic study is essential [6].

The author of the research described in this thesis hypothesised that dynamic scapula motion could be determined more accurately using non-invasive techniques to aids in the therapy, rehabilitation treatment and diagnosis. However, the effect of soft tissue movement over bony anatomy would require further investigation as this would probably have a significant effect on the accuracy of measurements, especially at the extremes of motion.

2.7.2 Shoulder Instability Assessment due to Muscle Patterning of Four Major Muscles

Wear activation patterns have been noticed in the major muscles of the shoulder, at the Pectoralis Major (PM), Latissimus Dorsi (LD), Deltoid (DT) and Trapezius (TP), in patients with recurrent shoulder instability due to muscle patterning [7, 79]. Low sensitivity in the pectoralis major, inferior and anterior deltoid has been found with the use of surface EMG [52]. These major muscles are strong enough to generate shoulder dislocation.

The Pectoralis Major has been found to be more active in shoulders with anterior instability (60%) [7]. For multidirectional instability, the pectoralis major has shown differences in the activation time in shoulder extension [27]. While the Latissimus dorsi activity level was found to be more active in 81% of the shoulders assessed with anterior instability and 80% in shoulders with posterior instability, the anterior part of the deltoid shows an inappropriate pattern in 22% of the cases with anterior instability. This could be explained by the stabilizer function of the deltoid muscle [7]. These percentages come from a recent study consisting of 140 participants with potential instability due to shoulder muscle patterning by Jaggi *et al.* [7]. The conclusion was that the Latissimus dorsi muscle influenced anterior/posterior instability whereas anterior instability was influenced by the pectoralis major. However the authors did not assess the orientation of the GHJ components at the time the wear pattern occurred. It has been demonstrated that, in patients with multidirectional instability, the activity of the pectoralis major muscle is reduced or suppressed, in order to keep the humeral head centralized in the glenoid fossa, while the arm is elevated in a continuous way in the scapular plane [101]. The reduction in the muscular activity is reflected in changes in the range of motion.

The upper part of the trapezius muscle is important in the flexion and abduction of the arm. Wear patterns have been found in this part of the muscle after shoulder arthroplasty [102]. Bad control of the trapezius muscle can generate non normal winging of the scapula that makes it rotate away from the ribcage. This action can result in subluxation or dislocation of the arm's humeral head from the glenoid fossa [77]. Differences in the activation time through the three different parts of the trapezius have

been reported for non traumatic instability [103]. This becomes important because any change, or imbalance in the forces generated by the activation time, can pull out the scapula generating the loss of the scapulohumeral balance [103]. Ludewig's [79] findings suggest alterations in the trapezius muscle, to compensate for a decrease in the muscle activity of the serratus anterior muscle, when the upward rotation of the scapula is occurring, in shoulders with impingement. The compensation was not enough to also generate a deficiency in the posterior tipping when the arm is holding a load. The participants of this study were prone to undertake overhead activities.

Electromyography Assessment of Four Major Muscles of the Shoulder

The Trapezius descendens is active in the first 60° of abduction, generating a large moment around the scapula-clavicular joint. When the arm is close to the 90° abduction position all parts of the Trapezius muscle become active to compensate the protracting forces generated by the other muscles. The clavicular portion of the trapezius presents its highest activity at 30° of abduction and at 90° ante-flexion [104].

The Deltoid muscle (DT) has its maximum peak of activity when the arm is abducted at 90° and 60° of ante-flexion, above 120° the deltoids generates a large counterbalance moment for the abduction motion according with Van Der Helm [104]. When the scapula is in a stable position, the external moments generated by the deltoid muscle in the humerus are counterbalanced [104].

Van Der Helm reports that the Latissimus dorsi muscle is not active during the antifixion and abduction of the humerus [104].

The Pectoralis Major muscle becomes active at high abduction of the arm, around 60° of ante-flexion. The PM muscle continue to be active for all the antifixion motion but for higher arm positions of antifixion it becomes more of a counterbalance muscle [104]. However the results obtained from a control group [101] suggest that sometimes the PM could be less, or not, active. The author of this work believed that this could be the result of a different neuromuscular technique used by the brain to reach the desired arm position.

2.8 Importance of the Quality and Accuracy of the Information

The orientation of the scapula is of great importance for the stability of the glenohumeral joint [47, 78]. The muscles move the bones so any imbalance in the muscles' activation time will be reflected in the humerus and scapula orientation under dynamic conditions [26]. Dynamic scapular assessment is more difficult due to the effect of the soft tissues under dynamic conditions. Deeper knowledge of the muscles' coordination and strength in shoulder instability is required for diagnosis and treatment [26]. It has been shown that scapular taping modifies the kinematics in asymptomatic subjects [105]. This highlights the importance of a good understanding of the instability mechanism and the influence of the muscles over the shoulder bones, particularly in the presence of pain or for injury prevention [105]. Studies suggest that the mechanism of the shoulder motion does not change in a linear way [106-107], especially at higher and lower arm elevations.

CHAPTER III: ANATOMY AND BIOMECHANICS OF THE SHOULDER

3.1 Introduction

The motion of the shoulder is achieved by the harmonic synchronisation of the dynamic and static stabilizers, which include muscles activation, the congruence between the shoulder joint bones and ligaments, thus allowing a wide range of motion of the arm through different planes. The shoulders allow the force transmission from the lower limbs to the arms.

3.2 Shoulder Anatomy

The shoulder bones are part of the Appendicular Skeleton. The Scapula and the Clavicle are located at the Pectoral Girdle (shoulder girdle). The Humerus is the only arm bone that has a direct link with the scapula in the upper limb area. Some bones, such as the ribs, also have an indirect effect on shoulder function [108-109].

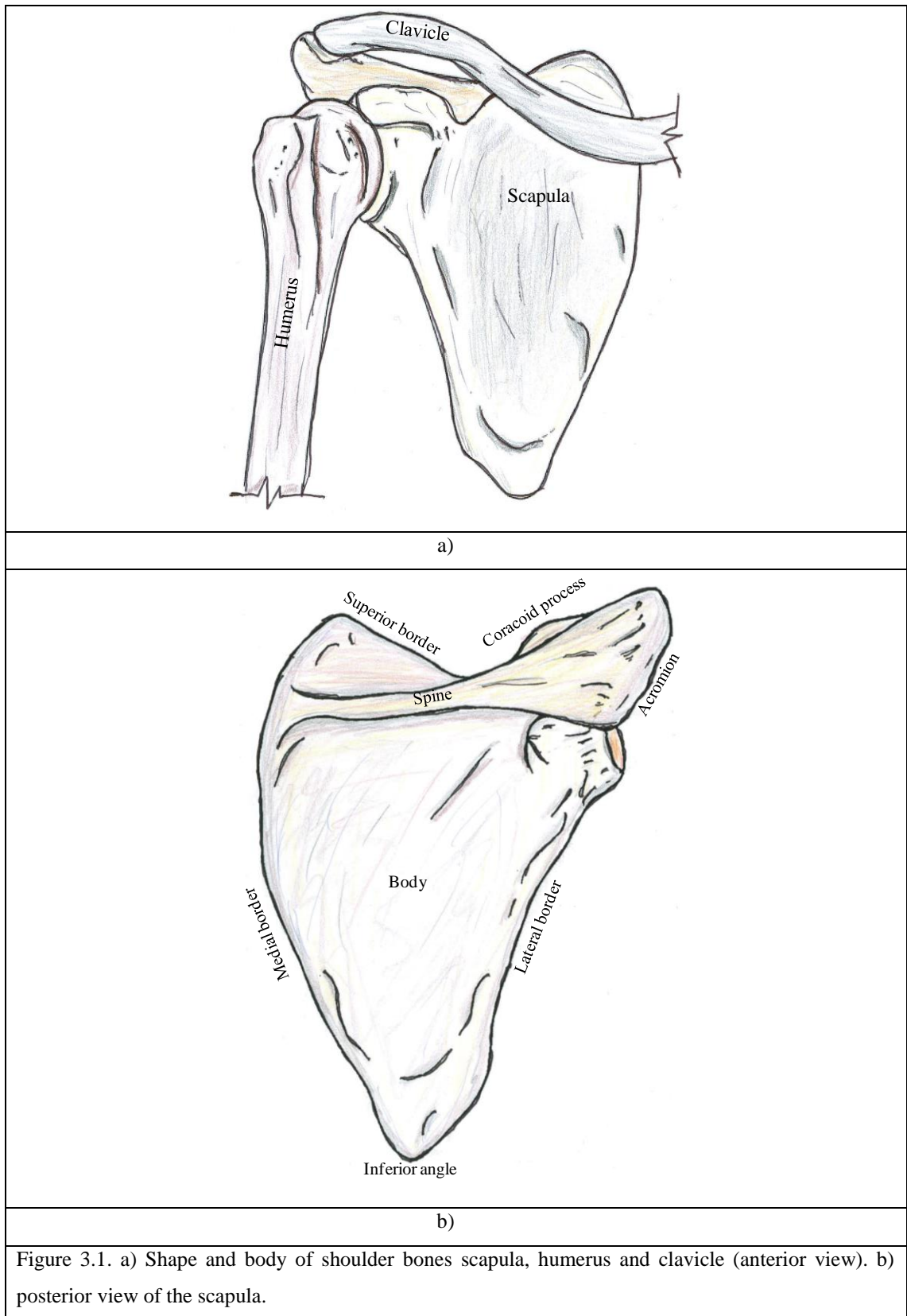
Being the hardest part of the glenohumeral joint, the shoulder bones provide structure and support to the shoulder muscles. The bones have been classified in several ways, according to the location (axial and appendicular) and the geometric shape (long, short, flat, and irregular bones) [108-110].

3.2.1 Shoulder Bones

The head of the humerus (Figure 3.1) links with the glenoid fossa of the scapula and the opposite side links with the radio-ulnar joint. The humeral head has a spherical shape with an angular value of 153° , that fits and moves in the glenoid fossa of the scapula. The humeral neck and head has an angle against the humeral shaft between 45° - 50° in a frontal plane, while in the transverse plane the neck is internally rotated against the shaft [111]. In terms of muscle attachment points, the greater and lesser tubercles are the humeral points where the shoulder muscles anchor [108-109, 112].

The clavicle or collar bone (Figure 3.1) is a long and slightly curved “S” form bone. The acromial side of the clavicle is the part of the bone that directly links with the Acromion process of the scapula, while the sternal side of the clavicle bone links with

the manubrium of the sternum, and the clavicle holding and helping to determine the position of the scapula [30, 96, 106, 112].



The Scapula or shoulder blade (Figure 3.1) has a flat triangular shape that provides stability to the glenohumeral joint. It acts as an attachment point for the shoulder muscle. The scapula helps with shoulder elevation and retracting/protracting of the shoulder girdle around the thorax [47, 112]. In a normal resting position the scapula is located around 30° with respect to the frontal plane [111]. The glenoid fossa of the scapula is the point that links with the humeral head. The glenoid has an angular radius of 75° in the frontal plane, while for the sagittal plane the angular value is around 50° [111]. Figure 3.1 shows the posterior view of the scapula and its components, while Figure 3.2 shows the lateral view of the scapula, where the glenoid fossa can be easily identified.

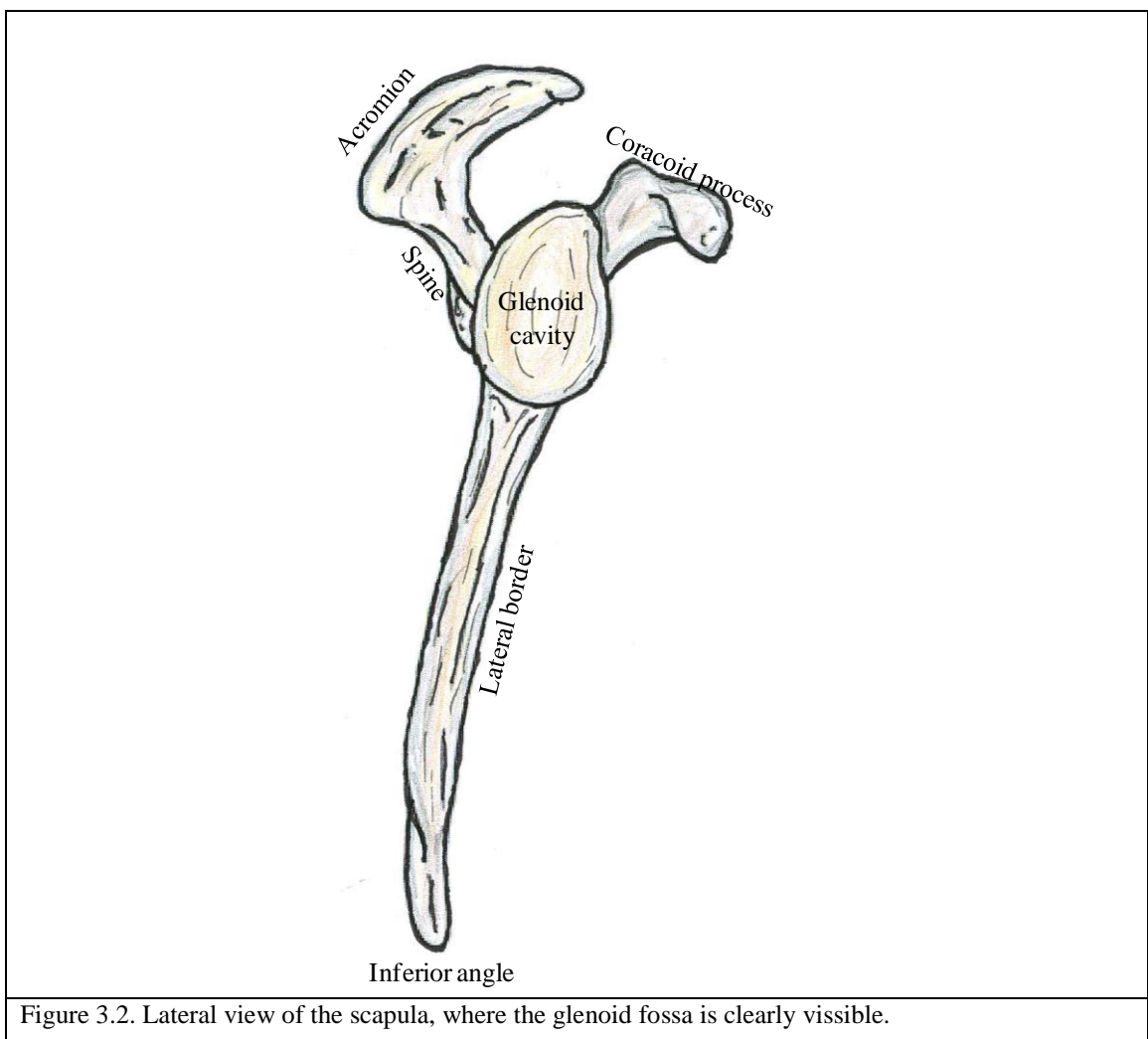


Figure 3.2. Lateral view of the scapula, where the glenoid fossa is clearly visible.

The main function of the shoulder bones, like the other bones in the human skeleton are to provide: support-shape, protection, storage, blood cell production and motion [108-109].

3.2.2 Shoulder Joints

The shoulder complex consists of five joints. Four of them are considerable, non- real joints (but contribute significantly to the mobility and stability of the shoulder, rhythm), [113-114]:

The glenohumeral joint (GHJ or true joint) is the place where the shoulder blade (scapula) links with the upper side of the humerus. This connection is made by the rounded end of the humerus and the cavity of the scapula (glenoid cavity), with a ratio of 153 ° provided by the humerus fitting, in a 75° concavity of the glenoid fossa [111]. As this kind of joint is unstable, it needs the surrounding muscles and ligaments to keep the whole entity together. The capsuloligamentous and musculotendinous are needed to keep the GHJ balanced. The work of the deltoid and the rotator cuff musculature are very well identified [115]. The GHJ has the advantage of having many degrees of freedom, but this range of freedom also makes it unstable.

Three rotation movements in the abduction and flexion planes, and through the long humeral axis (axial rotation), as well as 3 translation movements have been used to describe the kinematics of GHJ [39]. It has been documented that if the translation is up to 3 mm in the superior direction, this translation occurs in the first 60 degrees of abduction. While in the scapular plane this translation occurs up to 1 mm after this point with inferior translation occurring in the supine abduction [39]. These results highlight the relationship that is kept by the GHJ in terms of rotation and translations of the humerus and the glenoid fossa of the scapula. Around 22% to 25% of the humeral head works in the glenoid fossa (articulate) [116-117]. The humeral head has 21 to 22 cm² of articulated area, while the glenoid fossa articulated area is around 8 to 9 cm², so the maximum contact area is about 4 to 5 cm², which represents 22 % of the contact area working in the fossa [117].

Scapulothoracic Joint, (STJ) is located at the rear of the chest (ribs area), where the scapula interacts with the thorax. This joint is well known as the Scapulothoracic gliding plane. The scapulothoracic joint is not an articulated link through the scapula and thorax. It is considered to be joined because of the action of the surrounding muscles that constrain and enable the scapula to glide on the thorax [118]. The most important muscles working in this joint are the serratus anterior and the trapezius. The

first one helps to keep the scapula in position, while the second one helps in the rotation and elevation process of the scapula. As well as having 3 rotations, upward rotation (anterior/posterior axis), external rotation (superior/inferior axis), and posterior tilt (medio/lateral axis) [39], this joint also has 2 movements of translation. The predominant motion in the abduction and forward flexion of the scapula is the upward rotation (Hill, 2008)[39]. It has also been reported that around 120° of humeral abduction, the scapula has an upward rotation of 50°, posterior tilting 30°, and external rotation 24° [39].

Acromioclavicular Joint, (ACJ) is the articulation that anchors the clavicle to the scapula. This joint has four degrees of freedom and is dynamically stabilized by the deltoid and trapezius muscles. The ACJ articulation is surrounded by a synovial fluid [119]. The ACJ is surrounded by a capsule, restricting the rotation motion during elevation to around 20°. Other constraints are the clavicular ligaments which restrain rotation when the clavicle is depressed. The medial and lateral movements are restrained by the costoclavicular ligaments (anterior and posterior) [39]. Ludewig (2009) highlights that the first movement of this articulation includes the upward rotation and posterior tilt of the scapula in relation to the clavicle [120].

The Sternoclavicular Joint (SCJ) is a synovial joint that is formed by the clavicle (at its medial end), the manubrium (which has a notch in the clavicle side that works in the joint), and the first rib cartilage [113, 118]. This joint is the only one that really links with the axial skeleton via the clavicle. This joint is involved in all movements of the shoulder.

Ludewig states that the first movement of the SCJ in any plane (except in extension) is arm elevation (30°) and the retraction of the clavicle (around 15°) at the SCJ, and a slight elevation (less than 10°, in people without injuries or illness). This happens when the humerus is elevated in any plane (Ludewig, refers to Sahara) [120]. Hill suggests that sternoclavicular motion has a range between 30 to 35° in upward elevation, 35° in the anterior/posterior direction (approximately), and 44 to 50° in axial rotation [39].

Brox comments that if the shoulder is abducted by less than 40°, the bottom part of the joint capsule restricts the external rotation and helps to prevent forward dislocation [20]. The humeral head is stabilized by the rotator cuff (horizontal resultant force, the deltoid

muscle also has a 90° force resultant in the direction of the force). When the shoulder is in its natural position, 90° of shoulder abduction is possible without moving the scapula. However, the scapular moves there is active participation in the abduction within 80° to 140° according to Brox [20].

As the Subacromial joint lies over the rotator cuff and below the clavicle, Acromion, and the coracoacromial ligament; it is considered a synovial structure [50].

3.3 Biomechanics of the Shoulder

Biomechanics is the tool that allows people to develop a full range of studies regarding the mobility, statics and the behaviour of living entities, taking its basics from mechanics, and helping to make comparisons of the human body with mechanisms.

3.4 Human Planes

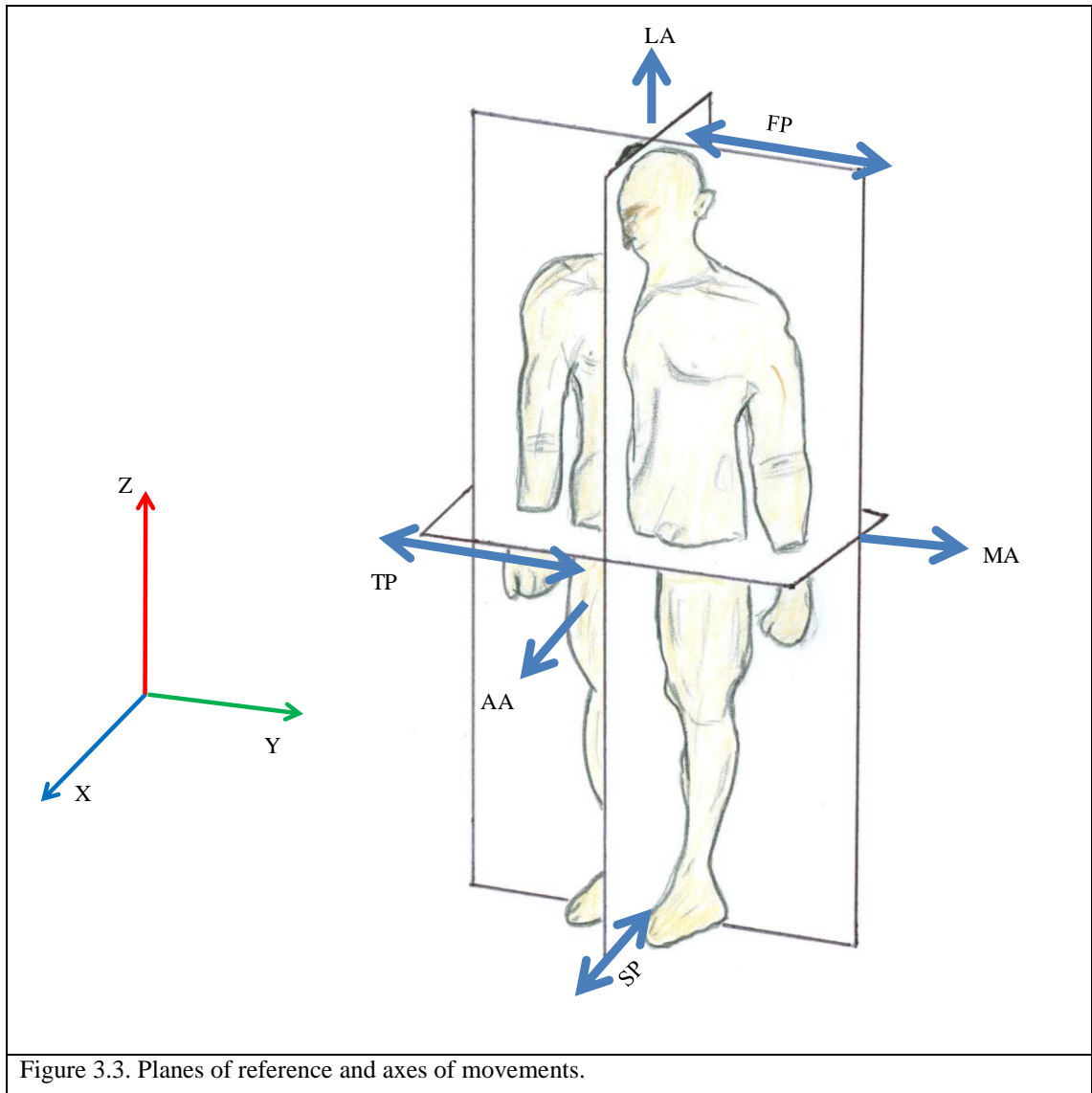
In order to describe the quantity, quality and the region of the movement, the body is divided into planes (reference system).

Three imaginary planes exist as a reference to describe movement. These planes are located at a 90 degree angle to each other, and the planes intersect at the mass centre (the mass centre is the place where all the planes converge). The main planes (or cardinal planes) are the following, Figure 3.3 [121]:

Sagittal Plane (SP) - the SP is the plane that cuts the body into two parts, dividing the body into the right and left parts. This plane runs along the “Z” axis, Figure 3.3. The SP can be observed as a plane that starts from the bottom (inferior area) to the top (superior area) or cranial area. The movement in this plane occurs through a Mediolateral Axis (MA) [121], Figure 3.3.

Frontal Plane (or coronal, FP) - the FP plane divides the body into the front and rear (back) parts (with motion occurring in the Anterior/posterior Axis, AA). The movements are quite unusual in this plane in comparison with the movements occurring in other planes. This plane starts at one side of the shoulder and ends on the opposite side of the other shoulder, through the “X” axis [121], Figure 3.3.

Transverse Plane (horizontal plane, TP) - the TP separates the body into two parts, the upper (head part) and lower part (lower limb part). The movements that occur in this plane occur in the Longitudinal Axis (LA) which is similar to the “Y” axis [121] shown in Figure 3.3.



In order to aid in the plane description and the orientation of segments of the body, special nomenclature is used, with reference to Figure 3.4:

Medial – anywhere near or in the middle of the body (SP).

Lateral - any place located far from the midline created by the sagittal plane.

Proximal - any position or body segment close to the sagittal plane of the body.

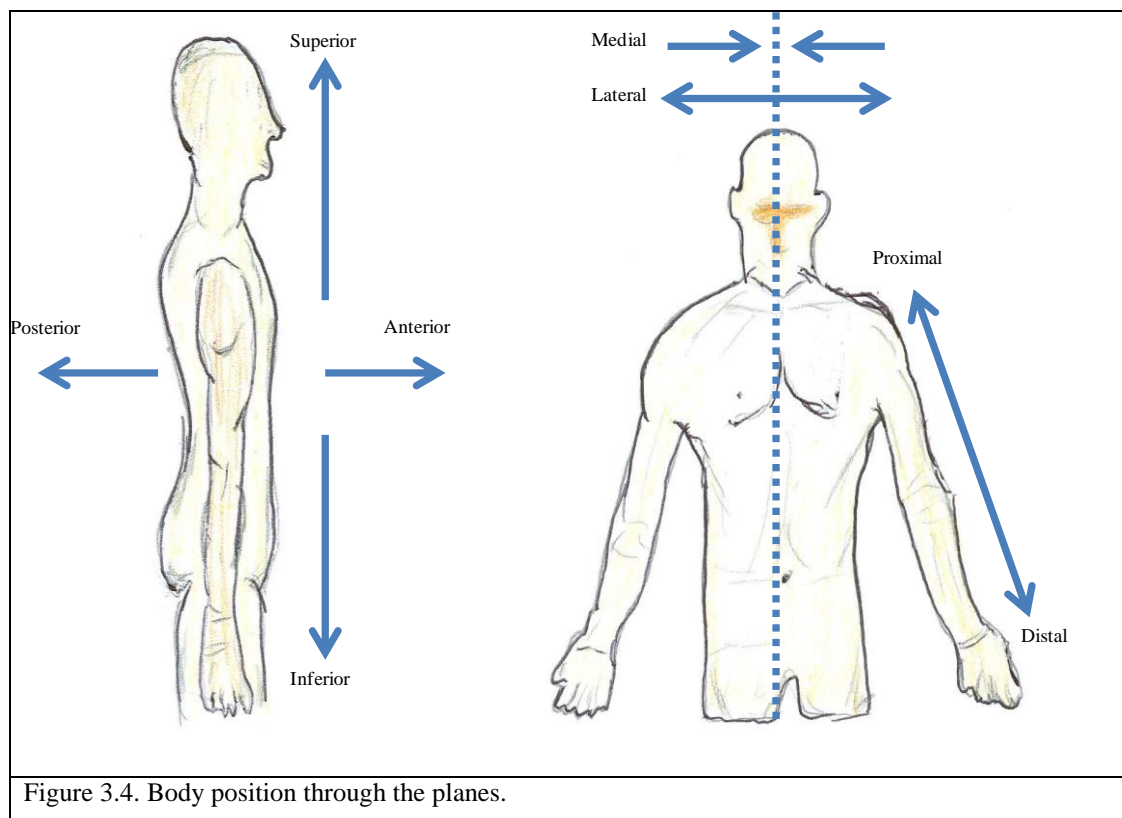
Distal - any position located far away from the sagittal plane of the body.

Superior - any position above a reference point (top), situated towards the vertex of the head.

Inferior - any position below a reference point (bottom), below or toward the feet.

Anterior (ventral surface) - this area is located in the frontal area of the body; the person must be looking at the chest to identify this place.

Posterior (Dorsal surface) - this area is located at the back of the human body; the person needs be looking at the buttocks to see this area.



3.5 Shoulder Dynamics

The shoulder joint is a diarthrosis joint (synovial joint) that can be compared with a ball and socket joint. As a result of this shape the shoulder has a wide range of motion (six degrees of freedom). The glenohumeral joint is not the only articulation working in the shoulder complex, there are others, but these are considered to be non real joints. For example the Acromioclavicular joint and Sternoclavicular joint are considered as non

real joint, and they are more restricted than the glenohumeral joint [39]. All the elements working in the shoulder complex help to keep the balance and to develop a wide range of movement. The shoulder range of motion is restricted by the static and dynamic stabilizers, that help to keep the humerus and the glenoid tied and centred.

Tözeren mentioned that movements that rotate around an axis and pass by the centre of a joint are known as “angular movements” [122], these movements are (Figure 3.5):

Flexion - occurs when two entities (bones) which lie together (side by side) get closer (trying to touch each other). It is considered a rotation movement, and occurs parallel to the sagittal plane [122].

Extension - is the opposing rotation movement to flexion, like flexion, it occurs in the sagittal plane [122].

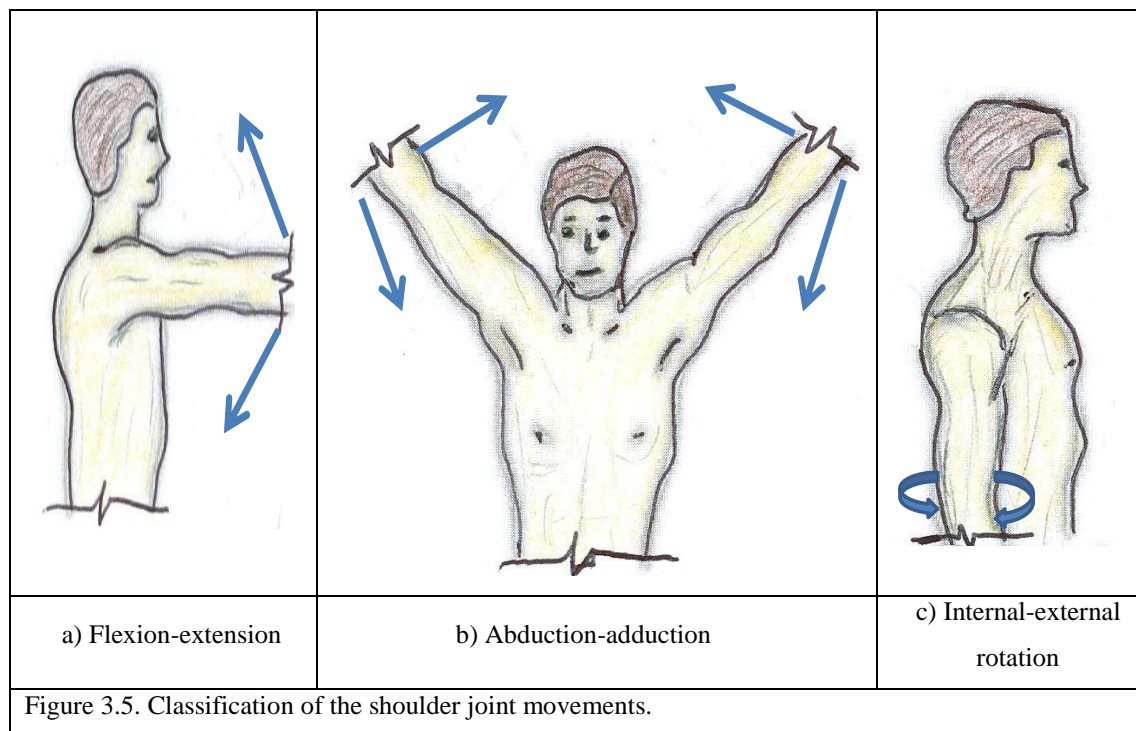
Abduction - is the movement of the extremities in the frontal plane. This is a distance motion from the longitudinal axis, which is a motion of the extremities to the back. [122].

Adduction - is the contrary movement to abduction, but it works in the same plane. This movement brings the extremities closer to the sagittal plane (mid line) [122].

If the extension movement exceeds the natural and relaxed anatomical position, this motion is known as hyperextension, while for the adduction motion it is known as hyperadduction. A study undertaken on a manual wheelchair shows that flexion, internal rotation and abduction involve the highest moments found in the shoulder joint [12].

Circumduction - is when the arm moves in a continuous angular position in a closed loop with a reference point over the sagittal plane, Figure 3.3, [122].

Humeral motion from its natural relaxed position to any position (plane) far from the thorax (humerothoracic motion) is known as elevation of the arm, while the coordinated motion between the scapula, humerus and thorax is known as the scapulohumerothoracic rhythm (SHT) [39].

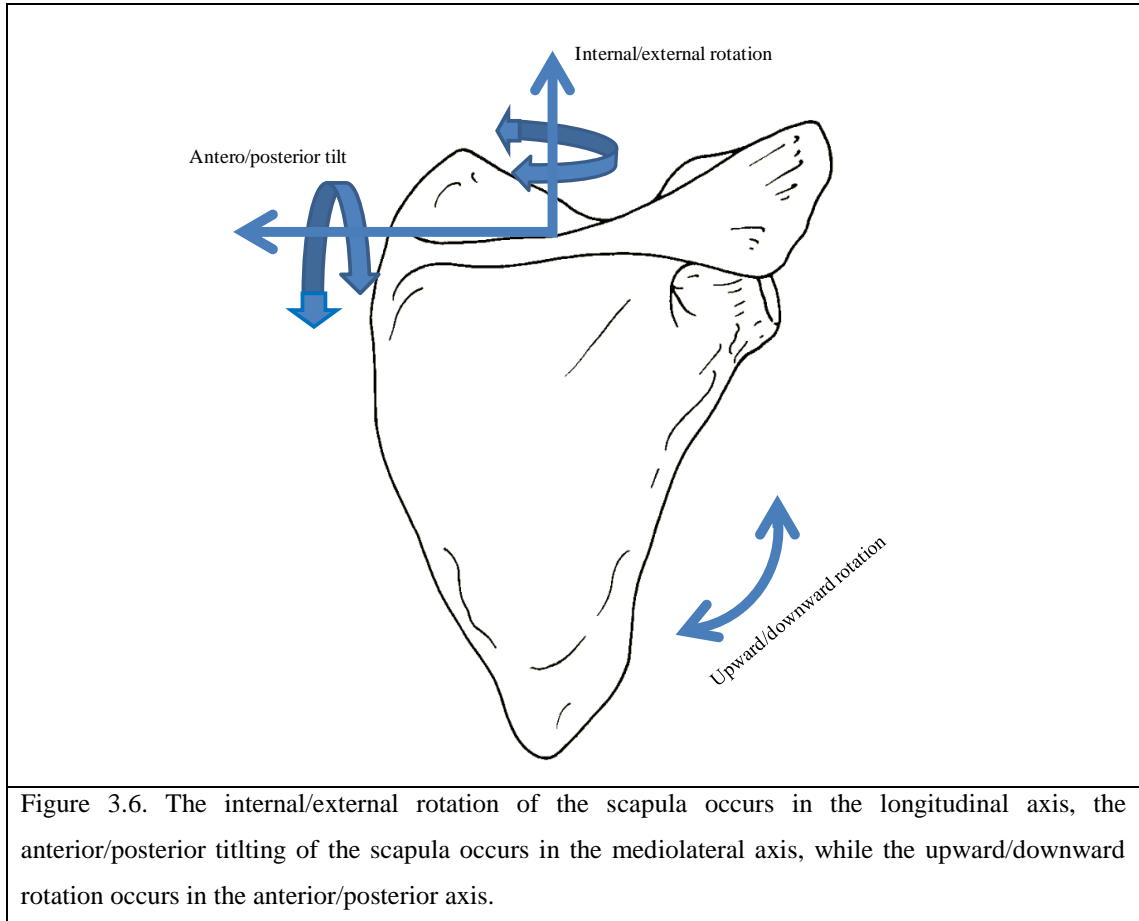


The relative motion between the glenohumeral components to generate the movements described above are produced by the static and dynamic stabilizers of the shoulder, which define the different patterns of motion of the shoulder joint; one clear example of this is represented by the Codman's paradox [123-124]. The Codman's paradox states how different rotations at the glenohumeral joint modifies the arm orientation, highlighting how important is to understand the rotations of the shoulder components, what is generating them, and their behaviour as well as the influence that those rotations could have in normal/pathological shoulder.

3.5.1 Scapular Rotations

Rotation of the scapula can be defined using different nomenclature, however the rotation of the scapula is usually described by the axis of occurrence. When the scapula rotates around a vertical axis it is known as internal/external rotation of the scapula. When the scapular bone rotates in a medial lateral axis it is known as scapular tilting (similar to a flexion-extension motion) and when it rotates in a frontal axis it is known as winging (similar to an abduction-adduction motion), Figure 3.6. This nomenclature is usually employed when the motion of the scapula is with respect to the thorax [125] provided that the planes of occurrence are well determined (global reference frame).

Researchers [106] have measured the rotation of the scapula in dynamic humeral elevations in the scapular plane. It was found while the arm is being elevated the scapula externally rotates around 24° , rotates upwardly 50° (mean value) and tilts posteriorly around 30° [106].




3.5.2 Glenohumeral Joint Orientations

The rotation of the GHJ and its components can be described using different combinations of Euler angles [125]. The International Society of Biomechanics (ISB) propose a number of bony land marks and joint coordinate systems to standardise shoulder rotations [126]. However, latent risks include the error generated by the technique being used, matrix multiplication or Gimbal Lock error due to the wide range of motion of the shoulder [127]. An alternative to avoid these problems is the use of inertial sensors. Inertial measurement units (IMU) integrate gyroscopes, accelerometers and magnetometers. These components of the inertial sensor help to determine a coordinate frame and the angular velocity by using the magnetic field, to specify the orientation of a rigid body in space in a three dimensional analysis.

The rotation of a unit vector ('**x**') with respect to a global reference frame (X, Y, Z) with origin at "Or"; Figure 3.7, can be defined as the components of a unit vector '**x**' divided by the length of the vector (1, in this case), as a result the cosine of the angle made with the component of a unit vector (x, y, z) of a local frame and the coordinate axes of the global reference frame are obtained [128]. The Direction Cosine Matrix (DCM) can be presented in the form of a rotation matrix (R), Eq 3.1.

Axes of the local system
(columns)



$$[R] = \begin{bmatrix} \cos X_x & \cos X_y & \cos X_z \\ \cos Y_x & \cos Y_y & \cos Y_z \\ \cos Z_x & \cos Z_y & \cos Z_z \end{bmatrix} \left. \vphantom{\begin{bmatrix} \cos X_x & \cos X_y & \cos X_z \\ \cos Y_x & \cos Y_y & \cos Y_z \\ \cos Z_x & \cos Z_y & \cos Z_z \end{bmatrix}} \right\} \begin{array}{l} \text{Axes of the global system} \\ \text{(rows)} \end{array}$$

Eq 3.1

For example, the $\cos Y_x$ represents the cosine of the angle with respect to the second axis of the global reference frame (Y) and the vector '**x**' (Figure 3.7) [128].

Usually to represent orientations in the 3D space, finite rotations are used to describe the motion of the object under study. The most common methods to represent those rotations are using Euler's angles and Quaternion's.

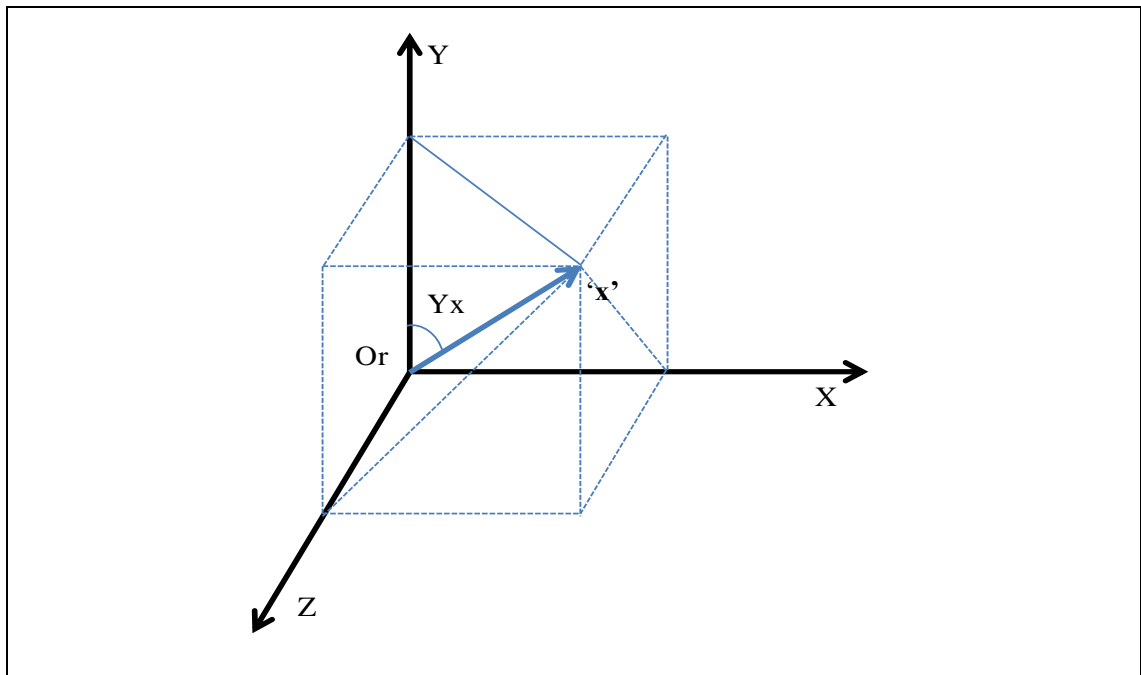


Figure 3.7. 'x' unit vector components in a global reference frame generated by the origin (Or) and the global axis X, Y and Z.

The Euler's method is based on three consecutive rotations; those rotations must be performed in a specific order, which are not commutative. There are twelve different sequences of rotations or Euler's conventions. One disadvantage of Euler's angle is that commonly it suffers from Gimbal's lock and requires significant matrix multiplications. Euler's angle can be represented by a 3 x 3 matrix similar to the cosine matrix. So a representative matrix for each axis of rotation is obtained and an Euler's sequence will be described as $[R_E] = [R_1] [R_2] [R_3]$, where the R_1 , R_2 and R_3 are 3 x 3 matrixes representing the sequential rotations [128]. For a ZYX Euler sequence the rotational matrix will be described as in Eq 3.2.

$$[R_E] = [R_z][R_y][R_x] \quad \text{Eq 3.2}$$

Where R_z , R_y and R_x represent a rotation for each axis and can be expressed as in Eq 3.3.

$$[R_E] = \begin{bmatrix} \cos \alpha & -\sin \alpha & 0 \\ \sin \alpha & \cos \alpha & 0 \\ 0 & 0 & 1 \end{bmatrix} \begin{bmatrix} \cos \beta & 0 & \sin \beta \\ 0 & 1 & 0 \\ -\sin \beta & 0 & \cos \beta \end{bmatrix} \begin{bmatrix} 1 & 0 & 0 \\ 0 & \cos \gamma & -\sin \gamma \\ 0 & \sin \gamma & \cos \gamma \end{bmatrix} \quad \text{Eq 3.3}$$

Where α , β and γ represent the angles for each rotation in Rz, Ry and Rx matrixes. Finally after performing the matrix multiplication the RE matrix is obtained as shown in Eq 3.4.

$$[R_E] = \begin{bmatrix} \cos \alpha \cos \beta & \cos \alpha \sin \beta \sin \gamma - \sin \alpha \cos \gamma & \cos \alpha \sin \beta \cos \gamma + \sin \alpha \sin \gamma \\ \sin \alpha \cos \beta & \sin \alpha \sin \beta \sin \gamma + \cos \alpha \cos \gamma & \sin \alpha \sin \beta \cos \gamma - \cos \alpha \sin \gamma \\ -\sin \beta & \cos \beta \sin \gamma & \cos \beta \cos \gamma \end{bmatrix} \quad \text{Eq 3.4}$$

The resultant matrix in Eq 3.4. is basically the representation of the direction cosines between axes of different reference frames but expressed as a function of Euler's angles. The direction cosine angle for the gravitational acceleration components will be represented by the third column of the rotation matrix.

3.6 Research Approaches for Glenohumeral Joint Tracking

Tracking the orientation of the scapula is difficult because it is surrounded by soft tissue, is held mainly by muscles and has only one direct point of attachment to the thorax, which gives the scapula a non fixed centre of rotation [90]. The three dimensional tracking of the scapula, by means of non invasive methods, is difficult because of the soft tissues that wrap the scapula [30].

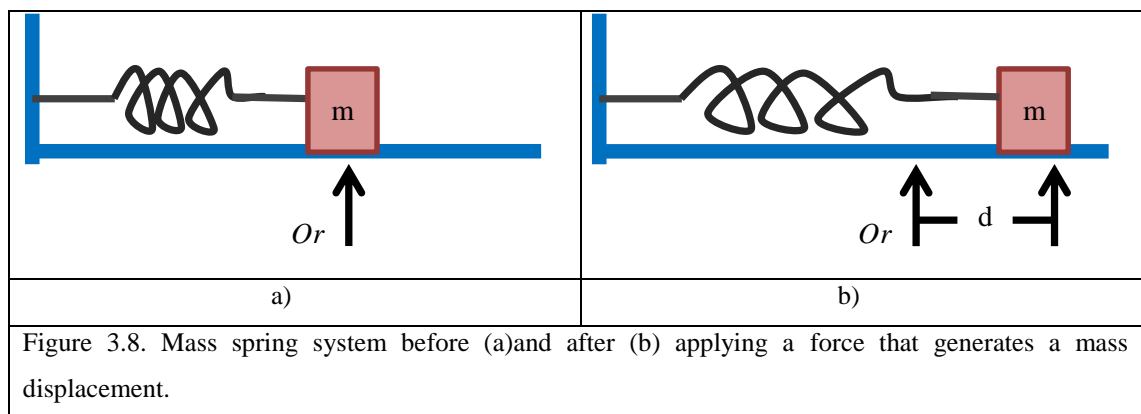
The work conducted by Godfrey *et al.* [121] and Dickerson [129-130] agree that biomechanical and kinesiology studies are necessary for good assessment of the shoulder motion, which will aid significantly in obtaining accurate representation of the shoulder motion and its relationship with various aspect of daily life [121]. This means that good, accurate information must be obtained to represent and assess shoulder behaviour. However, some studies state that measurement of GHJ motion, with non invasive methods using the skin, does not produce a sufficient level of accuracy for clinical practice [85]. This makes scapular tracking with non invasive methods a challenge.

One of the most common non invasive devices used to evaluate the glenohumeral joint tracking are electromagnetic and inertial sensors [30, 79, 84, 88, 92, 131], acromion markers clusters [87, 90] and locators (scapula locators, SL).

3.6.1 Electromagnetic and Inertial Sensors

Accelerometers are devices that measure the physical acceleration experienced by a body due to gravity. When an accelerometer is in a steady state, it will measure an acceleration of $g=9.81\text{m/s}^2$. Accelerometers are commonly used to measure tilt angles with respect to gravity (or vertical).

The easiest way to understand how an accelerometer works is by imaging a single axis spring mass system, where a mass 'm' is connected to a spring with a 'k' constant. The k constant is a function of the physical characteristic of the spring. If the system does not experience any acceleration, the mass of the system will stay in its original position Or , Figure 3.8. If the system experiences an acceleration 'a', the system's mass will be displaced a distance 'd' from its original position, Figure 3.8. Due to the nature of the system the motion of the mass system will be restricted by the spring. Bearing this in mind then by applying the concepts of Newton's second law of motion and Hooke's law it is possible to relate the mass and spring parameters to compute the amount of acceleration that is acting on the system to generate the mass displacement.



Newton's second law of motion states that if a mass is accelerated a force 'F' will be generated Eq 3.5, while Hooke's law states that within the elastic limits of a solid material, the deformation (strain) generated by a force (stress) is proportional to the force. If the elastic limits are not exceeded, the material will return to its original condition in terms of shape and size, as it was before the force was applied. Because the mass and spring system is connected, the spring will generate a force proportional to the force generating the displacement (d) but in the opposite direction. So it is possible to

relate Newton's second law and Hooke's law by Eq 3.6. By equating Eq 3.5 and Eq 3.6 it is possible to obtain the acceleration value, as presented in Eq 3.7.

$$F = m * a \quad \text{Eq 3.5}$$

$$F = k * x \quad \text{Eq 3.6}$$

$$a = \frac{k * x}{m} \quad \text{Eq 3.7}$$

Different types of accelerometer have been developed by researchers, which combine electrical and mechanical parts. It is possible to categorize these as mechanical (described above), solid state and silicon chips.

Solid-state accelerometers can be divided into vibratory, silicon, acoustic wave and quartz devices. This type of accelerometer uses small beams that bend when the acceleration is modified. Finally, it is possible to find Micro-electromechanical systems (MEMS) which are a combination of mechanical and solid state accelerometers. Accelerometers can be found in different configurations that allows acceleration measurement in one, two and three orthogonal axes. Tri-axial accelerometers have been used to assess the shoulder orientation, they are more accurate for predicting orientations than linear accelerometers [132-133].

Gyroscopes work on the principle of the conservation of angular momentum, and are useful for detecting rotational movement such as angular velocity (rad/s). By integrating angular velocity (ω , omega) it is possible to obtain the angle and the trajectory described by IMU. However, the angle and trajectory obtained by this means is prone to develop drift. Gyroscopes can be found in different designs such as laser gyroscopes (optical), vibrating mass gyroscopes (MEMS gyroscopes) and spinning rotor gyroscopes (mechanical).

The simplest mechanical gyroscope is a wheel that can spin; the wheel is mounted in a gimbaled structure which is capable of rotation in any orientation. Vibrating mass gyroscopes are smaller and cheaper than mechanical and optical gyroscopes, and work on the principle that when a mass is rotated, the mass experiences the Coriolis Effect, generating a vibration. The generated vibration is orthogonal to the original direction of

vibration, creating a deflection in the internal components, which is converted into the gyroscopes output.

Magnetometers measure the strength in a magnetic field as well as its direction. Magnetometers are influenced by the Earth's magnetic field, and are commonly used to calculate the heading of the device. Magnetometers are susceptible to magnetic materials close to them.

3.6.2 Locators and Clusters

Despite the fact that the scapula locator (SL) has the disadvantage of being restricted to quasi-static measurements [30, 81, 90, 131], it is still considered to be the “gold standard” to know the orientation of the scapula [90]. On the other hand whilst invasive techniques (implanted pins, [30, 80]) can be used under dynamic conditions, they require surgical treatment and anaesthesia and even these methods are prone to errors [80] or can be used only in a limited population.

3.6.3 Invasive Techniques to Track the Scapula

Invasive techniques are commonly considered as the best method to for comparing different techniques, devices or for validation [30, 90]. While imaging techniques such as Computer tomography scans (CT scan) [61], Magnetic resonance image (MRI) [83] or arthrography (MRA), X rays, fluoroscopic imaging [85] and ultrasonic methods [26] have been used to track the scapula, these methods can represent a potential hazard for the patient due to potentially long exposure times to radiation. Another limitation is that the glenohumeral joint has to be constrained to limited ranges of motion, or planes of elevation, when any of these techniques or devices is being used [79-81].

3.6.4 Glenohumeral Joint Tracking Quasi-static and Dynamic Conditions

The kinematics of the shoulder has been assessed under quasi-static conditions in order to explain the shoulder movement by utilising data from quasi-static test in conjunction with regression equations [81, 134], or under dynamic conditions [85, 100, 127].

The increase in the dynamic assessment of the shoulder can be explained by the fact that quasi-static assessment of the glenohumeral joint does not provide sufficient

information about the behaviour of the dynamic stabilizers of the shoulder. A good understanding of the muscles' role will aid in understanding shoulder pathologies and the influence of these on the kinematics of the joint.

In an attempt to match the quasi-static assessment of the GHJ to a dynamic assessment de Groot *et al.* [127] reported that velocity does not have an effect on shoulder motion, so the regression equations obtained from quasi-static measurements can be used for dynamically assessing the shoulder. Zhou *et al.* [100], also evaluated the upper limbs' motion at different velocities before arriving at the conclusion that their experimental work using electromagnetic sensors provides a good, reliable method for GHJ assessment at different velocities. These results suggest that velocity does not have a major effect on the shoulder kinematics, but it can affect the activation time of the shoulder muscles. These results as well as those reported by McClure *et al.* suggest a non-linearity behaviour in the shoulder components motion (scapula and humerus) when the humerus is elevated [81, 106, 134].

The use of the described tools in sections **3.6.1** to **3.6.3** allows the generation of regression type models. Quasi-static assessment of the shoulder using reflective markers placed over the skin were used to compare scapula kinematics under different loadings conditions for shoulder abduction in healthy volunteers, with a cubic polynomial proposed that used the humeral orientation as an input [97]. A linear equation was developed by Karduna *et al.* [30] to reduce the error generated in the upward rotation of the scapula under dynamic conditions by using wire magnetic tracking devices drilled to the bone; the proposed model was based on the assumption that the error is generated by the tissue artefact when the scapula is in motion; the input for the proposed model is the data from the scapula sensor placed directly over the skin. This type of invasive assessment has been taken as a base for validating techniques such as the locator-based methods; the proposed model was generated to correct the orientation in the main axis of rotation of the scapula. A linear regression model using the humerus as an input to correct the scapula orientation was developed by Lempereur *et al.* [94] and Matias *et al.* [2] by using optoelectronic/electromagnetic tracking systems and palpation techniques under quasi-static conditions. Palpation methods have been used [81, 135] to describe and quantify the source of variability in 3D shoulder motion, by using the humerus and initial conditions of the scapula and clavicle as inputs. Numerical evaluation based on

radiological processes to describe shoulder rhythm has also been used as well [134], the second order polynomial obtained uses the humerus location as an input. Shoulder component orientation has been described by using fifth order polynomials [135-136] and data from a wired electromagnetic tracking device. A linear model to describe shoulder rhythm based on thoracohumeral orientation by using static arm postures captured with reflective markers [137] has been developed too. Two types of regression models to predict the scapula orientation were developed using the humerus and the humerus plus individual factors such as anthropometry data, gender and age as predictors [138]. Both mathematical models developed were obtained by using a motion tracking system for different static humeral postures.

3.7 Healthy Shoulder Kinematics

A shoulder is considered to be healthy when the harmony and balance between the different shoulder joints is maintained, through any arm motion and with an absence of damage or neuromuscular problems.

3.7.1 Glenohumeral Joint Range of motion

The shoulder joint can achieve different actions due to its mobility through planes at different degrees. The normal range of motion of the glenohumeral joint through the different planes of motion can be described as follows [116, 139]:

To full abduction, palms up 180° (120° are provided by the joint and 60° by the rotation of the scapula).

- Flexion, 180°.
- Extension, 40°.
- Internal rotation, 55° approx.
- External rotation, 45° approx.

Fu comments that the shoulder joint motion ratio is: elevation (including the arm) 180°, rotation 150°, horizontal (sagittal) plane rotates to 170° [104, 115]. Similar results were presented by Van Der Helm for arm elevation and a ratio between 60° and 90° of endo/exo rotation (axial rotation, for the anatomical position) [104].

When the arm is abducted in the scapular plane, in the first 0° to 30° the lower mid portion of the scapula is used as a center of rotation, and from 60° and beyond the centre of rotation is moves towards the glenoid fossa, generating a large amount of motion of the inferior angle of the scapula [140].

The variability of the scapular centre of rotation generates a scapular twisting of 40° ±9° (external rotation of the scapula) and with external rotation of the humerus (after 90° of abduction) clearly indicates the synchronous motion of the humerus and the scapula [140]. Similar values have been reported for the abduction range of motion in the glenohumeral joint, around 64°-90°. By the time the joint reaches 90° the scapula has already rotated 25°-30°. It is important to comment that the closer the abduction motion is to the sagittal plane, the abduction motion is combined with forward flexion or backward extension [111]. The flexion-extension range presents values around 100°-150° with the larger values occurring in the flexion motion [111].

The combined range of motion of the entire shoulder is around 180° for forward flexion (120° in the glenohumeral joint and 60° in the clavicular joints).

3.8 Shoulder Stabilizers

The static and dynamic stabilizers of the shoulder work together to ensure the stability of the glenohumeral joint throughout a whole range of motion (RoM). The biomechanic equilibrium at the glenohumeral joint is maintained by the static and dynamic stabilizers which can be subdivided as shown in Table 3.1 [13, 141]:

Table 3.1. Shoulder Static and Dynamic stabilizers [13, 141].	
Stabilizers	Components
Static	<ul style="list-style-type: none"> • Bony anatomy • Negative intra-articular pressure • Glenoid labrum • Glenohumeral ligaments (along with the joint capsule) • Capsule
Dynamic	<ul style="list-style-type: none"> • Rotator cuff muscles • Other muscles surrounding the GHJ.

The static stabilizers can be summarised as being the geometry of the glenohumeral joint, the congruence between the scapula and humeral bone, the ligaments and the negative intra-articular pressure [59, 142]. The dynamic stabilization of the GHJ is generated basically by the strength, resistance and flexibility of the shoulder muscles that are coordinated by neuromuscular control and adequate proprioceptive input [142-143].

The other static stabilizers of the shoulder, apart from the bones, are:

Ligaments are soft tissue structures that connect bones with other bones. Eight ligaments have been identified in the shoulder area; these ligaments help to maintain the shoulder balance [48, 59]:

- 1) Inferior glenohumeral ligament (connects the humerus to the glenoid, stabilises and holds the shoulder).
- 2) Middle glenohumeral ligament (connects the humerus to the glenoid, stabilises and holds the shoulder).
- 3) Superior glenohumeral ligament (connects the humerus to the glenoid, stabilises and holds the shoulder).
- 4) Transverse humeral ligament.
- 5) Coraco-humeral ligament.
- 6) Coraco-acromial ligament.
- 7) Acromioclavicular ligament.
- 8) Coracoclavicular ligament.

Tendons are strong and flexible bands that connect the muscles with the bones. Their main function is to transmit the power generated by the muscles to the bones.

On the other hand the dynamic stabilizers of the GHJ are the muscles. There are 30 muscles in the shoulder muscle complex that work directly or indirectly in the joint [11]. In terms of stabilization and motion of the shoulder, some muscles have a direct impact in the shoulder joint. However, there are others muscles that help the shoulder bones, to hold their position or to increase the range of motion of the articulation. Also, some of them work in any of the non real articulations (platysma, sternocleidomastoid, and scalene). The muscles could be classified by the motion performed, see Table 3.2.

Table 3.2. Muscle actions [37, 108-109, 144-145].

MUSCLE ACTION						
MUSCLES INVOLVE	Retraction of the pectoral girdle	Protracting the pectoral girdle	Elevation of the pectoral girdle	Lateral rotation of the pectoral girdle	Medial rotation of the pectoral girdle	
	<ul style="list-style-type: none"> • Rhomboid minor • Rhomboid major • Trapezius 	<ul style="list-style-type: none"> • Serratus anterior • Pectoralis minor 	<ul style="list-style-type: none"> • Trapezius • Levator scapulae 	<ul style="list-style-type: none"> • Trapezius • Serratus anterior 	<ul style="list-style-type: none"> • Rhomboid major • Rhomboid minor • Pectoralis minor • Levator scapulae 	
	MUSCLE ACTION					
	Stabilizers of the clavicle	Abduction of the arm	Flexion of the arm	Extension of the arm	Medial rotation of the arm	Lateral rotation of the arm
	<ul style="list-style-type: none"> • Subclavius 	<ul style="list-style-type: none"> • Supraspinatus • Deltoid 	<ul style="list-style-type: none"> • Pectoralis major • Deltoid (anterior fibres) • Biceps brachii (long head) • Coracobrachialis 	<ul style="list-style-type: none"> • Latissimus dorsi • Teres major • Pectoralis major • Deltoid (posterior fibres) • Triceps brachii (long head) 	<ul style="list-style-type: none"> • Subscapularis • Teres major • Latissimus dorsi • Pectoralis major • Deltoid (anterior fibres) 	<ul style="list-style-type: none"> • Teres minor • Infraspinatus • Deltoid (posterior fibres)

3.8.1 Important Shoulder Muscle Mechanics

The muscle contraction starts with a stimulus coming from the central nervous system, which activates a flow of calcium resulting in the contraction of the muscle sarcomeres; if there is a limited quantity of calcium flowing to the sarcomeres in the musculoskeletal system this can be detrimental to the time reaction of the muscle [146].

In order to understand how the muscle contractions work, it is possible to compare the contraction mechanism of muscles with a man pulling ropes (one rope in each arm), gives a clear idea of the muscle contraction. Imagine the Myosin as the man in Figure 3.9, and the Actin as the ropes, when the ropes are pulled by the man towards the chest, this generates the bones' motion (muscle contraction).

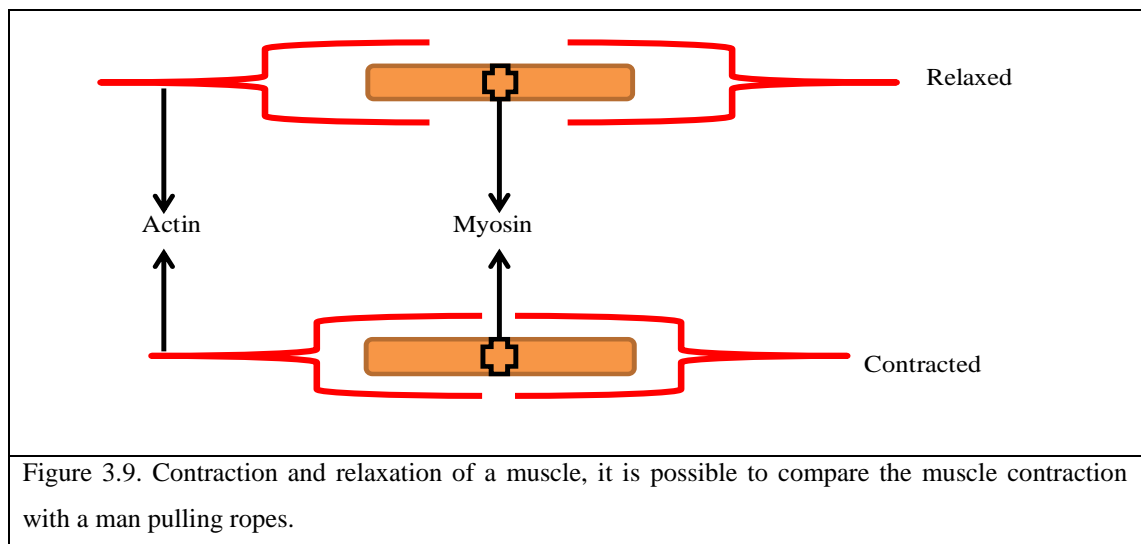


Figure 3.9. Contraction and relaxation of a muscle, it is possible to compare the muscle contraction with a man pulling ropes.

The process of contraction and relaxation of a muscle can change over time, depending on the muscle involved, and its muscular fibres, [147-149]:

Another factor that has influences the mechanism of muscle contraction is the alignment of the muscle fibres. The muscle fibres can adopt different orientations and geometric shapes. These configurations give the muscle a range of motion in certain degrees, and the quantity of force that a muscle can generate [109]:

The alignment, the type of muscle fibres and the neuromuscular activation sequence influence the activities performed by the muscles.

Muscle can adopt several shapes such as triangular, quadrangular, rhomboid, or fusiform. The configuration adopted by the muscles allows them to perform the following actions:

Motion - the muscle moves an entity, and one muscle makes the first movement (prime mover). The muscle fibres have equal or almost equal lines of action to the direction of the move intended by the articulation.

Opposition - when a muscle action runs contrary to the muscle that made the first move (prime mover).

Anchor- Stabilizes the source of the muscle that makes the first move.

Synergist - The synergist muscle helps the joints, keeping them safe from unwanted movements.

A good understanding of this function will aid in to determining the muscles involved in the muscle patterning (instability in the shoulder joint) [150].

The rotator cuff muscle for example plays an active participation in shoulder stability and in positioning the glenohumeral joint. It contains four muscles. Located near to the centre of the joint rotation, these muscles are able to support glenohumeral shear stresses. Each muscle has an independent function, but they work together as a whole entity in the stabilization of the GHJ (in the middle and final ranges of motion, rhythm). The humeral head is kept deep, and in a central position inside the glenoid fossa by these muscles. The rotator cuff muscles are [50-51]:

Supraspinatus, this muscle abducts, compresses, and externally rotates the arm. It has actively participates in the stabilization of the shoulder joint.

Infraspinatus, this muscle helps in the external rotation of the arm, stabilizes and fortifies the joint capsule.

Teres minor, it helps in the external rotation of the arm, and stabilizes the shoulder joint.

The rotator cuff muscles aids to keep the glenoid fossa and the humeral head centred and compressed, in a mechanism known as concavity-compression and helps in the stabilization of the glenohumeral joint components [151]. In the presence of abnormal concavity-pressure, normal displacing forces could generate subluxation or dislocation[152].

Subscapularis, this muscle abducts, and internally rotates the arm. It also stabilizes the shoulder.

Escamilla cites that the infraspinatus and subscapularis muscles (important muscles in scapular plane abduction, scaption), have the capacity to generate forces or three times greater than the Supraspinatus muscle, Table 3.3 [51].

The stability of the shoulder can be altered by the large torques acting on the shoulder produced by the Latissimus dorsi, Serratus anterior, Pectoralis major and the Deltoid (major muscles). In a certain position, it is possible to explain these torques by the cross sectional anatomy and the large distance from the rotation centre of the joint (which can generate instability) [13, 45].

Serratus anterior muscle: keeps the medial angle against the chest wall (the trapezius helps in synchrony with the movements made by the glenohumeral joint, and in the rotation and elevation of the scapula). The serratus anterior participates in all movements while the humerus is elevated (rotation, posterior tilt and external rotation); in the same way, it stabilizes the medial border and the inferior angle of the scapula [13, 51].

Deltoid muscle: the deltoid muscle helps in the abduction of the arm (90°). It contributes little in flexion and works in adduction (external rotation) [50].

Pectoralis major muscle: this muscle has the action of flexes/extends, rotates and abduct the humerus [37, 50].

Biceps brachii muscle: This is considered the principal flexor muscle of the arm and forearm (it acts in supination as a secondary action). The short head of this muscle participates in adduction, while the long head participates in internal rotation and abduction (the biceps brachii muscle stabilizes the shoulder joint) [50].

The two rhomboids and the levator scapulae work as retractors of the scapula (adductors), downward rotators and elevators.

Table 3.3. Muscle contribution to the abduction torque, measured by Escamilla [51].		
Muscle	Percent (%)	Forces (Newton's)
Middle deltoid	35-65	434
Subscapularis	30	283
Supraspinatus	25	117
Infraspinatus	10	205
Anterior deltoid	2	323

The forces generated by these muscles are not only used in abducting the shoulder, they also stabilize the glenohumeral joint, and neutralize contrary action, or antagonist motion. In the same way, the superior directed deltoid force produced by the deltoids (at lower abduction angles) is neutralized by an elevated force value generated by the rotator cuff muscles [51].

CHAPTER IV: METHODOLOGY FOR TRACKING THE SCAPULA

4.1 Introduction

In the previous chapters established that accurate tracking of the scapula under dynamic conditions is essential in order to be able to correctly identify, assess, and understand what the muscles are doing in the different kinds of shoulder instability. By knowing where the bones and how they move it is possible to estimate what the muscles are doing. A better understanding of shoulder kinematics and kinetics will help clinicians and therapists in the diagnosis and treatment of shoulder pathologies such as muscle patterning instability. To estimate scapula orientation accurately under dynamic conditions, particularly at high humeral elevations, using a non-invasive skin-based technique, then it is necessary to reduce the error generated by the soft tissue around the scapula. Current non invasive methods may be inaccurate at high humeral elevations because of the effect of the soft tissue artefact.

In this section a methodology is presented to reduce the soft tissue error by utilising scapula orientation data recorded using a scapula locator under quasi-static conditions to formulate a regression-type equation which can then applied to correct surface sensor measurements obtained under dynamic conditions.

The methodology presented in this section enables the human scapula to be tracked under dynamic conditions to scapula locator level accuracy using a non-invasive skin based technique.

4.2 Methodology

In order to obtain a mathematical expression to enable tracking of scapula orientation under dynamic conditions as if the scapula is being tracking with a scapula locator (considered as the best non invasive device to track the scapula), a methodology has been developed which utilises three inertial sensors. One is placed directly on the skin over the scapula, the second is located on the humerus and the third one is attached to a scapula locator device (SL). The methodology consists of two stages.

In the first stage: the subject is required to position the arm in a series of consecutive quasi-static humeral elevations. In each quasi-static position, data from three sensors

(scapula sensor, humeral sensor and SL sensor) are recorded for a period of time. The data are used to describe the scapula orientation under quasi-static conditions and to obtain a representative polynomial, by fitting the data from the humerus and the scapula IMUs to the locator data. The data recorded by the locator are less prone to be affected by the soft tissues surrounding the scapula, and so it is considered to provide a more accurate representation of scapula location.

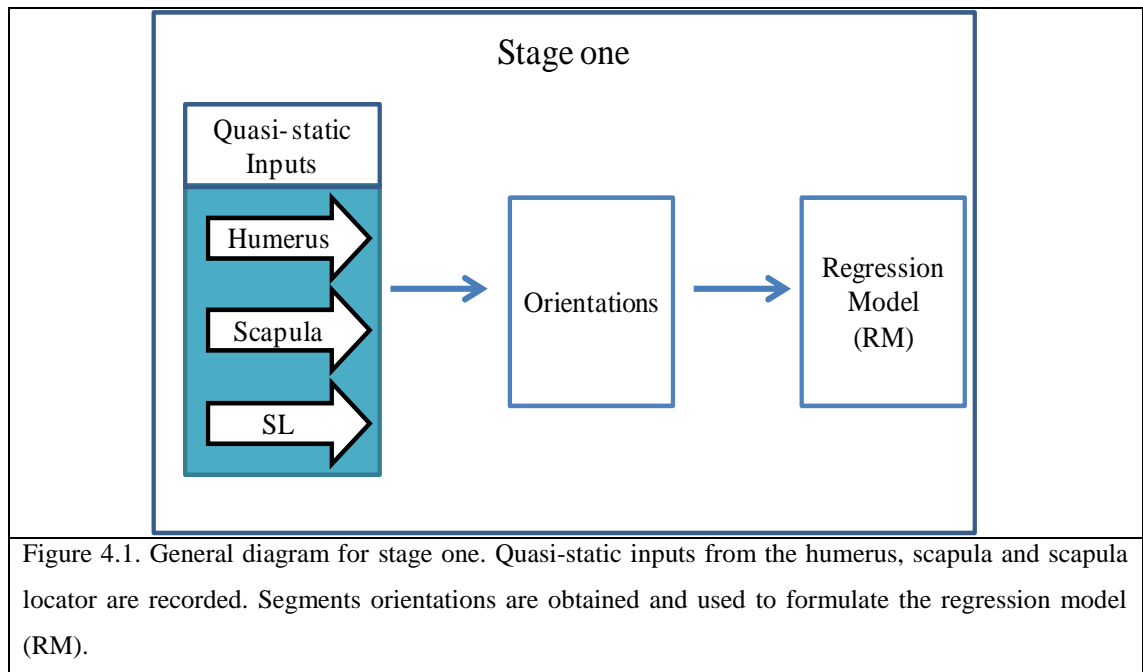
For the second stage: dynamic movements of the glenohumeral joint are performed by the subject. The locator is discarded at this stage (as it can only be used under quasi-static conditions) and data are recorded from the humeral and scapula IMUs during the dynamic movements. If the output from the scapula IMU sensor alone was used directly for the scapula location at this point, it would be subject to the error generated as a result of the soft tissue artefact. However, the data from the scapula and humeral sensors data are not employed directly but used as input to the representative polynomial in order to correct for the soft tissue artefact and provide an improved estimate of scapular orientation.

4.2.1 Stage One: Quasi-static Motion

(i) In this first stage a regression equation is developed utilising data from quasi-static motion trials (Figure 4.1). The method requires initial quasi-static tests to be undertaken for each subject using three IMUs and a SL for consecutive humeral orientations, enabling scapular and humeral orientation to be estimated. The multiple quasi-static humeral orientations need to be recorded at approximately equal intervals between an initial position (which for the clinical case will be the fundamental position) and an ending position, which represented the extreme of movement but did not force or exceed the natural range of motion of the shoulder joint; this is considered as one cycle. Two complete cycles are considered for each trial performed in the clinical settings to avoid fatigue in the participants.

(ii) Two IMUs are used to estimate the orientation of the scapula (S-IMU) and the humerus (H-IMU) during the quasi-static trials. These measurements are considered approximate as they are affected by factors including the soft tissue artefact, especially for high humeral elevations. A third IMU is placed over one arm of the scapula locator

(SL-IMU) in order to track the orientation of the scapula as determined by the SL. It is assumed here that the location provided by the SL is the more accurate compared with other non-invasive methods.



(iii) Data from the three IMUs are obtained from quasi-static trials performed by subjects. The SL-IMU data are obtained by palpation and relocation of the scapula locator over the scapula bony landmarks for the different H-IMU and S-IMU orientations recorded. The soft tissue artefact generated in a quasi-static position is expected to be lower than the one that is generated when the shoulder components are in motion. Quasi-static measurements allow palpation of scapula bony landmarks and location of the SL over them. It is recommended that the observer/researcher follows the consecutive motion of the scapula with his/her fingers as the humeral motion occurs to facilitate the bony landmark identification. The data obtained from the humerus (H-IMU) and scapula (S-IMU) IMUs are then related to the data obtained from the scapula locator IMU (SL-IMU) enabling a regression-type equation to be developed.

Developing a Regression Type Equation

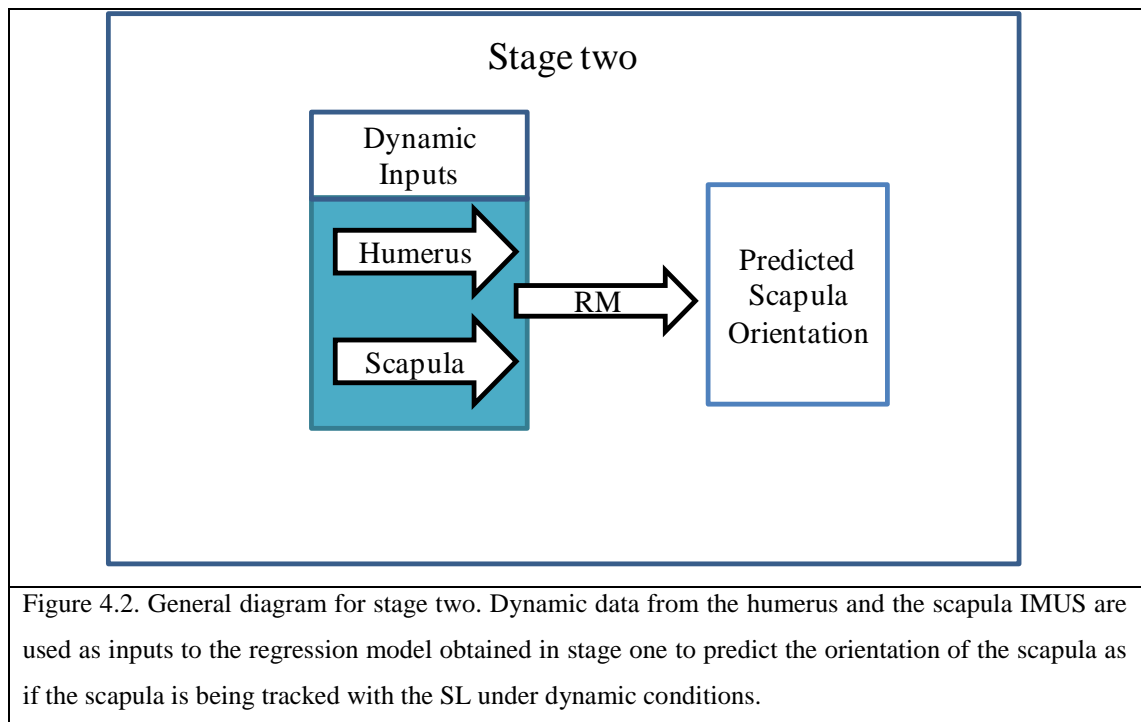
Once the sensor orientations were obtained (stage one) the S-IMU and H-IMU orientation data were fitted to the SL-Measured orientation using a least squares methodology. The least squares methodology can be used to determine the best fitting straight line through a series of data. The best fit is determined by specifying an equation to describe a model or a series of data that minimises the sum of the square distance between the real data and the fitted data from the proposed model.

4.2.2 Stage two: Dynamic Motion

The dynamic motion trials consist of recording the continuous motion of the shoulder components while the subject undertakes the same humeral movement patterns as are employed in stage one. The dynamic motion trials also help to assess the effect of the dynamic stabilizers of the glenohumeral joint. To assess the dynamic motion the following steps are undertaken:

(iv) The regression equation determined in stage one are used in conjunction with data obtained from the humerus (H-IMU) and scapula (S-IMU) IMUs to estimate scapular orientation during dynamic conditions without the need to use the SL, as shown in Figure 4.2.

In the clinical setting, patients undertake the trials as described in stage one, steps (i)-(iii). Having used the data from two different quasi-static trials to obtain the regression equation, the SL together with the SL-IMU are discarded and dynamic tests are undertaken using the humerus (H-IMU) and scapula (S-IMU) IMUs only.



The data from these two IMUs (scapula and humerus) are used in the regression equation obtained from the initial quasi-static trials enabling scapula orientation to be estimated during dynamic tests as though it was measured with the SL, highlighting the advantages of this technique. Employing the two sensors (scapula and humerus) in the methodology allows the observer/researcher to assess how the scapula is behaving both as an individual entity and as a part of the glenohumeral joint, as a function of both scapular orientation and humeral orientation. The methodology described has the advantage that it enables the human scapula to be tracked under dynamic conditions without resorting to invasive techniques, such as the use of bone pins. This methodology will allow researchers to assess shoulder patterns movements and shoulder pathologies such as muscle patterning instability.

4.3 Methodology Validation

Before applying the methodology presented to evaluate human scapula orientation, the technique was applied in a test performed on a wooden structure, to avoid distortions in the magnetic field. The aim was to prove that the proposed methodology worked and to understand the sensor behaviour for different initial orientations.

4.3.1 Materials and Methods

Two different scenarios a) and b) (see Figure 4.3) were considered in order to validate the proposed methodology in controlled conditions with orthogonal movement planes, without the influence of soft tissues, and with an environment clear of magnetic influence. These tests were also helpful to understand sensor behaviour before applying the methodology with human participants.

Scenario a) aims to validate the proposed methodology step by step, from the quasi-static measurements to the dynamic measurements, steps (i)-(iv).

It is widely acknowledged that observation of the actual motion of the scapula is confused by the soft tissues that surround it. Measuring the sensor orientation under quasi-static conditions in a controlled environment (i.e. no magnetic disturbance), without the presence of the tissue artefact will help in understanding the effect that the soft tissue can have on the sensors output for different initial orientations, see Figure 4.3.

Scenario b) aims to investigate the effect of different initial sensors orientation in order to see the behaviour respect to the gravitational acceleration vector.

A series of consecutive quasi-static positions was recorded for both scenarios a) and b) using three inertial unit sensors (IMUs). For scenario a) dynamic measurements were also performed. Dynamic measurements were discarded for scenario b) because of the difficulty of coordinating the motion of the sensors; this scenario therefore focuses on the orientation results under quasi-static conditions.

The sensors were placed on the surfaces of a wooden structure as if they were simulating measuring the humerus (virtual humerus, H-IMU) and scapula (virtual scapula, S-IMU) location. The third IMU was placed on a custom made scapula locator (SL-IMU). The wooden structure had orthogonal surfaces that were used in the test; for scenario a) the horizontal or top surface of the structure was used while for scenario b) several different surfaces were used.

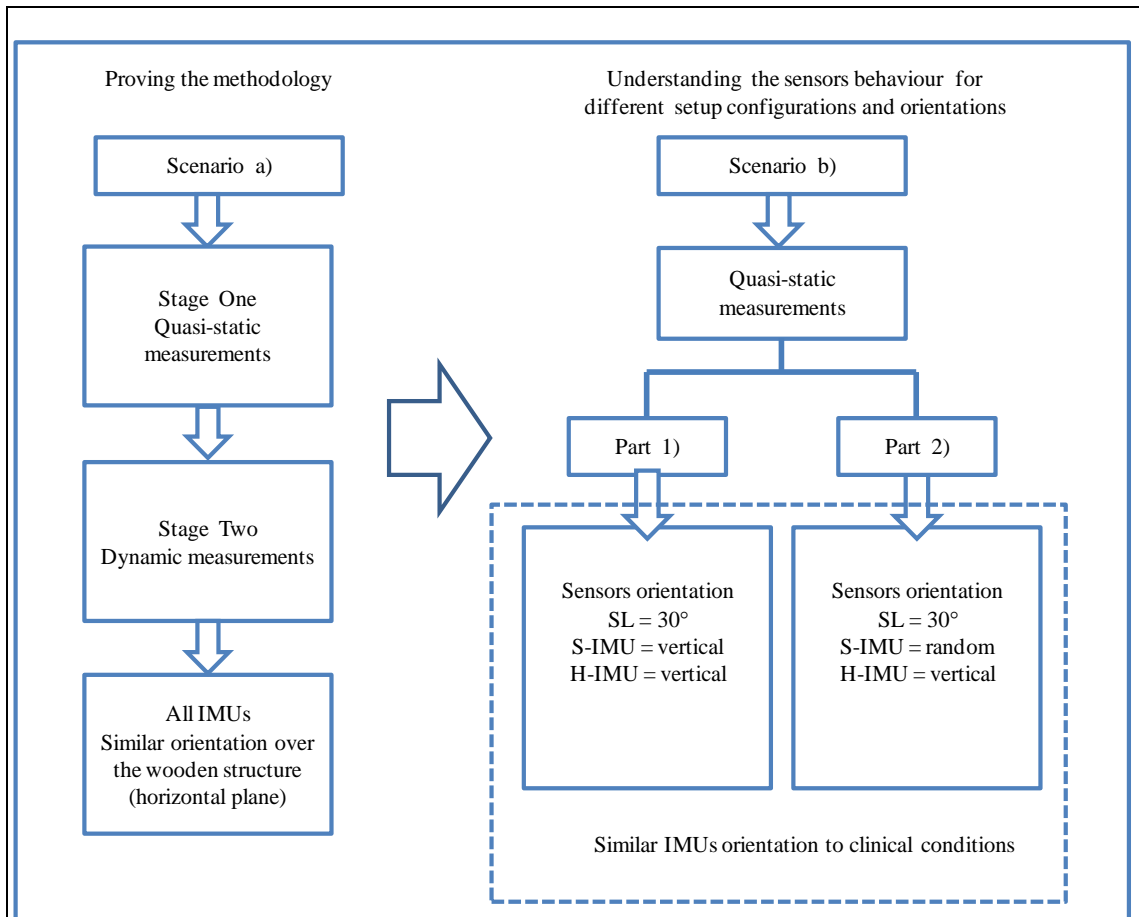


Figure 4.3. Flow diagram for scenario a) and b). Scenario a) aims to prove that the proposed methodology works. Scenario b) aims to understand the sensor behavior for different initial orientations.

4.3.2 Calibration

Three MTw sensors (Xsens Technologies, Enschede Netherlands) were used; each sensor has a mass of 27g, with a dynamic accuracy of 2° reported by the manufacturer [153]. One of the sensors used to measure the scapula orientation was positioned on a custom made Scapula Locator (SL-IMU) built from acrylic sheet with plastic pins to avoid distortion in the magnetic field around the IMUs (Figure 4.4). The angle as well as the distance between the pins can be adjusted by loosening and tightening the plastic pins. The sensor (SL-IMU) was held in place on the Scapula Locator using double-sided tape.

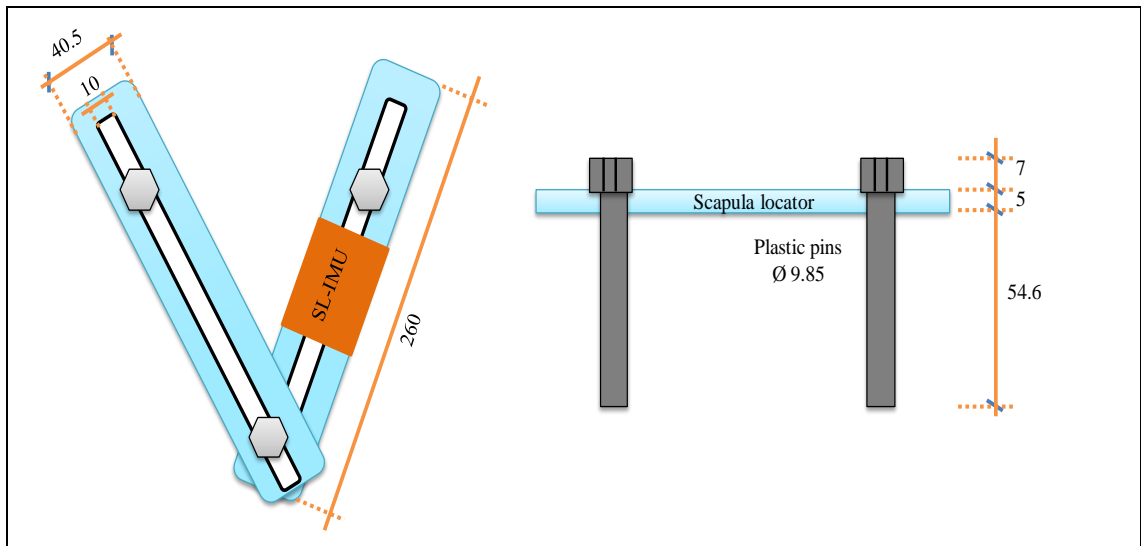


Figure 4.4. Acrylic custom made scapula locator (SL) with plastic pins. Dimensions are in mm. The SL-IMU was placed on one of the arms of the SL. The arm is aligned with the lateral border of the scapula.

Before data collection started a heading reset was applied to all IMUs on a flat surface, which aligned the global Z axis (Figure 4.5) and **the gravitational acceleration** [153].

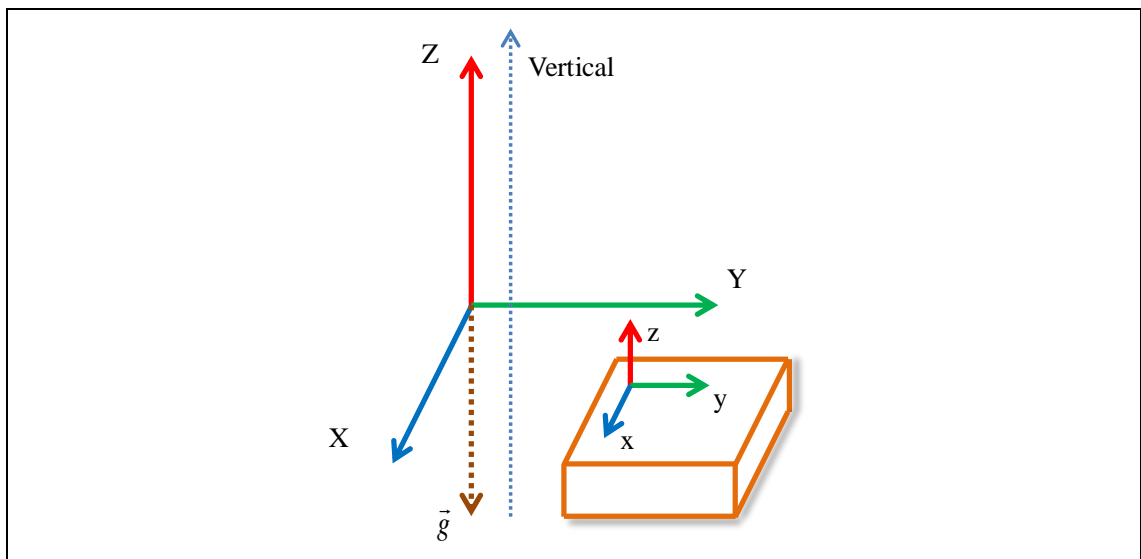


Figure 4.5. IMU calibration on a flat surface, which aligned the global Z axis and the gravitational acceleration vector where X, Y and Z are the vector components of \vec{g} and local axes of the sensor are represented by x, y and z.

4.3.3 Experimental Test Setup

Data from the three sensors were recorded for a series of consecutive quasi-static positions in both scenarios a) and b). The positions were recorded at variable and known intervals measured by goniometers.

Scenario a) Setup: For scenario a) two goniometers were placed over the top flat surface of the wooden structure. The goniometers were aligned on a flat surface of the structure to avoid motion in different axes, see Figure 4.6. The goniometers were employed to simulate the scapula and the humerus motion. The scapula (S-IMU) IMU was attached to one of the arms of the goniometer used to simulate scapula motion and the humerus (H-IMU) IMU was attached to one of the arms of the goniometer used to simulate humeral motion using double-sided tape. The SL sensor (SL-IMU) was aligned with the goniometer used to simulate the scapula motion (S-IMU) throughout the whole series of quasi-static tests, with the two pins of the SL aligned with the goniometer arm carrying the S-IMU. All the IMUs had a similar alignment as shown by Figure 4.6, with the local z-axis pointing upward.

The wooden structure was then rotated 20° around the local 'y' axis of the sensors to facilitate coordinated motion of the sensors placed over the goniometers in dynamic tests and to keep the local z-axis of the sensor on a known angle with respect to vertical.

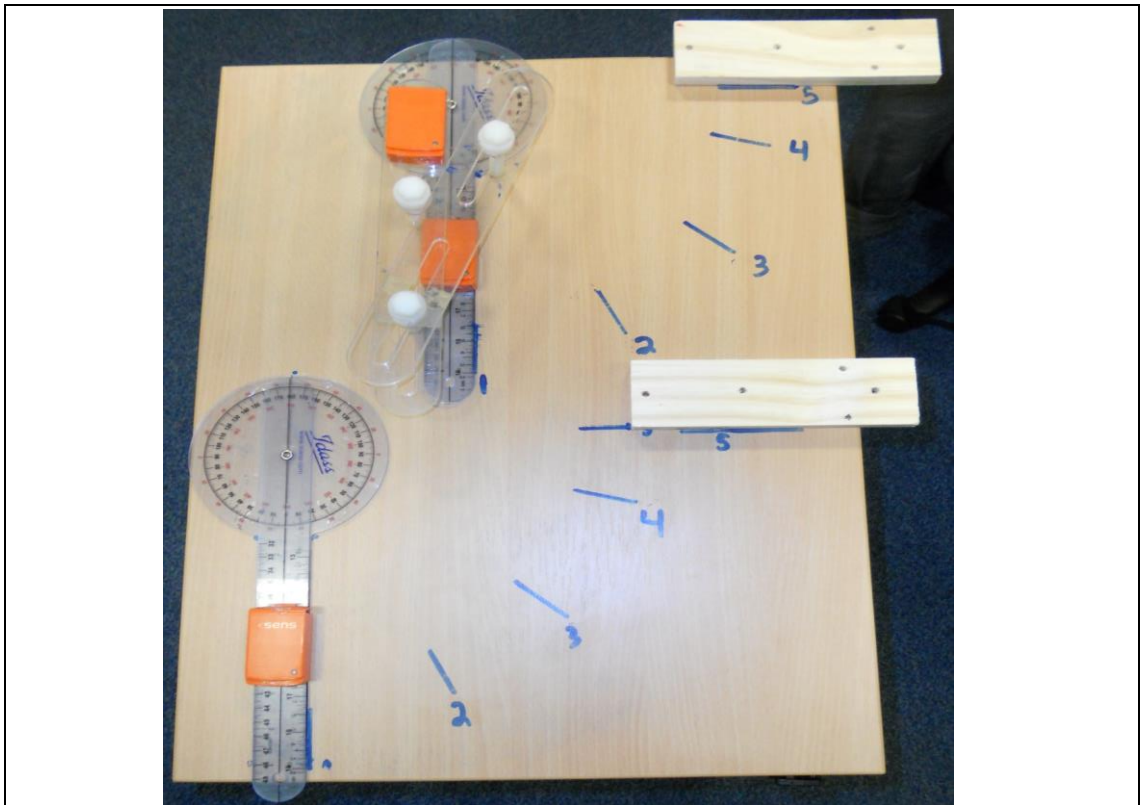


Figure 4.6. Wooden structure test used in scenario a) to simulate the humerus, the scapula and the SL. Quasi-static and dynamic measurements were performed on the wooden structure. Two extra pieces of wood were used to constrain the motion for the dynamic conditions and to help synchronise the dynamic motion.

Scenario b) Setup: For Part 1), the local x-axis of the S-IMU and H-IMU sensors were aligned with the gravitational accelerator vector on two surfaces of the wooden structure, in a similar way to that in human test (Figure 4.7). For the SL, the sensor was placed at a known angle with respect to the vertical (around 30°) over one arm of the SL, see Figure 4.7. The SL arm is simulating the x local axis of the sensor alignment with the lateral border of the scapula.

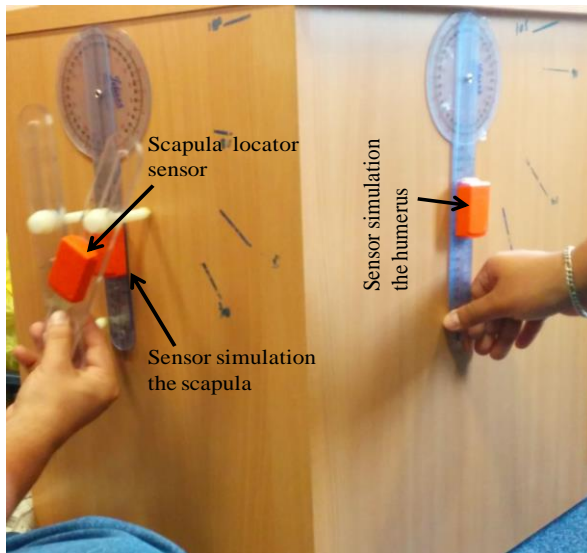


Figure 4.7. Scenario a), sensors placement over the wooden structure, with similar conditions to those in potential clinical trials. The local x-axes of the sensors simulating the scapula and humerus are close to vertical.

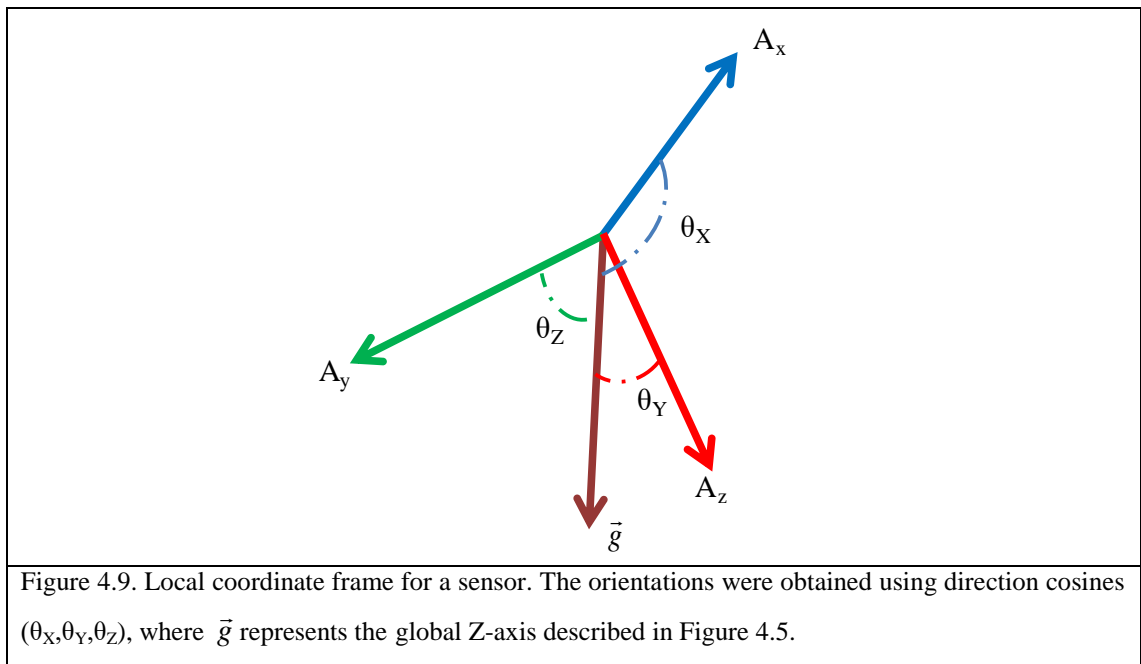
For Part 2) of Scenario b), the humerus and SL sensors were setup as they were for Part 1), while the scapula sensor was placed in different orientations and planes on a curved surface as shown in Figure 4.8. Each position was marked with double sided tape on the curved surface.



Figure 4.8. Scenario b), SL and humeral sensors placed on the wooden structure, simulating conditions similar to those found in clinical conditions. The scapula-sensor was placed in different orientations on a curved surface simulating the effect that the shoulder muscles can have on the shoulder.

4.3.4 Data Collection

The SL, humerus and scapula sensors measured orientation in three local axes (x, y, z) and the relative orientation between pairs of sensors (scapula-humerus-SL) was calculated using the gravitational acceleration vector (\vec{g}) as a global reference, see Figure 4.9. In terms of data recorded, each quasi-static position was held for a period of three to six second for all the tests performed, and then an average orientation was calculated for each quasi-static position.



4.3.5 Data Processing

The IMU orientation was calculated using a custom Matlab program (Mathworks, Version 7.10.0.499, R2010a). The orientation of the sensors was calculated from the direction cosines between the local axes and the global Z-axis as defined by \vec{g} .

4.3.6 Obtaining the Orientations

Stage One: the Direction Cosines

Three local acceleration components A_x, A_y, A_z were obtained as outputs from the inertial sensors, these outputs were used to obtain the magnitude of the gravitational acceleration vector ' \vec{g} ' as shown in Eq 4.1.

$$\vec{g} = \sqrt{A_x^2 + A_y^2 + A_z^2} \quad \text{Eq 4.1}$$

Where: A_x , A_y and A_z are the gravitational acceleration components of (\vec{g}) from each sensor under quasi-static conditions.

If three gravitational acceleration components are known (A_x , A_y , A_z), the direction cosine of the angle with respect to the vertical can be obtained by dividing the acceleration components by ' \vec{g} ' as shown in Eq 4.2. The \vec{g} value is obtained in Eq 4.1 for each quasi-static position.

$$\begin{aligned} \theta_x &= \cos^{-1} \frac{A_x}{\sqrt{A_x^2 + A_y^2 + A_z^2}} \\ \theta_y &= \cos^{-1} \frac{A_y}{\sqrt{A_x^2 + A_y^2 + A_z^2}} \\ \theta_z &= \cos^{-1} \frac{A_z}{\sqrt{A_x^2 + A_y^2 + A_z^2}} \end{aligned} \quad \text{Eq 4.2}$$

The direction cosine angle can be visualized and obtained by applying simple trigonometry in Figure 4.9, where the norm of the three acceleration components represents the vertical gravitational acceleration vector.

If the local A_z acceleration component is completely vertical the z-axis acceleration magnitude, as Figure 4.5 shows, will be equal $|g|$.

The local acceleration vectors provide the tilt of the xy, yz, and xz local planes in relation to the vertical (Figure 4.5), which defines the orientation of the sensor with respect to gravity (vertical and the global Z-axis).

Once the orientations were obtained, the scapula and humeral orientation were fitted to the SL orientation using a best fit polynomial derived from the data from the first two cycles of the quasi-static test as is shown in Figure 4.1. The mean coefficients calculated from the two cycles of the quasi static test were used in the regression equation to predict the scapula orientation in dynamic tests (Figure 4.2) using the relative orientation of the humerus and the IMU sensor placed directly over the scapula.

Stage Two: Dynamic Conditions

For stage two the dynamic orientation of the sensor was calculated using the regression equation obtained in stage one, as section 4.2.1 describes.

c) The dynamic orientation of the sensor was achieved by first evaluating the three local components of the angular velocity (ω_x , ω_y , ω_z) in the regression equation obtained on stage one of the protocol; this represents the tilt of the local planes in relation to the vertical or gravity, see Figure 4.9.

d) The three local components of the angular velocity (ω_x , ω_y , ω_z) and their quaternion representation were obtained as outputs from the inertial sensors. For stage two these local angular velocities were rotated into the global reference frame (calibration frame, see Figure 4.5) by applying a quaternion rotation [154].

A quaternion (q) may be interpreted as a four term of real numbers, Eq 4.3.

$$q = (q_0, q_1, q_2, q_3) \quad \text{Eq 4.3}$$

Where: q_0 , q_1 , q_2 and q_3 are scalars.

The complex conjugate of a quaternion (q^*) can be calculated by multiplying the last three terms of a quaternion by minus one.

$$q^* = (q_0, -q_1, -q_2, -q_3) \quad \text{Eq 4.4}$$

A quaternion (q_{GL}) represents the rotation from the local reference frame to the global reference frame.

$$q_{GL} = (q_0, q_1, q_2, q_3) \quad \text{Eq 4.5}$$

Hence, if a vector \mathbf{P} must be rotated from the local to the global reference frame and the relevant quaternion is known it may be rotated by applying a quaternion rotation:

$$P_G = q_{GL} * P_L * q_{GL}^* \quad \text{Eq 4.6}$$

Before the angular velocity vector is rotated into the global frame (quaternion rotation), the measured angular velocity magnitudes are substituted and evaluated using the polynomial obtained for each axis (stage 1, see Figure 4.2).

4.4 Results Scenario a): Stage One Quasi-static Orientations

The results of the quasi-static tests undertaken in stage one for scenario a), are presented in Figure 4.10.

The sensor orientation data of Figure 4.10 represent the average of two sets of quasi-static data considered for this test. The orientations are presented in degrees in the three global axes, θ_X , θ_Y and θ_Z , at virtual points throughout the quasi-static cycle of movement of the sensors simulating that of the shoulder joint components, Figure 4.10. These measurements correspond to the measurements recorded by the H-IMU, S-IMU and SL-IMU sensors.

The quasi-static orientation results of Figure 4.10 represent the angle between an axis and a plane, due to the configuration used for scenario a) (see Figure 4.3), which was quite similar to the calibration configuration used in Figure 4.5, the difference being the 20° tilt angle of the wooden structure after calibration. The 20° tilt with respect to the vertical can be observed in θ_Z , for the three sensors. For θ_X it can be seen that the component angle is close to 70° in the first data recorded which agrees with the 20° of misalignment in the initial position generated by the researcher ($90^\circ - 70^\circ = 20^\circ$), with a variation around 15° in the earliest stages of the humerus elevation. Finally for θ_Y , orthogonality is maintained with a similar variation to θ_X as the humerus sensor reached its maximum amplitude.

The small variations of less than 15° in the three axes (see Figure 4.3), were attributable to the flexibility of the goniometer arms in the different positions measured. However the local z axis kept its orientation of $17^\circ \pm 3^\circ$ with the global Z-axis throughout the whole test, which was similar to the initial conditions of the wooden structure test, highlighting the dependence of this axis on the remaining two axes (θ_X and θ_Y).

With few changes in the axis orientation with respect to the vertical, the next step was to assess the rotation of the sensors in each axis in terms of the angular velocity.

To assess the motion of the virtual joint in the wooden structure test it was necessary to coordinate the motion of the scapula (S-IMU) and the humerus (H-IMU) sensors which required a training period. The coordination motion consisted of moving the goniometers to a pre-determined position (Figure 4.6) in one second and returning both sensors to their initial also in one second. It was expected that the main rotation would occur in the local 'z' and global 'Z' axes, with small variation in the remaining two axes, as the quasi-static results in Figure 4.10 suggest.

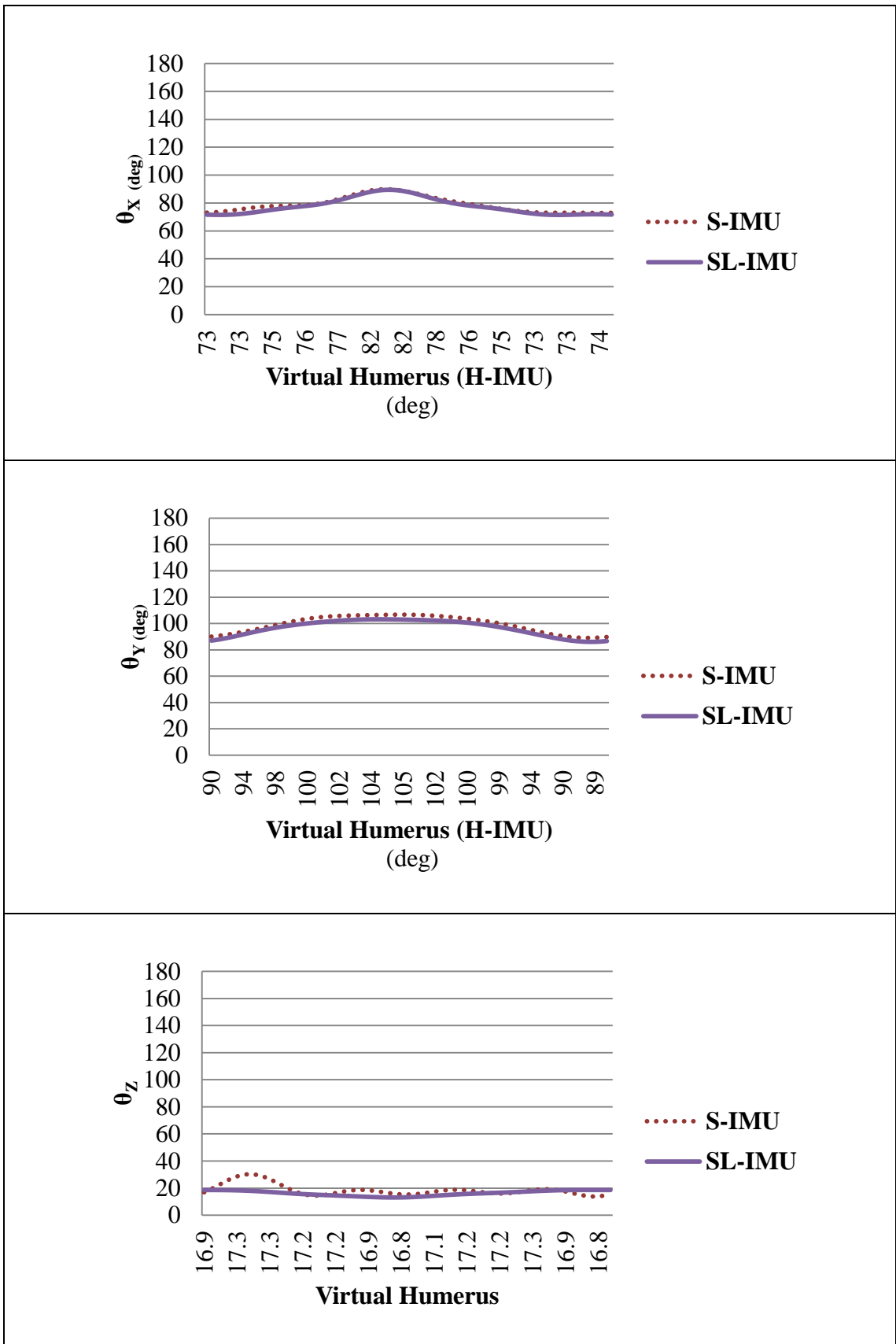


Figure 4.10. Orientations in the global axes (θ_x , θ_y and θ_z) for different quasi-static conditions, measured by the IMUs positioned on the humerus (H-IMU), scapula (S-IMU) and Scapular locator (SL-IMU).

The orientation obtained from the quasi-static measurements was used to obtain the representative regression equation for each axis as shown in Table 4.1. Here, the H and S terms of the best fit polynomials (Table 4.1) represent the angular velocity measured by the humeral and scapular sensor gyroscopes, $a_1...a_n$ represent the best fit coefficients obtained from the quasi-static tests and finally $SL_{\theta_x, \theta_y, \theta_z}$ represents the scapula orientation as if it was measured with the scapular locator device, for each axis.

Table 4.1. Best fit coefficients for the three axes of the wood drawer test.		
Table 4.1 a), Best fit coefficients for the X axis orientation (radians) for the virtual humerus and scapula of Trials 1 and 2 for the wooden drawer.		
Equation	$SL_{\theta_x}=a_1H+a_2S$	
Coefficients	a_1	a_2
Trial 1	0.1256	0.8603
Trial 2	-0.0926	1.0775
Average	0.0169	0.9689
Table 4.1 b). Best fit coefficients for the Y axis orientation (radians) for the virtual humerus and scapula of Trials 1 and 2 for the wooden drawer.		
Equation	$SL_{\theta_y}=a_1H+a_2S$	
Coefficients	a_1	a_2
Trial 1	0.4369	0.5434
Trial 2	0.0391	0.9291
Average	0.2380	0.7363
Table 4.1 c). Best fit coefficients for the Z axis orientation (radians) for the virtual humerus and scapula of Trials 1 and 2 for the wooden drawer.		
Equation	$SL_{\theta_z}=a_1H+a_2S$	
Coefficients	a_1	a_2
Trial 1	0.8358	0.0988
Trial 2	-1.0110	1.9462
Average	-0.0876	1.0225

4.5 Results Scenario a): Stage Two Dynamic Motion

For parts c) and d) (see, Dynamic conditions in section 4.3.6) a second order, zero phase lag, Butterworth filter with a cut-off frequency of 2.0 Hz (determined by using the power spectrum density; PSD) was applied to reduce noise in the angular velocity output signal from the humeral and scapular sensors. After filtering, the signals were split into the number of repetitions performed and then each individual repetition was integrated to obtain orientation.

The regression equation obtained in stage one (Table 4.1) was used to predict scapular position under dynamic conditions. The gyroscopes measure the angular velocity in three local axes in the dynamic test; the local angular velocities values were feed to the regression equation (Table 4.1). After the angular velocities were evaluated in the obtained polynomial to reduce the error generated by the soft tissue artefact, the new corrected angular velocities were integrated to obtain the orientations with respect to the vertical, see Figure 4.11.

Figure 4.11 shows the orientation results obtained as described in section 4.3.6 point c) at points throughout the dynamic cycle. The results represent the scapula orientation measurements (Measured, Figure 4.11) with respect to the vertical under dynamic conditions, and the predicted scapula orientation (Predicted, Figure 4.11) under dynamic conditions obtained by applying the regression equation developed from quasi-static measurements (first stage). The results are similar to the quasi-static results obtained in Figure 4.10 in terms of little variation in the three local rotation axes in the measured results, which may be attributed to the absence of soft tissues. For the dynamic tests, the change in orientation, and therefore, the difference between the predicted and measured values of θ_X and θ_Y in Figure 4.11 was less than 1° . Upon inspection of Figure 4.11 it can be seen that the predicted data are in good agreement with the measured data for both θ_X and θ_Y . The results presented in Figure 4.11 also agree with the measurements performed with the mechanical goniometer see Figure 4.6.

In contrast, the change in θ_Z (Figure 4.11) was significantly greater than for θ_X and θ_Y , having a maximum value of around 90° , indicating that this is the axis about which the main rotation occurs, which is in agreement with the condition shown in Figure 4.6. Predicted and measured data values are also in good agreement for this axis, with the maximum difference being around 5° .

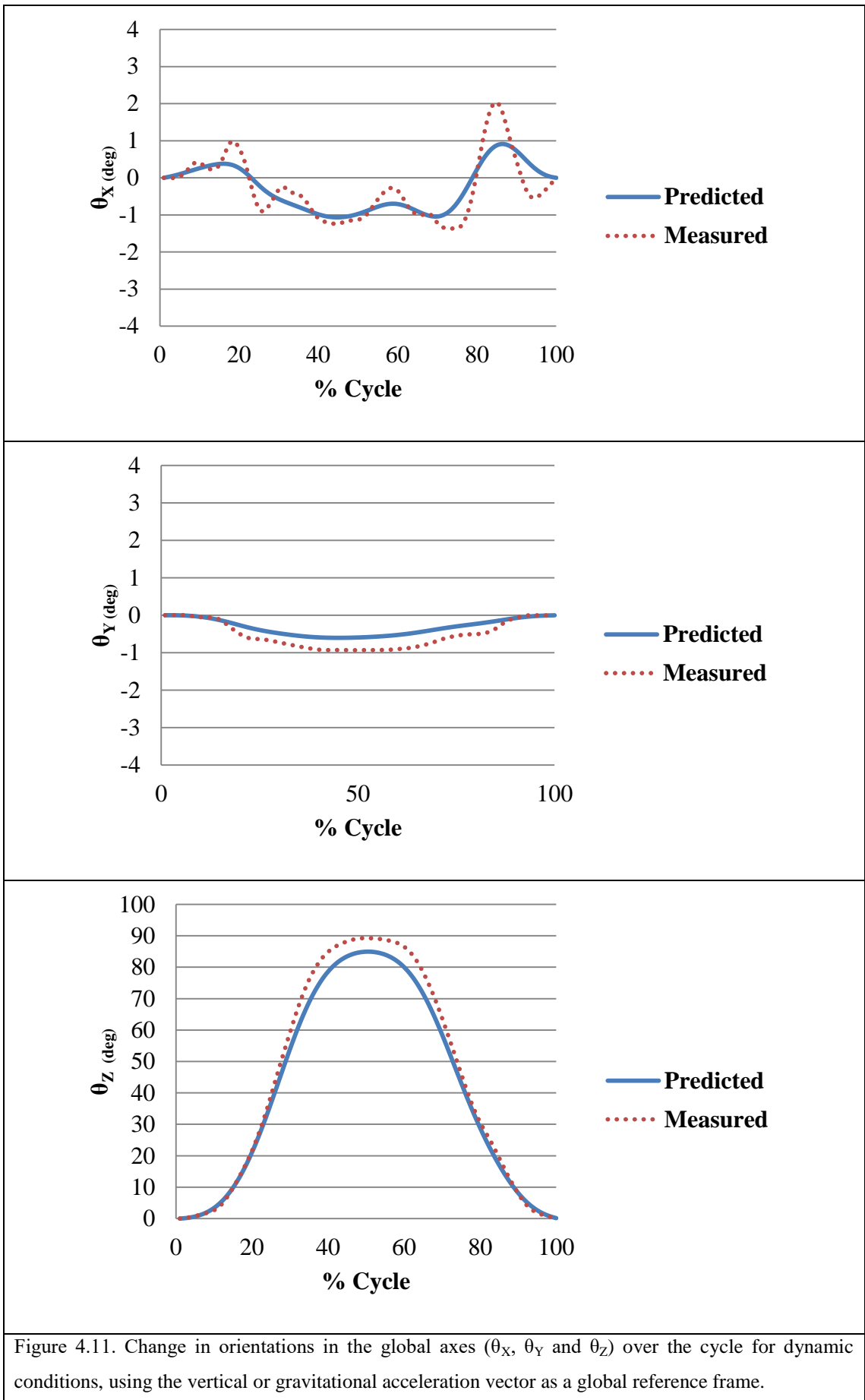


Figure 4.11. Change in orientations in the global axes (θ_x , θ_y and θ_z) over the cycle for dynamic conditions, using the vertical or gravitational acceleration vector as a global reference frame.

4.6 Results Scenario b): Stage One Different Quasi-static Conditions

The results for scenario b) only focus on the orientation results under quasi-static conditions for two different parts (1 and 2) described in Figure 4.3. This is as a result of the difficulties in synchronizing the sensor motion (humerus and scapula), generated mainly by the different orientations measured in the curved surface.

The measured angle between vertical and the local planes of the scapula and SL sensors is shown in Figure 4.12 for the first part of scenario b) (Part 1)). The humeral sensor, the scapula sensor and the SL sensor were placed vertically with the local x axis pointing up for this scenario, simulating the conditions that potentially could be found in clinical settings, which is different from in scenario a). The SL sensor was rotated around 30° over one arm of the SL device, as if the sensor were aligned with the lateral border of the scapula. It is important to remember that in terms of recording quasi-static data the scapula sensor and the SL sensor follow the same motion pattern as in scenario a), which means that two of the SL pins were aligned with the goniometer that held the scapula sensor, see Figure 4.7 and Figure 4.8.

The first value recorded in the initial section of the result for θ_X shown in Figure 4.12, indicates how the sensors were aligned with respect to the vertical or the gravitational acceleration vector; with θ_X having a value of around 0° for the scapula sensor and around 30° for the SL, which were the initial conditions for the sensors.

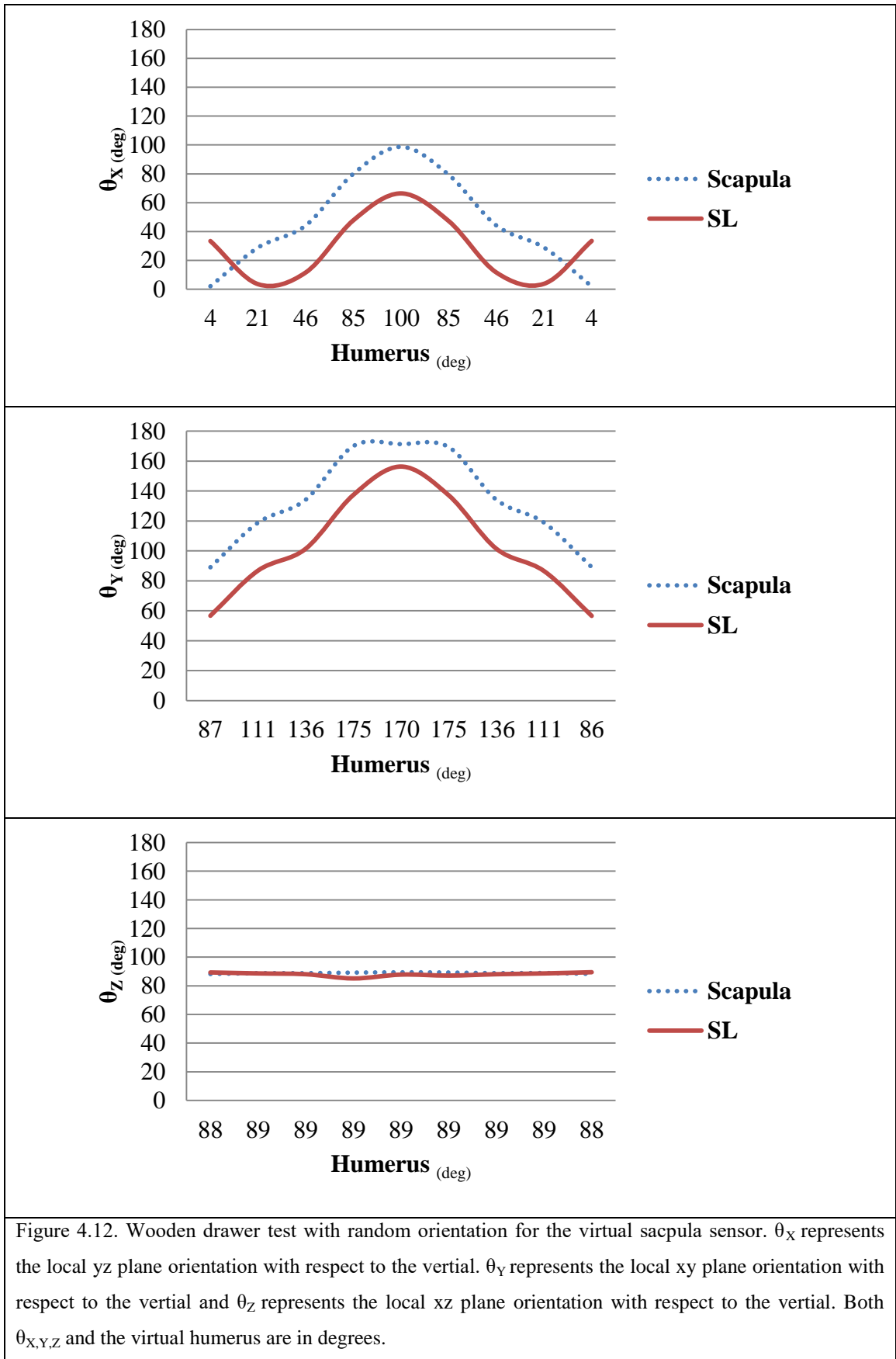
For the θ_X and θ_Y axes the difference between the scapula and the SL orientation remains around 30° throughout the whole test, which is as a result of the initial 30° misalignment with respect to the vertical of the θ_X and θ_Y axes intentional set by the observer/researcher.

Because θ_X and θ_Y axes change proportionally, the θ_Z axis, which is the main axis of rotation (see Figure 4.7), remains unchanged to the other two axes, which highlights how the orientation of θ_Z is dependent on the other two axes and the initial setup conditions.

When the sensor simulating the humerus reaches 20° with respect to the vertical or gravitational acceleration vector, the local x axis orientation of the SL-IMU crosses the

vertical see Figure 4.13, in other words the local yz plane is almost aligned with the ground, the local x axis of the SL orientation suffers an orientation change. The SL sensor follows the same pattern as the scapula sensor placed over the goniometer after this point as shown in Figure 4.12, θ_x . The scapula sensor does not present this problem because when the sensors rotate it never crosses the vertical or aligns with the ground (see Figure 4.13). The phenomenon experimented by θ_x in Figure 4.12 can be explained because due to the absence of gyroscopes and magnetometers it is difficult to determine the direction of the spin. However if a negative rotation is considered for the first 20° of the virtual humerus, which is when the yz plane almost aligns with the vertical, similar trends between the virtual scapula and the SL can be observed, this phenomena is very important for understanding sensor behaviour and can be easily visualized in Figure 4.13.

Figure 4.13 explains the source of the different patterns between the scapula and scapula locator shown in Figure 4.12 (θ_x). The initial conditions of the scapula and Scapula locator sensors for a clinical setting (a) and b)) are presented in Figure 4.13. It is possible to appreciate how the local x axis of the scapula sensor is aligned with the vertical (gravity) or the ground Figure 4.13 e), while the scapula locator sensor is tilted certain angle from the vertical Figure 4.13 b). After apply a rotation in the local z axis, the final orientation of the sensors are presented in Figure 4.13 c) and d). After a visual inspection it can be seen that the scapula locator local 'x' axis crossed the vertical while the scapula sensor did not. Due to the absence of gyroscopes and magnetometers, it is not possible to determinate if the spin of the scapula locator sensor when it crosses the vertical was positive or negative. The resulting orientation of the scapula locator sensor after applying the direction cosines was positive, explaining the 'w' pattern, which is different than the scapular sensor pattern that can be seen in Figure 4.12 (θ_x). In other words, if the motion of the scapula locator sensor is considered negative before the sensor crossed the vertical (Figure 4.13 b) and d)), the scapula and scapula locator sensor will present similar patterns.



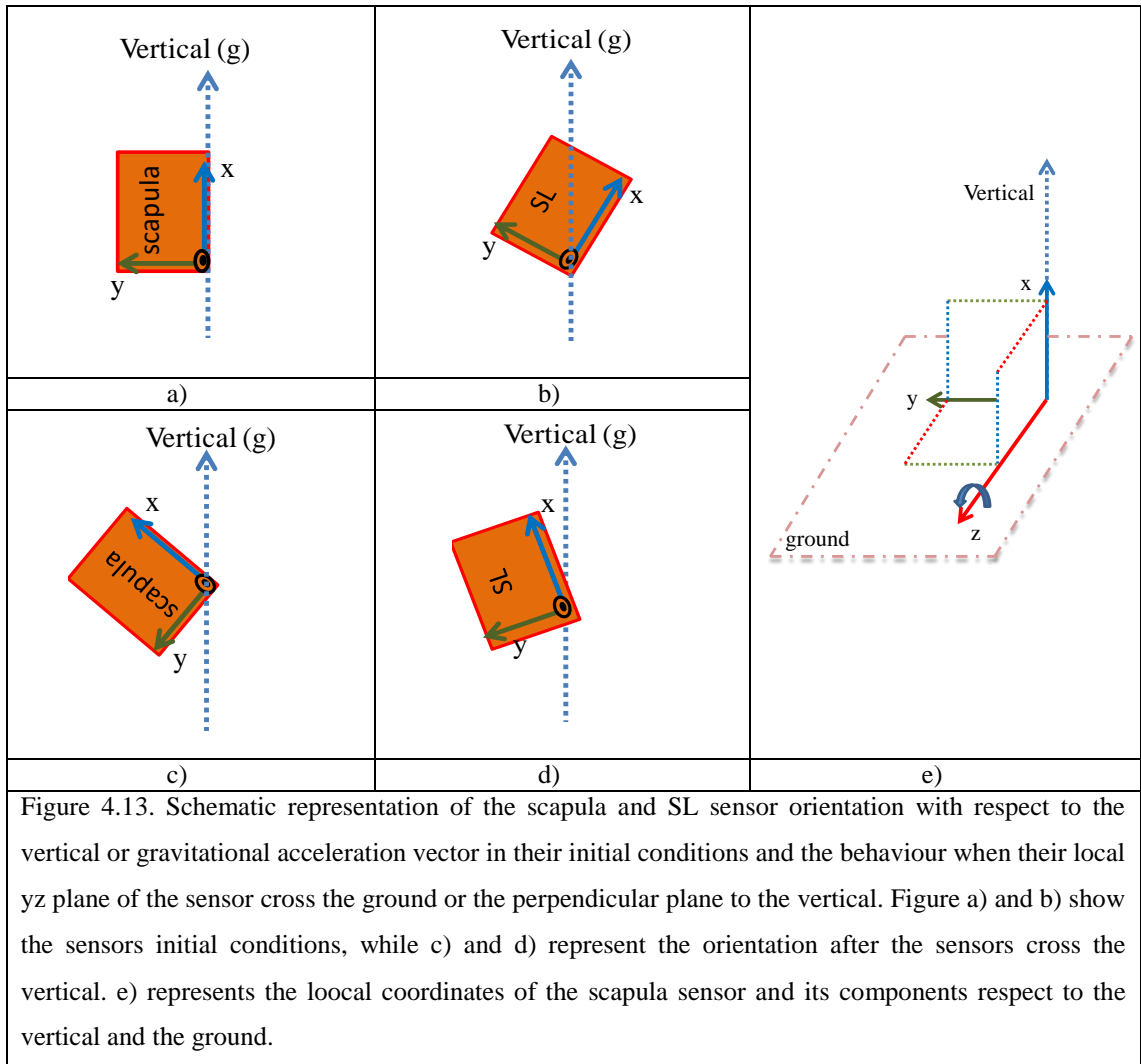


Figure 4.13. Schematic representation of the scapula and SL sensor orientation with respect to the vertical or gravitational acceleration vector in their initial conditions and the behaviour when their local yz plane of the sensor cross the ground or the perpendicular plane to the vertical. Figure a) and b) show the sensors initial conditions, while c) and d) represent the orientation after the sensors cross the vertical. e) represents the loocal coordinates of the scapula sensor and its components respect to the vertical and the ground.

For the second part (Part 2)) of scenario b) see Figure 4.3, the scapula sensor was rotated in to different directions over a round helmet instead of using the flat surface of the drawer wall. The results for this scenario are presented in Figure 4.14 and as was expected, the SL displays the same pattern as in Figure 4.12; however, it can be seen that the rotation through different planes affects the measured orientation of the scapula sensor.

The results of Figure 4.14 suggest that the scapula locator can effectively track the orientation of the virtual scapula, as can be seen from the results shown in Figure 4.12 and 4.14, which suggest that the main source of error when a locator is being used comes from the observer/researcher in accurately locating the device and keeping it in position. Figure 4.14 also suggests that variability in the input data (humerus and scapula) to the polynomial can generate large variability in scapula orientation

predictions. This could potentially have a significant effect when the dynamic stabilizers of the upper arm and shoulder pathologies are being assessed.

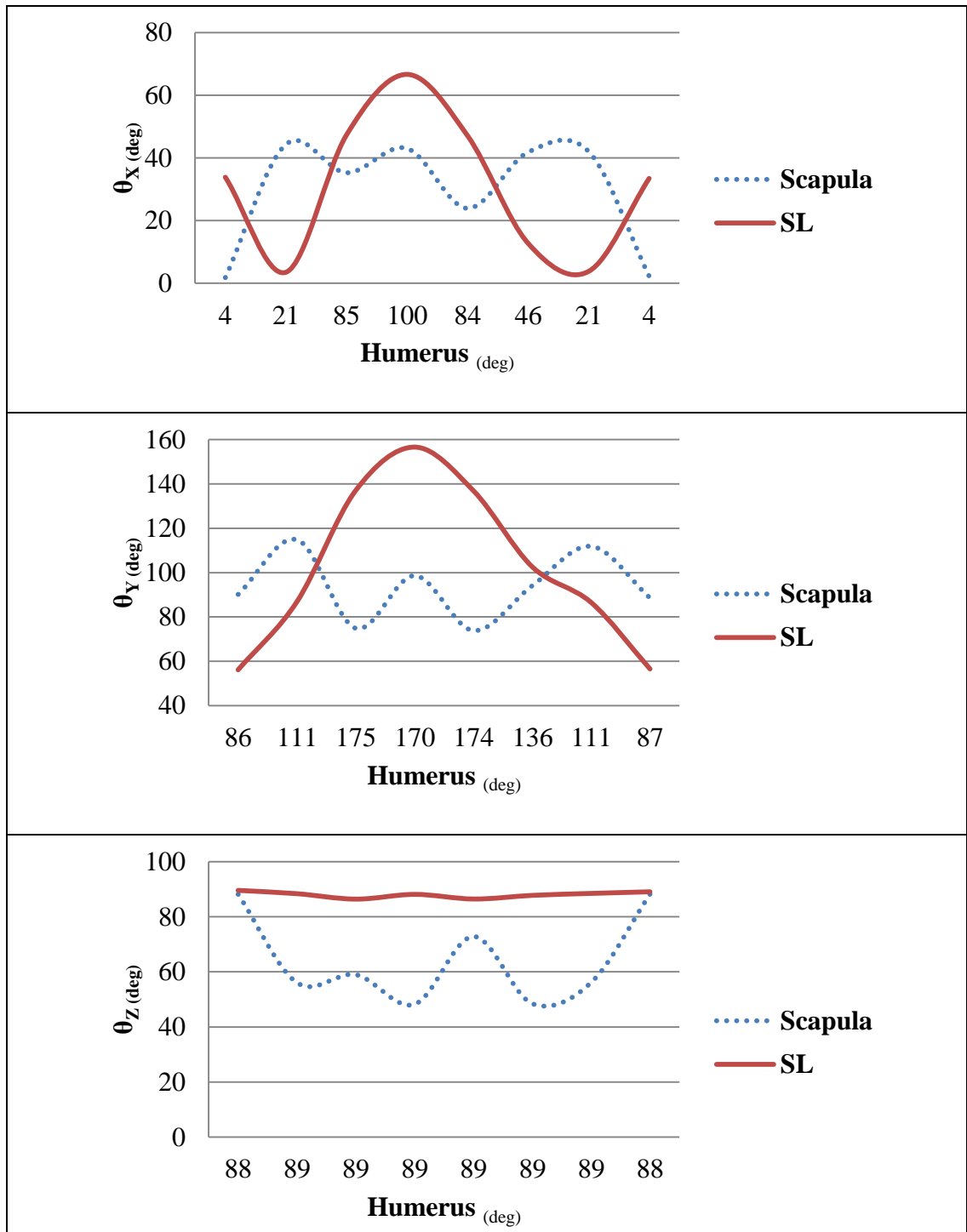


Figure 4.14. Helmet test with random orientation for the virtual scapula sensor. θ_x represents the local yz plane orientation with respect to the vertical. θ_y represents the local xy plane orientation with respect to the vertical and θ_z represents the local xz plane orientation with respect to the vertical. Both $\theta_{x,y,z}$ and the virtual humerus are in degrees.

CHAPTER V: TRACKING THE SCAPULA: PORCINE STUDY

5.1 Introduction

In the previous chapter (IV) a methodology was presented with the aim to reduce the error generated by the soft tissue and allows the dynamic tracking of the scapula orientation as if the scapula were tracked with a scapular locator device, by using a regression-type equation obtained from quasi-static conditions. The methodology presented in section IV enables the human scapula to be tracked under dynamic conditions to scapula locator level accuracy using a non-invasive skin based technique. However, in chapter IV, the methodology was tested over a wooden drawer which is not affected by soft tissues.

In this chapter a mechanism for simulating dynamic glenohumeral motion is established and tests undertaken on an intact porcine specimen. Following this, the tests were repeated after removing subcutaneous tissue and muscle layers covering the scapula enabling the scapula tracking technique described in Chapter IV to be assessed under dynamic conditions and the effect of skin deformation and subcutaneous tissue artefact to be estimated. In outline, the technique utilises data from a combination of IMUs and a SL recorded during quasi-static tests to develop a regression-type equation which is then applied to track the scapula under dynamic conditions using just two IMUs. Unlike other regression type techniques [30, 81, 94, 97, 134] this method uses both scapula and humeral orientations as inputs. A porcine cadaver was chosen for assessing the accuracy of the technique because of the physiologic and anatomic characteristics that swine share with humans [31-33], in particular the structural similarity of the skin [32-34].

5.2 Materials and Methods

In this section study tests were undertaken on a porcine cadaver in order to:

- a) assess the accuracy of the non-invasive methodology described in Chapter IV; and
- b) quantify the effect of the skin, tissue, and muscle artefact when the scapula was tracked under dynamic conditions.

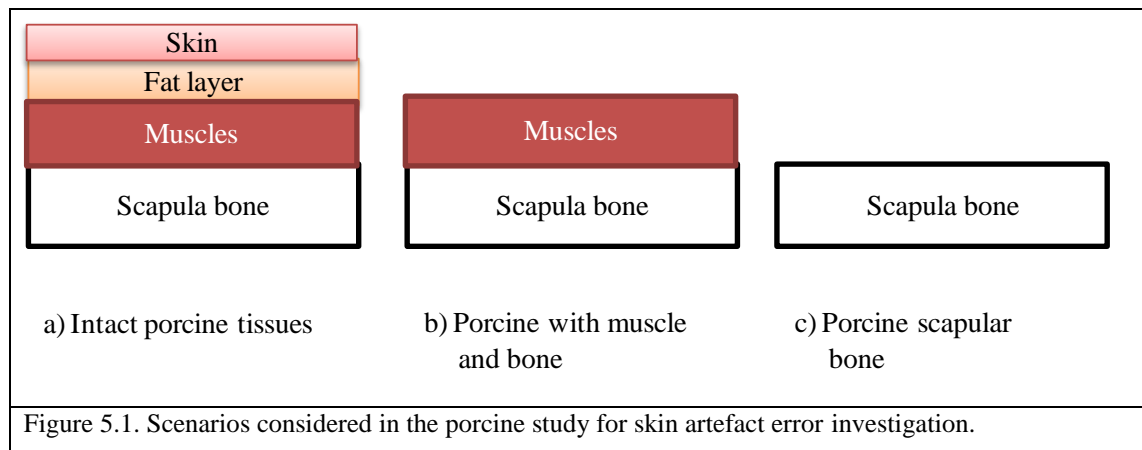
For these experiments only flexion-extension motions were investigated in the porcine model. The flexion-extension pig leg motion is the natural motion of the pig legs for its gait.

Passive movement trials were conducted under the following conditions:

On the intact animal, with the skin, subcutaneous tissue and muscle layers covering the scapula left intact, see Figure 5.1.

On the animal with muscle covering the scapula remaining after removing the epidermal, dermal and subcutaneous fat layers covering the scapula, see Figure 5.1.

On the animal with no tissue remaining over the scapula after excision of the epidermal, dermal, subcutaneous fat and muscle layers covering the scapula, see Figure 5.1.



5.2.1 Practice Dissection

To address the different conditions described in Figure 5.1, a preliminary dissection was performed on a pig shoulder as shown in Figure 5.2. This dissection allowed the researcher to become familiar with the different tissues that have to be removed as well as to become familiar with the shoulder pig anatomy and finally to plan the best way to perform the final assessment. The dissection also provided information about the range of motion expected in the tests.

The dissection was performed using a scalpel, which facilitated the tissue removal. The dissection also helped in practicing and identifying the best method for tissue removal; ensuring that unwanted extra tissue removal was avoided.

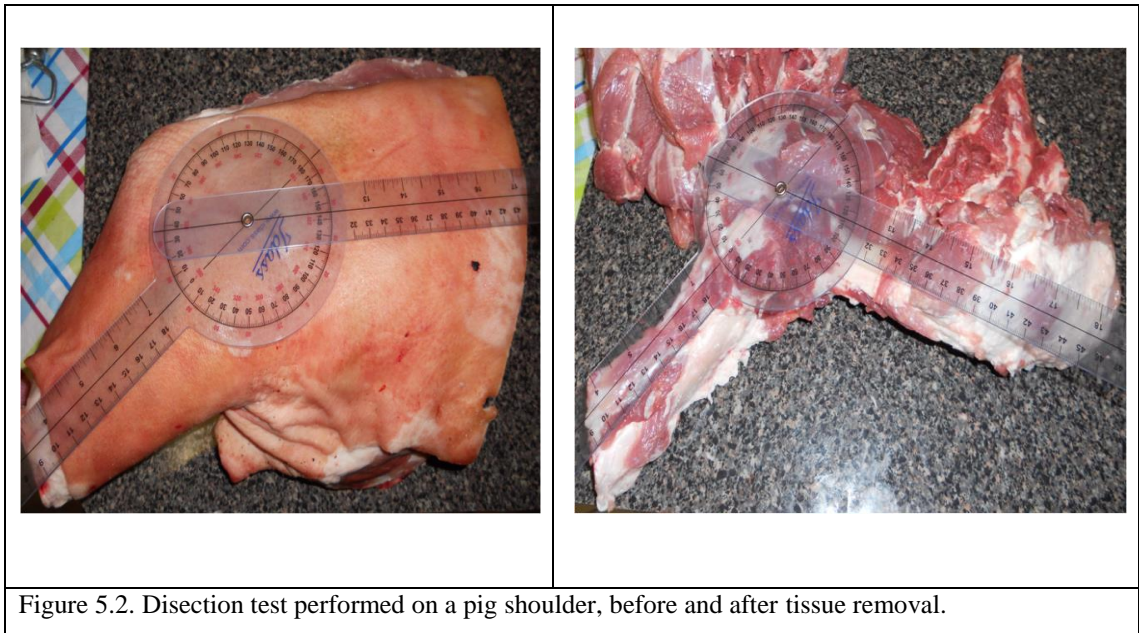


Figure 5.2. Dissection test performed on a pig shoulder, before and after tissue removal.

5.2.2 Porcine Assessment

Passive continuous motion tests were undertaken for the three conditions described above, and the intact animal was also used for quasi-static tests (see Figure 5.1). All tests were undertaken on a juvenile porcine cadaver within 1.5hrs of death. The animal showed no signs of disease or trauma, was aged 3.5 months with a body mass of 30kg at the time of slaughter, and had a combined fat and skin thickness of 2.8mm (\pm 0.3mm). The porcine specimen was bought from the local butcher and intended for human consumption.

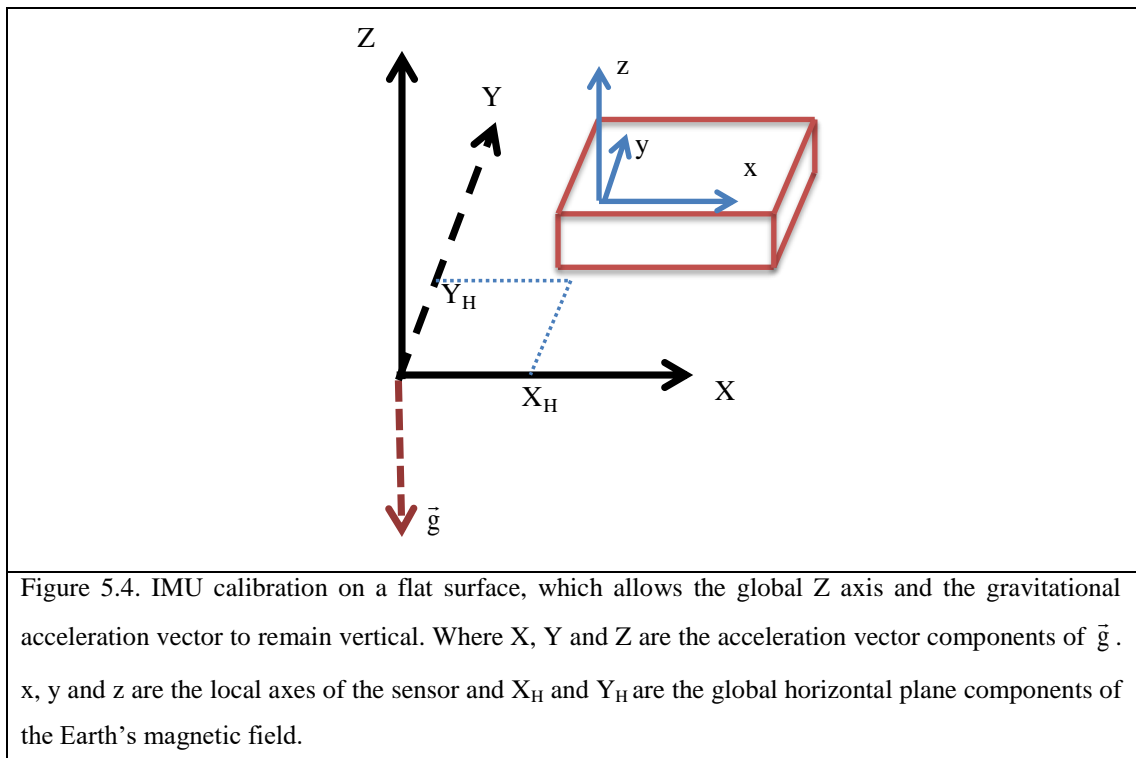
Four MTw sensors (Xsens Technologies, Enshede Netherlands) were used for the tests, each with a mass of 27gram and manufacturer reported dynamic accuracy of 2° [153], see Figure 5.3.



Figure 5.3. Four inertial measurement units (IMUs) were used for the porcine test.

All IMUs were calibrated by performing a heading reset on a flat surface which allowed the global Z axis (Figure 5.4) and the gravitational acceleration vector to remain parallel to each other [153].

A custom made SL was built to measure scapular orientation under quasi-static conditions. This SL was manufactured from acrylic sheet with three plastic and stainless steel locator pins as shown in Figure 5.5. The acrylic sheets were machined according to the dimension specified in Figure 5.5.



The upper portion of the pins was made from 9.8mm diameter plastic in order to minimise distortion in the magnetic field around the IMUs. The lower portion of the pins consisted of 3mm diameter stainless steel, machined to a relatively sharp point at the end in order to aid palpation of the scapula using the SL.

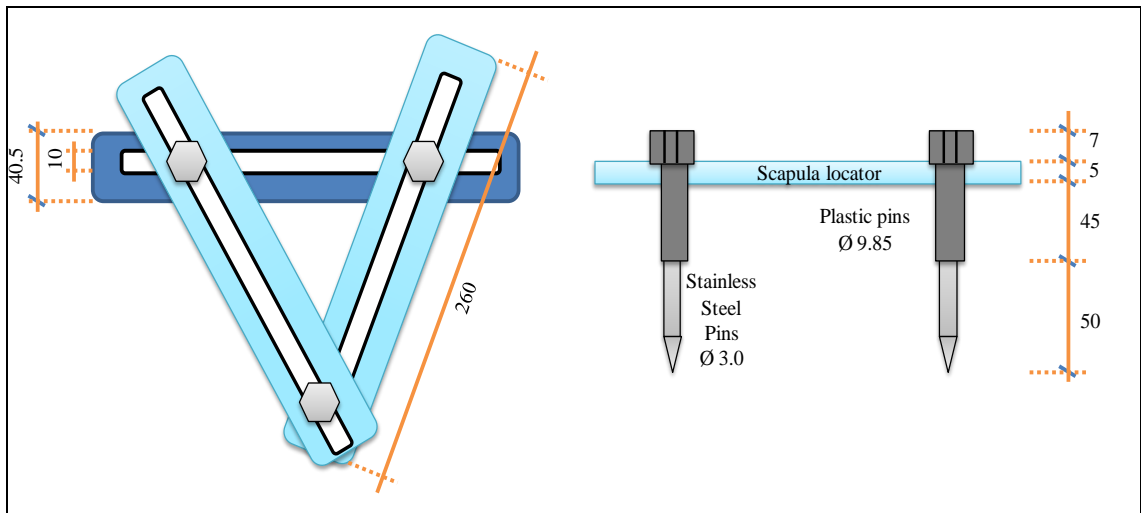


Figure 5.5. Acrylic custom made scapula locator (SL). Dimensions are in mm.

The animal was placed on a wooden table (Figure 5.6) in the left lateral recumbent position and secured in place using a mechanical clamping system in order to avoid unwanted motion.

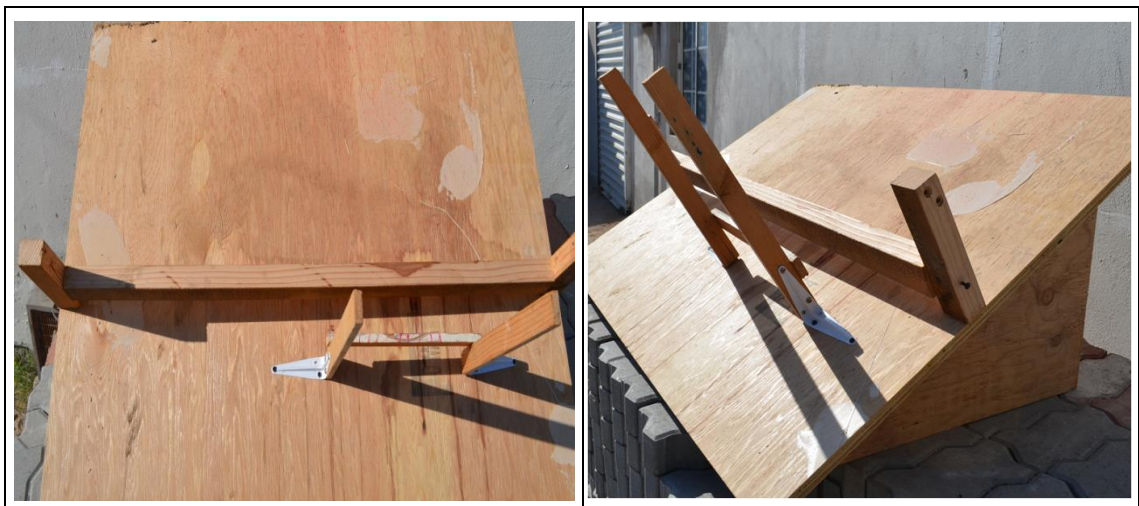


Figure 5.6. Frontal and lateral view of the wooden table used in the assessment.

A triangular shaped wooden base was screwed to the humerus and ulna to fix the elbow joint of the superior forelimb of the specimen (Figure 5.7) which was then rested on an H-shaped wooden jig screwed to the table (Figure 5.6 and Figure 5.8) in order to guide and limit the motion.



Figure 5.7. Traingular wooden base, used to fix the humerus and ulna of the pig leg and support the humeral sensor.

A schematic section view of the final setup configuration for the porcine assessment is presented in Figure 5.8.

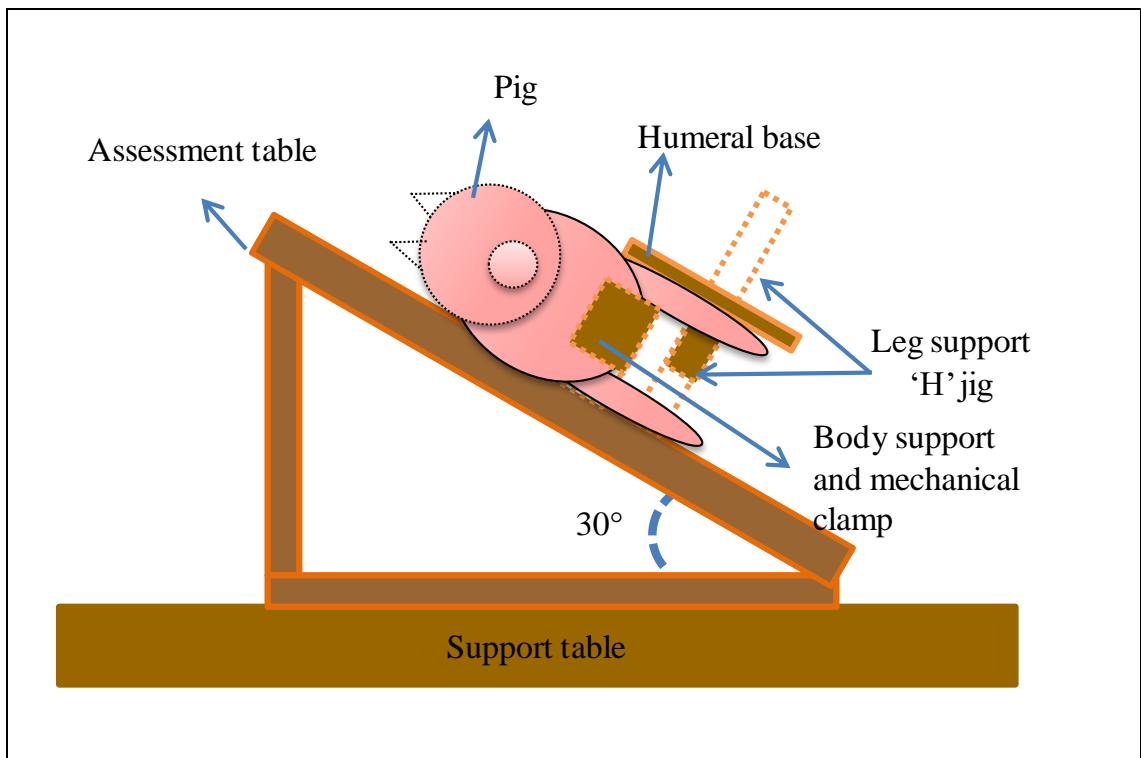


Figure 5.8. Section view showing the support table, the assessment table inclined at an angle of 30° to the horizontal plane of the support table, the pig held in position by the body support and mechanical clamp and the upper forelimb of the pig resting on the H-shape jig screwed to the assessment table.

A digital spirit level was employed to ensure that the table, H Jig and the humeral plane of motion remained parallel (Figure 5.9). Scapulo-humeral flexion-extension motion was induced in the superior, right forelimb of the specimen by moving the forelimb back and forth on the H-jig, which was screwed to the table and provided control of movement amplitude of the forelimb and ensured that movement remained in a sagittal plane.

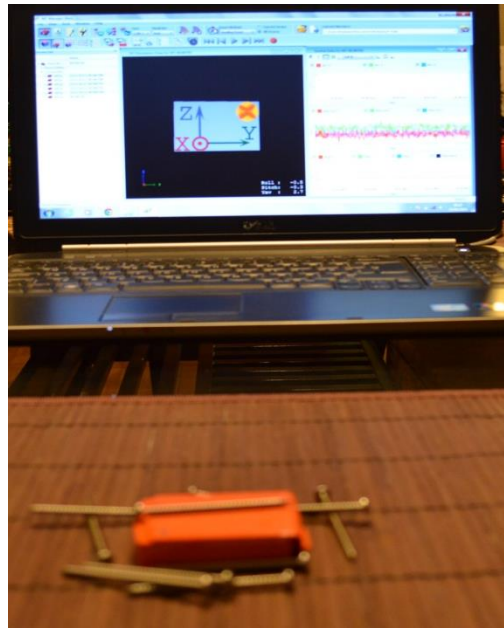


Once the mechanism to produce repeatable controlled flexion-extension motion of forelimb of the specimen was established, the IMUs were secured in place. The first IMU (S-IMU) was position over the scapula. To ensure that placement of the scapular sensor (S-IMU) occurred in the same position throughout the different tests performed, three 2" x 0.19" ϕ non magnetic stainless steel screws were drilled into the scapula and used as a guide.

Figure 5.10 shows a magnetic test performed over the sensors before the test with the stainless steel screws used in the assessment.



a)



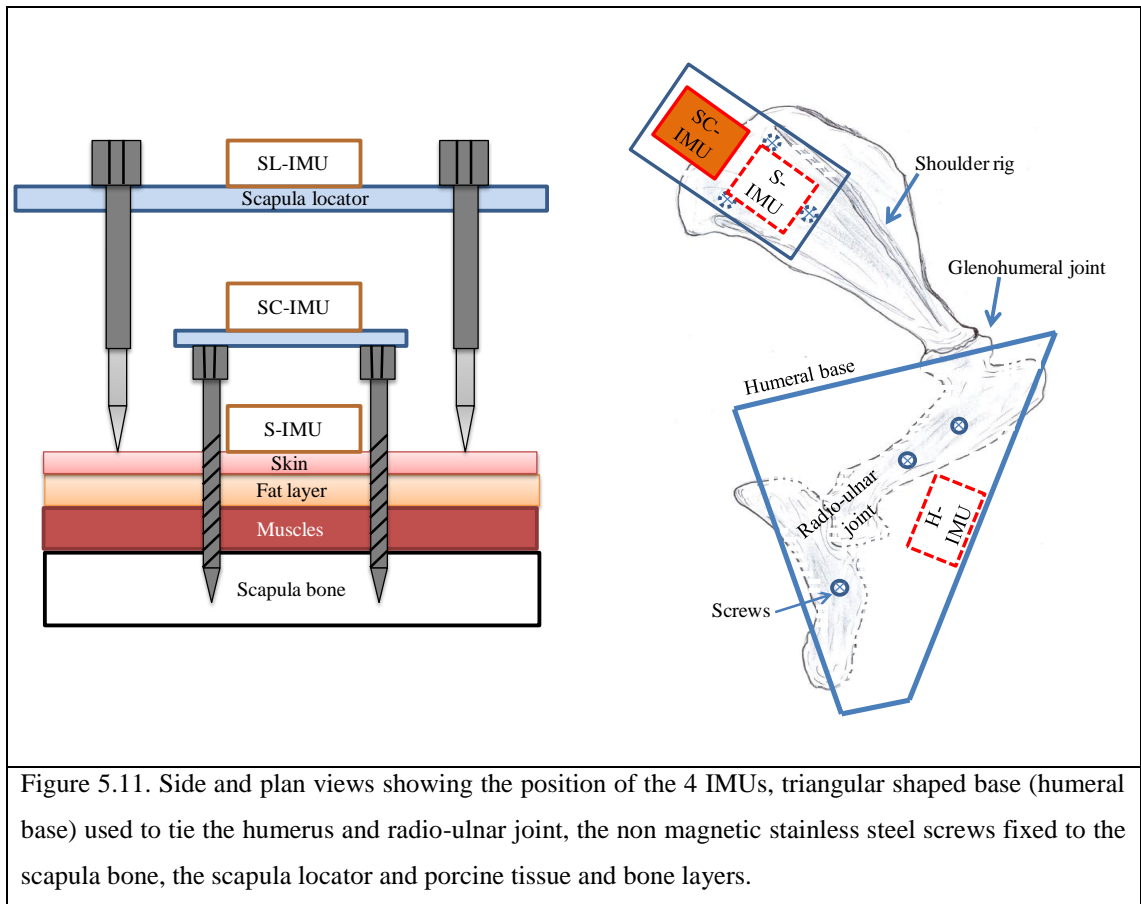
b)

Figure 5.10. a) A magnetic test was performed with the IMUs by locating the stainless steel screws close to them, Fig 5.10 a) also shows that there is not magnetic effect on the sensors, making their use suitable for the test. Fig 5.10 b).

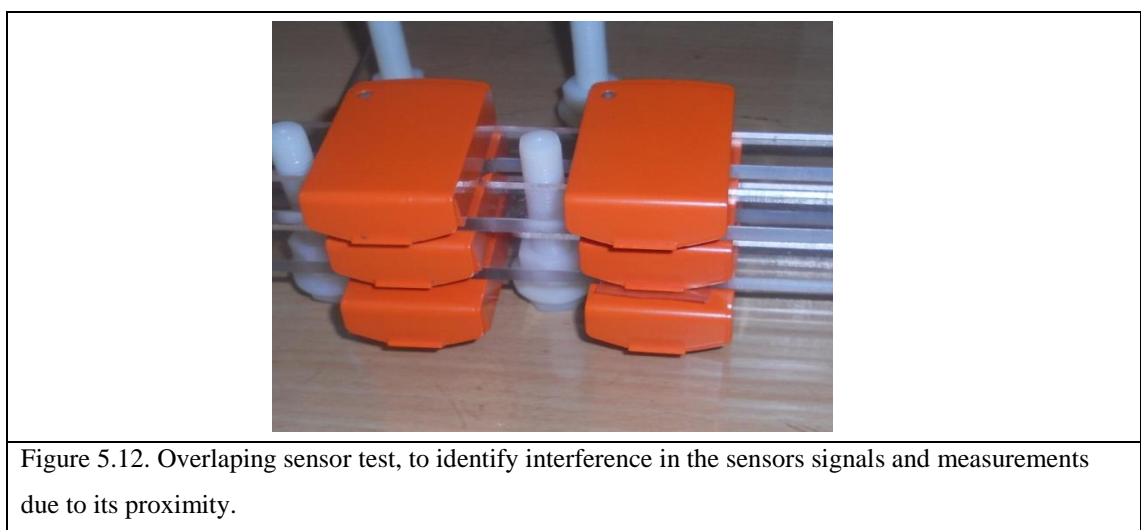
In addition, these screws were used to track the actual position of the scapula by attaching a second IMU (SC-IMU) on top of them. These three screws were positioned based on bony landmarks of the scapular as illustrated in Figure 5.11.

The screws were positioned by:

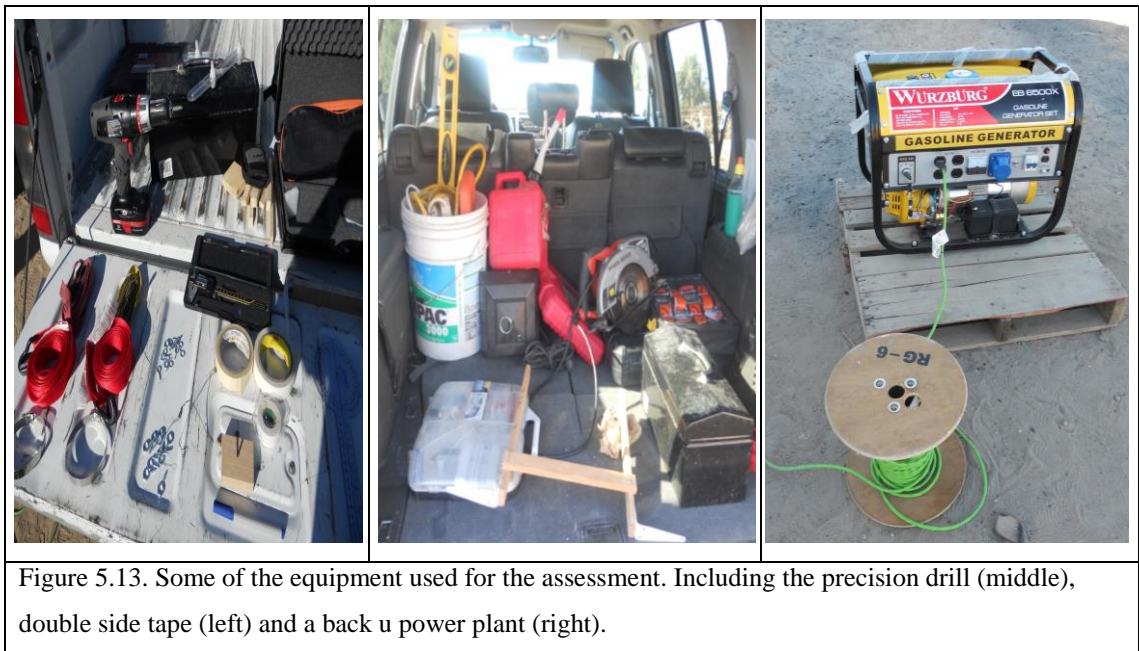
- 1) Identifying the scapula bony landmarks.
- 2) Inserting a needle to identify the scapula bone and placing an ink mark.
- 3) With a small precision drill a tiny holes were made in the scapula.
- 4) The precision drill provided the path to place the screws over the scapula.



Because the SC-IMU and the S-IMU were to be placed one over the other, separated by an acrylic base, an extra test was performed in order to identify any interference in the sensors signals and measurements due to their proximity. The test consisted in overlapping the sensors and looking for interference in the signal, Figure 5.12. The results of the test did not indicate any interference between the sensors signals due to the proximity of the sensors.

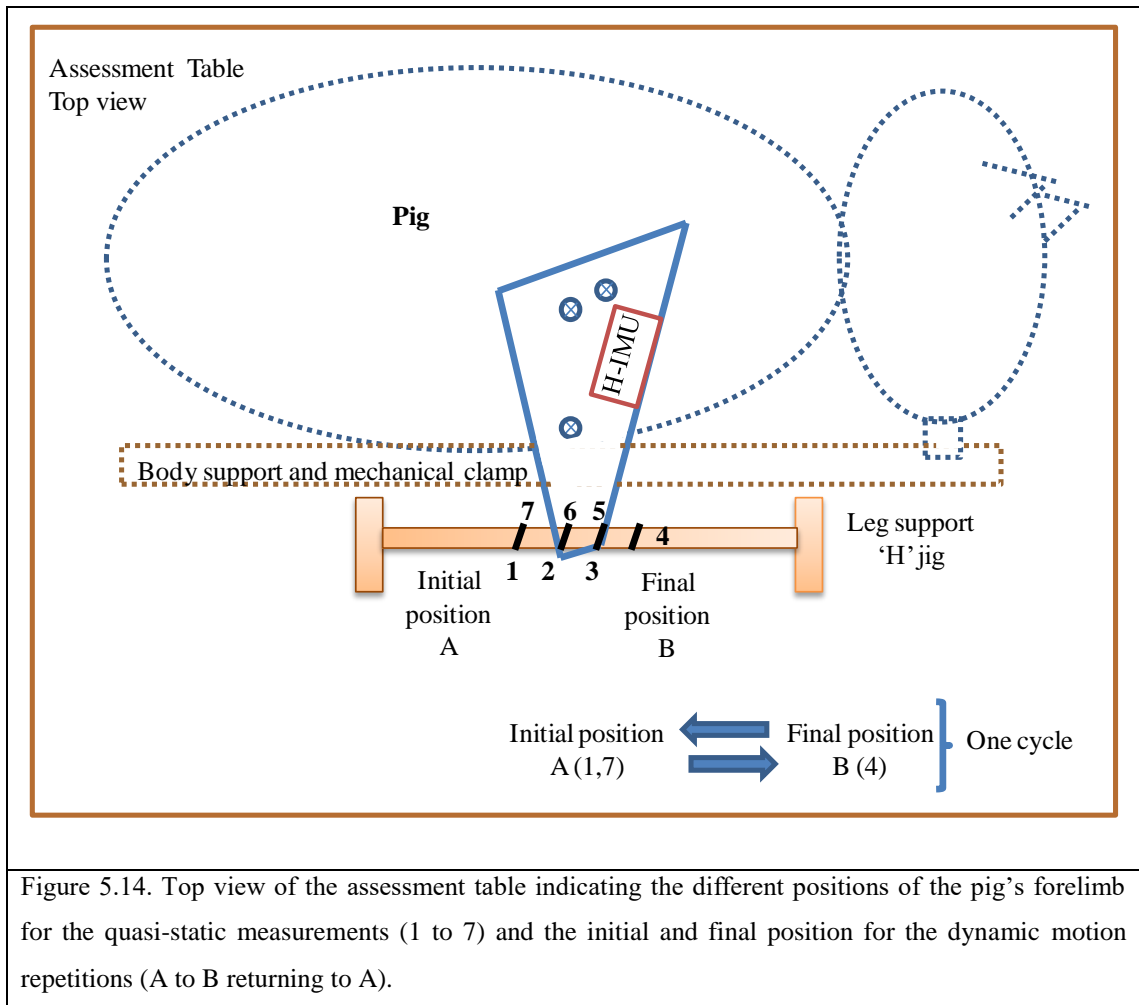


The third IMU, the humeral sensor (H-IMU), was placed on the wooden triangle screwed to the humerus and ulna; the process to screw the wooden triangle base into the bone was the same as the process followed to place the scapular screws. The edge of the humeral sensor (H-IMU) was aligned along the longest edge of the triangle, Figure 5.7 and 5.11. The last sensor was aligned along one of the arms of the scapula locator (SL-IMU) in order to track the orientation of the scapula as determined by the SL. All four sensors were attached using industrial double- sided tape. Figure 5.13 shows some of the equipment used in the assessment.



5.2.3 Stage One: Quasi-static Trials

The first stage consisted of multiple quasi-static humeral flexion-extension motions, recorded at approximately equal intervals between an initial and an end position which represented the extreme of movement but which did not force or exceed the natural range of motion of the elbow joint. Starting from the initial position, data were taken at intervals of $7^{\circ} \pm 2.5^{\circ}$ until the end position was reached (a total of 7 positions); at that point the forelimb was moved back to its initial position with data again taken at the same intervals; this was considered as one cycle, Figure 5.14. The intervals amplitude was identified by placing marks over the ‘H’ support, Figure 5.14. Each position recorded corresponds to a mark. The edge of the triangular wooden base was aligned for each position recorded.



At each position, motion was stopped and the scapular bony landmarks were palpated and the SL placed accordingly. Data from the four IMUs were then collected. The maximum amplitude obtained for the specimen in the quasi-static flexion-extension motion tests was $21^\circ \pm 8^\circ$ for the humerus and $10^\circ \pm 1.5^\circ$ for the scapula. The quasi-static test comprised 5 cycles.

5.2.4 Stage Two: Dynamic Trials

In this stage, the scapula locator and SL sensor (SL-IMU) were discarded and dynamic tests undertaken by inducing scapulo-humeral flexion-extension motions in a sagittal plane while data were recorded from the remaining three IMUs: the scapula and humerus IMUs and the IMU attached to the three screws tracking the actual position of the scapula. The initial and end positions remained the same as those used for the quasi-static test (stage one). A cycle in the dynamic tests consisted of moving the forelimb of the specimen from the initial position to the end position then back to the initial position

at a steady velocity, which took around two seconds to complete. Nine cycles (± 1) were performed continuously without stopping while data were recorded from the humerus (H-IMU), and scapula (S-IMU) IMUs and the IMU attached to the screws (SC-IMU). Each dynamic test was repeated 5 times. On average the maximum amplitude obtained for the specimen in the dynamic flexion-extension motion tests was $28^\circ \pm 2.5^\circ$ for humeral motion and $10^\circ \pm 3^\circ$ for the scapula. A detailed description of the range of motion for the performed tests is described in Table 5.1.

RoM in degrees ($^\circ$)							
Sensor	Measured layers	Axis X	stdv \pm	Axis Y	stdv \pm	Axis Z	stdv \pm
Humerus	All tissues	11.4	0.93	3.1	0.18	25.58	1.48
	Muscles	12.37	1.26	3.86	0.39	27.24	1.13
	Bone	15.42	1.11	4.75	0.1	30.06	0.47
Scapula	All tissues	3.88	0.42	4.61	0.36	7.21	0.36
	Muscles	4.33	0.89	5.58	0.87	10.13	0.63
	Bone	3.04	0.13	4.19	0.11	12.42	0.28
Screws sensor	All tissues	4.72	0.45	4.31	0.3	10.57	0.36
	Muscles	4.2	0.74	4.44	0.36	11.99	0.44
	Bone	3.29	0.13	4.18	0.11	12.37	0.28

5.3 Data Processing

The data obtained in stage one described in section 5.2.3 was processed to generate the coefficients of the regression equation. This equation was used to predict the location of the scapula during the dynamic tests (stage two).

5.3.1 Orientation Calculation from IMUs

The following data process procedure was employed to obtain the orientation for both stages one and two.

5.3.2 Stage One: Quasi-static

Three local acceleration components \mathbf{A}_x , \mathbf{A}_y , \mathbf{A}_z were obtained as outputs from the inertial sensors, which, in a static situation, sum to the gravitational acceleration vector (\vec{g}). The gravitational acceleration vector and the global Z-axis remain vertical. The

local acceleration vectors will provide the tilt of the xy, yz, and xz local planes in relation to the vertical (Z) by using direction cosines (see section 4.3.6), which defines the orientation of the sensor, but they will not provide enough information to indicate the direction of the tilt (i.e. to define the heading vector). In order to obtain the heading vector, another reference vector, provided by the Earth's magnetic field is used [155-156]. Because the motion mainly occurs in one plane for this test an electronic compass analogy is used.

Under quasi-static conditions, the pitch and roll of the sensor in relation to a global horizontal and vertical plane are given by Eq 5.1 and 5.2. The three magnetometer outputs in the local axes (X_m , Y_m , and Z_m) from the sensor and the calculated pitch and roll angles are used to rotate the Earth's magnetic field components into a global horizontal plane (Eq 5.3 and 5.4), Figure 5.4. When the magnetometer data are in the horizontal plane the heading or Z_θ orientation can be obtained [155-156], by applying Eq 5.5.

$$X_\theta = \tan^{-1} \frac{A_x}{\sqrt{A_y^2 + A_z^2}} \quad \text{Eq 5.1}$$

$$Y_\theta = \tan^{-1} \frac{A_y}{\sqrt{A_x^2 + A_z^2}} \quad \text{Eq 5.2}$$

$$X_H = X_m * \cos Y_\theta + Y_m * \sin X_\theta * \sin Y_\theta - Z_m * \cos X_\theta * \sin Y_\theta \quad \text{Eq 5.3}$$

$$Y_H = Y_m * \cos X_\theta + Z_m * \sin X_\theta \quad \text{Eq 5.4}$$

$$Z_\theta = -\tan^{-1} \frac{Y_H}{X_H} \quad \text{Eq 5.5}$$

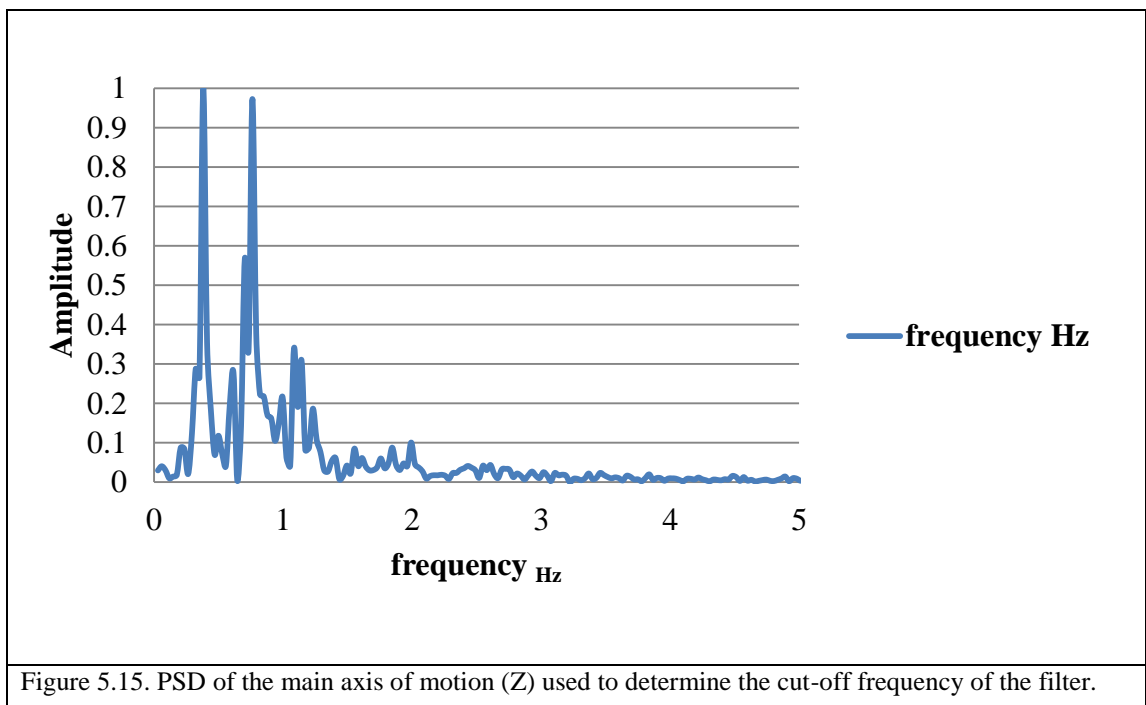
Where A_x , A_y and A_z represents the acceleration measured by the sensors in the three local axes; X_θ and Y_θ are the pitch and roll angles relative to the horizontal; and X_H and Y_H represent the components of the heading vector in the pitch and roll axes. Z_θ represents the new heading. This principle is commonly used in electronic compasses as can be found in mobile devices.

The scapular and humeral orientation were fitted to the SL orientation using a best fit polynomial for the data from each of the five cycles of the quasi-static test, as was suggested in section 4.2.1. The mean coefficients calculated from the five cycles of the

quasi static test were used in the regression equation to predict the scapular orientations in the dynamic tests from the relative orientation of the humerus and the IMU sensor placed directly over the scapula.

5.3.3 Stage Two: Dynamic Motions

For stage two the three local components of the angular velocity (ω_x , ω_y , ω_z) and their quaternion representation were obtained as outputs from the inertial sensors. The local angular velocity data were substituted into the polynomial obtained for each axis before they were rotated into the global reference frame (calibration frame) by applying a quaternion rotation (see section 4.3.6, **Stage Two: Dynamic Conditions**). With the angular velocity in the global frame a second order, zero phase lag, Butterworth filter with a cut-off frequency of 1.5 Hz (determined by using the power spectrum density; PSD, see Figure 5.15) was applied to reduce noise in the signal. After filtering, the signals were split into the number of repetitions performed and then each individual repetition was integrated to obtain the orientation of each axis in the global frame.



5.4 Results

The results obtained for the three scenarios described in Figure 5.1 and for the two stages described in sections 5.2.3 and 5.2.4 are presented as follows:

5.4.1 Stage One: Quasi-static Trials

Figure 5.16 shows the results from the quasi-static trials undertaken in stage one of the tests. The sensor data shown in the figure represents the average over the 5 quasi-static test cycles considered. The orientations in degrees in the global axes, θ_x , θ_y and θ_z , at points throughout the quasi-static cycle of movement of the shoulder joint are illustrated in this Figure. These measurements correspond to the readings recorded by the IMUs attached to the humerus and scapula surfaces and the IMU attached to the scapula locator. Also shown in this figure is the predicted scapula orientation obtained using the regression equation (Table 5.2) enabling a comparison to be made with the scapula location as measured by the SL sensor. The regression equation was subsequently used to predict scapular position under dynamic conditions (Table 5.2).

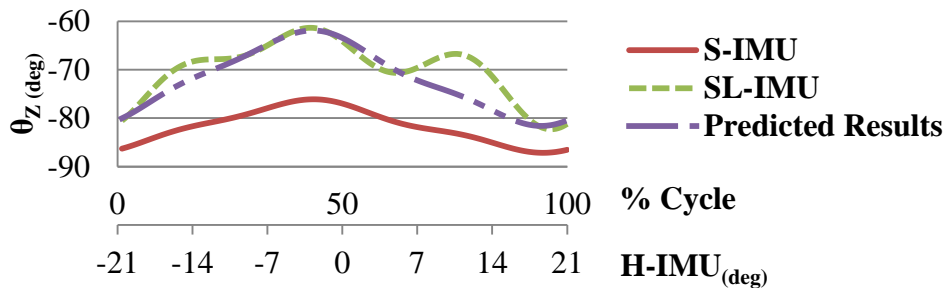
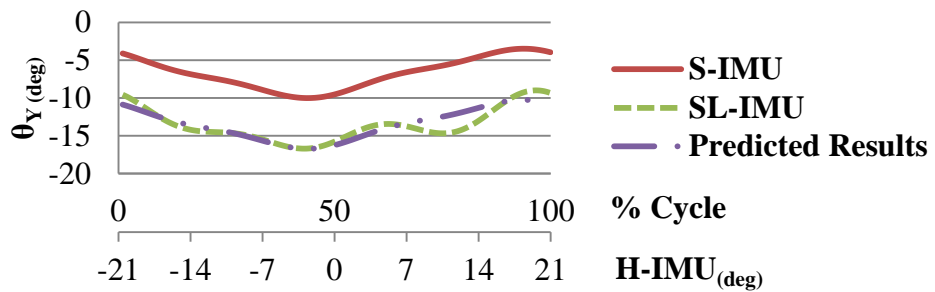
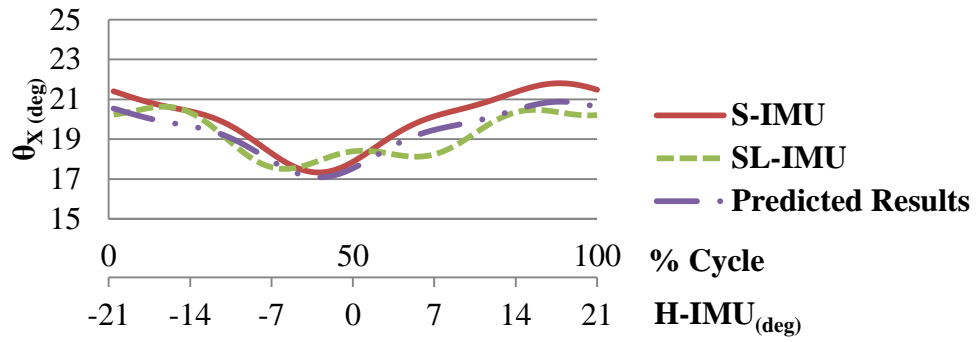


Figure 5.16. Orientations in the global axes (θ_x , θ_y and θ_z) over the cycle for quasi-static conditions, measured by IMUs positioned on the Humerus (H-IMU) and is represented in the second (bottom) longitudinal axis, Scapula (S-IMU) and Scapular locator (SL-IMU) and the predictions obtained using the regression equation.

Upon inspection of Figure 5.16 it can be seen that there is a difference between scapula location as determined by the IMU attached to the SL (SL-IMU) and that determined from the skin mounted scapula sensor (S-IMU); this is particularly notable in the Y and Z directions where the maximum difference and RMS error are 9.1° and 6.9° in Y and 16.5° and 12.1° in Z respectively. The difference can be attributed to the soft tissue artefact and gives an indication of the amplitude of error that can occur when surface based sensors alone are employed to track the scapula [30, 93-94]. The Z axis was the main axis about which motion took place and therefore it is expected that the effect of the soft tissue artefact would be more evident for this axis as it is associated with a larger range of motion.

From Figure 5.16 it can also be seen that the scapula location predicted by the regression equation is in relatively good agreement with actual scapula location as measured by the IMU attached to the scapula locator (SL-IMU). The maximum and RMS error between predicted and measured scapula location angles were 1.1° and 0.6° about the X-axis, 2.4° and 1.0° about the Y-axis, and 8.7° and 3.5° about the Z-axis respectively.

Table 5.2 shows the representative regression equation for each axis for each of the five quasi-static trials. Here, the H and S terms of the best fit polynomials (Table 5.2) represent the angular velocity measured by the humeral and scapula sensors' gyroscopes, $a_0...a_n$ represents the best fit coefficients obtained from the quasi-static tests and finally $SL_{\theta_x, \theta_y, \theta_z}$ represents the scapula orientation as if it was measured with the scapular locator device, for each axis.

Table 5.2. Best fit coefficients for the three axes of the porcine assessment.			
Table 5.2 a), Best fit coefficients for the X axis orientation (radians) for the porcine humerus and scapula of the five trials performed.			
Equation	$SL_{\theta x} = a_1 H + a_2 S$		
Coefficients	a_1	a_2	
Trial 1	-0.34	1.45	
Trial 2	-0.10	1.02	
Trial 3	0.42	0.39	
Trial 4	0.39	0.48	
Trial 5	0.22	0.70	
Equation	0.12	0.81	
Standard deviation (\pm)	0.33	0.44	
Table 5.2 b). Best fit coefficients for the Y axis orientation (radians) for the porcine humerus and scapula of the five trials performed.			
Equation	$SL_{\theta y} = a_0 + a_1 H + a_2 S$		
Coefficients	a_0	a_1	a_2
Trial 1	-0.234	0.416	-0.281
Trial 2	-0.103	0.043	1.334
Trial 3	-0.091	-0.126	1.380
Trial 4	-0.042	-0.755	2.165
Trial 5	-0.130	0.462	0.284
Average	-0.12	0.01	0.98
Standard deviation (\pm)	0.07	0.49	0.97
Table 5.2 c). Best fit coefficients for the Z axis orientation (radians) for the porcine humerus and scapula of the five trials performed.			
Equation	$SL_{\theta z} = a_0 + a_1 H + a_2 S$		
Coefficients	a_0	a_1	a_2
Trial 1	-4.978	1.452	-1.315
Trial 2	0.234	0.312	1.241
Trial 3	3.228	-0.123	3.022
Trial 4	5.606	-0.945	3.998
Trial 5	-2.581	0.522	-0.469
Average	0.30	0.24	1.30
Standard deviation (\pm)	4.27	0.88	2.25

5.4.2 Stage Two: Dynamic Trials

The results of the trials to investigate the effect that the skin, tissue and muscle artefact can induce in measurements when the scapula is tracked under dynamic conditions are shown in Figure 5.17.

The ‘intact’ measurements are the readings taken from the scapula IMU (S-IMU) mounted on the skin surface for the scenario where the skin, subcutaneous fat and muscle layers covering the scapula were present (Figure 5.17). The ‘Muscle’ measurements are the readings from the same IMU (S-IMU) when located on the surface of the muscle following removal of the epidermal, dermal and subcutaneous tissue layers covering the scapula. These results are compared with the actual scapula orientation (‘actual/screws’) as determined by the screw mounted IMU attached directly to the scapula (SC-IMU) during the ‘intact’ tests.

From Figure 5.17 it can be seen that the soft tissue artefact is substantial in the ‘intact’ test, as indicated by the difference between the ‘intact’ results and the actual/screws results, with the difference being as much as 3.4° or 4.1% about the Z axis, the main axis about which motion took place, compared to the actual scapula location. The difference resulting from the artefact is reduced considerably following excision of the epidermal, dermal and subcutaneous fat layers, with the maximum difference between the ‘muscle’ results and the actual/screws results being 0.5° or 0.6% for the Z axis, confirming that the majority of the contribution to the soft tissue artefact comes from the epidermal, dermal and subcutaneous fat layers.

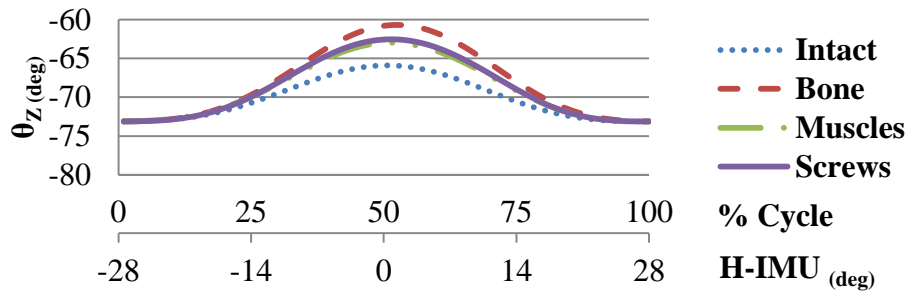
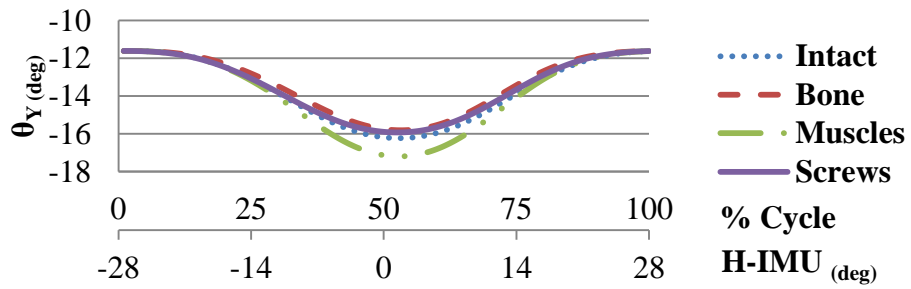
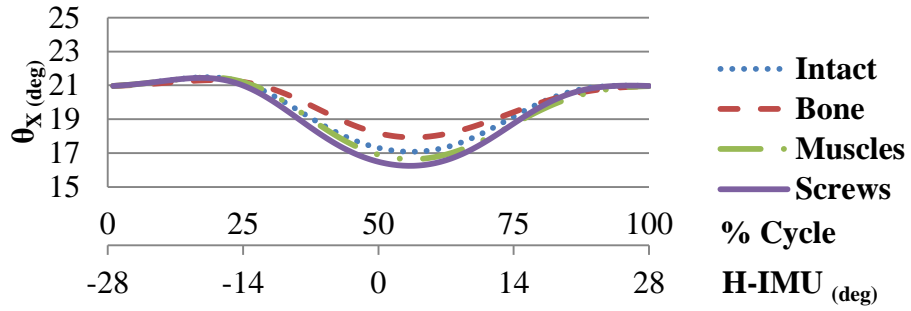


Figure 5.17. Orientations in the global axes (θ_x , θ_y and θ_z) over the cycle for dynamic conditions, measured by IMUs positioned on the skin (intact), bone, muscles and the screws (real orientation of the scapula). The second abscissa (bottom) represents the mean changes in angular orientation of the humeral sensor (H-IMU) in the three scenarios described with a maximum change of 28° and a standard deviation of $\pm 2.5^\circ$.

5.4.3 Comparison of Predicted and Measured Scapula Location in Dynamic Trials

Figure 5.18 shows the scapula location as predicted by the regression equation at points throughout the dynamic cycle alongside actual location as measured by the screw mounted IMU attached directly to the scapula (SC-IMU). Upon inspection of Figure 5.18 it can be seen that predicted and actual scapula orientation are in relatively good agreement. The maximum error between predicted and measured location are 0.25° or 1.0%, 0.2° or 1.3%, and 2.0° or 2.4% in the X, Y and Z axes respectively. The corresponding RMS errors in X, Y and Z are 0.1° , 0.15° and 1.0° respectively. The largest differences between predicted and measured scapula location occur about the Z axis, the main axis about which motion took place, at the higher humeral elevations when the effect of the skin and soft tissue movement with respect to the underlying bone would have been greater.

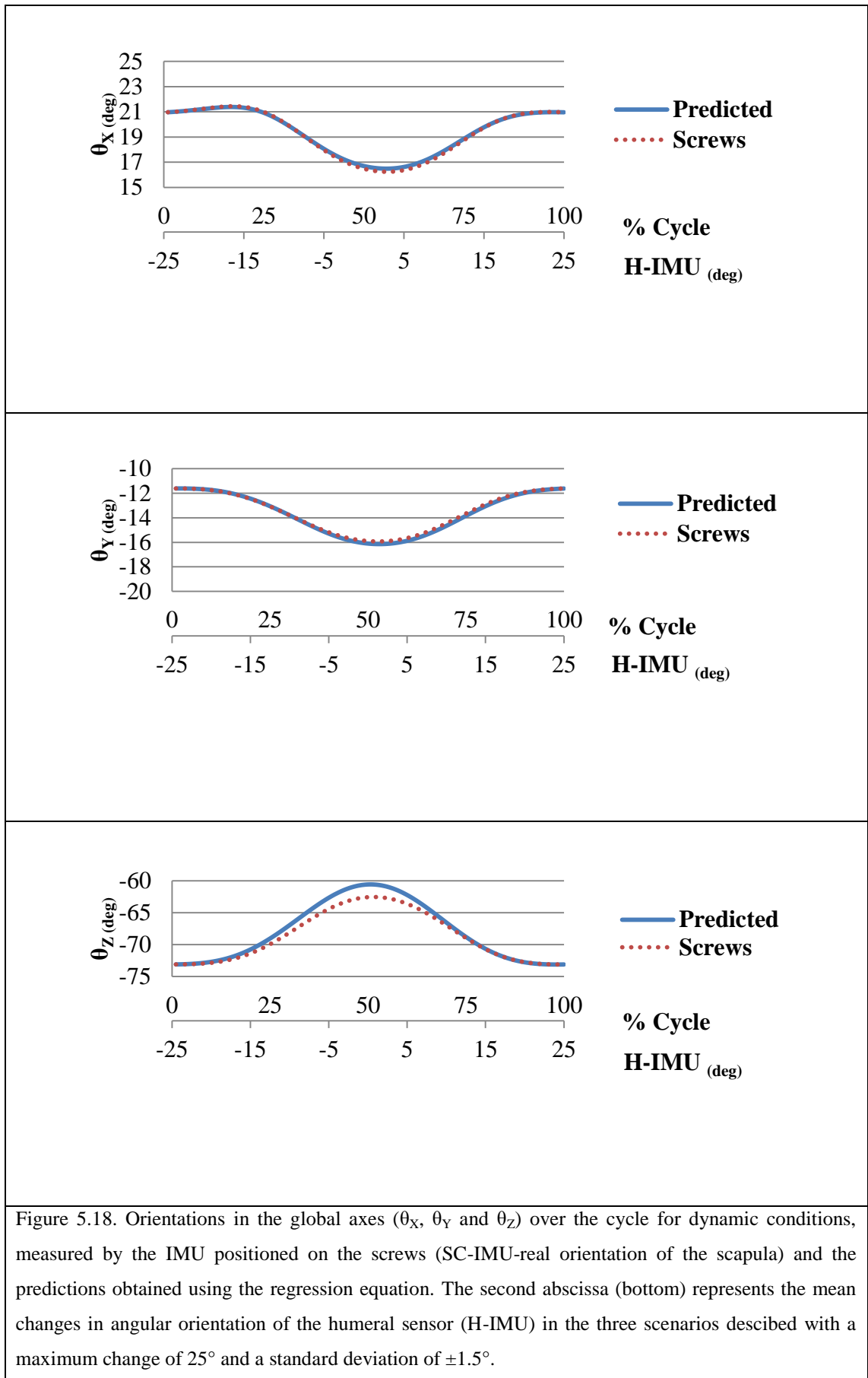


Figure 5.18. Orientations in the global axes (θ_x , θ_y and θ_z) over the cycle for dynamic conditions, measured by the IMU positioned on the screws (SC-IMU-real orientation of the scapula) and the predictions obtained using the regression equation. The second abscissa (bottom) represents the mean changes in angular orientation of the humeral sensor (H-IMU) in the three scenarios described with a maximum change of 25° and a standard deviation of $\pm 1.5^\circ$.

5.4.4 Assessing the Dynamic Pattern

The averaged scapular orientation and the screw sensor orientation were plotted for the three scenarios (Figure 5.19, Figure 5.20 and Figure 5.21) under dynamic conditions. The behaviour of the measured orientation of the scapula surrounded by different tissue layers (as measured by the S-IMU sensor) and the real motion of the scapula measured by the SC-IMU sensor for the X, Y and Z axes are presented in Figure 5.19, Figure 5.20 and Figure 5.21 (the orientations are plotted in degrees). Different tilts in the slope for the three different tests performed can be seen in the figures.

Figure 5.19 shows the results for the X axis. For scenario a) the soft tissues are causing the skin based sensor to under estimate the scapula orientation, while for scenario b) muscle and bone, the results are still close to the 45° in the tilt. As the pig leg increases its range of motion the orientation, without the skin influence, the sensor measurements tends to overestimate the scapula orientation, this could be explained by the fluttering and damping effect that the skin could have on the sensor for this axis. Even though the difference in the slope tilt, similarities in the motion pattern can be seen, however differences in the motion pattern increase as the humeral elevation increases.

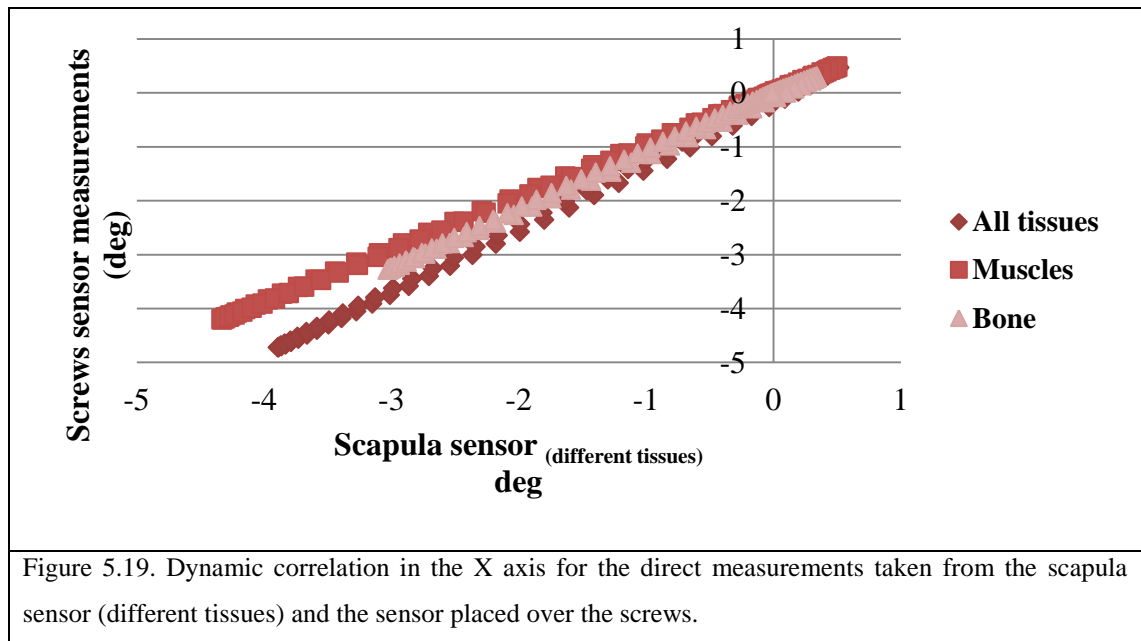


Figure 5.20 shows the results for the Y axis. For scenarios a) and b) again the surface mounted measurements under estimate the scapula orientation. Although the actual scapula location and scapula location as measured by the surface bases sensor and

follow a similar pattern, the difference between the two increases as the humeral elevation increases.

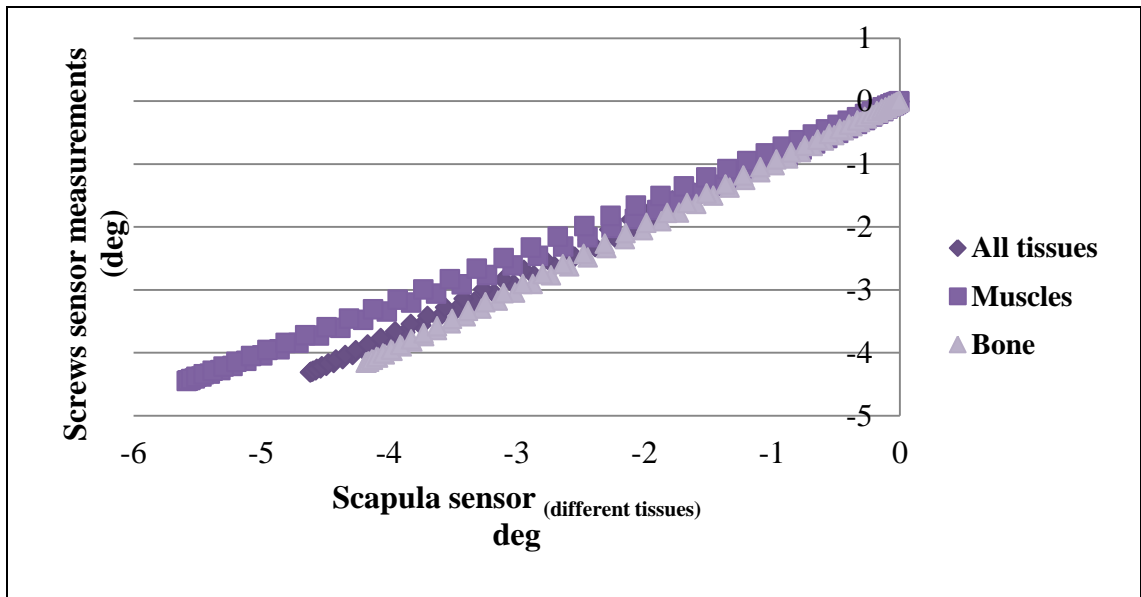


Figure 5.20. Dynamic correlation in the Y axis for the direct measurements taken from the scapula sensor (different tissues) and the sensor placed over the screws.

Figure 5.21 shows the results for the main axis of motion (Z), where it can be seen that for scenarios a) and b) the surface based sensor over estimates the real orientation of the scapulas measured by the SC-IMU sensor. This effect is more evident as the humeral range of motion increases.

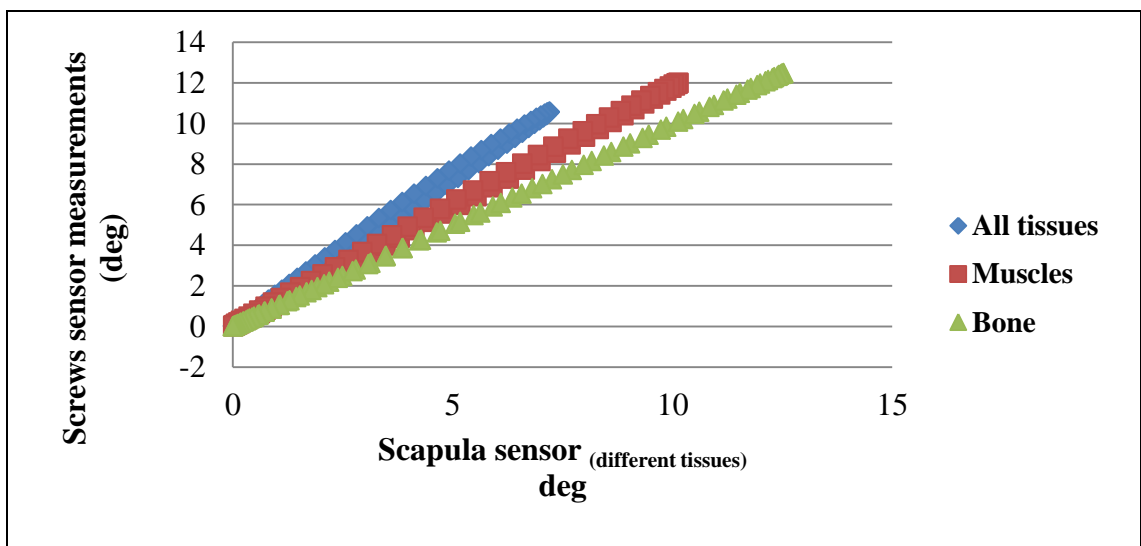


Figure 5.21. Dynamic correlation in the Z axis for the direct measurements taken from the scapula sensor (different tissues) and the sensor placed over the screws.

CHAPTER VI: GENERAL REPRESENTATIVE POLYNOMIAL FROM QUASI-STATIC MEASUREMENTS, HUMAN APPROACH

6.1 Introduction

The tests on the porcine cadaver detailed in Chapter V confirmed that skin based scapula tracking techniques can lose accuracy particularly at high humeral elevations and as the range of motion of the joint increases due to the soft tissue artefact, however, by using the methodology described in Chapter IV this error can be reduced.

In this section an approach to measure the scapula orientation in human subjects under quasi-static conditions by applying the methodology described in stage one of Chapter IV is presented in this chapter. The aim is to obtain a general representative equation from quasi-static trials, which can then be used under dynamic conditions to accurately track the scapula. In order to accomplish the aim different and consecutive humeral elevations under quasi-static conditions were recorded for two different humeral motions (flexion-extension and abduction-adduction) in three different trials. First, two trials were undertaken in order to obtain data to generate a regression type equation. A third trial was then performed to assess the accuracy of the equation.

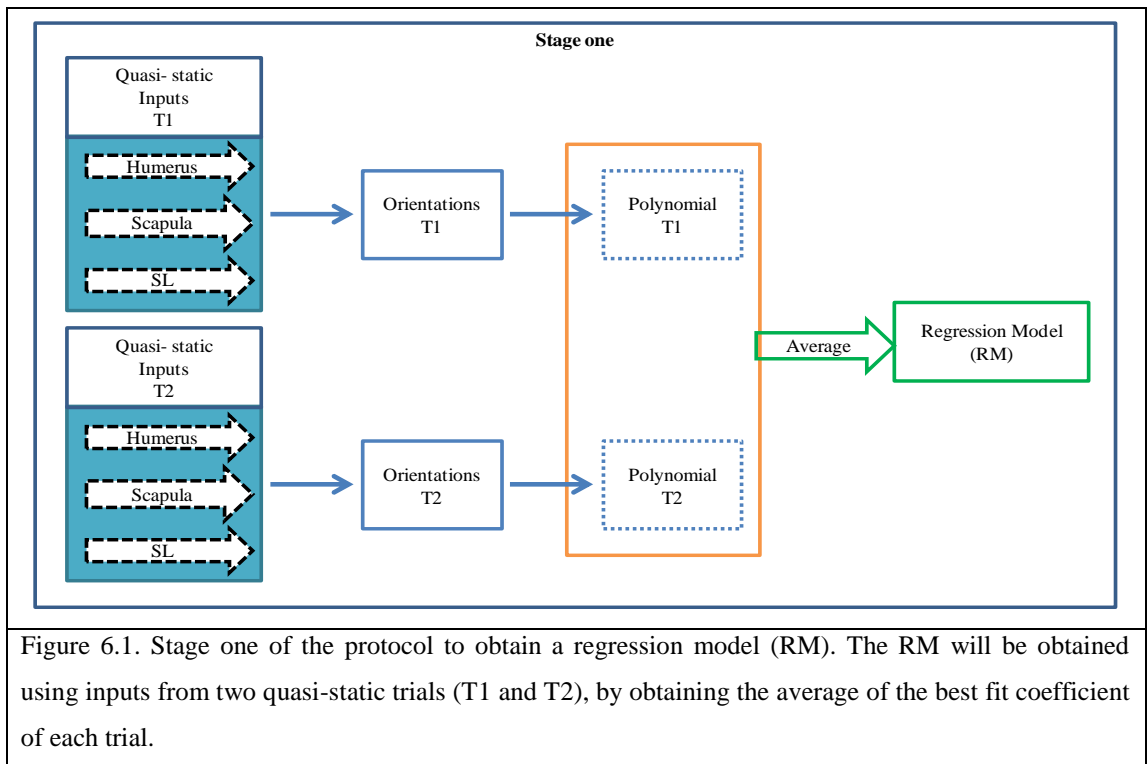
6.2 Materials and Methods

6.2.1 Methodology Overview: Obtaining a Polynomial from Quasi-static Measurements

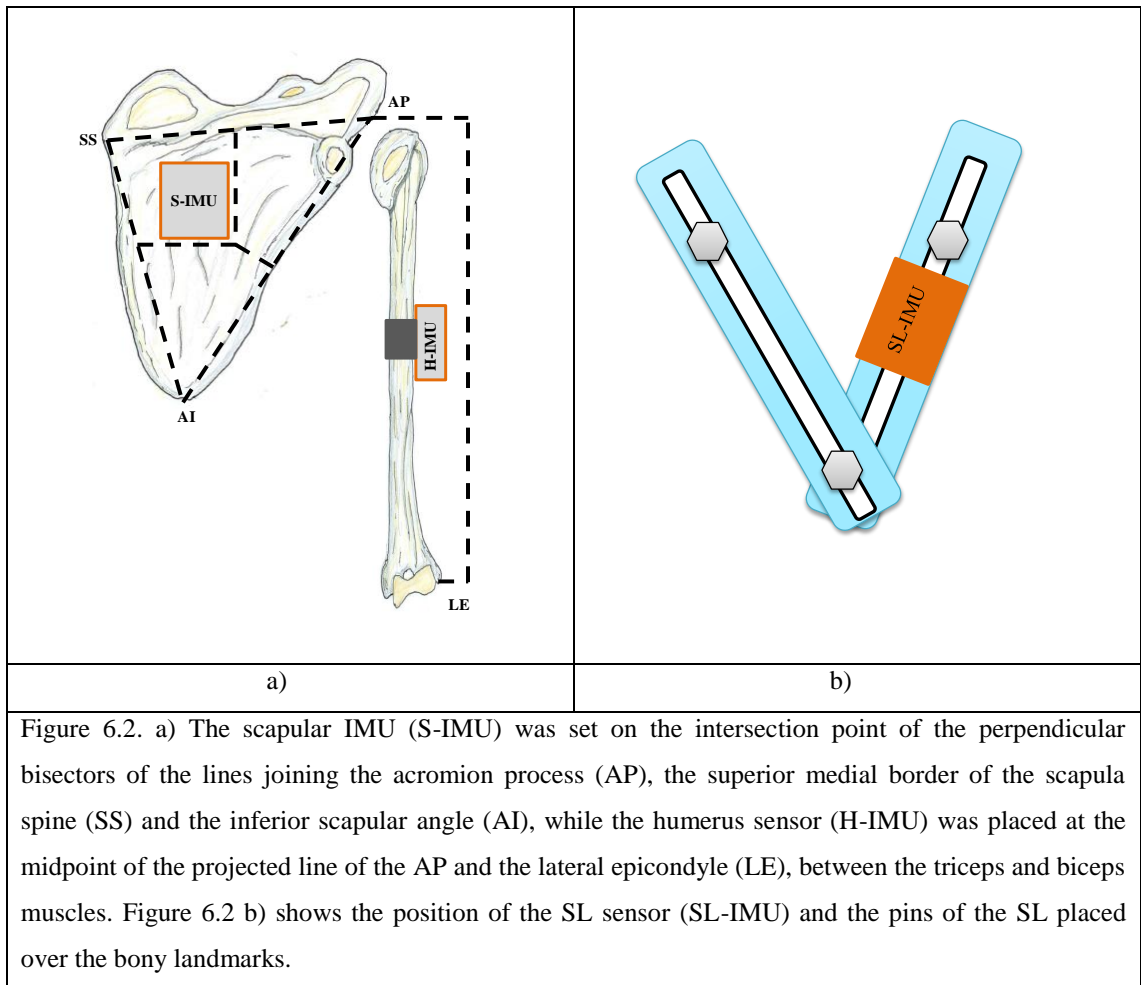
The protocol presented in this section was developed to obtain a general regression equation that allowed the correction of the error generated by the soft tissue surrounding the scapula under dynamic conditions by using non-invasive electromagnetic devices attached directly to skin of human subjects. This protocol uses accelerometry, to measure humeral and scapular orientation.

The experimental protocol consisted of multiple quasi-static humeral elevations and depressions in both a sagittal (flexion-extension) and a frontal plane (abduction-adduction) over three trials. Three IMUs and one scapula locator were used to record orientation data. The protocol is separated into two stages; an outline of the protocol is described as follows:

(i) Stage One: quasi-static motion. In this stage a regression equation is obtained from the first two trials (Figure 6.1) performed by each participant by obtaining the mean regression coefficients for the regression equation from the first two trials.



The regression equation is obtained by using the data from three IMUS, humerus (H-IMU), scapula (S-IMU) and one SL (SL-IMU), Figure 6.2.



(ii) Stage Two: Level of agreement. Having established the regression equation from stage one, the data measured from the humerus and scapula during a third trial are used in the regression equation to predict the orientation of the scapula. The new scapula orientation predictions are then compared with the actually scapula orientation as obtained from the scapula locator IMU (SL-IMU), in the third trial, see Figure 6.3.

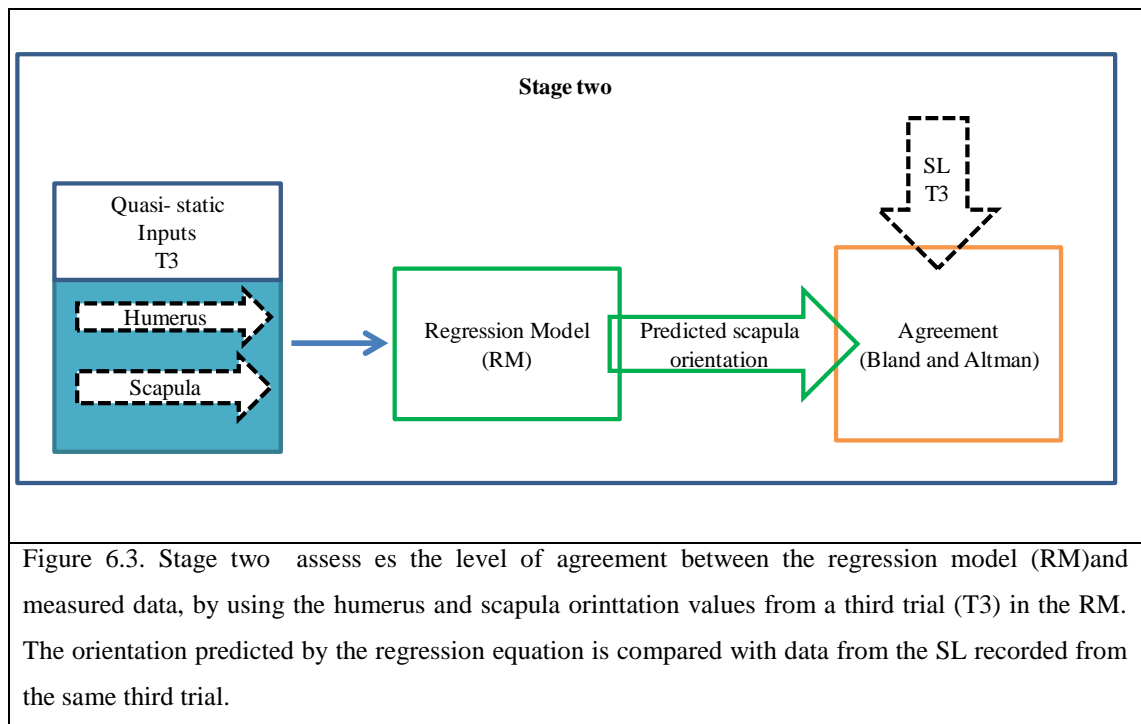


Figure 6.3. Stage two assess es the level of agreement between the regression model (RM)and measured data, by using the humerus and scapula orintntation values from a third trial (T3) in the RM. The orientation predicted by the regression equation is compared with data from the SL recorded from the same third trial.

6.2.2 Subjects

Ten healthy right handed male participants (mean age 28.1 ± 2.2 years, mean body mass 76.2 ± 11.8 kg, and mean height 1.74 ± 0.05 m) with no history of neuromuscular or musculoskeletal impairment participated in this study. One participant withdrew.

Written informed consent was obtained from the participants and the experimental procedures were evaluated and approved by the University of Manchester Research Ethics Committee, Ref 12143 (see Appendix A1).

6.2.3 Calibration

Before data collection started a heading reset was applied to the three MTw sensors [153]. The MTw sensors were used to measure the orientation of the scapula, scapula locator and humerus. The IMU calibration procedure employed was the same as that used calibration in the drawer test discussed in section 4.3.2 on a flat surface, allowing both the global Z axis (Figure 6.4) and the gravitational acceleration vector to remain vertical [153].

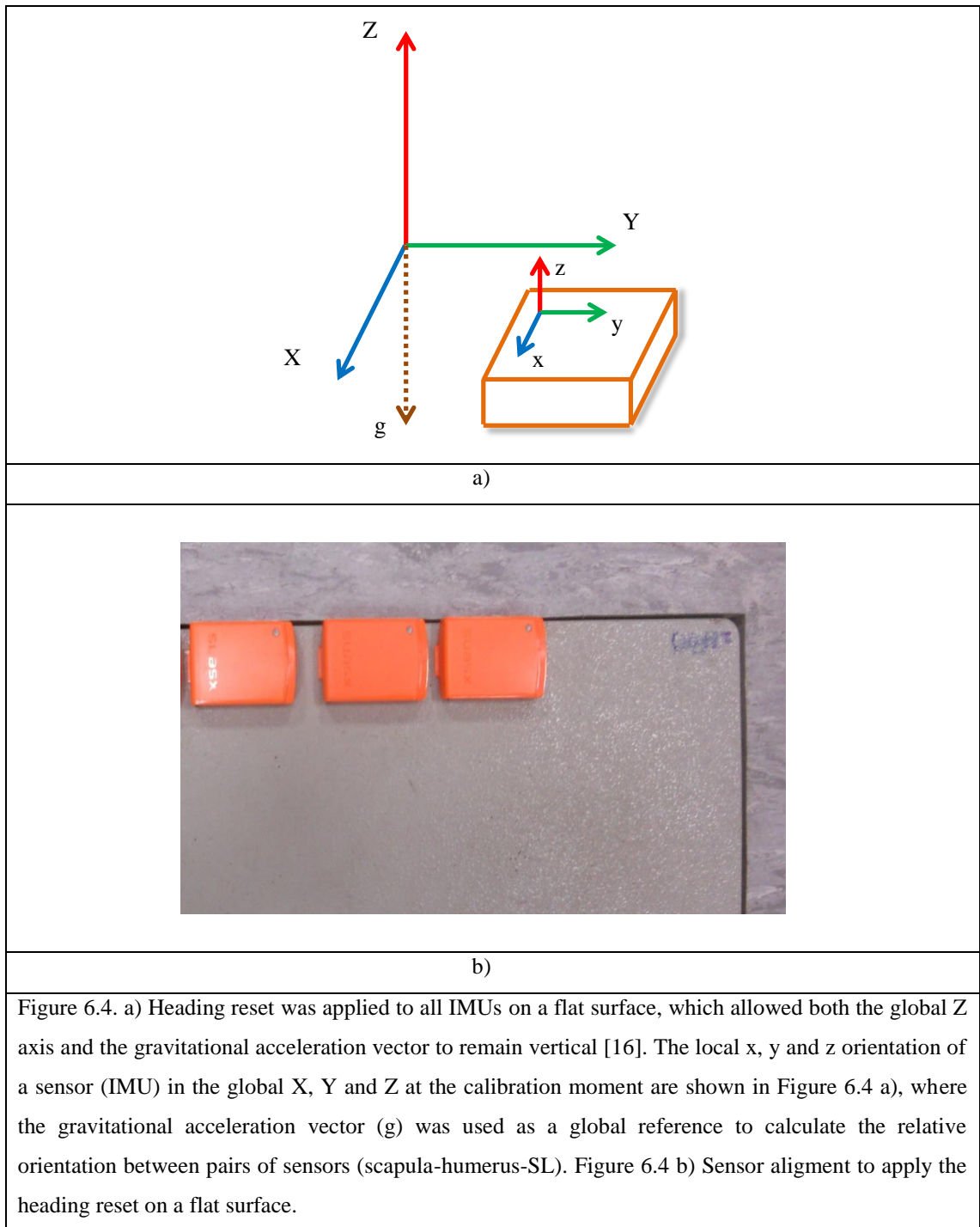


Figure 6.4. a) Heading reset was applied to all IMUs on a flat surface, which allowed both the global Z axis and the gravitational acceleration vector to remain vertical [16]. The local x, y and z orientation of a sensor (IMU) in the global X, Y and Z at the calibration moment are shown in Figure 6.4 a), where the gravitational acceleration vector (g) was used as a global reference to calculate the relative orientation between pairs of sensors (scapula-humerus-SL). Figure 6.4 b) Sensor alignment to apply the heading reset on a flat surface.

6.2.4 Experimental Set up

Participants were asked to stand comfortably in the fundamental position with their eyes fixed on a point directly in front of them and with their thumbs pointing forward (Figure 6.5), and the elbow fully extended. A total of 38 different consecutive positions were recorded for each trial at approximate intervals of 10° for each position. A complete trial consisted of 19 positions for arm elevation until the arm reached its maximum

amplitude followed by 19 positions for arm depression in both abduction-adduction and flexion-extension.



Figure 6.5. Participant in the fundamental position and SL placement with the three sensor used in the test.

After a training period to ensure that the participant understood the motion and could performed it repeatedly, the participants performed three trials following the procedure shown in Figure 6.6. Once the participants could comfortably and reliably produce the required motion the sensors were attached.

The scapular sensor (S-IMU) was set on the intersection point of the perpendicular bisectors of the lines joining the three bony landmarks, as described in Figure 6.2. The humeral sensor (H-IMU) was placed between the triceps and biceps muscles, at the midpoint between the bony landmarks.

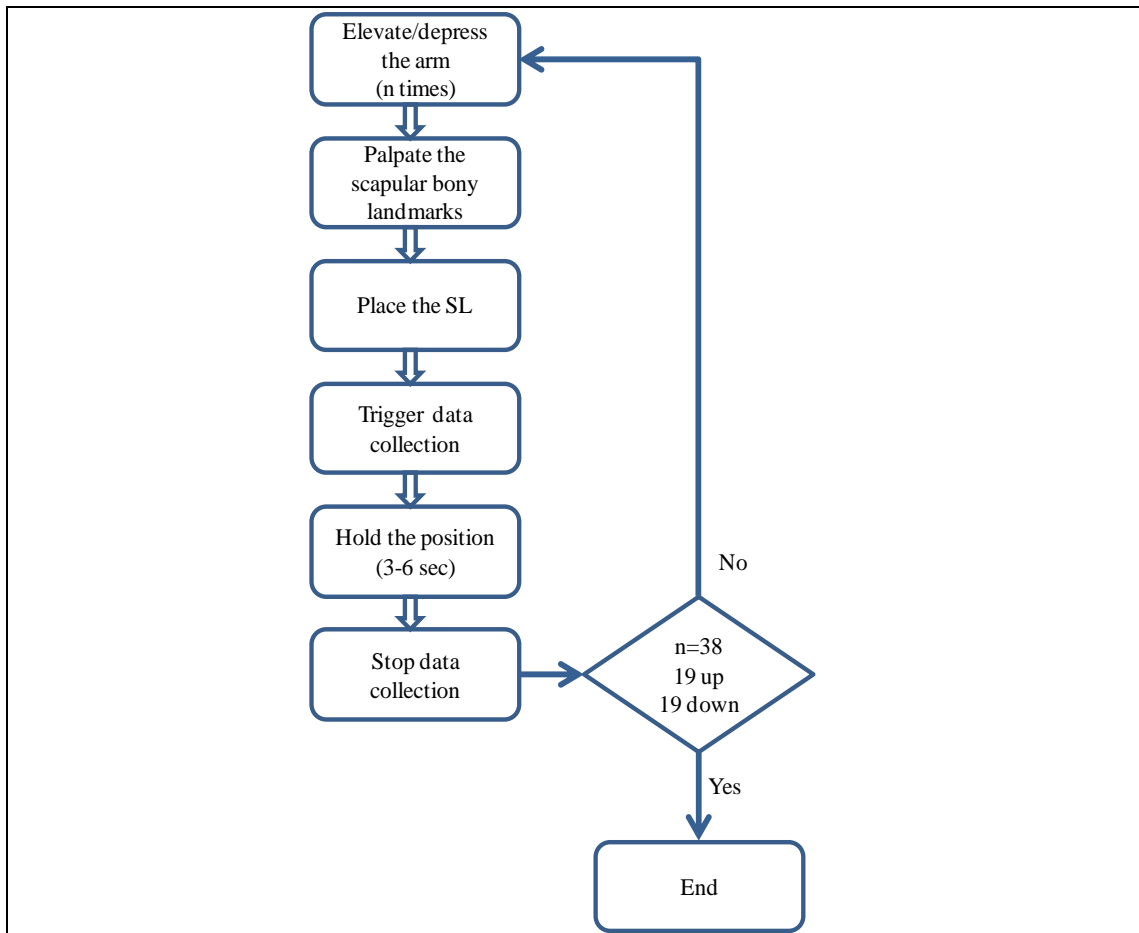


Figure 6.6. Procedure used in the trials. Three trials were performed by each participant in flexion-extension and abduction-adduction recording the humerus, scapula, and the SL orientations.

The SL sensor (SL-IMU) was aligned along one of the SL arms, parallel to the lateral border of the scapula as shown in Figure 6.2. The scapula and SL sensors were attached with double sided hypoallergenic tape, while the humerus sensor was attached using a Velcro strap.

6.2.5 Data Collection

Two IMUs were used to measure the orientation of the scapula (S-IMU) and the humerus (H-IMU) directly while a third IMU was placed over one arm of the scapula locator jig (SL-IMU) Figure 6.2. The IMU sensors measured orientation in three local axes (x, y, z) and the relative orientation between pairs of sensors (scapula-humerus-SL) was calculated using the gravitational acceleration vector (\vec{g}) as a global reference, Figure 6.4.

6.2.6 Data Processing

In order to obtain a mathematical expression that estimated the scapular orientation (S_{θ}) in different humeral orientations (H_{θ}) as if it were measured by the Scapula Locator (SL_{θ}), the global orientation of each sensor was calculated.

For stage one, the scapular and humeral orientation were fitted to the SL orientation using a best fit polynomial for the data from each of trials one and two (T1 and T2), see Figure 6.1. For stage two, the mean coefficients obtained from the first two trials were used in the regression equation along with the relative orientation of the humerus and the data from the sensor placed directly over the scapula (see Figure 6.3) to predict the scapular orientations of the third trial.

The level of correlation (r^2), and the standard deviation of the differences between the predicted and observed data (σ) were calculated, and the agreement between the measured and predicted SL orientation was assessed using the Bland and Altman method [157-158].

The Bland and Altman method [157-158] assesses the level of agreement between two series of data or measurements, by plotting the series data differences against their mean. This methodology also allows the clinical importance to be assessed by plotting the 95% confidence limits.

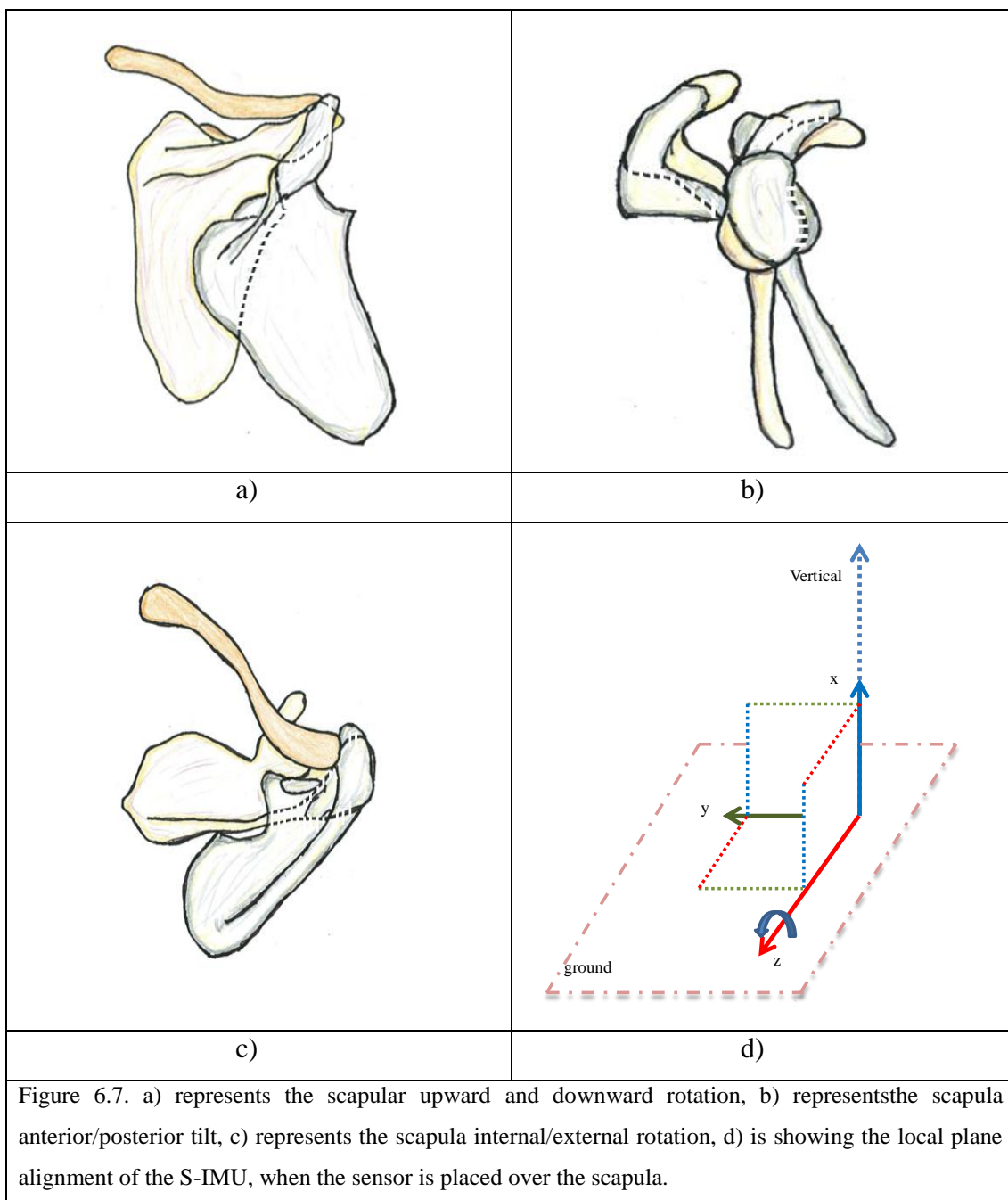
6.2.7 Obtaining the Orientations

The humeral orientation ($H_{\theta_x, \theta_y, \theta_z}$), scapula orientation ($S_{\theta_x, \theta_y, \theta_z}$) and SL orientation ($SL_{\theta_x, \theta_y, \theta_z}$) about the local x, y and z axes and the vertical were obtained using direction cosines (Figure 4.6) from Eq 4.2, for all the trials.

6.3 Shoulder Results

The results represent the angle between an axis and a plane, in this case the sensor axis and the planes formed by the gravitational acceleration vector (the vertical); it is important to understand what this information represents in terms of anatomical motion of the scapula.

The local xz plane (Figure 6.7, d)) orientation with respect to the vertical (human sagittal plane) represents the scapula internal/external rotation (Figure 6.7, c)). The internal external rotation is quite limited by the anatomical restrictions. The angle formed by the xz plane and the vertical is similar to a rotation about the global Z axis described in Figure 6.4.



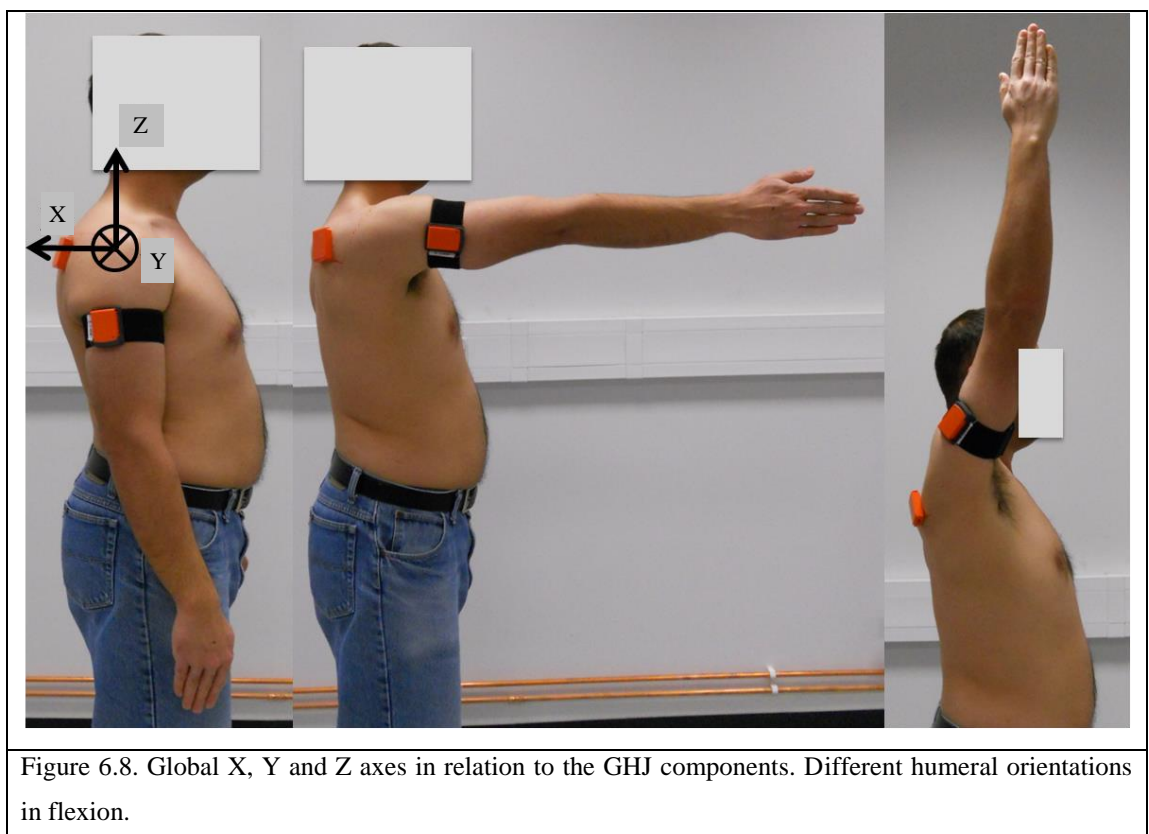
The local xy plane (Figure 6.7, d)) orientation with respect to the vertical (human coronal plane) represents the (anterior/posterior, Figure 6.7, b)) scapula tilt. The angle

formed by the xy plane and the vertical is similar to a rotation about the global Y axis, see Figure 6.4.

The local yz plane (Figure 6.7, d)) orientation with respect to the vertical (human transverse plane) represents scapula rotation (Figure 6.7, a)), it could be considered that this plane is almost parallel to the ground; the orientation of this plane is dependent on the orientation on the other two planes. The angle formed by the yz plane and the vertical is similar to a rotation about the global X axis as Figure 6.4 shows.

6.3.1 Humeral Flexion-Extension

Scapula and humerus orientation in humeral flexion-extension relative to the global gravitational acceleration vector X, Y and Z axes (Figure 6.4) is shown in Figure 6.8, where the main rotation occurs about the Y axis (medio-lateral).



The coefficients ‘ $a_1 \dots a_n$ ’ for the regression model used to describe the quasi-static orientation of the scapula were obtained for each trial and averaged to obtain a representative expression for the participant according to the procedure described in

section 4.2.1. Figure 6.9 shows the mean values from the first two trials performed in stage one from one participant.

Figure 6.9 (θ_x) shows the maximum arm elevation reached in the test was 133° and the maximum standard deviation value was $\pm 6.4^\circ$ at 70° humeral elevation. The maximum standard deviation for the scapula orientation measurements (S-IMU) was $\pm 6.1^\circ$ and occurred between 80° and 90° humeral elevation. On the other hand, the maximum standard deviation found for the scapula locator (SL-IMU), $\pm 4.6^\circ$, occurred at around 90° humeral elevation. Upon inspection of Figure 6.9 (θ_x) it can be seen that the scapula sensor shows a continuous change in scapula orientation (about 50°) up to 120° humeral elevation. However, the SL measured no change in scapula orientation until close to 90° humeral elevation starting at 70° humeral orientation representing a 15° of change in the scapula orientation and then a 30° change over the remainder cycle of humeral elevation/depression, in the opposite direction to the skin sensor data for the yz local plane with respect to the vertical. Figure 6.9 (θ_x) also shows a similar pattern in the upward and downward rotation of the scapula measured by the scapula sensor and the SL. The small changes in the pattern presented by the SL in the downward rotation of the scapula can be attributed to the influence of gravity on the scapula muscles that generates a smoother curve. The shape pattern in θ_x is highly dependent on the orientation of the other two planes, as well as the rotation and translation of the scapula under the soft tissues surrounding the scapula. This result suggests that the morphological characteristics of each participant are important.

Figure 6.9 (θ_y) shows that the maximum standard deviation for the anterior/posterior tilt of the scapula orientation measurements (S-IMU) was $\pm 6.1^\circ$ and occurred at around 80° and 90° humeral elevation. On the other hand, the maximum standard deviation found for the scapula locator (SL-IMU), $\pm 3.4^\circ$, occurred at around 90° of humeral elevation. Upon inspection of Figure 6.9 (θ_y) it can be seen that the scapula sensor and the SL sensor indicate a continuous change in scapula orientation (about 40°) up to 130° of humeral elevation. Figure 6.9 (θ_y) also shows a similar pattern in the anterior/posterior tilt of the scapula measured by the scapula sensor and the SL for the humeral flexion-extension motion. The offset between the two measurements was expected for the local xy plane and it is consistent through the entire test; this offset reflects the differences in orientation between the sensor directly attached to the scapula and the sensor placed

over the SL, which are mainly generated by the skin and subsequent tissue layers i.e. the muscles and fat.

Figure 6.9 (θ_z) shows that the maximum standard deviation for the internal/external rotation of the scapula orientation (S-IMU) measurements was $\pm 6.1^\circ$ and occurred around 50° and 60° of humeral elevation. On the other hand, the maximum standard deviation found for the scapula locator (SL-IMU), $\pm 5.4^\circ$ occurred at the same humeral elevation. Upon inspection of Figure 6.9 (θ_z) it can be seen that the scapula sensor and the SL sensor shows a continuous change in scapula orientation (about 20°) up to 130° of humeral elevation. Figure 6.9 (θ_z) also shows a similar pattern in the internal/external rotation of the scapula as measured by the scapula sensor and the SL for the humeral flexion-extension motion. As expected, the measurements for the local xz plane from the sensor directly attached to the scapula and the sensor placed over the SL are similar in magnitude for all humeral elevations, as Figure 6.9 (θ_z) shows. The internal and external rotation is quite limited by the anatomical restrictions.

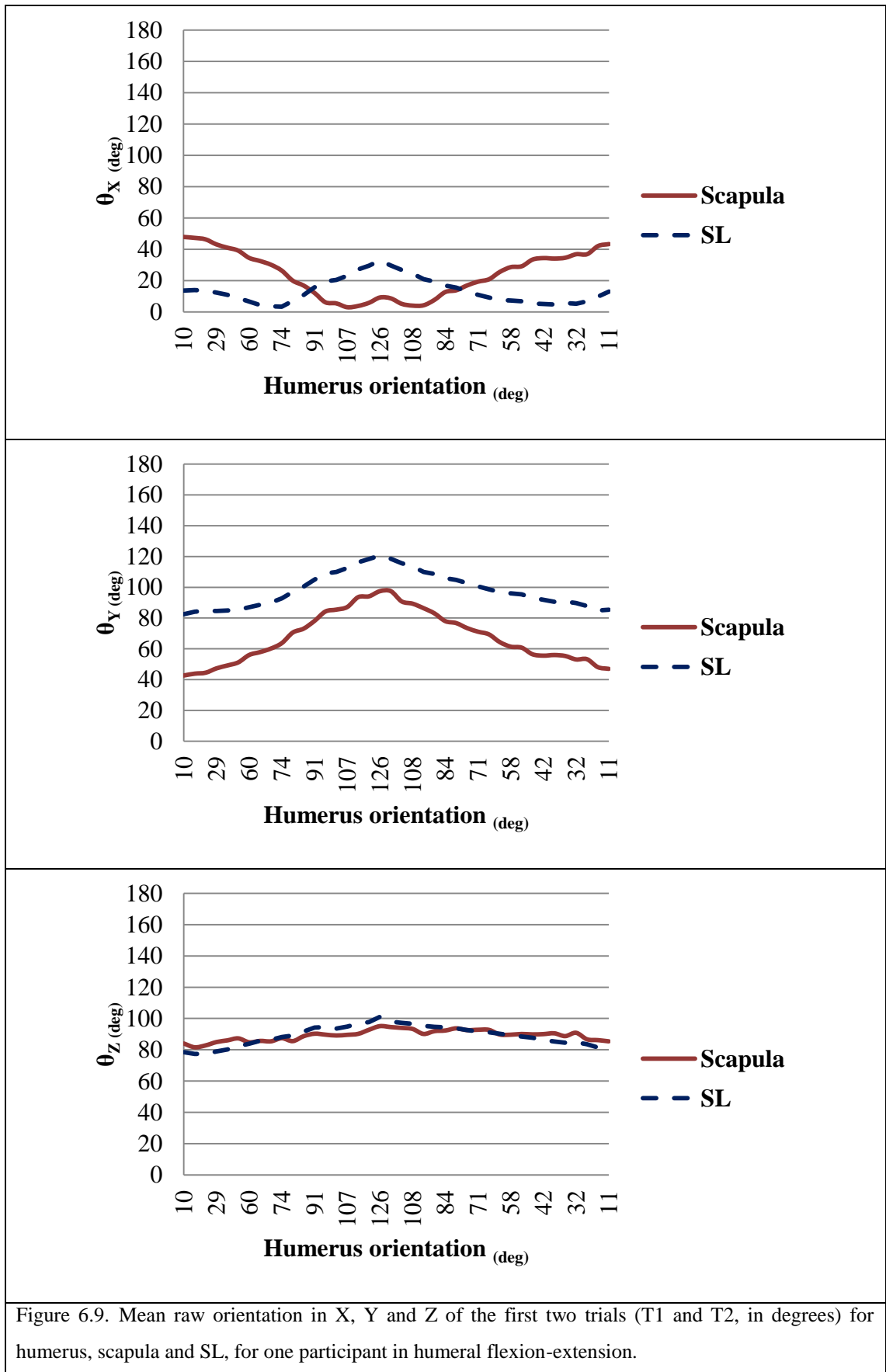


Figure 6.9. Mean raw orientation in X, Y and Z of the first two trials (T1 and T2, in degrees) for humerus, scapula and SL, for one participant in humeral flexion-extension.

The mathematical expressions used to predict the orientation of the scapula for each axis (SL_{θ_x} , SL_{θ_y} , SL_{θ_z}) are shown in Table 6.1 a), 6.1 b) and 6.1 c), for one participant, where H and S represent the orientation of the humerus and the scapula in radians for the X (Table 6.1 a)), Y (Table 6.1 b)) and Z (Table 6.1 c)) axes. The coefficients ‘a...a_n’ in the mathematical expression were obtained for each trial (T1 and T2) then averaged to obtain a representative expression for the participant; this was then used to predict the scapular orientation of a third trial in humeral flexion-extension.

Table 6.1. Best fit coefficients for the three axes of one participant for humeral flexion-extension.							
Table 6.1 a). Best fit coefficients for the X axis orientation (radians) for the humerus and scapula of Trials 1 and 2 for one of the participants and the average coefficient used in Trial 3.							
Equation	$SL_{\theta_x}=a+a_1H^3+a_2H^2+a_3H+a_4S^3+a_5S^2+a_6S$						
Coefficients	a	a ₁	a ₂	a ₃	a ₄	a ₅	a ₆
Trial 1	0.8510	0.0851	-0.5522	0.1692	0.2218	-2.6884	3.8316
Trial 2	0.8112	-0.1410	-0.3304	0.1207	0.9815	-6.5280	8.3609
Average	0.8311	-0.0280	-0.4413	0.1449	0.6017	-4.6082	6.0962
Table 6.1 b). Best fit coefficients for the Y axis orientation (radians) for the humerus and scapula of Trials 1 and 2 for one of the participants and the average coefficient used in Trial 3.							
Equation	$SL_{\theta_y}=a+a_1H+a_2S$						
Coefficients	A		a ₁		a ₂		
Trial 1	-1.4393		0.1319		1.3517		
Trial 2	-1.4162		0.1145		1.3603		
Average	-1.4277		0.1232		1.3560		
Table 6.1 c). Best fit coefficients for the Z axis orientation (radians) for the humerus and scapula of Trials 1 and 2 for one of the participants and the average coefficient used in Trial 3.							
Equation	$SL_{\theta_z}=a+a_1H+a_2S$						
Coefficients	A		a ₁		a ₂		
Trial 1	0.4986		0.1154		0.5959		
Trial 2	0.5392		0.1234		0.5685		
Average	0.5189		0.1194		0.5822		

The resultant average equations (Table 6.1) were used to predict the scapula orientation of the third trial in humeral flexion-extension as shown in Figure 6.10.

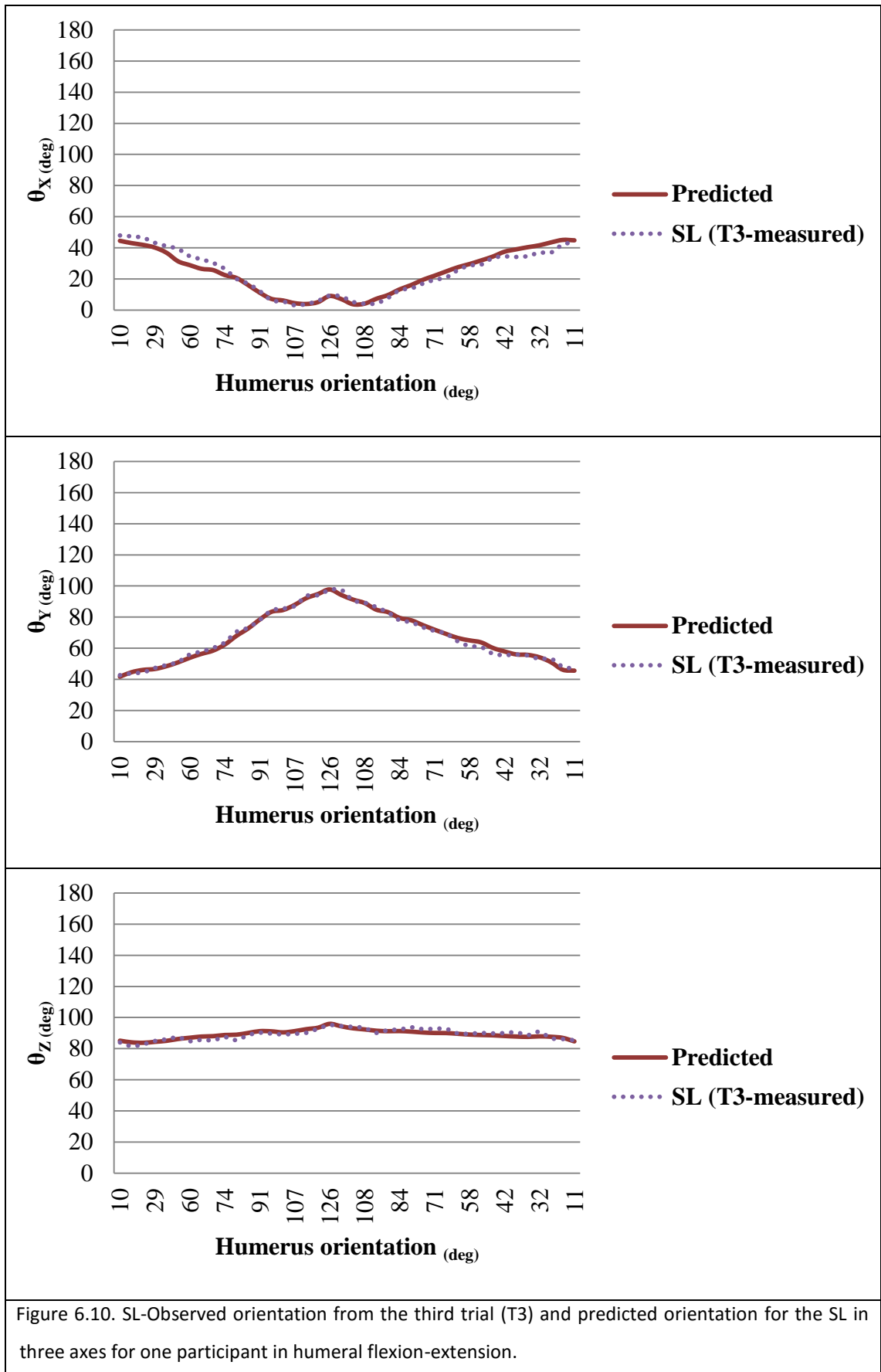


Figure 6.10. SL-Observed orientation from the third trial (T3) and predicted orientation for the SL in three axes for one participant in humeral flexion-extension.

Figure 6.10 shows the predicted results using the representative polynomial and the measurements of the third trial (T3), where it can be seen that predicted scapula orientation is in very good agreement with measured orientation, which indicates that, for the subject considered, the regression equation obtained is capable of predicting scapula orientation in humeral flexion-extension to good accuracy.

6.3.2 Humeral Abduction-Adduction

Scapula and humerus orientation in humeral abduction-adduction relative to the global X, Y and Z axes is shown in Figure 6.11, where the main rotation occurs in the X axis (anterior/posterior).

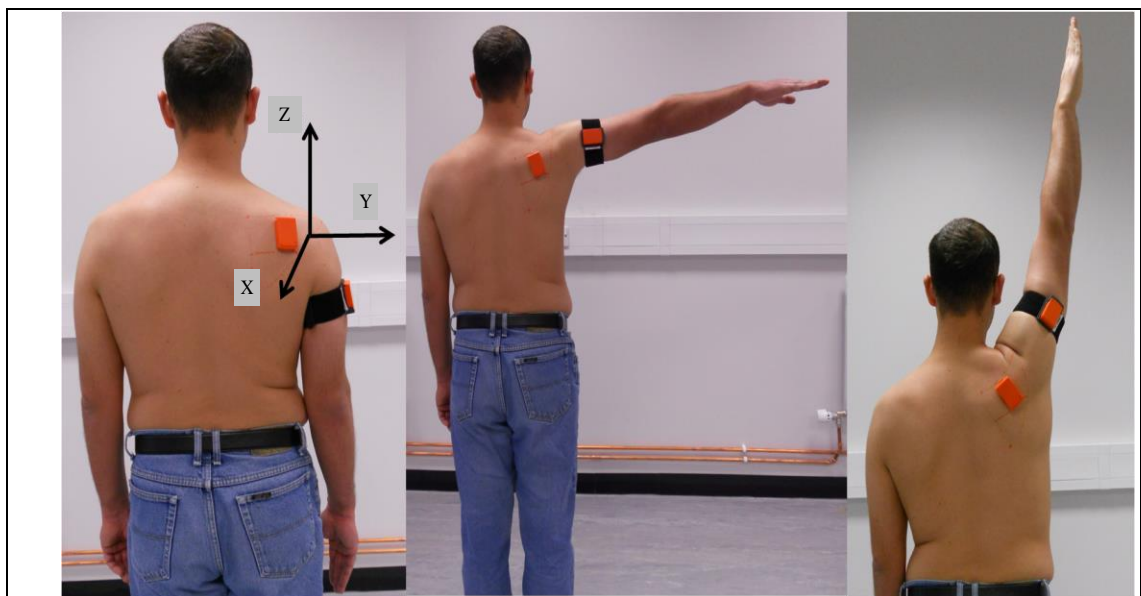


Figure 6.11. Global X, Y and Z axes in relation to the GHJ components. Different humeral orientations in abduction-adduction are shown: at rest position, one position around middle range of humeral abduction-adduction and one in an overhead position.

Figure 6.12 shows the mean values from the first two trials performed in stage one for the humeral abduction-adduction motion, that were used to obtain the coefficients ‘a...a_n’ for the representative mathematical expression for the participant as was described in section 4.2.1.

Figure 6.12 (θ_x) shows the maximum arm elevation reached in the test was 144° and the maximum standard deviation value was $\pm 7.7^\circ$ at 60° of humeral elevation. The maximum standard deviation for the scapula orientation measurements (S-IMU) was

$\pm 7.1^\circ$ and occurred between 130° and 150° of humeral elevation. On the other hand, the maximum standard deviation found for the scapula locator (SL-IMU), $\pm 5.9^\circ$, occurred around 60° humeral elevation. Upon inspection of Figure 6.12 (θ_x) it can be seen that the scapula sensor (S-IMU) shows a continuous change in scapula orientation (about 50°) up to 120° humeral elevation. However, the SL measured no change in scapula orientation until close to 90° humeral elevation and then a 20° change over the remainder motion, in the opposite direction to the skin sensor data for the yz local plane with respect to the vertical. Figure 6.12 (θ_x) also shows a similar pattern in the upward and downward rotation of the scapula measured by the scapula sensor and the SL. The small changes in the pattern presented by the SL in the downward rotation of the scapula can be attributed to the influence of gravity work on the scapula muscles that generates a smoother curve. The shape pattern in θ_x is highly dependent on the orientation of the other two planes, as well as the rotation of the scapula under the soft tissues surrounding the scapula. This result suggests that the morphological characteristics of each participant are important.

Figure 6.12 (θ_y) shows that the maximum standard deviation for the anterior/posterior tilt of the scapula orientation (S-IMU) measurements was $\pm 7.6^\circ$ and occurred at around 130° and 150° humeral elevation. On the other hand the maximum standard deviation found for the scapula locator (SL-IMU) was $\pm 6.7^\circ$ which occurred around 90° of humeral elevation. Upon inspection of Figure 6.12 (θ_y) it can be seen that the scapula sensor and the SL sensor indicate a continuous change in scapula orientation (about 40°) up to 140° of humeral elevation. Figure 6.12 (θ_y) also shows a similar pattern in the anterior/posterior tilt of the scapula as measured by the scapula sensor and the SL for the humeral abduction-adduction motion. The difference between the two measurements was expected for the local xy plane and it is consistent throughout the entire test; this offset is expected because it reflects the differences in orientation between the sensor attached directly to the scapula and the sensor placed over the SL, where the differences are mainly generated by the skin and subsequent tissues layer i.e. the muscles and fat.

Figure 6.12 (θ_z) shows that the maximum standard deviation for the internal/external rotation of the scapula orientation (S-IMU) measurement was 5.3° and occurred above 90° humeral elevation. The maximum standard deviation found for the scapula locator (SL-IMU) was $\pm 7.0^\circ$ which occurred at the same humeral elevation. Figure 6.12 (θ_z)

also shows a similar pattern in the internal/external rotation of the scapula measured by the scapula sensor and the SL for the humeral flexion-extension motion. As expected, the measurements for the local xz plane from the sensor directly attached to the scapula and the sensor placed over the SL are similar in magnitude over most of the humeral orientation. However, Figure 6.12 (θ_z) shows a difference between scapula sensor and SL sensor measurements of around 15° when the humeral elevation starts; this difference reduces as the humeral elevation reaches its maximum elevation. The internal and external rotation is quite limited by the anatomical restrictions, and for the humeral abduction-adduction the soft tissues have a major impact on the measurements. Despite this, the scapula sensor and the SL sensor measurement patterns remain similar throughout the test.

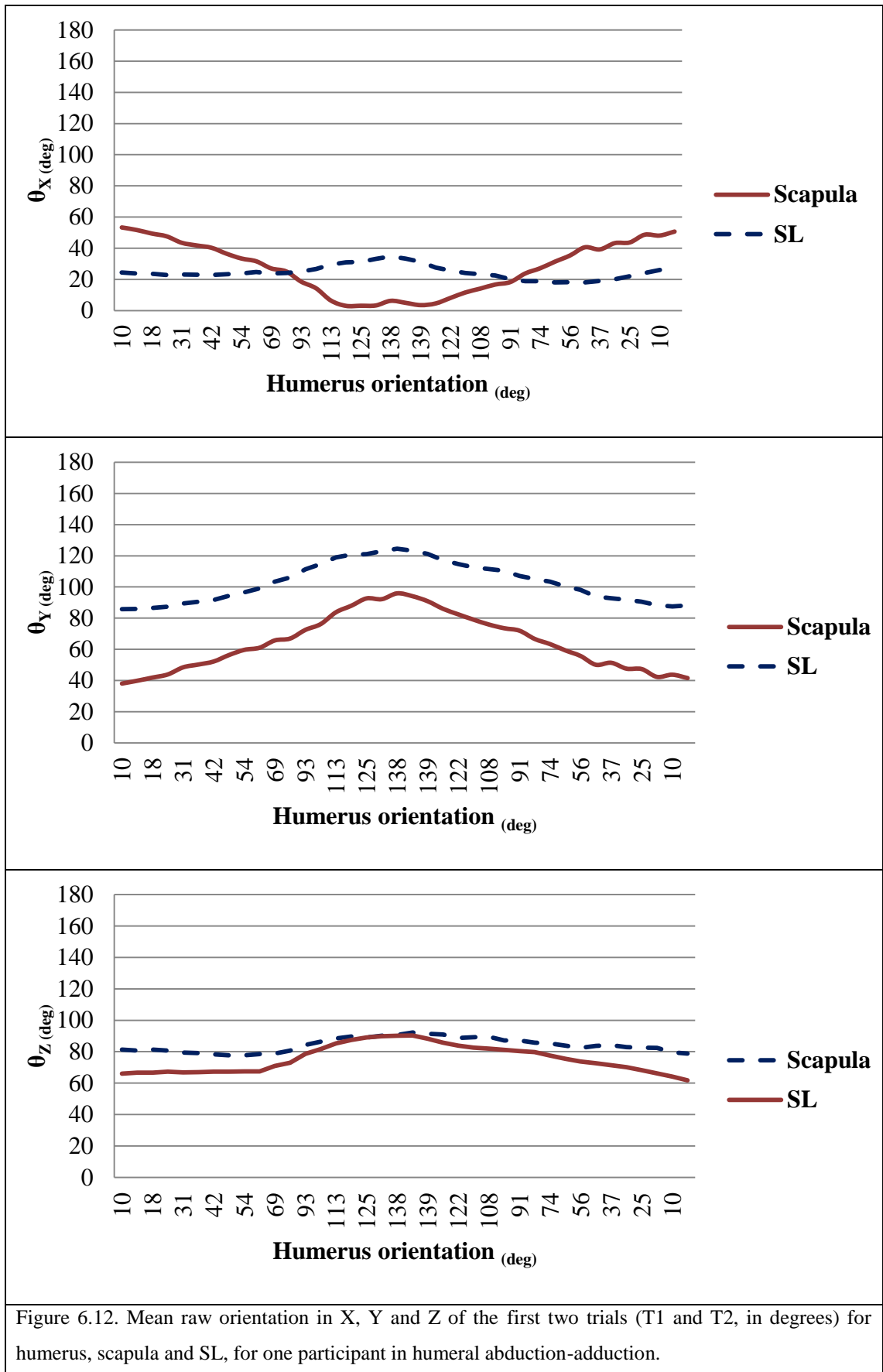


Figure 6.12. Mean raw orientation in X, Y and Z of the first two trials (T1 and T2, in degrees) for humerus, scapula and SL, for one participant in humeral abduction-adduction.

The mathematical expressions used to determine the orientation of the scapula are shown in Table 6.2 a), 6.2 b) and 6.2 c) where H and S represent the orientation of the humerus and the scapula in radians for the X (Table 6.2 a)), Y (Table 6.2 b)) and Z (Table 6.2 c)) axes in humeral abduction-adduction, for one participant and $SL_{\theta_x, \theta_y, \theta_z}$ represents the scapula orientation as if it was measured with the scapular locator device, for each axis. The coefficients ‘a...a_n’ in the mathematical expression for the polynomial were obtained for each trial (T1 and T2), then averaged to obtain a representative equation for the participant; this was then used to predict the scapular orientation of a third trial.

Table 6.2. Best fit coefficients for the three axes of one participant for humeral abduction-adduction.					
Table 6.2 a), Best fit coefficients for the X axis orientation (radians) for the humerus and scapula of Trials 1 and 2 for one of the participants and the average coefficient used in Trial 3.					
Equation	$SL_{\theta_x}=a+a_1H^2+a_2H+a_3S^2+a_4S$				
Coefficients	a	a ₁	a ₂	a ₃	a ₄
Trial 1	0.9422	-0.4030	0.0008	0.5238	-0.8959
Trial 2	1.9059	-0.6217	0.1144	-3.6613	3.4194
Average	1.4241	-0.5124	0.0576	-1.5687	1.2618
Table 6.2 b). Best fit coefficients for the Y axis orientation (radians) for the humerus and scapula of Trials 1 and 2 for one of the participants and the average coefficient used in Trial 3.					
Equation	$SL_{\theta_y}=a+a_1H+a_2S$				
Coefficients	a	a ₁	a ₂		
Trial 1	-1.2828	0.0051	1.3448		
Trial 2	-1.4385	-0.1037	1.5398		
Average	-1.3606	-0.0493	1.4423		
Table 6.2 c). Best fit coefficients for the Z axis orientation (radians) for the humerus and scapula of Trials 1 and 2 for one of the participants and the average coefficient used in Trial 3.					
Equation	$SL_{\theta_z}=a+a_1H+a_2S$				
Coefficients	a	a ₁	a ₂		
Trial 1	0.6792	0.1376	0.4823		
Trial 2	0.7065	0.1165	0.4727		
Average	0.6928	0.1270	0.4775		

The resultant average equations were used to predict the scapula orientation of the third trial in humeral abduction-adduction as shown in Figure 6.13.

Figure 6.13 shows the predicted results using the representative polynomial and the measurements of the third trial (T3), where it can be seen that predicted scapula

orientation is in very good agreement with measured orientation, which indicates that, for the subject considered, the regression equation obtained is capable of predicting scapula orientation in humeral abduction-adduction to good accuracy.

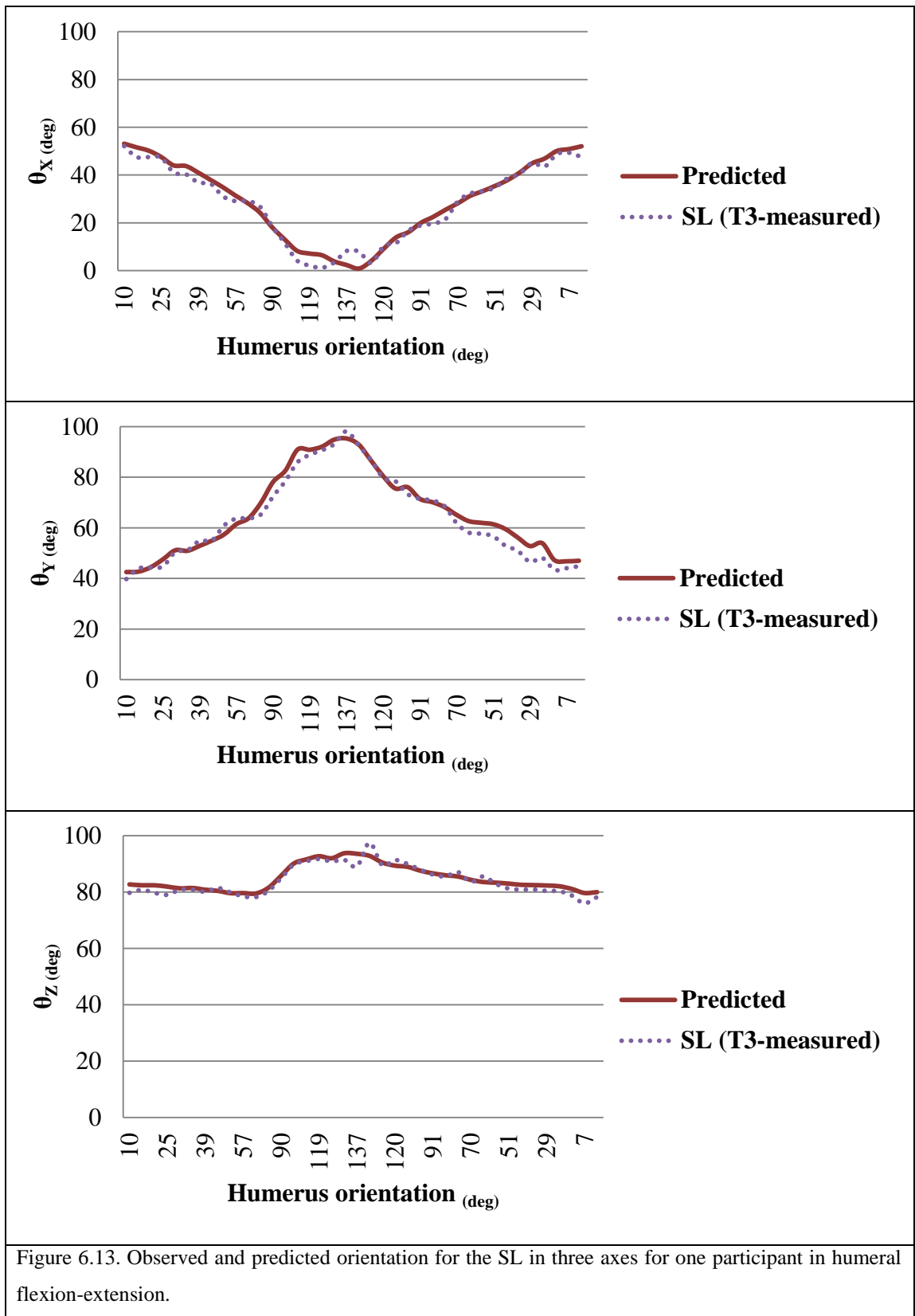


Figure 6.13. Observed and predicted orientation for the SL in three axes for one participant in humeral flexion-extension.

6.3.3 Control Group Results

The same analysis was applied to all nine subjects. The resultant regression equation obtained for each subject from the first two trials (stage one, described in section 6.2.1) was used to predict the scapula orientations of the subject in a third trial (stage two, described in section 6.2.1) for humeral flexion-extension. The results are presented in Table 6.3. Where H and S represent the orientation of the humerus and the scapula in radians for the X, Y and Z axes and $SL_{\theta_x, \theta_y, \theta_z}$ represents the scapula orientation as if it was measured with the scapular locator device, for each axis in humeral flexion-extension. The coefficients ‘a...a_n’ in the mathematical expression for the polynomial were obtained for each trial (T1 and T2) of each participant, then averaged to obtain a representative equation for each participant; this was then used to predict the scapular orientation of a third trial of each participant.

Table 6.3. Mean values of the best fit coefficients for the three axes from the first two trials for the nine participants in humeral flexion-extension. The coefficient values are in radians.							
Table 6.3 a). θ_x , for the humeral flexion-extension.							
Equation	$SL_{\theta_x}=a+a_1H^3+a_2H^2+a_3H+a_4S^3+a_5S^2+a_6S$						
Coefficients	a	a ₁	a ₂	a ₃	a ₄	a ₅	a ₆
P1	0.8311	-0.0280	-0.4413	0.1449	0.6017	-4.6082	6.0962
P2	0.8201	-0.5233	0.0820	-0.0021	1.5920	-7.1134	7.9642
P3	0.9398	-0.3600	0.0132	-0.0079	0.2071	-2.0545	2.4325
P4	1.1502	-0.1267	-0.1606	0.0416	-3.1888	8.4969	-7.5978
P5	0.6914	0.3652	-0.4374	0.0579	-1.3199	5.3952	-4.5055
P6	0.2213	0.2888	-0.6987	0.2070	4.1080	-8.3565	4.3461
P7	0.0629	-0.8516	0.0436	0.1404	17.4274	-85.9642	123.9587
P8	0.9418	-0.5511	0.0403	0.0324	-0.6207	0.9415	-0.8146
P9	2.0282	-0.9318	0.5783	-0.1847	-0.38	-5.1502	6.3049
Mean	0.854	-0.302	-0.109	0.048	2.047	-10.935	15.354
Standard deviation (±)	0.563	0.463	0.377	0.114	6.106	28.697	41.061
Table 6.3 b). θ_y , for the humeral flexion-extension.							
Equation	$SL_{\theta_y}=a+a_1H+a_2S$						
Coefficients	a	a ₁	a ₂				
P1	-1.4277	0.1232	1.3560				
P2	-1.2150	0.0104	1.3643				

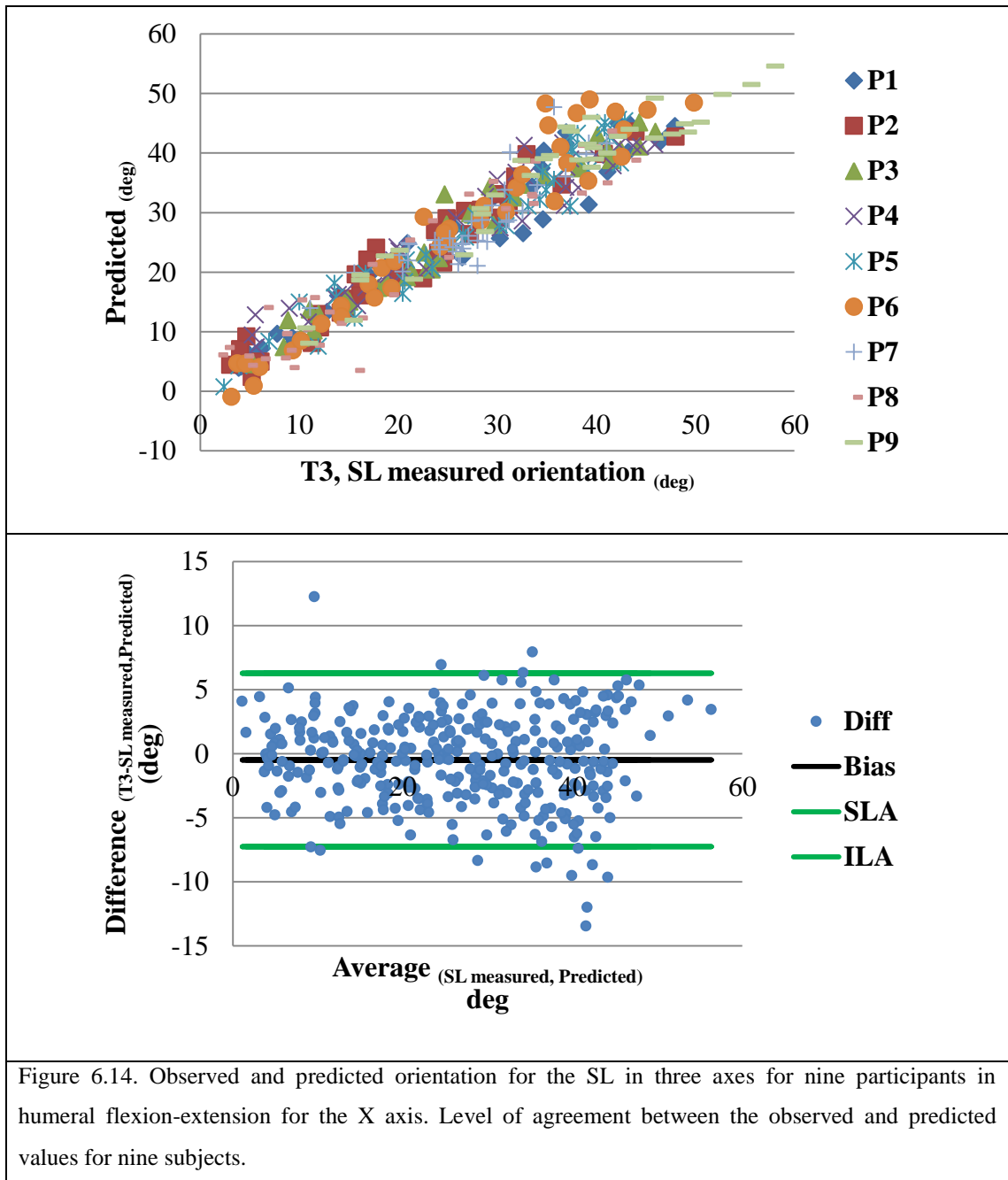
P3	-1.3021	0.0797	1.2351
P4	-1.3325	0.0747	1.2697
P5	-1.2785	0.1186	1.2126
P6	-1.0438	0.0429	1.1313
P7	-0.9369	0.0953	1.0705
P8	-0.9513	0.0700	1.1473
P9	-1.0714	-0.0331	1.2009
Mean	-1.173	0.065	1.221
Standard deviation (\pm)	0.177	0.051	0.099
Table 6.3 c). θ_z , for the humeral flexion-extension.			
Equation	$SL_{\theta_z}=a+a_1H+a_2S$		
Coefficients	a	a ₁	a ₂
P1	0.5189	0.1194	0.5822
P2	0.0498	0.4509	0.6097
P3	0.1262	0.3187	0.6769
P4	0.7767	0.0975	0.4373
P5	0.5503	0.2105	0.4700
P6	0.4631	0.0496	0.6821
P7	0.7362	0.0203	0.5002
P8	0.3225	0.2546	0.5908
P9	0.4755	0.2951	0.4267
Mean	0.447	0.202	0.553
Standard deviation (\pm)	0.246	0.142	0.098

The predicted and observed orientation for the SL, and the level of agreement between them for all nine subjects are presented in Figure 6.14 to Figure 6.16 for humeral flexion-extension.

Even though there are differences in the coefficient values of SL_{θ_x} between the participants (shown in Table 6.3), especially for participants P7 and P9, which increases the standard deviation value, the predicted and observed scapula locator orientation measurements presented in Figure 6.14 for all participants show a good level of agreement and correlation, which strongly indicates that the polynomials obtained are highly participant dependent.

Figure 6.14 shows the predicted scapula orientation obtained using the representative participant polynomial in Table 6.3 and the measured orientation for the third trial with

the SL (T3-SL measured orientation) for humeral flexion-extension for the nine participants in the global X-axis.



The r^2 value between the predicted orientation and the SL measured orientation of the third trial (T3) for all nine participants in θ_x is 0.90 which indicates the mean square deviation of the slope is acceptable, as Figure 6.14 shows. The agreement values indicate a BIAS line close to zero, with the scatter points distributed above and below of the line, which indicates no systematic error.

Figure 6.15 shows the predicted and measured orientation of trial three for the humeral flexion-extension motion for the nine participants in the global Y-axis.

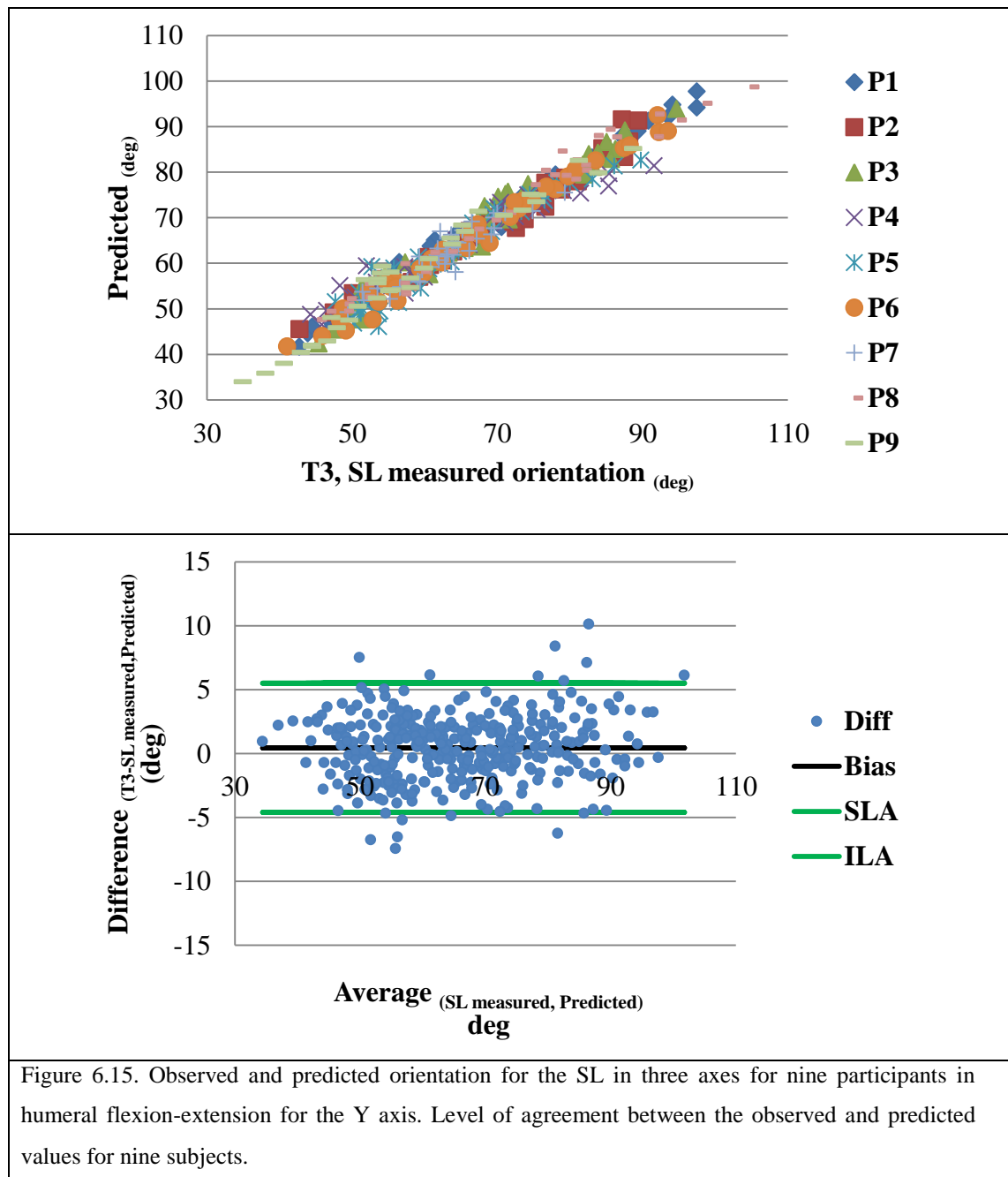


Figure 6.15. Observed and predicted orientation for the SL in three axes for nine participants in humeral flexion-extension for the Y axis. Level of agreement between the observed and predicted values for nine subjects.

The r^2 value between the predicted orientation and the SL measured orientation of the third trial (T3) for all nine participants in θ_Y is 0.95 which indicates the mean square deviation of the slope is acceptable, as Figure 6.15 shows. The agreement values indicate a BIAS line close to zero, with the scatter points distributed above and below the line, which indicates no systematic error.

Figure 6.16 shows the predicted and measured orientation of trial three for the humeral flexion-extension motion for the nine participants in the global Z-axis.

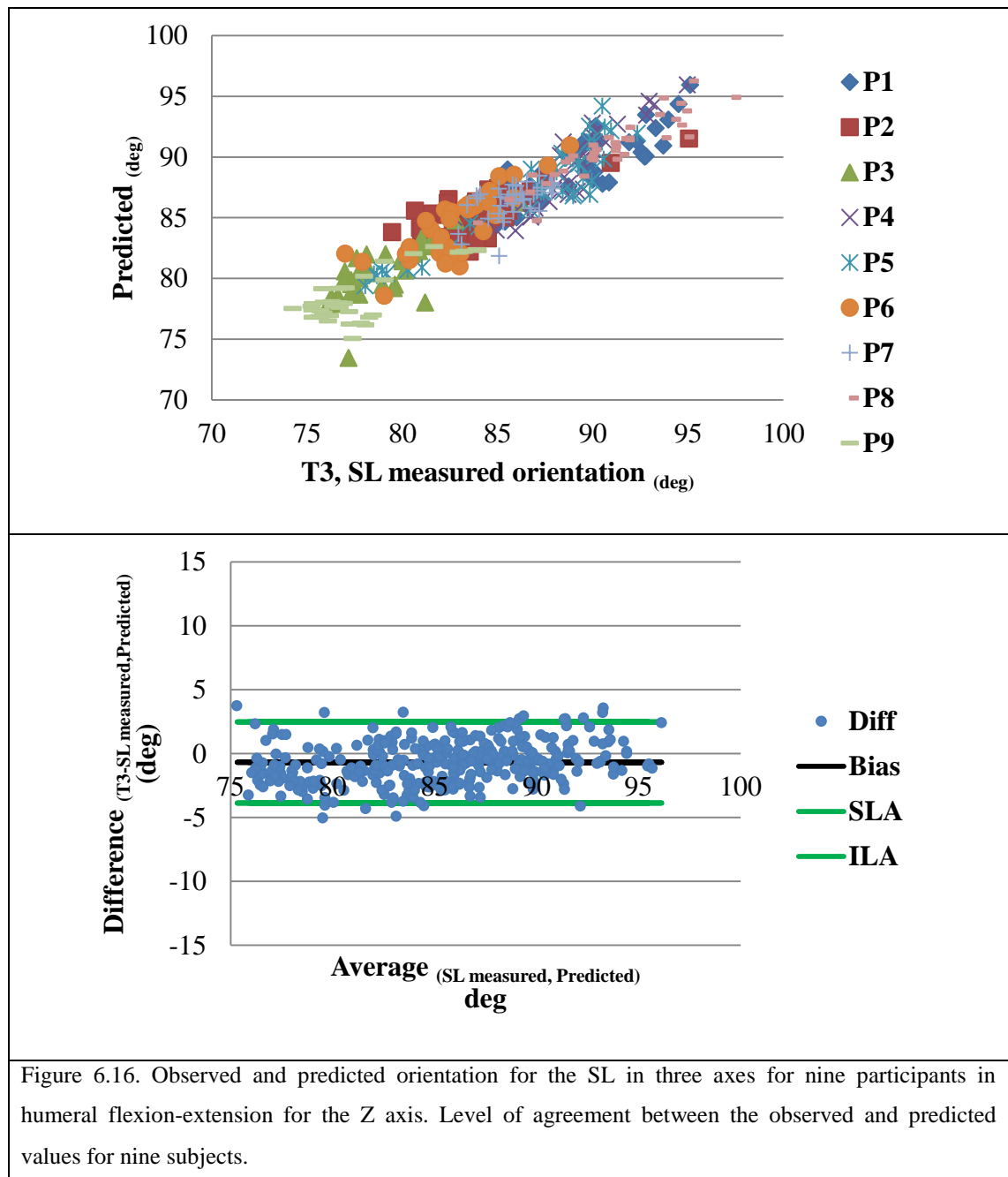


Figure 6.16. Observed and predicted orientation for the SL in three axes for nine participants in humeral flexion-extension for the Z axis. Level of agreement between the observed and predicted values for nine subjects.

The r^2 value between the predicted orientation and the SL measured orientation of the third trial (T3) for all nine participants in θ_z is 0.64 which indicates the mean square deviation of the slope or the level of correlation is not high. However, a low level of correlation is expected in θ_z due to the anatomical restrictions of the participants, the scapula translation and the surrounded soft tissues which complicates the measurement of the internal/external rotation of the scapula. The agreement values indicate a BIAS

line close to zero, with the scatter points distributed above and below the line, which indicate no systematic error, however it can be seen that the regression equation slightly under estimates scapula location between 75° and 80° and over estimates it above the 90°.

For the humeral abduction-adduction motion the representative equations used to predict the scapula orientations of the third trial are presented in Table 6.4. Where H and S represent the orientation of the humerus and the scapula in radians for the X, Y and Z axes in humeral abduction-adduction, for one participant and $SL_{\theta_x, \theta_y, \theta_z}$ represents the scapula orientation as if it was measured with the scapular locator device, for each axis. The coefficients ‘a...a_n’ in the mathematical expression for the polynomial were obtained for each trial (T1 and T2) of each participant, then averaged to obtain a representative equation for each participant; this was then used to predict the scapular orientation of a third trial of each participant.

Table 6.4. Mean values of the best fit coefficients for the three axes from the first two trials for the nine participants in humeral abduction-adduction. The coefficient values are in radians.					
Table 6.4 a). θ_x , for the humeral abduction-adduction.					
Equation	$SL_{\theta_x}=a+a_1H^2+a_2H+a_3S^2+a_4S$				
Coefficients	a	a ₁	a ₂	a ₃	a ₄
P1	1.4919	-0.6204	0.1801	-3.4177	3.3784
P2	0.7015	-0.9442	0.2850	2.1982	-3.7407
P3	2.7024	-0.5557	0.0895	-7.5469	7.6531
P4	0.5036	-0.8033	0.1993	2.7148	-3.5287
P5	1.9031	-0.1516	-0.1291	-5.6102	7.4354
P6	1.4241	-0.5124	0.0576	-1.5687	1.2618
P7	1.4654	-1.0325	0.3578	-1.0988	-0.7066
P8	1.0970	-0.9678	0.3233	-0.2298	-1.1004
P9	2.4837	-0.2512	-0.1397	-5.7043	5.4304
Mean	1.530	-0.649	0.136	-2.251	1.787
Standard deviation (±)	0.739	0.315	0.183	3.587	4.413
Table 6.4 b). θ_y , for the humeral abduction-adduction.					
Equation	$SL_{\theta_y}=a+a_1H+a_2S$				
Coefficients	a	a ₁	a ₂		
P1	-1.4275	0.0726	1.3507		
P2	-0.9206	0.0303	1.1269		
P3	-1.1196	0.1013	1.1600		

P4	-1.2098	0.446	1.2195
P5	-1.0944	0.1331	1.0521
P6	-1.3606	-0.0493	1.4423
P7	-0.8574	0.2577	0.7849
P8	-1.3349	0.0253	1.4133
P9	-1.1086	-0.0280	1.2574
Mean	-1.159	0.110	1.201
Standard deviation (\pm)	0.194	0.156	0.204
Table 6.4 c). θ_z for the humeral abduction-adduction.			
Equation	$SL_{\theta_z}=a+a_1H+a_2S$		
Coefficients	a	a ₁	a ₂
P1	1.005	0.0291	0.3558
P2	0.4927	0.2481	0.5259
P3	0.4889	0.0546	0.6576
P4	0.6928	0.1270	0.4775
P5	0.5033	0.1864	0.5301
P6	0.7933	0.0969	0.3954
P7	0.7467	0.0937	0.4191
P8	0.4121	0.2590	0.5317
P9	0.5728	0.1909	0.4895
Mean	0.634	0.143	0.487
Standard deviation (\pm)	0.190	0.156	0.204

Figure 6.17 to Figure 6.19 shows the predicted orientation obtained using the representative participant polynomial in Table 6.4 and the orientation measured by the SL (T3, SL measured orientation) for trial three for the humeral abduction-adduction motion for the nine participants.

Figure 6.17 shows the predicted and measured orientation of trial three for the humeral abduction-adduction for the nine participants in the global X-axis. The representative coefficients from the nine participants are more consistent for humeral abduction-adduction than for the humeral flexion-extension which is reflected in the lower standard deviation value.

The r^2 value between the predicted orientation and the SL measured orientation of the third trial (T3) for all nine participants in θ_x is 0.93 which indicates the mean square deviation of the slope is close to the 45° which is acceptable as Figure 6.17 shows. The

agreement values indicate a BIAS line close to zero, with the scatter points distributed above and below the line, which indicate no systematic error.

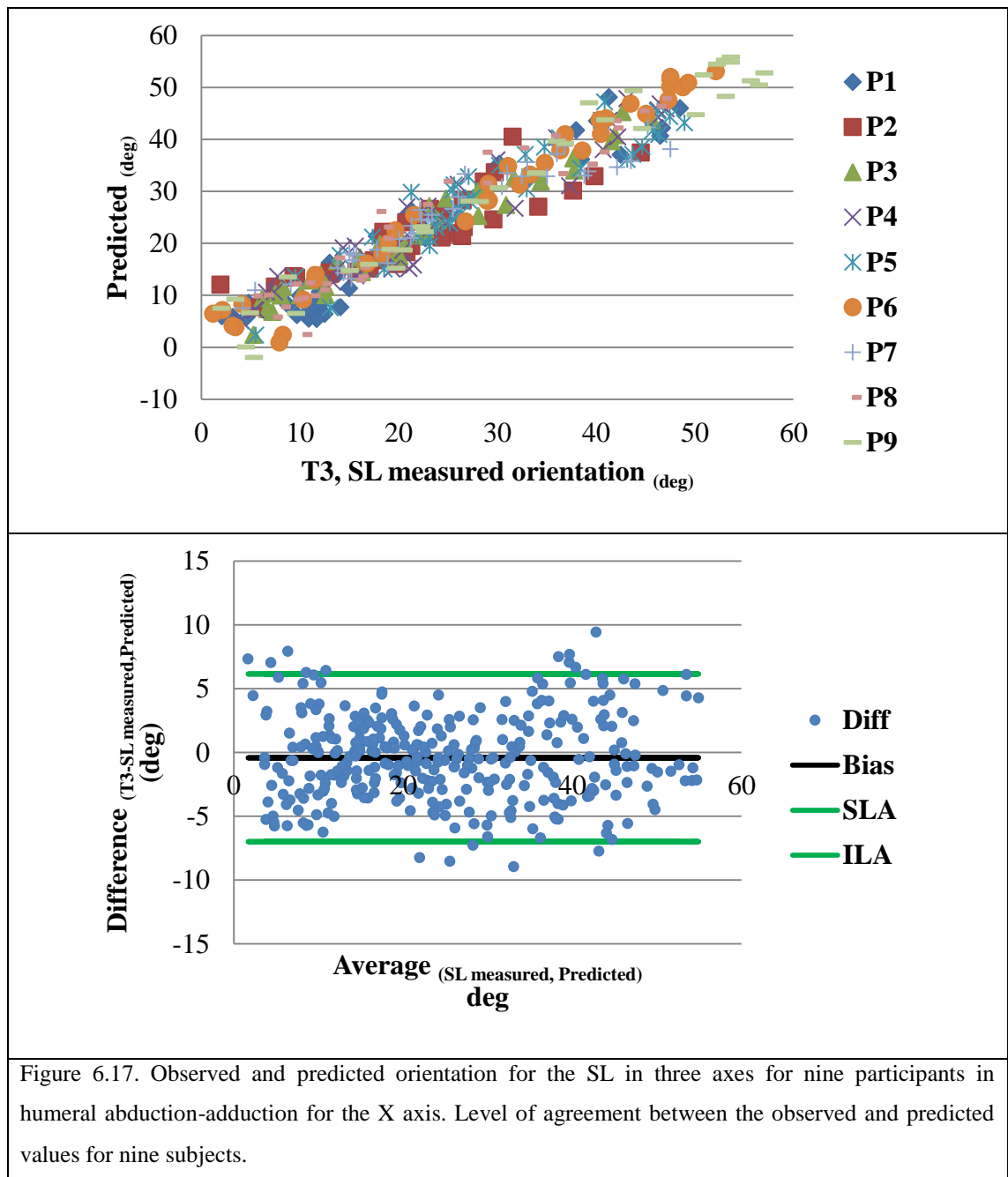


Figure 6.17. Observed and predicted orientation for the SL in three axes for nine participants in humeral abduction-adduction for the X axis. Level of agreement between the observed and predicted values for nine subjects.

Figure 6.18 shows the predicted and measured orientation of trial three for the humeral abduction-adduction for the nine participants in the global Y-axis.

The r^2 value between the predicted orientation and the SL measured orientation of the third trial (T3) for all nine participants in θ_Y gives is 0.95 which indicates the mean square deviation of the slope is acceptable, as Figure 6.18 indicates. The agreement

values indicate a BIAS line close to zero, with the scatter points distributed above and below the line, which indicates no systematic error.

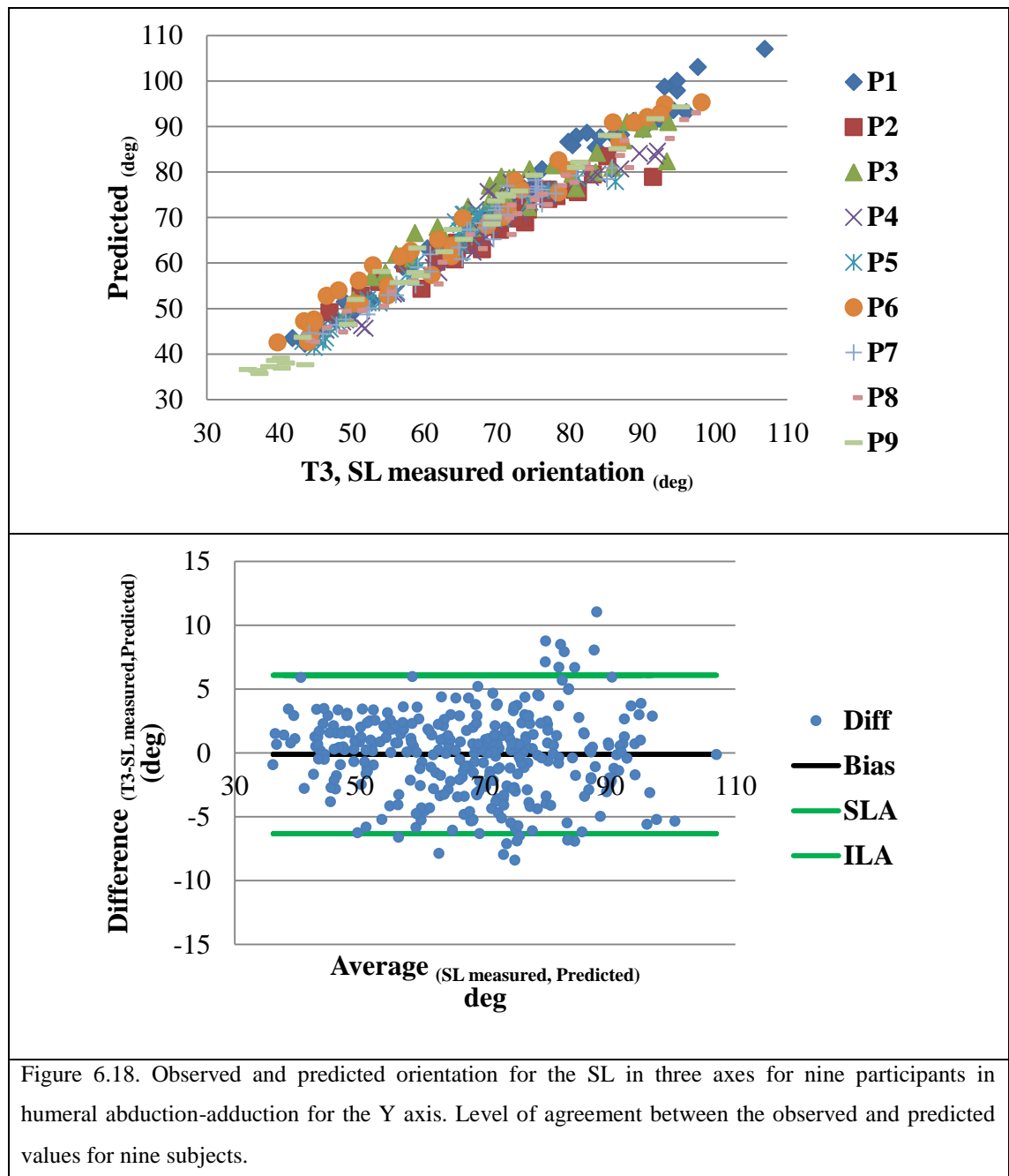


Figure 6.18. Observed and predicted orientation for the SL in three axes for nine participants in humeral abduction-adduction for the Y axis. Level of agreement between the observed and predicted values for nine subjects.

Figure 6.19 shows the predicted and measured orientation of trial three for the humeral abduction-adduction for the nine participants in the global Z-axis.

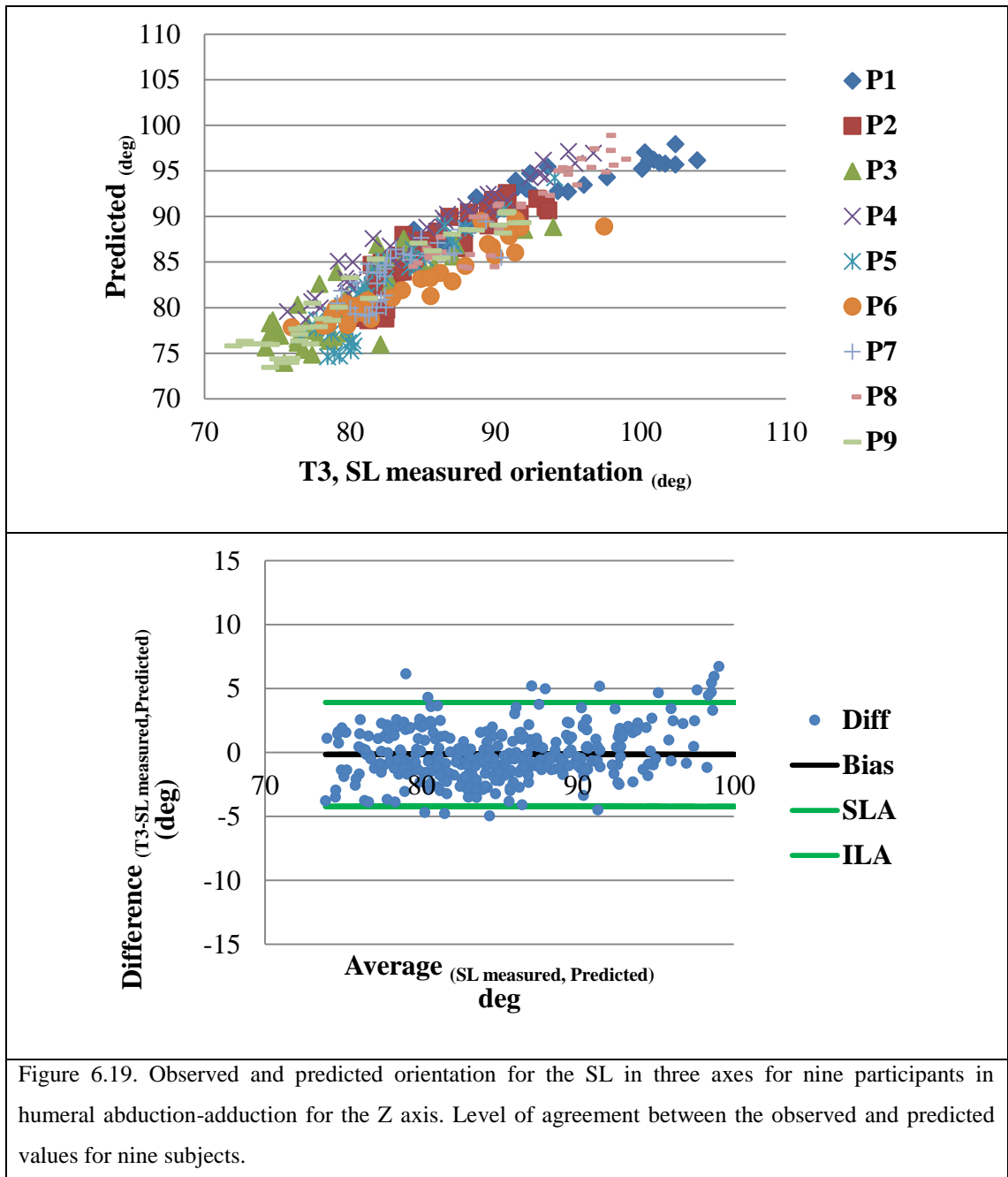


Figure 6.19. Observed and predicted orientation for the SL in three axes for nine participants in humeral abduction-adduction for the Z axis. Level of agreement between the observed and predicted values for nine subjects.

The r^2 value between the predicted orientation and the T3 SL measured orientation for all nine participants in θ_z is 0.79 which indicates the mean square deviation of the slope or in other words the level of correlation is not high. However a low level of correlation is expected in θ_z due to the anatomical restrictions of the participants, the scapula translation (which is smaller than for the humeral flexion-extension) and the surrounded soft tissues that complicates the measurement of the internal/external rotation of the scapula,. The agreement values indicate a BIAS line close to zero, with the scatter points distributed above and below the line, which indicates no systematic error.

Table 6.5 shows the averaged results from nine participants in terms of level of correlation (r^2), the standard deviation of the differences between the predicted and observed data (σ), and the agreement between the measured and predicted SL orientation (Bland and Altman method). The results in Table 6.5 indicate that there is a strong correlation between the observed and predicted scapular orientation about the Y (flexion-extension) and X (abduction-adduction) axes, while the correlations about the Z axis were moderate.

Table 6.5. Averaged results from nine participants for humeral flexion-extension and abduction-adduction.					
Humeral motion	Axis	r^2	Bland and Altman		RMSe ($^\circ$)
			BIAS($^\circ$)	σ ($^\circ$)	
Flexion-extension	X	0.90	-0.5	3.4	3.0
	Y	0.95	0.4	2.5	3.3
	Z	0.64	-0.4	1.6	4.9
Abduction-adduction	X	0.93	-0.4	3.3	3.2
	Y	0.95	-0.1	2.7	8.1
	Z	0.79	-0.1	2.0	2.7

However, the level of agreement analysis indicated that there was no systematic difference between the observed and predicted orientation and that the 95% confidence limits of the mean differences between the predicted and observed data (Bland and Altman methodology, [157]) were less than $\pm 7^\circ$ for all axes.

CHAPTER VII: CASE STUDY

7.1 Introduction

In the previous chapter it has been found that it is not possible to have a general regression model, so each participant assessed needs to have his/her own mathematical model developed to describe their scapula orientation. In this section tests were undertaken on two different participants by generating their own representative polynomials, in order to apply the methodology described in Chapter IV. One case presented hyper-elasticity; this participant will be considered as a healthy participant, although it is believed that persons with a hyper-lax joint are prone to develop muscle patterning [43]. The volunteer did not present any symptoms of pain or shoulder dysfunction; it is important to mention that when laxity at the shoulder joint becomes symptomatic, it is considered as instability. The second participant presented muscle patterning instability in one shoulder, while the contra-lateral shoulder had undergone several shoulder surgery procedures and so could not be considered a normal control.

7.2 Materials and Methods

The methodology described in Chapter IV was applied in two different case studies in which flexion-extension and abduction-adduction motions were investigated. The first part (Part 1) of each study involved recording scapula-humeral motion under quasi-static conditions using two sensors directly placed over the scapula, humerus and one over a scapula locator device (see Chapter IV). The second part (Part 2) of each study involved data acquisition from humerus and scapula under dynamic conditions without using the scapula locator (see Chapter IV).

7.2.2 Subjects

Two different volunteers participated in the test: one volunteer presented hyper-elastic joints, scoring five points in the Beighton test [57, 159]; the volunteer was 31 years old, 175cm tall, and had a body mass of 75kg at the time of the assessment. The second volunteer had been diagnosed with muscle patterning instability in the left shoulder, while the right shoulder had undergone surgical procedures, including: soft tissue anterior stabilization, anterior bony stabilization and posterior soft tissue stabilization

(hyper lax capsule). This volunteer was 25 years old, 188cm tall, and had a body mass of 90kg at the time of the assessment.

Written informed consent was obtained from both participants. The experimental procedures were evaluated and approved by the University of Manchester Research Ethics Committee, Ref 12143 (see Appendix A1), for the hyper elastic volunteer. For the muscle patterning volunteer the experimental procedures were evaluated and approved by the NHS Committee, REF: 13/NW/0128 (see Appendix A2).

7.2.3 Calibration

A heading reset was applied to all sensors on a flat surface. The heading reset allows the vertical Z axis and the gravity vector to remain vertical (see Chapter IV for an in depth explanation).

7.2.4 Experimental Setup

Participants were standing in the fundamental position with the elbow fully extended; eyes fixed on a point directly in front of them, and thumb pointing forward. Participants were trained to reproduce the flexion-extension and abduction-adduction motion, without bending the elbow, rotating the trunk or head and to synchronize the arms during elevation and depression in the dynamic tests. In Part 1, different and consecutive quasi-static orientations were recorded. While for Part 2, both arms were elevated and depressed at the same time. The elevation of the arms was synchronized to 1s up and 1s down; this will be considered as a complete repetition or cycle. The motion synchronisation was achieved by using a metronome.

The scapula sensor (S-IMU) were set on the intersections point of the perpendicular bisectors of the lines joining the three bony landmarks described in Figure 7.1 for the left scapula. The humeral sensor (H-IMU) were placed at the midpoint between the bony landmarks described in Figure 7.1; the H-IMUs were pointing posteriorly instead of laterally (see Chapter VI) to facilitate the humeral motion under dynamic condition. This modification comes as a result of the discomfort generated by the strap locking system used to attach the humeral sensors. The scapula and the SL sensors were attached with double sided tape, to fix the sensors in place.

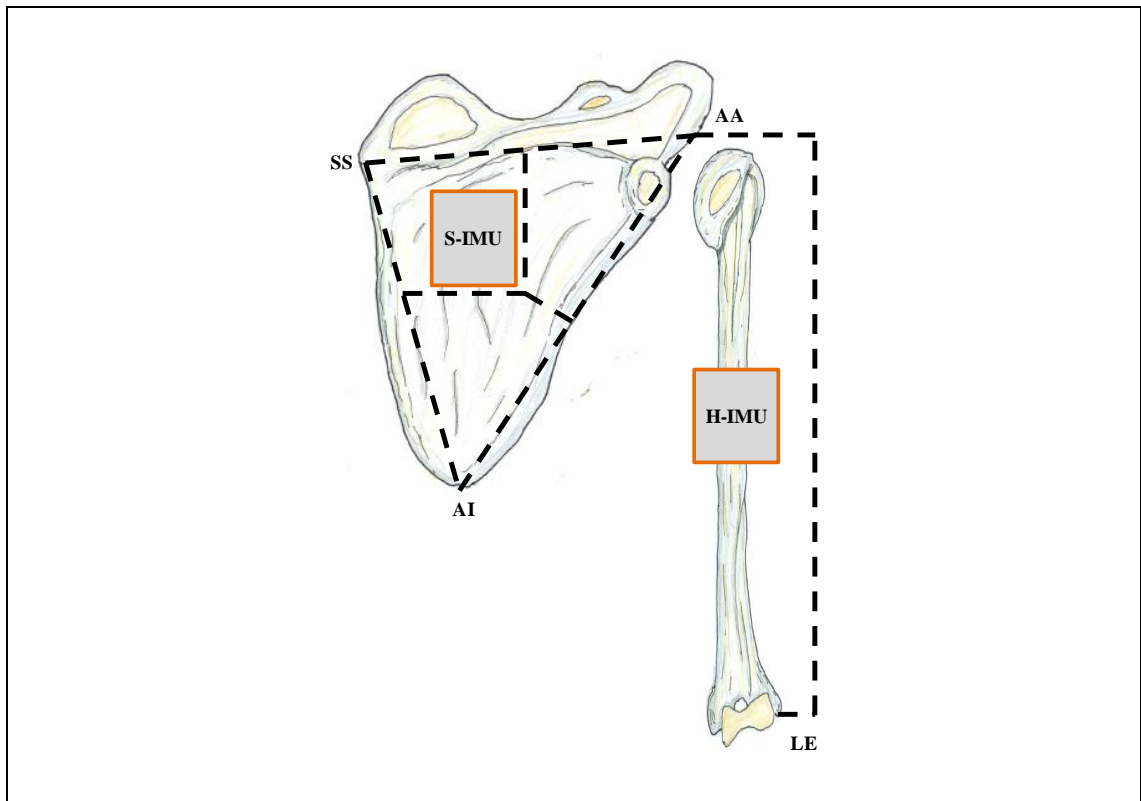


Figure 7.1. The scapula IMU (S-IMU) was set on the intersection point of the perpendicular bisectors of the lines joining the acromion inferior angle (AA), superior medial border of the scapula spine (SS) and the inferior scapular angle (AI), while the humerus sensor (H-IMU) was placed at the midpoint of the projected line of the AA and the lateral epicondyle (EL), pointing posteriorly.

7.2.5 Data Collection

Quasi-static Part 1): Quasi-static measurements were recorded for different humeral orientations according to the procedure used in Chapter VI, section 6.2.4. The participant presenting muscle patterning completed fewer quasi-static positions (10 ± 2), because of the effort and discomfort during the data collection process.

Dynamic Part 2): Participants were instructed to perform elevations and depressions in both the sagittal (flexion-extension) and the frontal plane (abduction-adduction) for both shoulders at the same time. A total of 10 consecutive repetitions were performed for each movement. One repetition consisted of the motion of the arm from the fundamental position to the maximum amplitude reached by the participants and return to the initial position. Even though approximately 20 electrodes for electromyography recording were located in the major muscle of the shoulder to assess the muscle behaviour (see Appendix 3), no electromyography results were presented, due to equipment malfunction.

7.2.6 Data Processing

In terms of data processing for Parts 1) and 2) the orientations and the predicted new scapula orientation under dynamic conditions were obtained by applying the data processing steps described in Chapter IV, section 4.3.5 and 4.3.6.

7.3 Quasi-Static Results Part 1), Humeral Flexion-Extension

The results obtained from the quasi-static and dynamic measurements for both participants in both humeral flexion-extension and abduction-adduction are presented as follows: The scapula upward/downward rotation result is represented by the local orientation of the yz plane (human transverse plane) with respect to the vertical, or the gravitational acceleration vector, and these results are presented in this section. The local yz plane is almost parallel to the ground, and the orientation of this plane is dependent on the orientation of the other two planes, where the local xz plane orientation with respect to the vertical (human sagittal plane) represents the scapula Internal/external rotation, and the local xy plane orientation (human coronal plane) represents the anterior/posterior scapula tilt.

7.3.1 Part 1), Hyper Elastic Participant: Humeral Flexion-Extension

Figure 7.2 shows the result from the quasi-static trials undertaken in stage One for the humeral flexion-extension test for the left shoulder of the hyper elastic (HE) participant. The sensor data shown in the figure represents the average over two quasi-static trials for the HE-participant. The orientations in degrees in the global axes θ_x , θ_y and θ_z (with respect to the vertical), at points throughout the quasi-static cycle of movement (0% to 100%) of the shoulder joint are illustrated in this Figure. These measurements correspond to the readings recorded by the IMUs attached to the humerus and scapula surfaces and the IMU attached to the scapula locator. These data were used to obtain the mathematical model, as described in Chapter IV. The regression equation was subsequently used to predict scapular position under dynamic conditions.

Upon inspection of Figure 7.2 appreciable differences can be seen in the pattern between the scapula (S-HE) and the scapula locator measurements (SL-HE) recorded with the respective IMUs sensors for the hyper elastic participant. The scapula sensor

orientation in the θ_x (upward and downward rotation of the scapula) shows a 'w' pattern and the SL sensor shows a 'v' pattern; this came as a result of the S-HE sensor alignment with the ground (see chapter IV), while the SL-HE sensor did not cross the vertical. The gap between sensors (S-HR and SL-HE) in the θ_x and θ_y axes is expected to be produced for the initial alignment of the sensors with respect to the vertical and can be attributed to the morphological characteristic of the participant, such as the muscles and fat layers that have the potential to modify the orientation of the sensors. On the other hand, a minimum gap in the θ_z axis that represents the internal/external rotation of the scapula is expected, as Figure 7.2 shows. This can be attributed to the almost parallel alignment of the local x axis with the vertical.

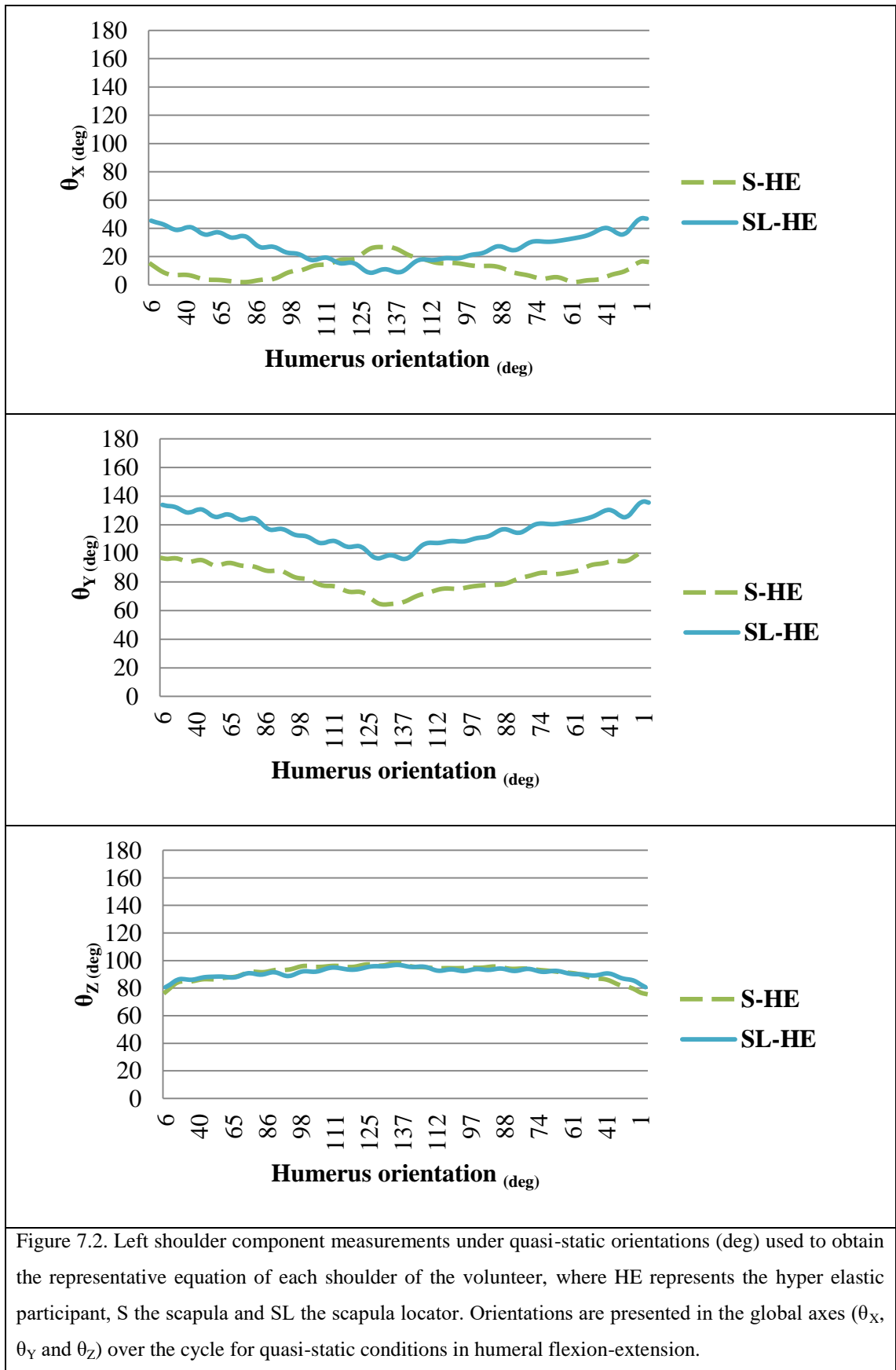


Figure 7.2. Left shoulder component measurements under quasi-static orientations (deg) used to obtain the representative equation of each shoulder of the volunteer, where HE represents the hyper elastic participant, S the scapula and SL the scapula locator. Orientations are presented in the global axes (θ_X , θ_Y and θ_Z) over the cycle for quasi-static conditions in humeral flexion-extension.

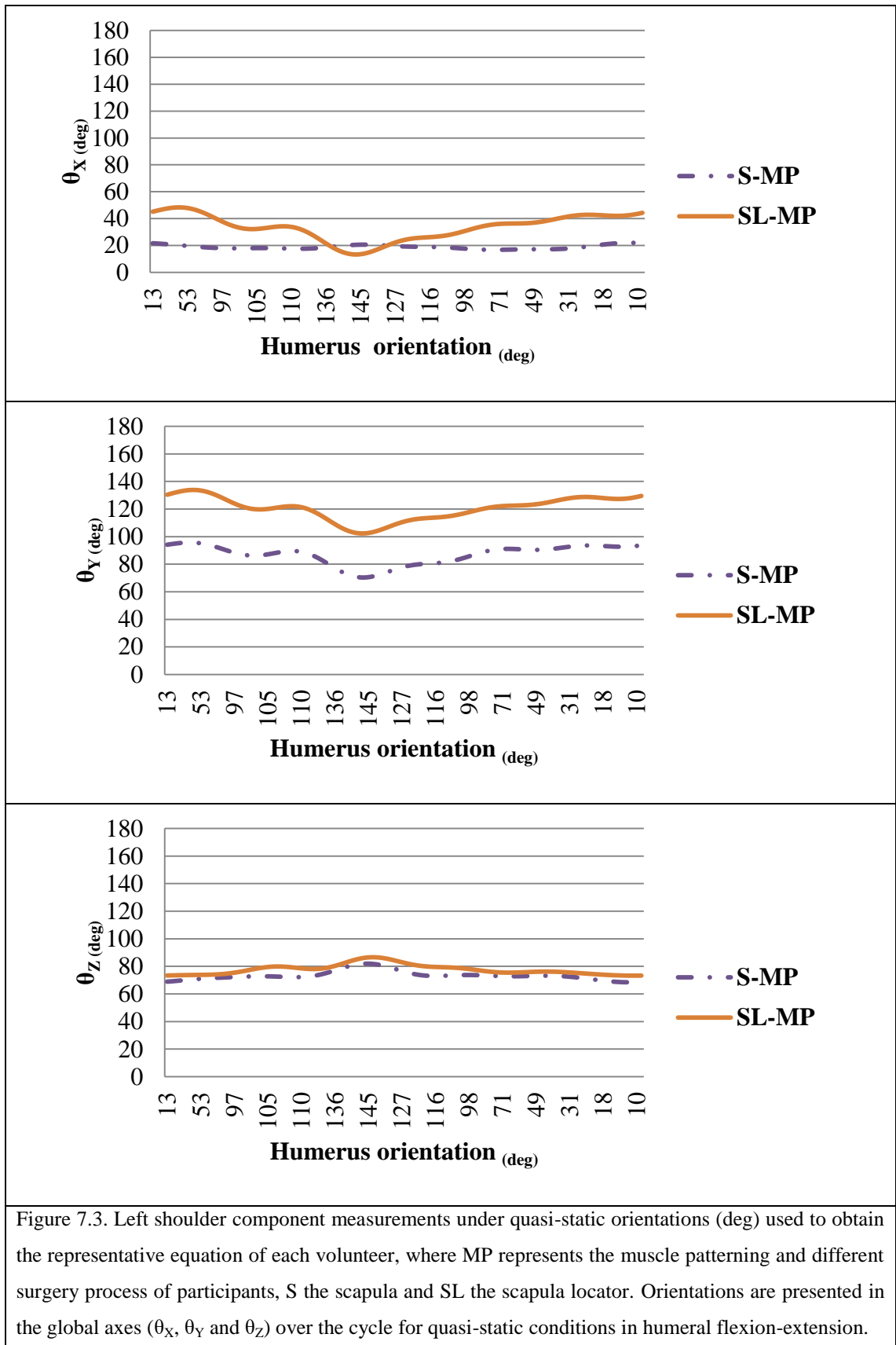
The scapular and humeral data of Figure 7.2 were used to obtain representative mathematical models (Table 7.1) that were used to predict scapular position under dynamic conditions as if the scapula orientation were being measured with the SL device.

Table 7.1 presents the equations obtained from the quasi-static inputs shown in Figure 7.2 for the three axes of the hyper elastic participant. H and S represent the orientation of the humerus and the scapula in radians for the three axes and $SL_{\theta_x, \theta_y, \theta_z}$ represents the scapula orientation as if it was measured with the scapular locator device, for each axis. The coefficients ‘ a_1, a_2 ’ in the mathematical expression represent the mean of the best fit values obtained from trial T1 and T2.

Table 7.1. Best fit coefficients for the three axes for the hyper elastic participant in humeral flexion-extension.		
Table 7.1 a), Best fit coefficients for the X global axis scapular orientation (radians) of Trials 1 and 2.		
Shoulder side	Left Shoulder	
Equation	$SL_{\theta_x} = a_1 H + a_2 S$	
Coefficients	a_1	a_2
Trial 1	0.2866	-0.2757
Trial 2	0.1424	0.5898
Average	0.2145	0.1571
Table 7.1 b), Best fit coefficients for the Y global axis scapular orientation (radians) of Trials 1 and 2.		
Equation	$SL_{\theta_y} = a_1 H + a_2 S$	
Coefficients	a_1	a_2
Trial 1	-0.0513	1.4395
Trial 2	-0.0710	1.4338
Average	-0.0612	1.4366
Table 7.1 c), Best fit coefficients for the Z global axis scapular orientation (radians) of Trials 1 and 2.		
Equation	$SL_{\theta_z} = a_1 H + a_2 S$	
Coefficients	a_1	a_2
Trial 1	-0.0150	1.0221
Trial 2	0.0032	0.9876
Average	-0.0059	1.0049

7.3.2 Part 1), Muscle Patterning Participant: Humeral Flexion-Extension

Figure 7.3 corresponds to the readings of the sensors with respect to the vertical for the participant with muscle patterning (MP). It is important to say that the right side of the participant with muscle patterning is the side that has undergone different surgical procedures, so it cannot be used to compare between shoulders. As can be seen, there is no discernible gap in the internal/external rotation of the scapula (θ_z), while for the upward and downward rotation of the scapula and the anterior/posterior tilt of the scapula (θ_x and θ_y) measured by the scapular (S-MP) sensor the gap exists as was expected; this can be attributed to the initial alignment of the sensor when located in place, where it is affected by the soft tissues. However the differences in the orientation pattern between the scapula sensor (S-MP) and the scapula locator sensor (SL-MP) in the θ_x axis are clear. While the SL-MP still shows the 'v' patterns (see Figure 7.2), the S-MP shows linear behaviour without almost any tilt, or the 'w' pattern observed in previous results, see Figures 6.9 and 7.2. From this figure it can also be observed that the participant could perform more quasi-static measurements during the extension motion of the test, and this can be confirmed from the visual feedback at the moment of the test, when the participant was extending the arm with fewer symptoms of discomfort.



As for the hyper-elastic participant, the data of Figure 7.3 were used to obtain representative mathematical models (Table 7.2) to predict scapular position under dynamic conditions.

Table 7.2 presents the equations obtained from the quasi-static inputs shown in Figure 7.3 for the three axes of the MP-participant. H and S represent the orientation of the humerus and the scapula in radians for the three axes, and $SL_{\theta_x, \theta_y, \theta_z}$ represents the scapula orientation as if it was measured with the scapular locator device, for each axis. The coefficients ‘ $a...a_n$ ’ in the mathematical expression represent the mean of the best fit values obtained from trials T1 and T2.

Table 7.2. Best fit coefficients for the three axes for the muscle patterning participant in humeral flexion-extension.		
Table 7.2 a), Best fit coefficients for the X global axis scapular orientation (radians) of Trials 1 and 2.		
Shoulder side	Left Shoulder	
Equation	$SL_{\theta_x}=a_1H+a_2S$	
Coefficients	a_1	a_2
Trial 1	-0.1400	2.3652
Trial 2	-0.1588	2.4489
Average	-0.1494	2.4071
Table 7.2 b), Best fit coefficients for the Y global axis scapular orientation (radians) of Trials 1 and 2.		
Equation	$SL_{\theta_y}=a_1H+a_2S$	
Coefficients	a_1	a_2
Trial 1	-0.0019	1.3749
Trial 2	0.5681	0.9500
Average	0.2831	1.1625
Table 7.2 c), Best fit coefficients for the Z global axis scapular orientation (radians) of Trials 1 and 2.		
Equation	$SL_{\theta_z}=a_1H+a_2S$	
Coefficients	a_1	a_2
Trial 1	0.0073	1.0374
Trial 2	-0.0042	1.0774
Average	0.0016	1.0574

7.3.3 Quasi-static Results Comparison

Clear differences can be appreciated in the coefficients of the obtained polynomials between participants (Table 7.1 and Table 7.2) and between the shoulder orientations of each participant (see Figure 7.2 and Figure 7.3), which can be attributed to the unique anatomical and physical characteristics of each participants and the shoulder instability presented for one of the participants. The participant with muscle patterning presents higher values in the coefficients obtained (Table 7.1) than the participant with hyper elasticity (Table 7.2). One difference that arises after the comparison between Figure 7.2 and Figure 7.3, is that in the upward and downward rotation of the scapula (θ_x) a clear difference in the behaviour of the scapular sensor for both participants can be observed, while the sensor placed over the scapula of the hyper elastic participant (S-HE) shows a 'w' pattern. The measurements recorded by the scapular sensors of the muscle patterning participant present flat and linear behaviour. The remaining two axes show similar patterns. Differences in the magnitudes between participants of around 20° in the upward/downward rotation (θ_x) and the posterior anterior tilt of the scapula (θ_y) can be seen in Figure 7.2 and Figure 7.3. The humeral elevations reached by each participant were quite similar under quasi-static conditions. The HE-participant reaches a maximum humeral elevation of around 140°, while the MP-participant reaches a different humeral elevation of around 145°. The MP-participant struggles more to hold the humeral position, especially after 30° of humeral elevation.

7.4 Dynamic Results Part 2): Humeral Flexion-Extension

The angular velocity results measured in Part 2) are presented in this section, where: ω_x represents the upward and downward rotation of the scapula, ω_y represents the anterior/posterior tilt of the scapula and finally ω_z represents the internal/external rotation of the scapula in global coordinates. The Omega measurements presented in Figure 7.4 correspond to the readings recorded by the IMUs attached to the scapula (Raw) in the global frame before and after the data correction (Corrected) by applying a representative polynomial, see Chapter IV for a deeper explanation.

7.4.1 Part 2), Hyper Elastic Participant: Humeral Flexion-Extension

Figure 7.4 shows the Omega (ω) result from the scapula undertaken in stage two of the test for the humeral flexion-extension, for the left shoulder of the hyper elastic (HE) participant. The sensor data shown in the figure represent the average over ten dynamic trials. The Omega data are in radians over second (rad/s) in the three global axes, ω_x , ω_y and ω_z . The data can be identified as points throughout the quasi-static cycle of movement of the shoulder joint and are illustrated in this Figure.

Small differences in the pattern and magnitude can be observed for the HE-participant before (Raw) and after correction of omega (Corrected) in Figure 7.4. Because Omega is presented in global coordinates, it is expected that the main rotation occurs about the global X axis (which is pointing posteriorly).

The data were rotated by using a quaternion rotation and integrated to obtain the angular orientation, and the results are presented in Figure 7.5.

Figure 7.5 shows the scapula orientation in degrees before (HE-Raw) and after the correction (HE-Corrected), for the three global axes. Similarities in shape can be appreciated for the HE-participant. However, there are small changes in the magnitudes between the raw measurements and the corrected scapula orientation, with an RMS error between the corrected orientation of the scapula and the orientation measured directly from the scapula sensor of 2.2° in the scapula upward/downward rotation, 3.8° in the anterior/posterior tilt of the scapula and 2.2° in the internal/external rotation of the scapula.

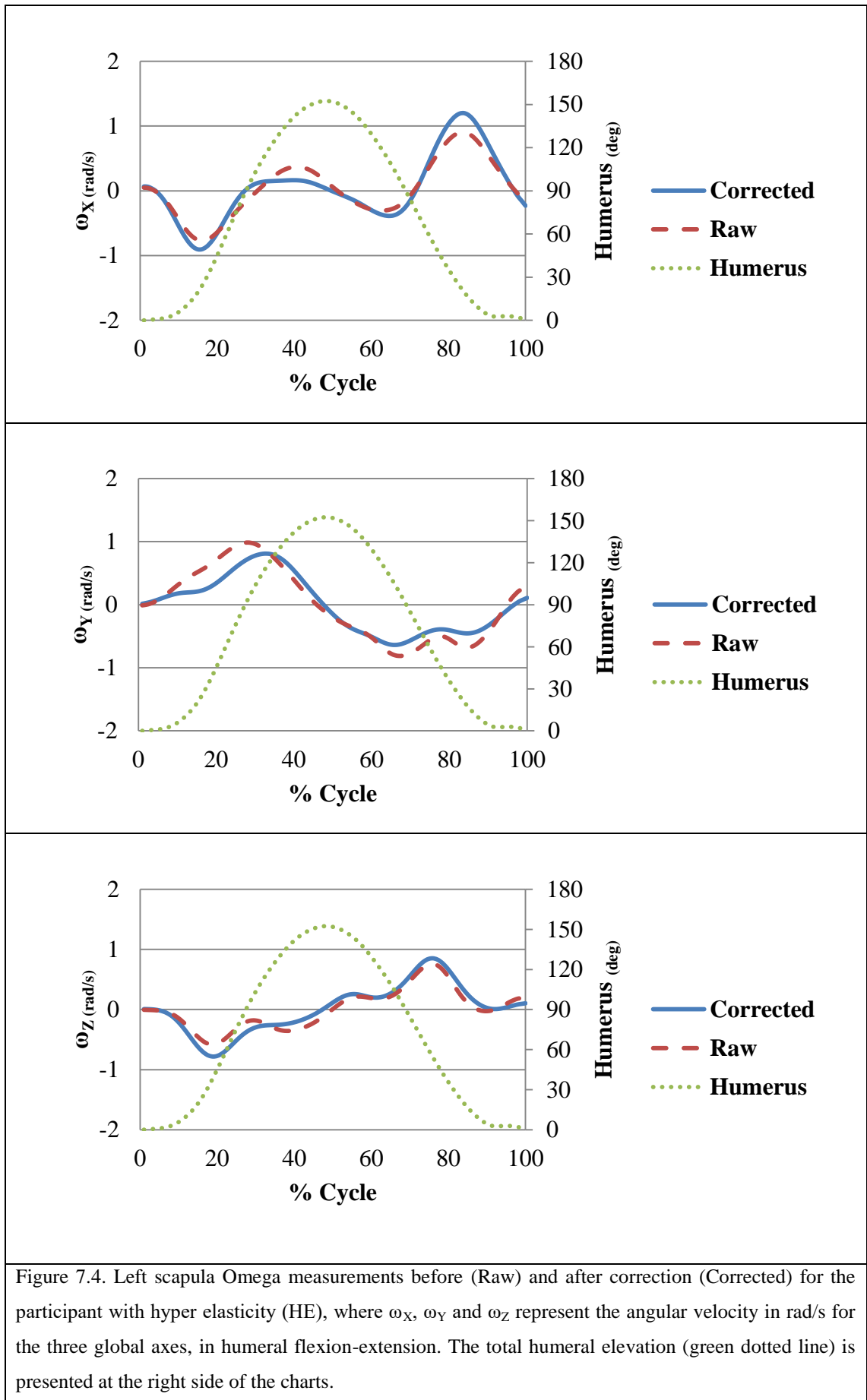
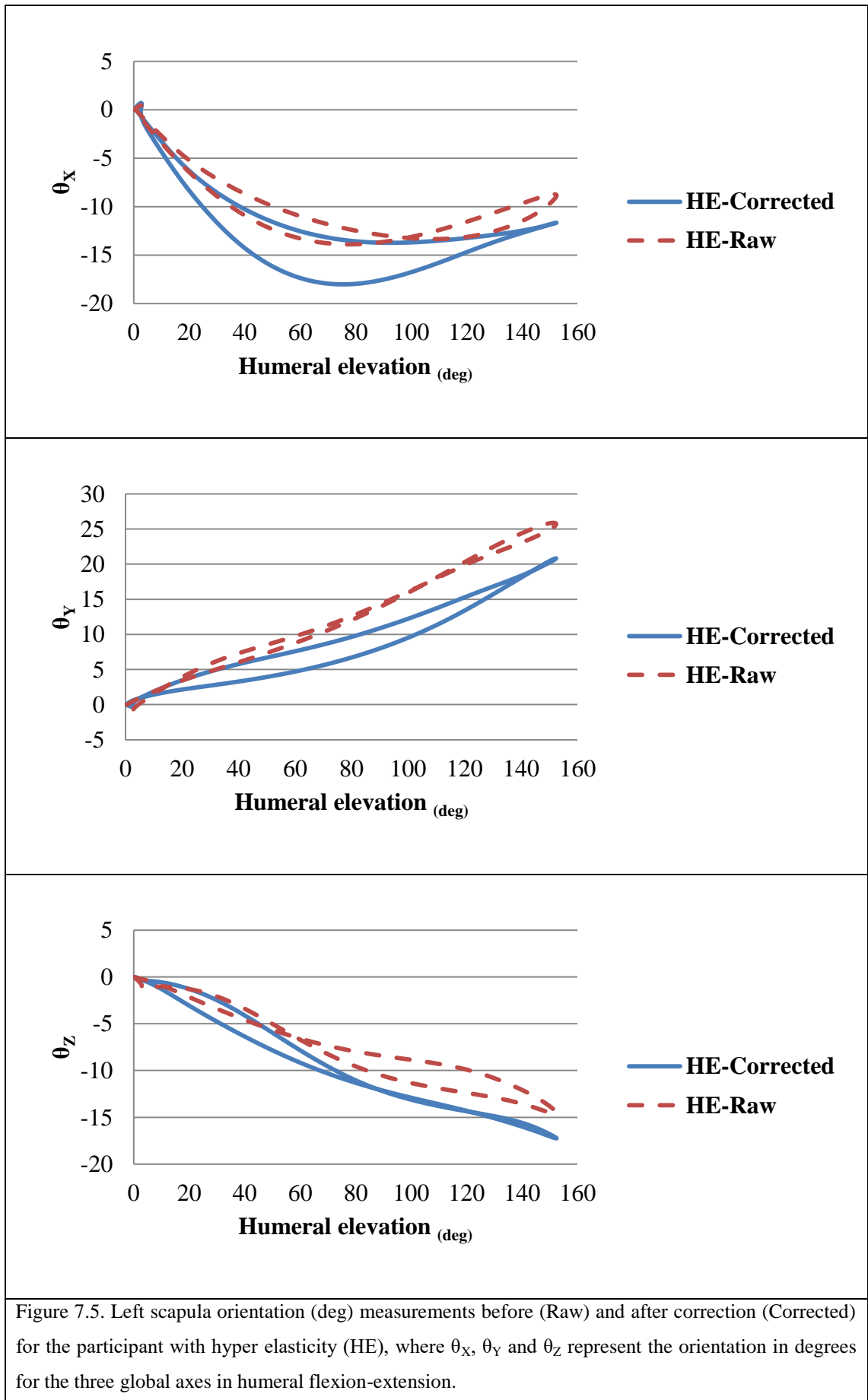


Figure 7.4. Left scapula Omega measurements before (Raw) and after correction (Corrected) for the participant with hyper elasticity (HE), where ω_X , ω_Y and ω_Z represent the angular velocity in rad/s for the three global axes, in humeral flexion-extension. The total humeral elevation (green dotted line) is presented at the right side of the charts.



7.4.2 Part 2, Muscle Patterning Participant: Humeral Flexion-Extension

Figure 7.6 shows the Omega (ω) results for the left scapula undertaken in stage two for humeral flexion-extension for the muscle patterning (MP) participant. The scapular sensors data presented in this figure represent the average over ten dynamic trials or repetitions. The Omega data are in rad/s in the three global axes, ω_X , ω_Y and ω_Z .

The participant with muscle patterning shows similar patterns before and after the omega correction but considerable differences in magnitude.

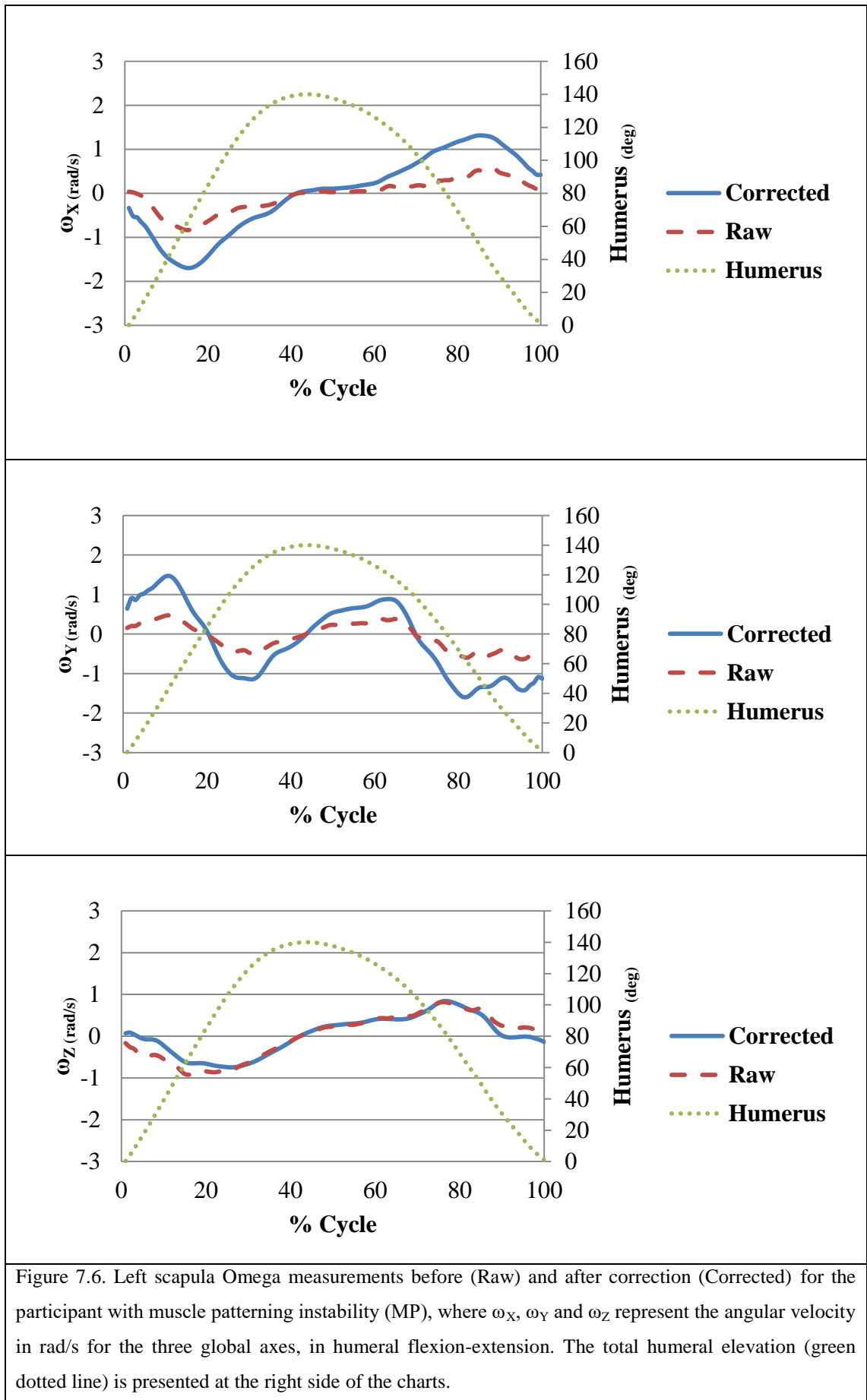


Figure 7.6. Left scapula Omega measurements before (Raw) and after correction (Corrected) for the participant with muscle patterning instability (MP), where ω_x , ω_y and ω_z represent the angular velocity in rad/s for the three global axes, in humeral flexion-extension. The total humeral elevation (green dotted line) is presented at the right side of the charts.

The corrected data were rotated by using a quaternion rotation and integrated to obtain the angular orientation and the results are presented in Figure 7.7.

Figure 7.7 shows the scapula orientation in degrees before (MP-Raw) and after the correction (MP-Corrected) in three global axes for the MP-participant. Discernible differences in magnitude can be seen in θ_X , θ_Y and θ_Z between the direct measurements of the scapula orientation by the scapular sensor (S-IMU) and the corrected orientation of the scapula by applying the obtained polynomial (Table 7.3). The shoulder diagnosed with muscle patterning shows a change in the pattern around 90° and 120° of humeral elevation in the anterior/posterior motion of the scapula; according to the volunteer this humeral elevation is when he feels the humeral dislocation. It was observed by the researcher how the MP-participant, in order to reach the maximum humeral elevation, needed to rotate the trunk, reducing the discomfort generated by the humeral motion. There was an RMS error between the corrected orientation of the scapula and the orientation measured directly from the scapula sensor of 29° in the scapula upward/downward rotation, 21° in the anterior/posterior tilt of the scapula, and 7.5° in the internal/external rotation of the scapula. This increment in the RMS error could be explained by the differences in the motion pattern between the quasi-static and dynamic measurements experimented by the MP-participant.

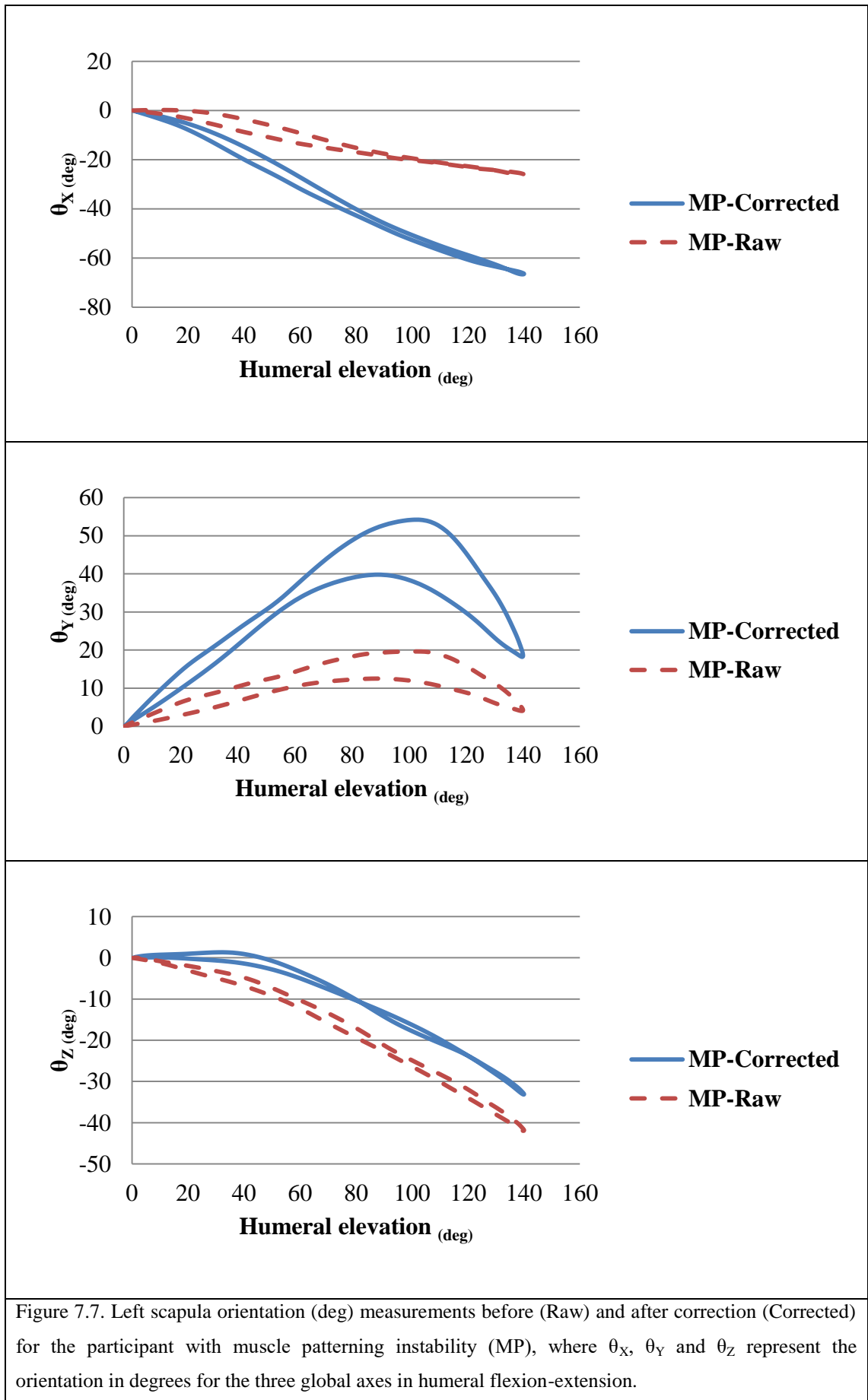


Figure 7.7. Left scapula orientation (deg) measurements before (Raw) and after correction (Corrected) for the participant with muscle patterning instability (MP), where θ_X , θ_Y and θ_Z represent the orientation in degrees for the three global axes in humeral flexion-extension.

7.4.3 Dynamic Results Comparison for the Humeral Flexion-Extension

If the results of both participants from Figure 7.4 and Figure 7.6 are compared, even though some similarities in the scapular angular velocity pattern were registered by the scapular sensors, clear differences can be appreciated, especially in the ω_Y , which represents the anterior/posterior tilt of the scapula and in the upward/downward rotation of the scapula (ω_X) between participants. The internal/external rotation of the scapula (ω_Z) result suggests that there is less variability in this axis. The MP-participant between 10% and 80% of humeral elevation in the anterior/posterior tilt of the scapula shows more variability than the HE-participant. However, at the moment of initiating the humeral motion, and at the end when the motion is being dampened this seems more stable. ω_X represents the upward and downward rotation of the scapula and the HE-participant seems to dampen the motion quicker (around 30% of the cycle) than the MP-participant (around 40% of the cycle).

In terms of humeral elevation, the range of motion of both participants was quite similar. The maximum humeral elevation was around 150° for the HE-participant and 140° for the MP-participant. The maximum measured magnitudes were greater under dynamic conditions than those reached in the quasi-static trials. The maximum humeral elevation for the MP-participant occurred at around 40% to 45% of the cycle, instead of at the expected 50% like the HE-participant, which could explain the failure of the MP-participant to coordinate the motion to one second up and one second down the motion. Another difference can be seen in the generated shape of the humeral elevation between participants, the shape generated by the HE-participant being smoother and thinner than the shape generated by the MP-Participant. Considerable differences in magnitude between participants, especially in the corrected results for the MP-participant, can be observed if Figure 7.5 and Figure 7.7 are compared. The results of both participants seem to be more consistent in the pattern but the resultant magnitudes are still larger for the MP-participant than for the HE-participant, which indicates that one of the inputs to the polynomial might follow a different trajectory from the orientations recorded in the quasi-static trials, or that the velocity may have an effect in the prediction of the scapula orientation in pathological shoulders. Around 75° of humeral elevation change in the trace appears for the MP-Participant (Figure 7.7) in the anterior/posterior tilt of the

scapula, if the results are compared with the HE-Participant (Figure 7.5); however, it is around this area that the MP-participant feels the click or the dislocation of the humerus.

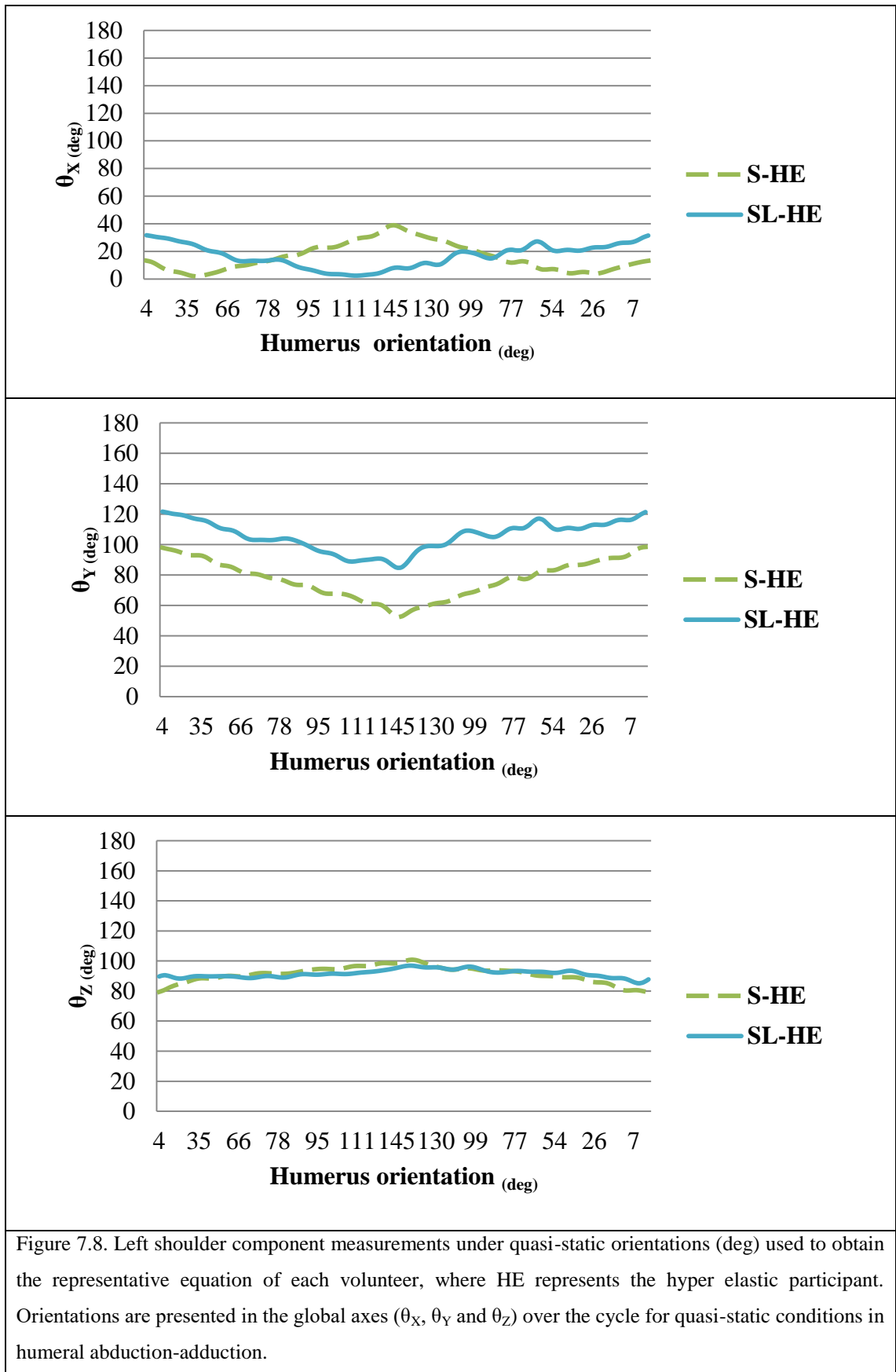
7.5 Quasi-Static Results Part 1), Humeral Abduction-Adduction

The Quasi-static results from both participants in humeral abduction-adduction are presented in the following sections.

The scapula upward/downward rotation result is represented by the local orientation of the yz plane (human transverse plane) with respect to the vertical or the gravitational acceleration vector, and the results are presented in this section. This plane is almost parallel to the ground and the orientation is dependent on the orientation of the other two planes, where the local xz plane orientation with respect to the vertical (human sagittal plane) represents the scapula Internal/external rotation, and the local xy plane orientation with respect to the vertical (human coronal plane) represents the anterior/posterior scapula tilt.

7.5.1 Part 1), Hyper Elastic Participant: Humeral Abduction-Adduction

Figure 7.8 shows the results from the quasi-static trial undertaken in stage One for the humeral abduction-adduction test for the left shoulder of the HE-participant. The sensor data shown in the figure represent the average over two quasi-static trials for the hyper elastic participant (HE). The orientations in degrees in the global axes θ_x , θ_y and θ_z , at points throughout the quasi-static cycle of movement (0% to 100%) of the shoulder joint are illustrated in this Figure. These measurements correspond to the readings recorded by the IMUs attached to the humerus and scapula surfaces and the IMU attached to the scapula locator. These data were used to obtain the mathematical model that was described in Chapter IV. The regression equation was subsequently used to predict scapular position under dynamic conditions.



Upon inspection of Figure 7.8, differences in the pattern between the scapula (S-HE) and the scapula locator measurements (SL-HE) for the HE-participant can be seen. The scapula sensor orientation in θ_X (upward and downward rotation of the scapula) shows a 'w' pattern, while the SL sensor shows a 'v' pattern; this was a result of the S-HE sensor alignment with the ground, while the SL-HE did not cross the vertical. The gap between sensor S-HR and SL-HE in the θ_X and θ_Y axes is produced for the initial alignment of the sensors with respect to the vertical and can be attributed to the anatomical characteristics of the participant, such as the muscles and fat layers that have the potential to modify the orientation of the sensors. The gap in the θ_X and θ_Y axes is expected, as described above, while for the θ_Z axis that represents the internal/external rotation of the scapula a minimum gap is expected, as Figure 7.8 shows.

The scapular and humeral data of Figure 7.8 were used to obtain a representative mathematical model (Table 7.3) that will be used to predict scapular position under dynamic conditions, as if the scapula orientation were measured with the SL device.

Table 7.3 presents the equations obtained from the quasi-static inputs shown in Figure 7.8 for the three axes for the hyper elastic participant, where H and S represent the orientation of the humerus and the scapula in radians for the three axes and $SL_{\theta_x, \theta_y, \theta_z}$ represent the scapula orientation as if it was measured with the scapular locator device, for each axis. The coefficients ' a_1, a_2, \dots, a_n ' in the mathematical expression represent the mean of the best fit values obtained for trials T1 and T2.

Table 7.3. Best fit coefficients for the three axes for the hyper elastic participant in humeral abduction-adduction.		
Table 7.3 a), Best fit coefficients for the X global axis scapular orientation (radians) of Trials 1 and 2.		
Shoulder side	Left Shoulder	
Equation	$SL_{\theta X}=a_1H+a_2S$	
Coefficients	a_1	a_2
Trial 1	0.1523	-0.1399
Trial 2	0.1465	-0.0329
Average	0.1494	-0.0864
Table 7.3 b), Best fit coefficients for the Y global axis scapular orientation (radians) of Trials 1 and 2.		
Equation	$SL_{\theta Y}=a_1H+a_2S$	
Coefficients	a_1	a_2
Trial 1	0.3039	1.0950
Trial 2	0.3313	1.1265
Average	0.3176	1.1108
Table 7.3 c), Best fit coefficients for the Z global axis scapular orientation (radians) of Trials 1 and 2.		
Equation	$SL_{\theta Z}=a_1H+a_2S$	
Coefficients	a_1	a_2
Trial 1	-0.1257	1.1806
Trial 2	-0.0609	1.0753
Average	-0.0933	1.1280

7.5.2 Part 1), Muscle Patterning Participant: Humeral Abduction-Adduction

Figure 7.9 corresponds to the readings of the sensors with respect to the vertical for the participant with muscle patterning (MP). As expected there is no discernible gap in the internal/external rotation of the scapula (θ_Z), while for the upward and downward rotation of the scapula (S-MP) and the anterior/ posterior tilt of the scapula (θ_X and θ_Y) the gap exists, as was expected. However the difference in the orientation pattern between the scapula (S-MP) and the scapula locator (SL-MP) in the θ_X axis is clear. While the SL-MP still shows the ‘v’ patterns (see Figure 7.9), the S-MP shows flat and linear behaviour with hardly any tilt, and no sign of a ‘w’ pattern as could be expected, see Figure 6.12 and Figure 7.8.

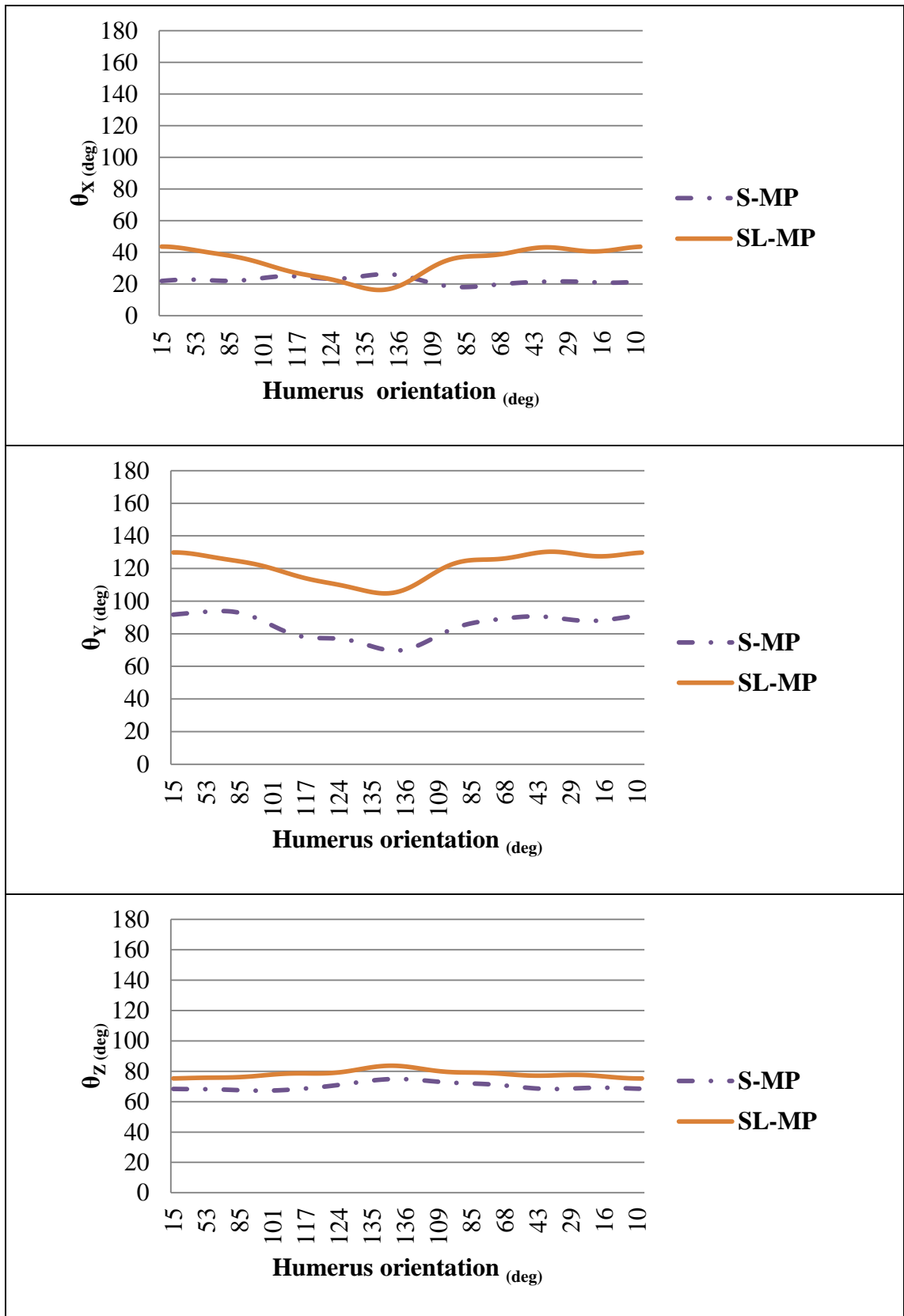


Figure 7.9. Left shoulder component measurements under quasi-static orientations (deg) used to obtain the representative equation of each volunteer, where MP is the muscle patterning and different surgery process participant, S the scapula and SL the scapula locator. Orientations are presented in the global axes (θ_X , θ_Y and θ_Z) over the cycle for quasi-static conditions in humeral abduction-adduction.

The scapular and humeral data of Figure 7.9 were used to obtain a representative mathematical model (Table 7.4) that will be used to predict scapular position under dynamic conditions, as if the scapula orientation were measured with the SL device. The best fit coefficients obtained from Figure 7.9 for the three axes for the MP-participant are presented in Table 7.4, where H and S represent the orientation of the humerus and the scapula in radians for the three axes, and $SL_{\theta_x, \theta_y, \theta_z}$ represents the scapula orientation as if it was measured with the scapular locator device, for each axis. The coefficients ‘ $a...a_n$ ’ in the mathematical expression represent the mean of the best fit values obtained for trials T1 and T2.

Table 7.4. Best fit coefficients for the three axes for the muscle patterning participant in humeral abduction-adduction.		
Table 7.4 a), Best fit coefficients for the X global axis scapular orientation (radians) of Trials 1 and 2.		
Shoulder side	Left Shoulder	
Equation	$SL_{\theta_X}=a_1H+a_2S$	
Coefficients	a_1	a_2
Trial 1	-0.2259	2.2635
Trial 2	-0.2332	2.3665
Average	-0.2296	2.3150
Table 7.4 b), Best fit coefficients for the Y global axis scapular orientation (radians) of Trials 1 and 2.		
Equation	$SL_{\theta_Y}=a_1H+a_2S$	
Coefficients	a_1	a_2
Trial 1	0.2079	1.2618
Trial 2	0.5346	0.9991
Average	0.3712	1.1305
Table 7.4 c), Best fit coefficients for the Z global axis scapular orientation (radians) of Trials 1 and 2.		
Equation	$SL_{\theta_Z}=a_1H+a_2S$	
Coefficients	a_1	a_2
Trial 1	-0.0247	1.1546
Trial 2	0.0700	0.9911
Average	0.0227	1.0729

7.5.3 Quasi-static Results Comparison

Clear differences between participants can be observed in the coefficients of the polynomials obtained (Table 7.3 and Table 7.4) and between different shoulders orientation of each participant (see Figure 7.8 and Figure 7.9), which can be attributed

to the unique anatomical and physical characteristics of each participant and the shoulder instability presented by one of the participants. The MP-participant presents higher values in the coefficients obtained (Table 7.4) than the participant with hyper elasticity (Table 7.3). One difference that arises after the comparison between Figure 7.8 and Figure 7.9 is in the upward and downward rotation of the scapula (θ_x), where a clear difference in the behaviour of the scapula sensor for both participants can be observed. While the sensors placed over the scapula of the hyper elastic participant (S-HE) show a 'w' pattern, the measurements recorded by the scapula sensor of the muscle patterning participant present flat and linear behaviour. The remaining two axes show similar patterns. Differences between participants in the magnitudes of around 10° in the upward/downward rotation (θ_x) and the anterior/posterior tilt of the scapula (θ_y) can be observed in Figure 7.8 and Figure 7.9. Another difference is in the humeral elevation reached by each participant. The HE-participant reached a maximum humeral elevation of around 150° , and the MP-participant reached a maximum humeral elevation of around 136° .

7.6 Dynamic Results Part 2), Humeral Abduction-Adduction

The angular velocity results measured in Part 2) are presented in this section, where: ω_x represents the upward and downward rotation of the scapula, ω_y represents the anterior/posterior tilt of the scapula, and finally ω_z represents the internal/external rotation of the scapula.

7.6.1 Part 2), Hyper Elastic Participant: Humeral Abduction-Adduction

Figure 7.10 shows the Omega (ω) result from the scapula undertaken in Part 2), for the humeral abduction-adduction of the left shoulder from the HE-participant. The sensor data shown in the figure represent the average over ten dynamic trials. The Omega data are in rad/s in the three global axes, ω_x , ω_y and ω_z ; the data can be identified as points throughout the quasi-static cycle of movement of the shoulder joint as illustrated in this Figure.

The Omega measurements presented in Figure 7.10 correspond to the readings recorded by the IMUs attached to the scapula (Raw) in the global frame before and after the correction (Corrected) by applying the representative polynomial (see [Table 7.3](#)) in the

global reference frame. Differences in the pattern and magnitude can be appreciated for the hyper elastic (HE) participant before (HE-Raw) and after correction of omega (HE-Corrected) in Figure 7.10.

The scapular and humeral angular velocity data were used in the mathematical model obtained (Table 7.3) to reduce the soft tissues error generated and to track the scapular orientation under dynamic conditions (Corrected, see Figure 7.10), as if the scapula orientation were being measured with the SL device. The corrected data were rotated by using a quaternion rotation to the global reference frame and integrated to obtain the angular orientation, presented in Figure 7.11.

Figure 7.11 shows the scapula orientation in degrees before (HE-Raw) and after the correction (HE-Corrected), for the three global axes, where similarities in shape can be observed for the HE-participant, with changes in the magnitudes between the raw measurements and the corrected scapula orientation, with an RMS error between the corrected orientation of the scapula and the orientation measured directly from the scapula sensor of 7.4° in the scapula upward/downward rotation, 4.7° in the anterior/posterior tilt of the scapula and 11.5° in the internal/external rotation of the scapula.

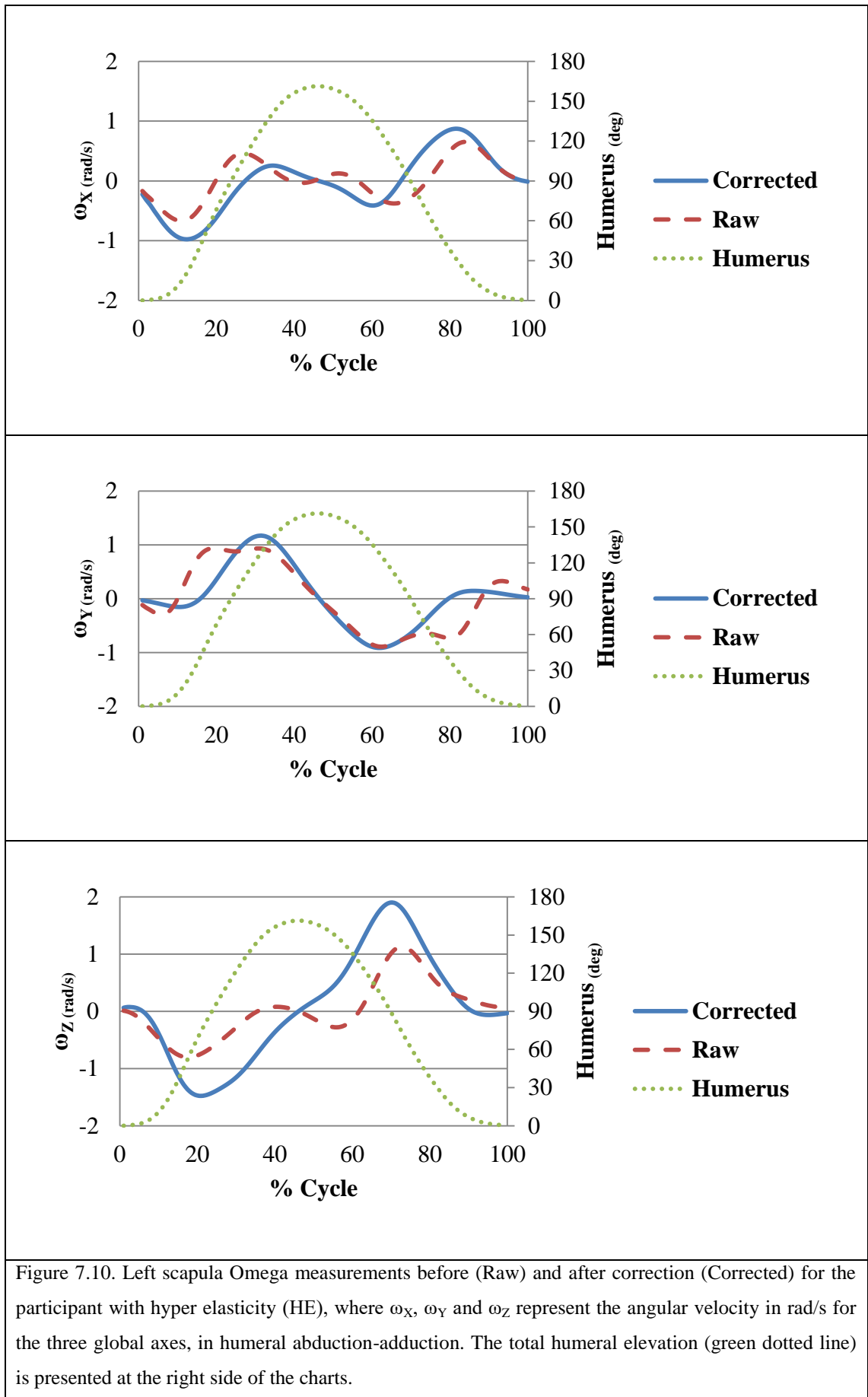


Figure 7.10. Left scapula Omega measurements before (Raw) and after correction (Corrected) for the participant with hyper elasticity (HE), where ω_x , ω_y and ω_z represent the angular velocity in rad/s for the three global axes, in humeral abduction-adduction. The total humeral elevation (green dotted line) is presented at the right side of the charts.

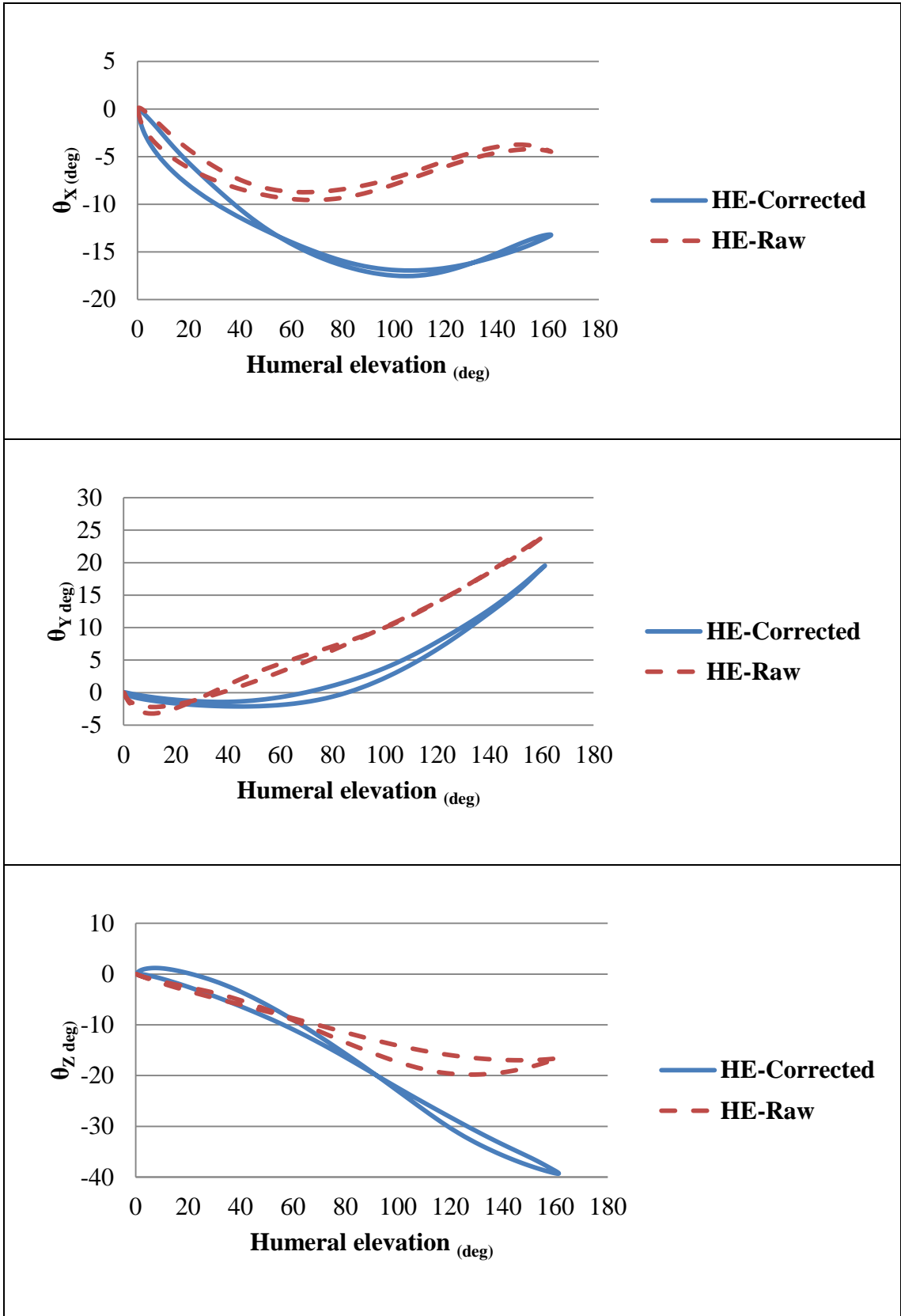


Figure 7.11. Left scapula orientation (deg) measurements before (Raw) and after correction (Corrected) for the participant with hyper elasticity (HE), where θ_X , θ_Y and θ_Z represent the orientation in for the three global axes, in humeral abduction-adduction.

7.6.2 Part 2), Muscle Patterning Participant: Humeral Abduction-Adduction

Figure 7.12 shows the Omega (ω) result from the scapula undertaken in Part 2) for the humeral abduction-adduction, of the left shoulder of the MP-participant. The sensor data shown in the figure represent the average over ten dynamic trials. The Omega data are in rad/s in the three local axes, ω_x , ω_y and ω_z ; the data can be identified as points throughout the quasi-static cycle of movement of the shoulder joint, as illustrated in this Figure.

The angular velocity results measured in Part 2) are presented in this section, where ω_x represents the upward and downward rotation of the scapula, ω_y represents the anterior/posterior tilt of the scapula, and finally ω_z represents the internal/external rotation of the scapula. The Omega measurements presented in Figure 7.12 correspond to the readings recorded by the IMUs attached to the scapula (Raw) in the global frame before and after the correction by applying the representative polynomial (see Table 7.4). The data presented in Figure 7.12 show the omega measurements after applying the quaternion rotation to the global reference frame (see Chapter IV).

The participant with muscle patterning failed to coordinate the elevation and depression of the arm. However, the MP-participant was able to reach his maximum amplitude, but failed in the time coordination, especially after the 30° of arm elevation.

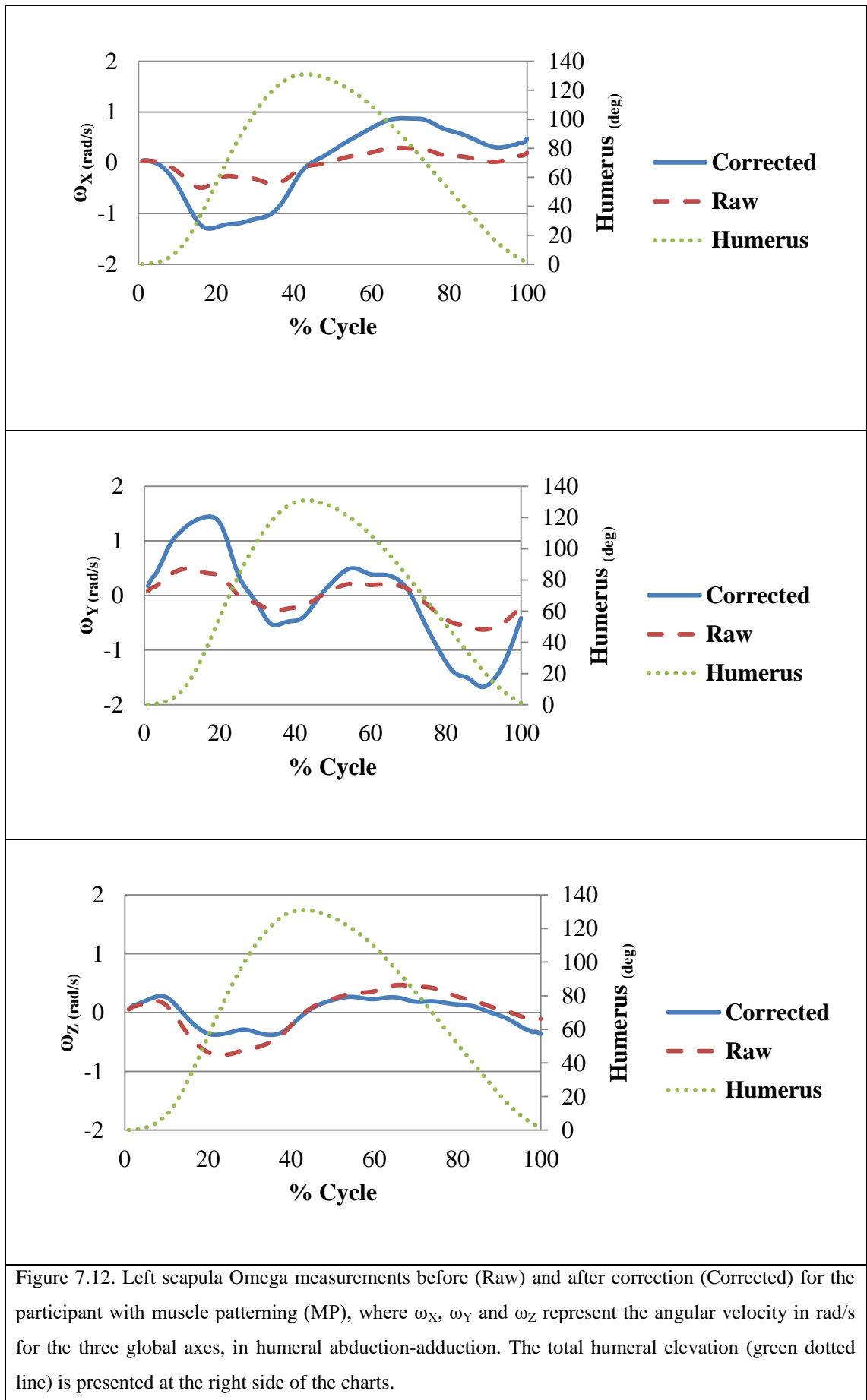
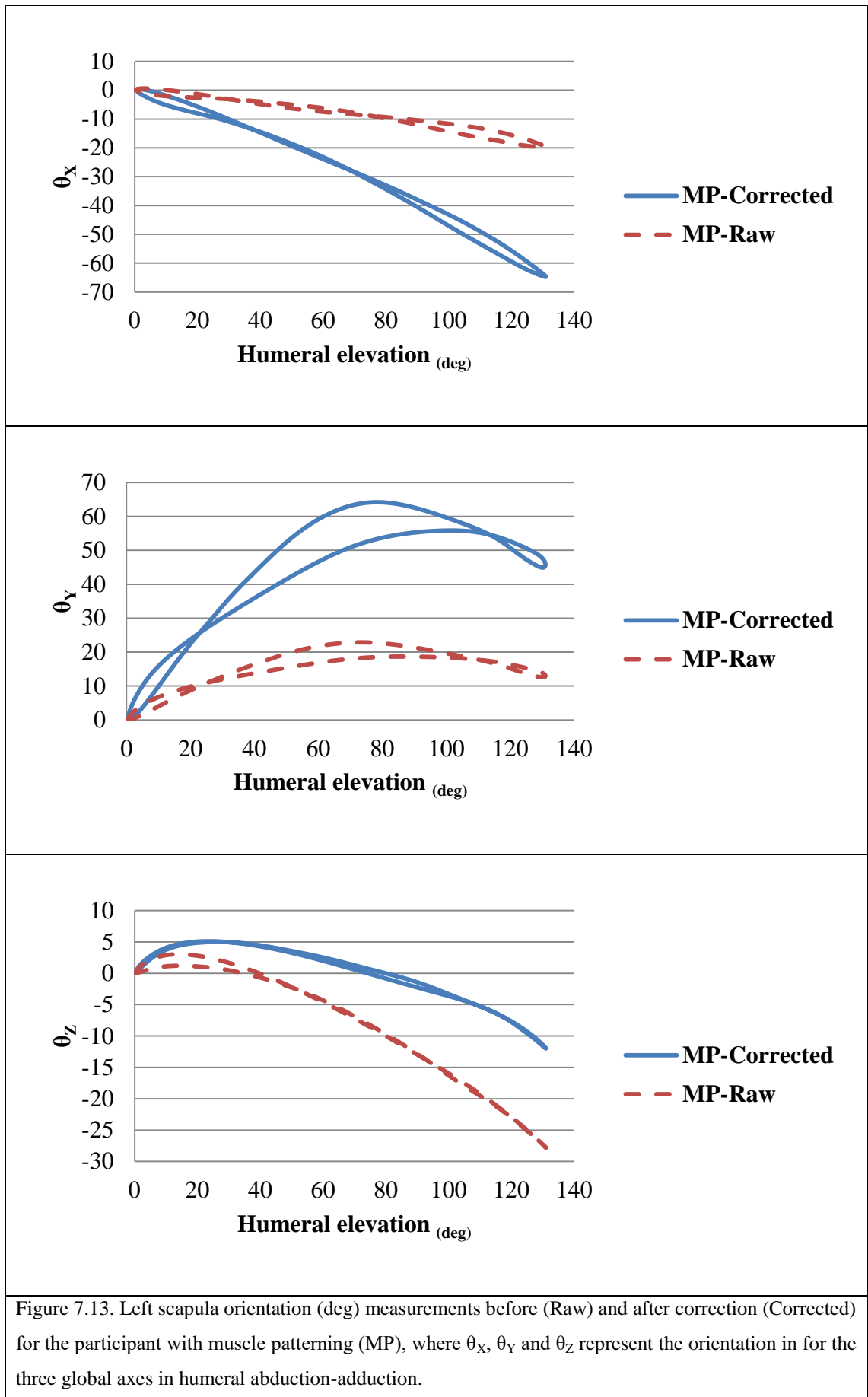


Figure 7.12. Left scapula Omega measurements before (Raw) and after correction (Corrected) for the participant with muscle patterning (MP), where ω_X , ω_Y and ω_Z represent the angular velocity in rad/s for the three global axes, in humeral abduction-adduction. The total humeral elevation (green dotted line) is presented at the right side of the charts.

The corrected data were rotated by using a quaternion rotation and integrated to obtain the angular orientation, and the results are presented in Figure 7.13.

The MP-participant (Figure 7.13), shows discernible differences in magnitude and shapes that can be observed in θ_X , θ_Y and θ_Z between the direct measurements of the scapula orientation by the scapular sensor (S-IMU) and the corrected orientation of the scapula by applying the polynomial obtained (Table 7.4). An interesting result can be seen in the θ_Y anterior/posterior tilt of the scapula: a change in the pattern appears after 75° of humeral elevation until the arm reaches its maximum amplitude, which can be confirmed from the visual feedback during the assessment. It is also in this part of the humeral elevation, above 75° , that the MP-participant feels the arm dislocation. There is an RMS error between the corrected orientation of the scapula and the orientation measured directly from the scapula sensor of 27° in the scapula upward/downward rotation, 30° in the anterior/posterior tilt of the scapula and 10° in the internal/external rotation of the scapula. This increment in the RMS error could be explained by differences in the motion pattern between the quasi-static and dynamic motion executed by the MP-participant.



7.6.3 Dynamic Results Comparison for Humeral Abduction-Adduction

If the results of both participants from Figure 7.10 and Figure 7.12 are compared, even though some similarities in the pattern of the scapula angular velocity were registered by the scapula sensors, clear differences can be observed in the magnitude.

The anterior/posterior tilt of the scapula (ω_Y) is the axis with more variability in shape between participants; the MP-participant shows less activity (MP-Raw) than the HE-participant. The patterns between the corrected and the raw measurements were consistent in the internal/external rotation of the scapula (ω_Z); the MP-participant shows flatter behaviour, compared with the HE-participant. The HE-participant seems to damp the motion quicker (around 30% of the cycle) than the MP-participant (around 40% of the cycle) in the upward and downward rotation of the scapula (ω_X).

In terms of humeral elevation, the range of motion reached was around 160° for the HE-participant, while for the MP-participant it was around 130° . Another difference in the humeral elevation between participants is the maximum humeral elevation reached by the MP, occurring at around 40% of the cycle and not at the 50%. Considerable differences between participants in shape and magnitude can be observed, especially for the MP-participant, if Figure 7.11 and Figure 7.13 are compared. Results seem to be consistent in terms of shape between the predicted and measured results of each participant but the differences in magnitude are still greater for the MP-participant than for the HE-participant. The trajectory followed by the scapula for the MP-participant is different from the one followed by the HE-participant; this can be attributed to differences in neuromuscular control between participants.

It is also important to comment that the abduction-adduction motion was the most difficult movement to perform for the volunteers.

CHAPTER VIII: DISCUSSIONS AND CONCLUSIONS

8.1 Methodology for Tracking the Scapula

The two stages methodology proposed in this work delivered good results when it was tested over a wooden structure, suggesting that it is possible to track the orientation of a virtual scapula in three axes under dynamic conditions, by using a polynomial obtained from quasi-static measurements. The polynomial uses humeral and scapula orientations obtained from inertial sensors measurements fitted to SL data recorded in quasi-static measurements.

The SL is considered the best option to track the scapula [90]; but it is well known that it is limited to quasi-static measurements [30, 81, 90, 131]. On the other hand, the use of invasive techniques (implanted pins, [30, 80]) necessitates surgical treatment and anaesthesia and even those methods are prone to errors [80] or have to be used in a limited population. Another limitation is that glenohumeral joint motion has to be constrained to a limited range, when any of those techniques or devices is being used [79-81]. One potential advantage of the proposed methodology in Chapter IV is that it can be used for different shoulder motions through different planes; however, whatever movement of the shoulder joint must be assessed using the proposed methodology, specific quasi-static measurements must be undertaken that match the GHJ motion to be assessed.

The kinematics of the shoulder has been assessed under quasi-static conditions [81, 134] with the aim of explaining the shoulder movement by obtaining regression equations, or under dynamic conditions [85, 100, 127]. The increase in the dynamic assessment of the shoulder could be explained by the quasi-static assessment of the glenohumeral joint not providing enough information about the behaviour of the dynamic stabilizers of the shoulder. The proposed methodology in Chapter IV has the advantage of mixing the scapula locator measurements obtained in a preliminary stage and the dynamic inputs of the scapula and humerus measured in a secondary stage. This technique also allows us to determine the amount of potential error generated by the soft tissues in each of the participants assessed. It has been reported that the velocity does not have an effect on the shoulder motion, so the regression equations obtained from quasi-static

measurements can potentially be used for dynamically assessing the shoulder [100, 127].

The studied motion over the structure test can be described under quasi-static conditions by applying a linear regression, but caution must be exercised, because researchers have suggested the non-linearity of the shoulder motion when the humerus is elevated [81, 106, 134].

This work also opens the possibility to analyse the data by using accelerometry as a base, taking the vertical or the gravitational acceleration vector as global reference frame. But caution must be exercised in the data interpretation when the motion occurs in several planes, as Figure 4.14 shows. Changes in orientation can be induced by the effect of different rotations and translations of the scapula and humerus, as well as the motion of the different surrounding tissue layers. The results from Chapter IV suggest how important it is to place the sensor in the same orientation, especially when the sensors measuring the orientation of the shoulder components are aligned with the ground (perpendicular plane to the gravitational acceleration vector). One advantage of using the inertial sensors is the use of tri-axial accelerometers embedded in the sensors, which are more accurate in predicting orientations than linear accelerometers [132-133], which is an advantage considering that the protocol is based on accelerometry.

Researchers [2, 19, 160] have commented that multiple quasi-static data could not represent the real dynamic motion and this may be as a result of the soft tissues artefact. However the results of the structure test could help to understand the potential behaviour of the sensors as a result of the soft tissues effect.

Chapter IV has proved that the proposed methodology based on inertial sensors (accelerometers, magnetometers and gyroscopes) and locator devices works effectively, which agrees with previous work [30, 88, 91-92, 99-100]. But unlike other regression techniques [30, 81, 94, 97, 134] our method uses both scapula and humeral orientations, as inputs to predict the scapula orientation as if it were measured with a locator device, by potentially reducing the soft tissues effect. Even though the methodology presented has proved its functionality, the soft tissues effect needs a deeper understanding. The tissues effect and the accuracy of the methodology are discussed in the next section.

8.2 Tracking the Scapula: Porcine Study

In this section, the general methodology described in Chapter IV for non-invasive tracking of the scapula under dynamic conditions was put forward, which involves combining data from two surface mounted sensors using a regression-type equation developed from quasi-static trials undertaken using a scapula locator and two IMUs. The accuracy of the technique was investigated using experimental tests undertaken on a porcine cadaver by comparing results with a bone based technique (pins). Tests were also undertaken to investigate the level of error that can be induced by the soft tissue artefact when the scapula was tracked by a standard surface based method.

The investigation into the effect of the skin artefact found that the majority of the contribution to this artefact comes from the epidermal, dermal and subcutaneous fat layers and confirmed that skin based measurements are sensitive to the motion of the skin in relation to the underlying bone and that therefore these methods can lose accuracy.

The results from our quasi static trial demonstrate that it is possible to predict scapula location to SL-comparable accuracy under quasi static conditions by combining data from surface mounted sensors using a suitable regression type equation. Having established the regression equation using data from the quasi static trials, we then demonstrated that it was possible to accurately track the scapula under dynamic conditions non-invasively, utilising data from just two surface mounted IMUs in combination with this regression equation. In the dynamic trials undertaken on the porcine cadaver the maximum error in scapula orientation as determined by our methodology was 2.0° or 2.4% compared to 3.4° or 4.1% for the surface mounted scapula sensor, indicating that our methodology is more accurate in determining scapula location than using only a standard skin-based approach.

The thickness of the epidermal, dermal, subcutaneous tissue layer of the porcine cadaver specimen used in our tests was, at $2.8\text{mm} \pm 0.3\text{mm}$, relatively low; and therefore the skin mounted scapula sensor was able to provide a reasonable estimate of the scapula location (to within 3.4° or 4.1%). This finding supports those of other researchers, who have argued that surface based methods can provide reasonable accuracy if used on young and lean subjects [30]. However, in cases where soft tissue layers are more

substantial, standard skin based scapula sensor methods lose accuracy, particularly at large humeral elevations [30]. By employing a regression-type equation that is formulated using subject-specific data, our technique provides a skin based, non-invasive methodology for accurately tracking the scapula under dynamic conditions in subjects regardless of individual body morphology and as such can potentially aid in the diagnosis and rehabilitation of shoulder pathology.

An increase in the range of motion indicates the important effect of the soft tissue in the integrity of the joint. Any modification in the shoulder structure (tissue removal) may affect the joint motion behaviour through its range of motion. For clinical purposes, shoulder pathologies such as muscle laxity or shoulder instability can modify the pattern and range of motion of the shoulder joint in different axes by generating unwanted rotation or unbalanced forces over the joint.

8.3 General Representative Polynomial from Quasi-static Measurements, Human Approach

The results of Chapter VI suggest that it is possible to determine scapular orientation about three axes using IMUs directly attached to the scapula and humerus through the whole range of motion, as if the scapula was tracked with the SL. Although the general form of the relationships found between predicted and observed orientation was consistent across participants, which agreed with previous results [30, 160], the coefficients of the best fit polynomials for each participant were unique, as Tables 6.3 and 6.4 shows.

The offset in the orientation in the upward/downward rotation or X axis (Figure 6.9 and 6.12) reflects the differences in orientation between the sensor directly attached to the scapula and the sensor placed over the SL; these differences are mainly generated by the skin and subsequent tissues layers. The orientation switch in this axis is generated by the rotation of the scapula under the soft tissues surrounding the scapula. As a result of the local y and z axis, rotation applied to the yz plane generates the 'w' shape in the sensor placed directly to the scapula (Figure 6.9 and 6.12). Similar patterns have been reported by Klopčar [161]. On the other hand the SL does not present this problem, because the SL is not affected by the soft tissues. A similar offset can be appreciated in the axis where the anterior/posterior tilt occurs (Y axis); see Figure 6.9 and 6.12. The

offsets for both axes X and Y are constant throughout the test, while for the internal/external rotation of the scapula the measured orientations almost overlap each other; this can be explained by the constrained motion of the scapula due to the anatomical characteristic of the shoulder. It is important to highlight that due to the independent anatomical characteristics of the participants, it is possible to correct the pattern of the orientation by using the direction cosine, which simplifies the mathematical procedures.

This work focussed on the relative orientation of the humerus and scapula, using the gravitational acceleration vector as a global reference, and did not take into account the thoracic and clavicular motion, which makes it quite difficult to compare the results with those from previous studies, which commonly use the thorax as a reference. However, the results (in terms of the differences between methods of estimating scapula orientation) are generally similar to those obtained in previous work. Brochard *et al.* [93] compared scapula orientation from a palpation method using a metal rod with that obtained from optoelectronic tracking of passive markers. The differences reported range between 2.14° and 6.65° about the medio/lateral and anterior/posterior axes respectively, while the differences about the vertical axis ranged between 4.94° and 11.05° . Similarly, in an earlier study, Lempereur *et al.* [94] reported differences of 1.74° and 3.98° between palpation by using a locator rod and optoelectronic methods of recording scapula orientation, which are close to the differences reported in Table 6.5.

Karduna *et al.* [30] investigated the accuracy of measuring three-dimensional dynamic scapular kinematics with a magnetic tracking device by comparing orientations from tracking devices attached to the skin with those from devices attached to bone pins. For humero-thoracic elevations up to 90° , the study found differences of less than 5° in all axes for the posterior tilt of the scapula (the results reported here give differences between 1.6° and 3.4° for a similar motion). However, the differences increased rapidly as arm elevation increased beyond 90° up to the maximum elevation of 150° ; similar results were presented by Karduna *et al.* and MacLean *et al.* [30, 160], and these results indicate that caution must be exercised in measuring high humeral elevation. The RMS reported by Karduna *et al.* [30] over the entire RoM ranged between 4.7° and 8.6° for scapular posterior tilt, 2.0° and 4.2° (after a correction factor) for the scapular upward rotation and 3.2° to 11.4° for external rotation of the scapula. The RMSe results

reported here ranged between 3.0° and 3.2° for the scapular upward/downward rotation, 3.3° and 8.1° for the anterior/posterior tilt of the scapula, and 2.7° to 4.9° for the internal/external rotation of the scapula, and so concur well with the data from Karduna *et al.* [30].

It is considered that, to determine shoulder instability (polar type II and III of the Stanmore classification triangle) where poor scapular control or unbalanced muscle actions are occurring (altering the GHJ posture), assessment of the GHJ under dynamic conditions is necessary [6]. Consequently, the SL, which is limited to quasi-static measurement, is unsuitable for assessment of shoulder instability, even though it may be the most accurate way to determine scapular orientation. We have shown that it is possible to track scapular orientation dynamically, using an IMU attached to the skin over the scapula with acceptable accuracy, as though it were determined by the SL, especially at extreme humeral elevation. This approach allows investigation of the influence of dynamic shoulder stabilizers on GHJ kinematics over the whole range of motion in subjects with shoulder instability problems; however, caution must be exercised in the palpation of the anatomical bony landmarks and in the influence that the dynamic stabilizers of the shoulder may have under dynamic conditions.

The literature suggests that the Acromion is the most common sensor attachment point [30, 89, 162]. However, during the preliminary stages of this research the muscle belly formed in the Acromioclavicular area at high humeral elevations caused insuperable problems. The sensor placed over the acromion tracked the muscle deformation instead of the scapula bone (Acromion) at high humeral elevations over 120° . However, placing the sensor on the flat surface of the scapula, where the muscle coverage of the scapula was lower, provided a solution for scapular tracking at high humeral elevations. This work indicates that an IMU sensor on the flat surface of the scapula provides reliable and accurate tracking of the GHJ orientation.

Karduna *et al.* commented that one possible restriction in the use of IMUs to determine scapular orientation was that they must be used in young, thin participants [30]. However, if a representative polynomial relationship may be obtained for each participant, as shown in this work, IMUs could be used reliably to evaluate shoulder pathology under dynamic conditions with minimal effects from individual body

morphology. Furthermore, a tri-axial analysis over the whole range of motion, as presented in this work, is more useful than a single axis analysis, especially in the diagnosis and rehabilitation of shoulder pathology, when instability is present and shoulder postural alignment is required (inter-relation of vertex II and III of the Stanmore classification triangle). This work also suggests that preliminary diagnosis could be made using IMUs; by keeping this in mind, this work could be used as a basis for future diagnosis based on standard accelerometers such as those found in mobile devices. The information recorded by those devices could be sent to the expert prior to the appointment, giving them more time to decide the treatment.

It is possible to describe tri-axial GHJ orientation as if the scapula were tracked with the SL, by using a specific polynomial relationship for each of the participants. The subsequent reduction in the error generated by the soft tissue deformation (a consequence of individual body morphology) over the whole RoM will help in the diagnosis of shoulder disorders, especially in the earliest stages of shoulder pathology. The methodology presented in this work could help in the investigation and diagnosis of shoulder instability, and potentially reduce the need to subject patients to invasive or radiological investigations, if an early detection is made.

8.4 Case Study

This section discusses the obtained results from the two volunteers assessed in Chapter VII by applying the methodology described in Chapter IV.

In terms of participants, it is important to remember that the volunteer with hyper elasticity is considered a healthy participant, although people with hyper lax joints are prone to develop muscle patterning [43]. The hyper elastic participant did not present any signs of pain or discomfort throughout the tests; the volunteer only showed symptoms of fatigue after finishing the tests. In contrast, the volunteer with muscle patterning and different surgical processes showed symptoms of fatigue and discomfort throughout the tests.

One important observation between participants comes as a result of the number of quasi-static measurements performed by each participant (see Chapter IV, stage a) of the protocol). The hyper elastic participant was able to perform multiple consecutive

measurements (arm up and down) with no visual symptoms of discomfort or pain, merely fatigue. The muscle patterning volunteer showed clear visual symptoms of discomfort and effort to hold the arms in small periods of time, especially after the 30° of humeral elevation. The discomfort sensed by the volunteer, increased as his arms worked against the gravity effect; the most difficult part of the test being at around 90° and 120° of humeral elevation/ depression. This occurred in both motions assessed (flexion-extension and abduction-adduction).

The author of this work believes that the number of quasi static measurements used to describe the shoulder orientation is important, especially when the scapula orientation in shoulder pathologies is needed. The number of quasi-static measurements recorded is important for the description of the full range of motion (RoM). The output from the polynomial that has been obtained from few quasi-static measurements has the potential to generate a large error, not only through the soft tissues effect, but also by the transition from quasi-static to dynamic measurements, as a result of the strategy followed by the shoulder muscles in dynamic motion to reach the maximum humeral elevation through the whole RoM. The number of quasi static measurements used to describe the shoulder orientation is important, especially when the scapula orientation in shoulder pathologies is needed, because the strategy followed by the shoulder muscles to perform the motion could be different even though the arm reached its maximum elevation. If an interpolation is performed with a few quasi-static measurements for different humeral orientations to generate the polynomial, the output from the polynomial obtained has the potential to generate a large error when the transition from quasi-static to dynamic measurements is performed, because the motion pattern could be different, which agrees with the comments of MacLean *et al.* [160], who suggest that the transition from quasi-static to dynamic measurements could over or under estimate the angular orientation of the shoulder components. The results from Chapter VI (Figure 6.9 and 6.12) and the quasi-static result of the hyper elastic participant and the muscle patterning participant (see Figure 7.2, 7.3, 7.8 and 7.9), highlight how important the effect of the soft tissues is; these results together with the results presented in section **5.4.3** agree with the results of MacLean *et al.* [160].

In this work the researcher tried to cover the whole RoM with the recorded quasi-static measurements to obtain the representative mathematical models, even though a better

description of the range of motion is possible by obtaining several quasi-static measurements, as in the study performed by Meskers *et al.* [136] and the work presented in this thesis. However, asking the participants to perform several quasi-static measurements could be a disadvantage in terms of the time required for them to perform the test. The author of this work agrees that the reduction of the quasi-static measurements recorded on a test is common, practical and functional in shoulder assessment, being a common practice among researchers [2, 81, 94, 97, 107, 134, 138].

Different research studies have been done trying to describe the scapular orientation with mathematical models based on quasi-static and dynamic measurements of the shoulder, by using different devices/techniques, polynomial orders (from linear to a fifth degree) and inputs [2, 30, 81, 94, 97, 107, 134-136, 138]; the humerus is the most common input to the polynomials. The methodology presented uses both the scapula and humerus as direct predictors in a linear model. After the inspection of the mathematical models in Table 7.1, 7.2, 7.3 and 7.4, clear differences between participants can be observed. It was expected that by reducing the number of variables and degrees in the mathematical model, the differences would be smaller. However, the influence of non natural movement of the humeral head [1], the scapula [163] and dominant side, large amounts of fat covering the scapular area are factors that have the potential to modify the results obtained from the mathematical model. Based on the results presented, it seems that unwanted humeral rotations or different neuromuscular control could have a larger effect in the prediction of the scapular orientation than the soft tissues.

The advantage of using two inputs in the polynomial is that in the case of variability in one of the inputs, the prediction of the scapula orientation could generate large errors easy to identify. These observations suggest that this kind of polynomial has the potential to be used as an approach to diagnose shoulder instability or to assess the level of efficiency of the physiotherapy process, by obtaining and comparing different equations through the physiotherapy as well as patterns of motion and orientation of the shoulder components. Another important discussion is that even though in Chapter VI cubic and quadratic polynomials were suggested as the best option to describe the scapula orientation under quasi-static conditions, a linear model was used in Chapter VII, which potentially reduces the generated error by reducing the number of variables

in the mathematical model. Inspection of the mathematical models in Table 7.1, 7.2, 7.3 and 7.4 clearly indicates the differences between participants, highlighting how unique each participant was.

When the volunteers were requested to perform dynamic motion (Part 2)), problems in the coordination time were faced by the participant with MP; this type of coordination problem has been previously reported [7, 164]. The coordination problems began for the MP volunteer after the relative motion between the humerus and the scapula reached 30° of humeral elevation when the arms are flexing/abducting, and around 120° of arms extension/adduction, see Figure 7.6 and 7.12. The HE participant did not present this type of coordination problem.

The dynamic measurements of the hyper elastic participant from Figure 7.4 and 7.10 suggest that quasi-static measurements can be used for dynamically assessing the shoulder with low variability between the direct scapular measurements (Raw) and the corrected measurements (Corrected) by using the obtained polynomial. The low variability shown in Figure 7.4 and 7.10 for the hyper elastic participant between the direct measurements of the scapular angular velocity (Raw) and the corrected angular velocity (Corrected) suggest the lower effect that velocity had in healthy participants. This effect has been observed in healthy participants before by Zhou *et al.* and De Groot *et al.* [100, 127]. From this work it can be assumed that similarities in the scapula motion pattern in healthy participants under quasi-static and dynamic conditions can be used to assess shoulder pathologies based on the motion patterns [161] and on its range of motion [30, 88, 91-92, 99-100], by keeping in mind the amount of error that could be expected in each participant. The amount of error can be obtained following the procedure described in Part 1). Even though this methodology works for people without any symptoms of shoulder pathologies, caution must be exercised when quasi-static data is used to predict dynamic orientation. These findings agree with the work of McLean *et al.*[160], who suggested that differences may exist between quasi-static and dynamic measurements when using scapula locator devices, especially in free shoulder motion. Because this methodology is based on the omega correction, the kinetics parameters of the joint can be obtained [165] by processing the relative angular velocity of the joint (humerus-scapula, see Appendix A3).

The HE-participant results (in terms of the differences between methods of estimating scapula orientation) are generally similar to those obtained in previous work [30, 93, 160] and discussed in section 8.3. The RMSe results reported here ranged between 2.2° and 7.4° for the scapular upward/downward rotation, 3.8° and 4.7° for the anterior/posterior tilt of the scapula, and 2.2° to 11.5° for the internal/external rotation of the scapula, these results concur well with the data from Karduna *et al.* [30] described in section 8.3. The result suggests that the methodology presented works in healthy participants.

On the other hand the results from the muscle patterning participant (Figure 7.6 and 7.12) suggest that differences in the shoulder components motion at the glenoid fossa together with the humeral velocity [81, 106, 134], when the arm is elevated/depressed on pathological shoulders, could have a big impact in the scapula orientation prediction (see Figure 7.7 and 7.13). In atraumatic instability, it is common for patients to feel uncomfortable with arms elevation, it being common for them to avoid high humeral positions; and it has been also found that the scapula would follow the glenohumeral motion [83]. But what generates the humeral dislocation is still a challenge, highlighting the possibility of poor neuromuscular imbalance [83], which agrees with the results of Matias *et al.* [2], suggesting that a failure in the muscular control could generate an excessive protraction or a delay in the scapula retraction, as well as a major tilted position of the scapula or a delay in its posterior tilt, probably resulting from poor control of one of the biggest shoulder largest muscles such as the Trapezius.

The errors reported in the prediction of the scapula orientation in pathological shoulders concur well with the differences reported before as in the work presented by Matias *et al.* [2], where differences in shapes and errors can reach values up to 25° for participants assessed under quasi-static conditions, suggesting how different the neuromuscular control could be in each participant and the importance of the different morphologies and specific pathologies that each participant can present. The maximum RMS error reported for the MP participant was 30° and it occurs in the anterior/posterior tilt of the scapula being this axis the one with more variability as well as the axis where the potential dislocation of the shoulder occurs. The reported error measured under dynamic conditions concurs well with the results presented by Matias *et al.*[2], suggesting that this amount of error could potentially arise from the transition from quasi-static to

dynamic measurements indicating a different muscular control performed by the body in the joint motion. The author of this work believed that the error is not only caused by differences between quasi-static and dynamic measurements, but is a result of a combination of factors. Those factors could include differences in the muscular control exerted by the shoulder muscles between quasi-static and dynamic movements, misalignment in the sensor placements as a result of the physiological characteristics of each participant, and unwanted rotations, e.g. trunk rotations. It has been reported before that trunk rotations have a relationship with joint laxity [166] that potentially develops in a muscle patterning problem [43]. Trunk rotation and shoulder shrugging to compensate the motion and reduce pain were observed by the researcher at the moment of the muscle patterning participant assessment.

This methodology has shown that it can be used to predict the scapula orientation in participants by using two inputs in a polynomial obtained from quasi-static measurements.

8.5 General Conclusions

- This work illustrates that it appears possible to improve scapula tracking under dynamic conditions and reduce the amount of error generated by the soft tissues by applying the two stage methodology described in this work, by using data from inertial sensors to assess dynamic motion and a regression equation to reduce error generated by the soft tissues.
- The results presented in the first stage of the methodology suggest that the polynomial fit for quasi-static data are participant dependant. However, similar patterns were observed between participants.
 - ❖ In the second stage of the methodology, the least square fit is used to improve scapular orientation, with good results in the prediction of a simulated scapula orientation over a wooden structure and without the influence of soft tissues.
- The two stage methodology was effective in passive flexion-extension motion of the glenohumeral motion of a porcine specimen, which was used because of the similarities that the animal has with the human shoulder, including the soft tissue artefact. In conclusion the two stage methodology explains most of the soft

tissue error generated by the different layers of tissues covering the porcine scapula in quasi-static and passive motion.

- The two stage methodology appeared effective in a healthy human participant in dynamic tests, where there was no indication of shoulder instability.
 - ❖ This work agrees with previous work and validates the assumption made by Karduna *et al.* [30], that the skin is the main source of error when determining the orientation of the scapula. However, when quasi-static data are being recorded further variability can arise from failure to position the scapula locator in an appropriate way.
 - ❖ When the methodology was applied to a pathological shoulder with symptoms of muscle patterning, variability in the data measurements, especially in the transition from quasi-static to dynamic conditions were evident. The variability could have significant effects when the dynamic stabilizers of the upper arm and shoulder pathologies are being assessed with this methodology.
- Differences in the activation patterns of the muscles producing potentially unwanted rotation could influence the inputs of the polynomials, by modifying the muscular mechanism that moves the arm this could be the situation with the MP-participant, in which differences occurs between the muscular strategies to hold the arm in certain quasi-static position and in the kinematics of the arm under dynamic conditions. However, the lack of EMG means that the causes cannot be identified.
- The work presented here can be used as a framework for developing diagnosis protocols.
- It is not possible to eliminate the error generated by the soft tissues but it can be reduced considerably as demonstrated in this work. However, it may be more difficult to reduce the error generated by the soft tissues in people with shoulder pathologies due to possible differences in neuromuscular control.

8.6 Limitations of the Work

Several limitations are discussed in this section. In terms of the animal assessment used to validate the technique and quantify the amount of error presented in Chapter V of this

work. The porcine specimen is restricted to a small range of motion due to the natural anatomical constraints of the animal, especially if it is compared with the range of motion of a human shoulder joint. Another limitation was that even though that the radioulnar joint motion was controlled using a rigid humeral base, the potential error generated by the soft tissues surrounding the humerus is not being assessed. However a similar assumption was made for the clinical trial in humans, considering that the humeral sensor was fixed in place by strap with a plastic base, which is similar to the sensor mounted over the wooden base for the animal assessment. Another potential limitation of the animal assessment is that the motion occurs in one plane, which may vary from a clinical scenario in humans. However for a clinical setting, specific mathematical models are obtained for each axis, considering the motion through different planes. Finally the passive motion induced in the animal forelimb potentially omits any change in the muscle belly volume.

On Chapter VI and VII, the main limitation found was the time taken to perform the three quasi-static trials, and the different level of fatigue that were experimented by the volunteers, after performing each trial. Finally on chapter VII, the main limitation was generated by the difficulty to find volunteers with shoulder instability due to muscle patterning willing to take part in the assessment.

8.7 Future Work

Further development could be undertaken, based on the proposed methodology, even though the results have demonstrated the functionality of the methodology for a participant without shoulder pathology.

- Perform more validations and in vivo assessment of participant with shoulder pathologies such as muscle patterning, especially in pre and post surgical procedures, and throughout the rehabilitation process.
- Apply the methodology in patients with shoulder instability due to muscle patterning in one shoulder, while the remaining shoulder does not present any type of pathologies.
- Kinematic and electromyography assessment of the shoulder muscles should be done at the same time.

Original publications that rise from this work

Submitted

Durazo-Romero, E. S, Alonso T., Walmsley A., Watts A., Dynamic tracking of the scapula: study, Journal of Biomechanics, 2015. (Review)

Podium presentations

Durazo-Romero, E. S, Alonso T., Walmsley A., Watts A., A methodology for dynamically tracking scapular orientation over the complete range of motion, Wrightington gold Medal Research Day, Celebrating 80 years of Wrightington Hospital, 14th June 2013.

Durazo-Romero, E. S, Alonso T., Walmsley A., Watts A., Tracking the scapula orientation under dynamic conditions, Wrightington gold Medal Research Day, 20th June 2014.

REFERENCES

- 1 Kuhn JE. A new classification system for shoulder instability. *British Journal of Sports Medicine*. 2010, vol. 44, 341-346.
- 2 Matias R and Pascoal AG. The unstable shoulder in arm elevation: A three-dimensional and electromyographic study in subjects with glenohumeral instability. *Clinical Biomechanics*. 2006, vol. 21, S52-S58.
- 3 Bak K. Nontraumatic glenohumeral instability and coracoacromial impingement in swimmers. *Scandinavian Journal of Medicine and Science in Sports*. 1996, vol. 6, 132-144.
- 4 Chahal J, Kassiri K, Dion A, MacDonald P, and Leiter J. Diagnostic and treatment differences among experienced shoulder surgeons for instability conditions of the shoulder. *Clinical Journal of Sport Medicine*. 2007, vol. 17, 5-9.
- 5 Halder AM, Zhao KD, O'Driscoll SW, Morrey BF, and An KN. Dynamic contributions to superior shoulder stability. *Journal of Orthopaedic Research*. 2001, vol. 19, 206-212.
- 6 Jaggi A and Lambert S. Rehabilitation for shoulder instability. *British Journal of Sports Medicine*. 2010, vol. 44, 333-340.
- 7 Jaggi A, Noorani A, Malone A, Cowan J, Lambert S, and Bayley I. Muscle activation patterns in patients with recurrent shoulder instability. *International Journal of Shoulder Surgery*. 2012, vol. 6, 101-107.
- 8 Cordasco FA. Understanding Multidirectional Instability of the Shoulder. *Journal of Athletic Training*. 2000, vol. 35, 278-285.
- 9 Allain J, Goutallier D, and Glorion C, *Long-Term Results of the Latarjet Procedure for the Treatment of Anterior Instability of the Shoulder** vol. 80, 1998.
- 10 Funk L, Rotator Cuff Biomechanics, For MSc Orthopaedic Engineering, ed, 2005. https://www.shoulderdoc.co.uk/education/rotator_cuff_mechanics.pdf.
- 11 Veeger HEJ and van der Helm FCT. Shoulder function: The perfect compromise between mobility and stability. *Journal of Biomechanics*. 2007, vol. 40, 2119-2129.

- 12 Desroches Guillaume, Raphaël D, Didier P, Philippe V, François-Xavier L, and Laurence C. Upper limb joint dynamics during manual wheelchair propulsion. *Clinical Biomechanics*. 2010, vol. 25, 299-306.
- 13 Lugo RK, Kung P, and Ma CB. Shoulder biomechanics. *European Journal of Radiology*. 2008, vol. 68, 16-24.
- 14 Higham TE, Biewener AA, and Delp SL. Mechanics, modulation and modelling: How muscles actuate and control movement. *Philosophical Transactions of the Royal Society B: Biological Sciences*. 2011, vol. 366, 1463-1465.
- 15 Pulavarti RS, Symes TH, and Rangan A. Surgical interventions for anterior shoulder instability in adults. *Cochrane Database of Systematic Reviews*. 2009,
- 16 ANTHONY HEARN DEN DT. The cost of shoulder arthroscopy: a comparison with national tariff. *The Royal College of Surgeons of England*. 2008, vol. 90, 587–591.
- 17 Adla DN, Rowsell M, and Pandey R. Cost-effectiveness of open versus arthroscopic rotator cuff repair. *Journal of Shoulder and Elbow Surgery*. 2010, vol. 19, 258-261.
- 18 Kibler WB. Management of the Scapula in Glenohumeral Instability. *Techniques in Shoulder and Elbow Surgery*. 2003, vol. 4, 89-98.
- 19 Ogston JB and Ludewig PM. Differences in 3-Dimensional Shoulder Kinematics Between Persons With Multidirectional Instability and Asymptomatic Controls. *The American Journal of Sports Medicine*. August 1, 2007, vol. 35, 1361-1370.
- 20 Brox JI. Shoulder pain. *Bailliere's Best Practice and Research in Clinical Rheumatology*. 2003, vol. 17, 33-56.
- 21 Niska R, MD, M.P.H., F.A.C.E.P.; Bhuiya F, M.P.H.; and Jianmin Xu, M.S. National Hospital Ambulatory Medical Care Survey: 2007 Emergency Department Summary. *National Health Statistics Reports*. August 6, 2010 2010, vol. 26,
- 22 Chun-Ju Hsiao PDDKC, M.S.; Paul C. Beatty, Ph.D.; and Elizabeth A. Rechtsteiner, M.S. National Ambulatory Medical Care Survey: 2007 Summary. *National Health Statistics Reports*. 2010, vol. 27,

- 23 Linsell L, Dawson J, Zondervan K, Rose P, Randall T, Fitzpatrick R, and Carr A. Prevalence and incidence of adults consulting for shoulder conditions in UK primary care; patterns of diagnosis and referral. *Rheumatology*. 2006, vol. 45, 215-221.
- 24 Owens BD, Agel J, Mountcastle SB, Cameron KL, and Nelson BJ. Incidence of glenohumeral instability in collegiate athletics. *American Journal of Sports Medicine*. 2009, vol. 37, 1750-1754.
- 25 Lewis A, Kitamura T, and Bayley JIL. (ii) The classification of shoulder instability: New light through old windows! *Current Orthopaedics*. 2004, vol. 18, 97-108.
- 26 Wuelker N, Korell M, and Thren K. Dynamic glenohumeral joint stability. *Journal of Shoulder and Elbow Surgery*. 1998, vol. 7, 43-52.
- 27 Barden JM, Balyk R, Raso VJ, Moreau M, and Bagnall K. Atypical shoulder muscle activation in multidirectional instability. *Clinical Neurophysiology*. 2005, vol. 116, 1846-1857.
- 28 Jan J, Benkalfate T, and Rochcongar P. The impact of recurrent dislocation on shoulder rotator muscle balance (a prospective study of 102 male patients). *Annals of Physical and Rehabilitation Medicine*. 2012, vol. 55, 404-414.
- 29 Stålhand J, Klarbring A, and Holzapfel GA. A mechanochemical 3D continuum model for smooth muscle contraction under finite strains. *Journal of Theoretical Biology*. 2011, vol. 268, 120-130.
- 30 Karduna AR, McClure PW, Michener LA, and Sennett B. Dynamic measurements of three-dimensional scapular kinematics: A validation study. *Journal of Biomechanical Engineering*. 2001, vol. 123, 184-190.
- 31 Busscher I, Ploegmakers JW, Verkerke G, and Veldhuizen A. Comparative anatomical dimensions of the complete human and porcine spine. *European Spine Journal*. 2010/07/01 2010, vol. 19, 1104-1114.
- 32 Douglas WR. Of pigs and men and research - A review of applications and analogies of the pig, *sus scrofa*, in human medical research. *Space Life Sciences*. 1972, vol. 3, 226-234.
- 33 Swindle MM, Makin A, Herron AJ, Clubb Jr FJ, and Frazier KS. Swine as Models in Biomedical Research and Toxicology Testing. *Veterinary Pathology*. 2012, vol. 49, 344-356.

- 34 Sullivan TP, Eaglstein WH, Davis SC, and Mertz P. The pig as a model for human wound healing. *Wound Repair and Regeneration*. 2001, vol. 9, 66-76.
- 35 Rowe CR, Pierce DS, and Clark JG. Voluntary dislocation of the shoulder. A preliminary report on a clinical, electromyographic, and psychiatric study of twenty-six patients. *Journal of Bone and Joint Surgery - Series A*. 1973, vol. 55, 445-460.
- 36 Tyson LL. Imaging of the painful shoulder. *Current Problems in Diagnostic Radiology*. 1995, vol. 24, 111-140.
- 37 Schachter AK, McHugh MP, Tyler TF, Kreminic IJ, Orishimo KF, Johnson C, Ben-Avi S, and Nicholas SJ. Electromyographic activity of selected scapular stabilizers during glenohumeral internal and external rotation contractions. *Journal of Shoulder and Elbow Surgery*. 2010, vol. 19, 884-890.
- 38 Dawson J, Fitzpatrick R, and Carr A. The assessment of shoulder instability. *Journal of Bone and Joint Surgery - Series B*. 1999, vol. 81, 420-426.
- 39 Hill AM, Bull AMJ, Richardson J, McGregor AH, Smith CD, Barrett CJ, Reilly P, and Wallace AL. The clinical assessment and classification of shoulder instability. *Current Orthopaedics*. 2008, vol. 22, 208-225.
- 40 Nyiri P, Illyés Á, Kiss R, and Kiss J. Intermediate biomechanical analysis of the effect of physiotherapy only compared with capsular shift and physiotherapy in multidirectional shoulder instability. *Journal of Shoulder and Elbow Surgery*. 2010, vol. 19, 802-813.
- 41 Silliman JF and Hawkins RJ. Classification and physical diagnosis of instability of the shoulder. *Clinical Orthopaedics and Related Research*. 1993, 7-19.
- 42 King LJ and Healy JC. Imaging of the painful shoulder. *Manual Therapy*. 1999, vol. 4, 11-18.
- 43 Barrett C. The clinical physiotherapy assessment of non-traumatic shoulder instability. *Shoulder & Elbow*. January 1, 2015 2015, vol. 7, 60-71.
- 44 Bohnsack M and Wülker N. (iv) Shoulder instability. *Current Orthopaedics*. 2002, vol. 16, 32-40.
- 45 Labriola JE, Lee TQ, Debski RE, and McMahon PJ. Stability and instability of the glenohumeral joint: The role of shoulder muscles. *Journal of Shoulder and Elbow Surgery*. 2005, vol. 14, S32-S38.

- 46 Endo H, Takigawa H, Takata K, and Miyoshi S. Loose shoulder: Diagnosis and treatment. [Translated by Eiji Itoi, MD, PhD* from the original paper in Japanese published in *Central Jpn J Orthop Surg Traumatol* 1971;14:630-2.]. *Journal of Shoulder and Elbow Surgery*. 2012, vol. 21, 1782-1784.
- 47 Kibler WB. The role of the scapula in athletic shoulder function. *American Journal of Sports Medicine*. 1998, vol. 26, 325-337.
- 48 William N. Levine ELF. The Pathophysiology of Shoulder Instability. *THE AMERICAN JOURNAL OF SPORTS MEDICINE*. 2000, vol. 28, 7.
- 49 Stark TW, Seebauer J, Walker B, McGurk N, and Cooley J. Severe aberrant glenohumeral motor patterns in a young female rower: A case report. *Chiropractic and Osteopathy*. 2007, vol. 15,
- 50 Precerutti M, Garioni E, Madonia L, and Draghi F. US anatomy of the shoulder: Pictorial essay. *Journal of Ultrasound*. 2010, vol. 13, 179-187.
- 51 Escamilla RF, Yamashiro K, Paulos L, and Andrews JR. Shoulder muscle activity and function in common shoulder rehabilitation exercises. *Sports Medicine*. 2009, vol. 39, 663-685.
- 52 Jaggi A, Malone AA, Cowan J, Lambert S, Bayley I, and Cairns MC. Prospective blinded comparison of surface versus wire electromyographic analysis of muscle recruitment in shoulder instability. *Physiotherapy Research International*. 2009, vol. 14, 17-29.
- 53 Yuk S, GP, Straker LM, and O'Sullivan PB. Neck-shoulder muscle activity in general and task-specific resting postures of symptomatic computer users with chronic neck pain. *Manual Therapy*. 2009, vol. 14, 338-345.
- 54 Rouleau DM, Faber K, and MacDermid JC. Systematic review of patient-administered shoulder functional scores on instability. *Journal of Shoulder and Elbow Surgery*. 2010, vol. 19, 1121-1128.
- 55 McFarland EG, Garzon-Muvdi J, Jia X, Desai P, and Petersen SA. Clinical and diagnostic tests for shoulder disorders: A critical review. *British Journal of Sports Medicine*. 2010, vol. 44, 328-332.
- 56 Brox JI. Shoulder pain. *Best Practice & Research Clinical rheumatology*. 2003, vol. 17, 33-56.
- 57 Beighton P, Solomon L, and Soskolne CL. Articular mobility in an African population. *Annals of the Rheumatic Diseases*. 1973, vol. 32, 413-418.

- 58 Simpson MR. Benign joint hypermobility syndrome: Evaluation, diagnosis, and management. *Journal of the American Osteopathic Association*. 2006, vol. 106, 531-536.
- 59 Omoumi P, Teixeira P, Lecouvet F, and Chung CB. Glenohumeral joint instability. *Journal of Magnetic Resonance Imaging*. 2011, vol. 33, 2-16.
- 60 Allen GM and Wilson DJ. Ultrasound of the shoulder. *European Journal of Ultrasound*. 2001, vol. 14, 3-9.
- 61 Baeyens JP, Van Roy P, De Schepper A, Declercq G, and Clarijs JP. Glenohumeral joint kinematics related to minor anterior instability of the shoulder at the end of the late preparatory phase of throwing. *Clinical Biomechanics*. 2001, vol. 16, 752-757.
- 62 Hug F. Can muscle coordination be precisely studied by surface electromyography? *Journal of Electromyography and Kinesiology*. 2011, vol. 21, 1-12.
- 63 ISEK. Standards for reporting EMG data. *Journal of Electromyography and Kinesiology*. 1997, vol. 7, I-II.
- 64 Barr KM, Miller AL, and Chapin KB. Surface electromyography does not accurately reflect rectus femoris activity during gait: Impact of speed and crouch on vasti-to-rectus crosstalk. *Gait and Posture*. 2010, vol. 32, 363-368.
- 65 Frigo C and Crenna P. Multichannel SEMG in clinical gait analysis: A review and state-of-the-art. *Clinical Biomechanics*. 2009, vol. 24, 236-245.
- 66 Piccinini L, Cimolin V, D'Angelo MG, Turconi AC, Crivellini M, and Galli M. 3D gait analysis in patients with hereditary spastic paraparesis and spastic diplegia: A kinematic, kinetic and EMG comparison. *European Journal of Paediatric Neurology*. 2011, vol. 15, 138-145.
- 67 Jaspers E, Feys H, Bruyninckx H, Harlaar J, Molenaers G, and Desloovere K. Upper limb kinematics: Development and reliability of a clinical protocol for children. *Gait & Posture*. 2011, vol. 33, 279-285.
- 68 White SC and Winter DA. Predicting muscle forces in gait from EMG signals and musculotendon kinematics. *Journal of Electromyography and Kinesiology*. 1992, vol. 2, 217-231.

- 69 Amarantini D, Rao G, and Berton E. A two-step EMG-and-optimization process to estimate muscle force during dynamic movement. *Journal of Biomechanics*. 2010, vol. 43, 1827-1830.
- 70 Gatti CJ, Doro LC, Langenderfer JE, Mell AG, Maratt JD, Carpenter JE, and Hughes RE. Evaluation of three methods for determining EMG-muscle force parameter estimates for the shoulder muscles. *Clinical Biomechanics*. 2008, vol. 23, 166-174.
- 71 Louis N and Gorce P. Surface electromyography activity of upper limb muscle during wheelchair propulsion: Influence of wheelchair configuration. *Clinical Biomechanics*. 2010, vol. 25, 879-885.
- 72 Lin C and Lei R. The influence of intrinsic muscle properties on musculoskeletal system stability: A modelling study. *Journal of Bionic Engineering*. 2010, vol. 7, S158-S165.
- 73 Brown SHM and McGill SM. Muscle force-stiffness characteristics influence joint stability: A spine example. *Clinical Biomechanics*. 2005, vol. 20, 917-922.
- 74 Potvin JR and Brown SHM. An equation to calculate individual muscle contributions to joint stability. *Journal of Biomechanics*. 2005, vol. 38, 973-980.
- 75 Brown SHM and Potvin JR. Constraining spine stability levels in an optimization model leads to the prediction of trunk muscle cocontraction and improved spine compression force estimates. *Journal of Biomechanics*. 2005, vol. 38, 745-754.
- 76 Trebs AA, Brandenburg JP, and Pitney WA. An electromyography analysis of 3 muscles surrounding the shoulder joint during the performance of a chest press exercise at several angles. *Journal of Strength and Conditioning Research*. 2010, vol. 24, 1925-1930.
- 77 Takwale VJ, Calvert P, and Rattue H. Involuntary positional instability of the shoulder in adolescents and young adults. *Journal of Bone and Joint Surgery - Series B*. 2000, vol. 82, 719-723.
- 78 Kibler WB and McMullen J. Scapular dyskinesis and its relation to shoulder pain. *The Journal of the American Academy of Orthopaedic Surgeons*. 2003, vol. 11, 142-151.

- 79 Ludewig PM and Cook TM. Alterations in shoulder kinematics and associated muscle activity in people with symptoms of shoulder impingement. *Physical Therapy*. 2000, vol. 80, 276-291.
- 80 Bourne D, Choo A, Regan W, MacIntyre D, and Oxland T. Accuracy of digitization of bony landmarks for measuring change in scapular attitude. *Proceedings of the Institution of Mechanical Engineers, Part H: Journal of Engineering in Medicine*. 2009, vol. 223, 349-361.
- 81 De Groot JH and Brand R. A three-dimensional regression model of the shoulder rhythm. *Clinical Biomechanics*. 2001, vol. 16, 735-743.
- 82 Jansen JHW, de Gast A, and Snijders CJ. Glenohumeral elevation-dependent influence of anterior glenohumeral capsular lesions on passive axial humeral rotation. *Journal of Biomechanics*. 2006, vol. 39, 1702-1707.
- 83 Inui H, Sugamoto K, Miyamoto T, Yoshikawa H, Machida A, Hashimoto J, and Nobuhara K. Three-dimensional relationship of the glenohumeral joint in the elevated position in shoulders with multidirectional instability. *Journal of Shoulder and Elbow Surgery*. 2002, vol. 11, 510-515.
- 84 Roren A, Lefevre-Colau MM, Roby-Brami A, Revel M, Fermanian J, Gautheron V, Poiraudreau S, and Fayad F. Modified 3D scapular kinematic patterns for activities of daily living in painful shoulders with restricted mobility: A comparison with contralateral unaffected shoulders. *Journal of Biomechanics*. 2012, vol. 45, 1305-1311.
- 85 Massimini DF, Warner JJP, and Li G. Non-invasive determination of coupled motion of the scapula and humerus-An in-vitro validation. *Journal of Biomechanics*. 2011, vol. 44, 408-412.
- 86 Matsuki K, Matsuki KO, Mu S, Yamaguchi S, Ochiai N, Sasho T, Sugaya H, Toyone T, Wada Y, Takahashi K, and Banks SA. In vivo 3-dimensional analysis of scapular kinematics: Comparison of dominant and nondominant shoulders. *Journal of Shoulder and Elbow Surgery*. 2011, vol. 20, 659-665.
- 87 Warner MB, Chappell PH, and Stokes MJ. Measuring scapular kinematics during arm lowering using the acromion marker cluster. *Human Movement Science*. 2012, vol. 31, 386-396.
- 88 Vermeulen HM, Stokdijk M, Eilers PHC, Meskers CGM, Rozing PM, and Vliet Vlieland TPM. Measurement of three dimensional shoulder movement patterns

- with an electromagnetic tracking device in patients with a frozen shoulder. *Annals of the Rheumatic Diseases*. 2002, vol. 61, 115-120.
- 89 Shaheen AF, Alexander CM, and Bull AMJ. Effects of attachment position and shoulder orientation during calibration on the accuracy of the acromial tracker. *Journal of Biomechanics*. 2011, vol. 44, 1410-1413.
- 90 Van Andel C, Van Hutten K, Eversdijk M, Veeger D, and Harlaar J. Recording scapular motion using an acromion marker cluster. *Gait & Posture*. 2009, vol. 29, 123-128.
- 91 Price CI, Rodgers H, Franklin P, Curless RH, and Johnson GR. Glenohumeral subluxation, scapula resting position, and scapula rotation after stroke: A noninvasive evaluation. *Archives of Physical Medicine and Rehabilitation*. 2001, vol. 82, 955-960.
- 92 Cutti AG, Giovanardi A, Rocchi L, Davalli A, and Sacchetti R. Ambulatory measurement of shoulder and elbow kinematics through inertial and magnetic sensors. *Medical and Biological Engineering and Computing*. 2008, vol. 46, 169-178.
- 93 Brochard S, Lempereur M, and Rémy-Néris O. Accuracy and reliability of three methods of recording scapular motion using reflective skin markers. *Proceedings of the Institution of Mechanical Engineers, Part H: Journal of Engineering in Medicine*. 2011, vol. 225, 100-105.
- 94 Lempereur M, Brochard S, Burdin V, and Rémy-néris O. Difference between palpation and optoelectronics recording of scapular motion. *Computer methods in biomechanics and biomedical engineering*. 2010, vol. 13, 49-57.
- 95 Yano Y, Hamada J, Tamai K, Yoshizaki K, Sahara R, Fujiwara T, and Nohara Y. Different scapular kinematics in healthy subjects during arm elevation and lowering: Glenohumeral and scapulothoracic patterns. *Journal of Shoulder and Elbow Surgery*. 2010, vol. 19, 209-215.
- 96 De Groot JH, Van Woensel W, and Van Der Helm FC. Effect of different arm loads on the position of the scapula in abduction postures. *Clinical Biomechanics*. 1999, vol. 14, 309-314.
- 97 Forte FC, Peduzzi de Castro M, Mahnic de Toledo J, Ribeiro DC, and Loss JF. Scapular kinematics and scapulohumeral rhythm during resisted shoulder

- abduction - Implications for clinical practice. *Physical Therapy in Sport*. 2009, vol. 10, 105-111.
- 98 Magermans DJ, Chadwick EKJ, Veeger HEJ, and van der Helm FCT. Requirements for upper extremity motions during activities of daily living. *Clinical Biomechanics*. 2005, vol. 20, 591-599.
- 99 Rezzoug N, Jacquier-Bret J, and Gorce P. A method for estimating three-dimensional human arm movement with two electromagnetic sensors. *Computer methods in biomechanics and biomedical engineering*. 2010/12/01 2010, vol. 13, 663-668.
- 100 Zhou H, Hu H, Harris ND, and Hammerton J. Applications of wearable inertial sensors in estimation of upper limb movements. *Biomedical Signal Processing and Control*. 2006, vol. 1, 22-32.
- 101 Illyés Á and Kiss RM. Kinematic and muscle activity characteristics of multidirectional shoulder joint instability during elevation. *Knee Surgery, Sports Traumatology, Arthroscopy*. 2006, vol. 14, 673-685.
- 102 Walker D, Wright TW, Banks SA, and Struk AM. Electromyographic analysis of reverse total shoulder arthroplasties. *Journal of Shoulder and Elbow Surgery*. 2014, vol. 23, 166-172.
- 103 Alexander CM. Altered control of the trapezius muscle in subjects with non-traumatic shoulder instability. *Clinical Neurophysiology*. 2007, vol. 118, 2664-2671.
- 104 Van Der Helm FCT. Analysis of the kinematic and dynamic behavior of the shoulder mechanism. *Journal of Biomechanics*. 1994, vol. 27, 527-550.
- 105 Shaheen AF, Villa C, Lee YN, Bull AMJ, and Alexander CM. Scapular taping alters kinematics in asymptomatic subjects. *Journal of Electromyography and Kinesiology*. 2013, vol. 23, 326-333.
- 106 McClure PW, Michener LA, Sennett BJ, and Karduna AR. Direct 3-dimensional measurement of scapular kinematics during dynamic movements in vivo. *Journal of Shoulder and Elbow Surgery*. 2001, vol. 10, 269-277.
- 107 Grewal TJ and Dickerson CR. A novel three-dimensional shoulder rhythm definition that includes overhead and axially rotated humeral postures. *Journal of Biomechanics*. 2013, vol. 46, 608-611.

- 108 Martini FH, *Fundamentals of anatomy & Physiology (international Edition)*, Seventh Edition ed. San Francisco: Pearson-Benjamin Cummings, 2006.
- 109 Seeley RR, *Anatomy & Physiology*, Third Edition ed. St. Louis Missouri: Mosby, 1995.
- 110 Gray H. (2000). *Gray's Anatomy of the Human Body (Twentieth ed.)*. Available: <http://www.bartleby.com/107/>
- 111 Steindler A, *Kinesiology of the human body under normal and pathological conditions / by A. Steindler*. Springfield, Illinois, U.S.A.: Charles C Thomas, 1955.
- 112 Di Giacomo G, NP, Costantini A and De Vita A. (2008). *Atlas of Functional Shoulder Anatomy [electronic resource]*. Available: <http://www.springerlink.com/content/p74854/#section=154364&page=1>
- 113 Pronk G, *THE SHOULDER GIRDLE, analysed and modelled kinematically*, 1991.
- 114 Hess SA. Functional stability of the glenohumeral joint. *Manual Therapy*. 2000, vol. 5, 63-71.
- 115 Fu FH, Seel MJ, and Berger RA. Relevant shoulder biomechanics. *Operative Techniques in Orthopaedics*. 1991, vol. 1, 134-146.
- 116 House J and Mooradian A. Evaluation and management of shoulder pain in primary care clinics. *Southern Medical Journal*. 2010, vol. 103, 1129-1135.
- 117 Hurov J. Anatomy and Mechanics of the Shoulder: Review of Current Concepts. *Journal of Hand Therapy*. 2009, vol. 22, 328-343.
- 118 McArdle PJ, Kalbassi R, and Ilankovan V. Stability of the sternoclavicular joint: A retrospective study. *British Journal of Oral and Maxillofacial Surgery*. 2003, vol. 41, 12-15.
- 119 Sellards R. Anatomy and biomechanics of the acromioclavicular joint. *Operative Techniques in Sports Medicine*. 2004, vol. 12, 2-5.
- 120 Ludewig PM and Braman JP. Shoulder impingement: Biomechanical considerations in rehabilitation. *Manual Therapy*. 2011, vol. 16, 33-39.
- 121 Godfrey A, Conway R, Meagher D, and ÓLaighin G. Direct measurement of human movement by accelerometry. *Medical Engineering and Physics*. 2008, vol. 30, 1364-1386.

- 122 Tözeren A. (2000). *Human Body Dynamics: Classical Mechanics and Human Movement*. Available: <http://www.nu.edu.sa/userfiles/mksaleh/A.Tozeren%20-%20Human%20Body%20Dynamics%20-%20classical%20mechanics%20and%20human%20movement.pdf>
- 123 Pearl ML, Sidles JA, Lippitt SB, Harryman Ii DT, and Matsen Iii FA. Codman's paradox: Sixty years later. *Journal of Shoulder and Elbow Surgery*. 1992, vol. 1, 219-225.
- 124 Cheng PL. Simulation of Codman's paradox reveals a general law of motion. *Journal of Biomechanics*. 2006, vol. 39, 1201-1207.
- 125 Karduna AR, McClure PW, and Michener LA. Scapular kinematics: Effects of altering the Euler angle sequence of rotations. *Journal of Biomechanics*. 2000, vol. 33, 1063-1068.
- 126 Wu G, van der Helm FCT, Veeger HEJ, Makhsous M, Van Roy P, Anglin C, Nagels J, Karduna AR, McQuade K, Wang X, Werner FW, and Buchholz B. ISB recommendation on definitions of joint coordinate systems of various joints for the reporting of human joint motion--Part II: shoulder, elbow, wrist and hand. *Journal of Biomechanics*. 2005, vol. 38, 981-992.
- 127 De Groot JH, Valstar ER, and Arwert HJ. Velocity effects on the scapulo-humeral rhythm. *Clinical Biomechanics*. 1998, vol. 13, 593-602.
- 128 Zatsiorsky VM, *Kinematics of human motion / Vladimir M. Zatsiorsky*. Champaign, Ill.: Champaign, Ill. : Human Kinetics, 1998.
- 129 Dickerson CR, Chaffin DB, and Hughes RE. A mathematical musculoskeletal shoulder model for proactive ergonomic analysis. *Computer methods in biomechanics and biomedical engineering*. 2007, vol. 10, 389-400.
- 130 Dickerson CR, Hughes RE, and Chaffin DB. Experimental evaluation of a computational shoulder musculoskeletal model. *Clinical Biomechanics*. 2008, vol. 23, 886-894.
- 131 Shaheen AF, Alexander CM, and Bull AMJ. Tracking the scapula using the scapula locator with and without feedback from pressure-sensors: A comparative study. *Journal of Biomechanics*. 2011, vol. 44, 1633-1636.
- 132 Amasay T, Zodrow K, Kincl L, Hess J, and Karduna A. Validation of tri-axial accelerometer for the calculation of elevation angles. *International Journal of Industrial Ergonomics*. 2009, vol. 39, 783-789.

- 133 Amasay T, Latteri M, and Karduna AR. In vivo measurement of humeral elevation angles and exposure using a triaxial accelerometer. *Human Factors*. 2010, vol. 52, 616-626.
- 134 Hogfors C, Peterson B, Sigholm G, and Herberts P. Biomechanical model of the human shoulder joint-II. The shoulder rhythm. *Journal of Biomechanics*. 1991, vol. 24, 699-709.
- 135 De Groot JH. The variability of shoulder motions recorded by means of palpation. *Clinical Biomechanics*. 1997, vol. 12, 461-472.
- 136 Meskers CGM, Vermeulen HM, de Groot JH, van der Helm FCT, and Rozing PM. 3D shoulder position measurements using a six-degree-of-freedom electromagnetic tracking device. *Clinical Biomechanics*. 1998, vol. 13, 280-292.
- 137 Grewal T-J and Dickerson CR. A novel three-dimensional shoulder rhythm definition that includes overhead and axially rotated humeral postures. *Journal of Biomechanics*. 2013, vol. 46, 608-611.
- 138 Xu X, Lin J-h, and McGorry RW. A regression-based 3-D shoulder rhythm. *Journal of Biomechanics*. 2014, vol. 47, 1206-1210.
- 139 Steindler A, *Kinesiology of the human body under normal and pathological conditions / by A. Steindler*: Thomas, 1955.
- 140 Poppen NK and Walker PS. Normal and abnormal motion of the shoulder. *Journal of Bone and Joint Surgery - Series A*. 1976, vol. 58, 195-201.
- 141 Terry GC and Chopp TM. Functional Anatomy of the Shoulder. *Journal of Athletic Training*. 2000, vol. 35, 248-255.
- 142 Finnoff JT, Doucette S, and Hicken G. Glenohumeral instability and dislocation. *Physical Medicine and Rehabilitation Clinics of North America*. 2004, vol. 15, 575-605.
- 143 Myers JB and Lephart SM. Sensorimotor deficits contributing to glenohumeral instability. *Clinical Orthopaedics and Related Research*. 2002, 98-104.
- 144 Palastanga NF, Derek.; Soames, Roger. (2002). *Anatomy and Human Movement: Structure and Function (4Th Ed. ed.)*. Available: <http://www.netlibrary.com/Details.aspx?ProductId=114782&Terms=shoulder&ReturnLabel=lnkSearchResults&ReturnPath=/Search/SearchResults.aspx>
- 145 Eldra PS, RRS, Adragna PJ, Human Anatomy & Physiology, S. C. Publishing, Ed., Second Edition ed. United States of America, 1990.

- 146 Lee D. A Survey of Modeling and Simulation of Skeletal Muscle. 2010, vol. 28,
147 McComas AJ and Thomas HC. Fast and slow twitch muscles in man. *Journal of
the Neurological Sciences*. 1968, vol. 7, 301-307.
- 148 Bottinelli R and Reggiani C. Human skeletal muscle fibres: molecular and
functional diversity. *Progress in Biophysics and Molecular Biology*. 2000, vol.
73, 195-262.
- 149 Westerblad H, Bruton JD, and Katz A. Skeletal muscle: Energy metabolism,
fiber types, fatigue and adaptability. *Experimental Cell Research*. 2010, vol.
316, 3093-3099.
- 150 Brown JMM, Wickham JB, McAndrew DJ, and Huang XF. Muscles within
muscles: Coordination of 19 muscle segments within three shoulder muscles
during isometric motor tasks. *Journal of Electromyography and Kinesiology*.
2007, vol. 17, 57-73.
- 151 Kibler WB and Sciascia A. The role of the scapula in preventing and treating
shoulder instability. *Knee Surgery, Sports Traumatology, Arthroscopy*. 2016,
vol. 24, 390-397.
- 152 Mulcahey MK, Mc Neil JW, II, and Provencher MT, Recurrent anterior shoulder
instability, in *Shoulder Arthroscopy: Principles and Practice*, ed: Springer-
Verlag London Ltd, 2014, pp. 181-199.
- 153 XSens T. (2010, *MTw User Manual (2010-2011 ed.)* [Equipment User Manual].
Available: www.xsens.com
- 154 Kuipers JB, *Quaternions and rotation sequences : a primer with applications to
orbits, aerospace, and virtual reality / Jack B. Kuipers*. Princeton, N.J.:
Princeton, N.J. : Princeton University Press, 1999.
- 155 Cannan J and Hu H, A Multi-sensor armband based on muscle and motion
measurements, in *2012 IEEE International Conference on Robotics and
Biomimetics, ROBIO 2012*, Guangzhou, 2012, pp. 1098-1103.
- 156 Caruso MJ. Applications of magnetic sensors for low cost compass systems.
IEEE 2000 Position, Location and and Navigation Symposium. 2000, 177-184.
- 157 Bland JM and Altman DG. Statistical methods for assessing agreement between
two methods of clinical measurement. *Lancet*. 1986, vol. 1, 307-310.
- 158 Bland JM and Altman DG. Agreed statistics: Measurement method comparison.
Anesthesiology. 2012, vol. 116, 182-185.

- 159 Beighton P and Horan F. Orthopaedic aspects of the Ehlers-Danlos syndrome. *Journal of Bone and Joint Surgery - Series B*. 1969, vol. 51, 444-453.
- 160 MacLean KFE, Chopp JN, Grewal TJ, Picco BR, and Dickerson CR. Three-dimensional comparison of static and dynamic scapular motion tracking techniques. *Journal of Electromyography and Kinesiology*. 2014, vol. 24, 65-71.
- 161 Klopčar N and Lenarčič J. Bilateral and unilateral shoulder girdle kinematics during humeral elevation. *Clinical Biomechanics*. 2006, vol. 21, S20-S26.
- 162 Fayad F, Hoffmann G, Hanne-ton S, Yazbeck C, Lefevre-colau MM, Poirau-deau S, Revel M, and Roby-Brami A. 3-D scapular kinematics during arm elevation: Effect of motion velocity. *Clinical Biomechanics*. 2006, vol. 21, 932-941.
- 163 Yang JI, Chang CW, Chen SY, and Lin Jj. Shoulder kinematic features using arm elevation and rotation tests for classifying patients with frozen shoulder syndrome who respond to physical therapy. *Manual Therapy*. 2008, vol. 13, 544-551.
- 164 Struyf F, Cagnie B, Cools A, Baert I, Brempt JV, Struyf P, and Meeus M. Scapulothoracic muscle activity and recruitment timing in patients with shoulder impingement symptoms and glenohumeral instability. *Journal of Electromyography and Kinesiology*. 2014, vol. 24, 277-284.
- 165 Zatsiorsky VM, *Kinetics of human motion / Vladimir M. Zatsiorsky*. Champaign, IL: Champaign, IL : Human Kinetics, 2002.
- 166 Erkula G, Kiter AE, Kilic BA, Er E, Demirkan F, and Sponseller PD. The relation of joint laxity and trunk rotation. *Journal of Pediatric Orthopaedics Part B*. 2005, vol. 14, 38-41.

APPENDIX

Appendix A1: University Ethical Approval Ref 12143



Secretary to Research Ethics Committee 5
Faculty Office - Devonshire House

Tel: 0161 275 0288

Email: jared.ruff@manchester.ac.uk

Emmanuel S Durazo Romero
Bioengineering group, School of MACE

8th August 2012

Dear Emmanuel

Research Ethics Committee 5 (Flagged Humanities) - Project Ref 12143

Kinematics in patients with recurrent shoulder instability due to "patterning"

I am writing to inform you that the above project was reviewed by University Ethics Committee 5 (Flagged Humanities) on 23rd July 2012. This letter formally confirms approval for the above project and that no further changes are required to the documentation submitted to the committee.

This approval is effective for a period of five years and if the project continues beyond that period it must be submitted for review. It is the Committee's practice to warn investigators that they should not depart from the agreed protocol without seeking the approval of the Committee, as any significant deviation could invalidate the insurance arrangements and constitute research misconduct. We also ask that any information sheet should carry a University logo or other indication of where it came from, and that, in accordance with University policy, any data carrying personal identifiers must be encrypted when not held on a university computer or kept as a hard copy in a location which is accessible only to those involved with the research.

Finally, I would be grateful if you could complete and return the attached form at the end of the project.

I hope the research goes well.

Yours sincerely

A handwritten signature in black ink, appearing to read "Jared Ruff".

Jared Ruff
Senior Research Manager
Faculty of Humanities and Secretary to UREC 5 (Flagged Humanities)
0161 275 0288
[Jared.ruff@manchester.ac.uk](mailto:jared.ruff@manchester.ac.uk)

Appendix A2: NHS Ethical Approval Ref 13/NW/0128

Wrightington, Wigan and Leigh 
NHS Foundation Trust

Mr Adam Research and Development Dept
Wrightington Hospital
Hall Lane
Appley Bridge
Wigan
WN6 9EP

Dr Yeng Ang – Clinical Director of Research and Development
Mrs Christine Birchall – Head of Innovation, R & D and Clinical Trials
Mrs Pamela Johnson – Head of Innovation, R & D and Clinical Trials
Mrs Sandra Latham – Research and Development Co-ordinator

Tel: 01257 256465
Fax: 01257 256398

Christine.Birchall@wwl.nhs.uk
Pamela.Johnson@wwl.nhs.uk
Sandra.Latham@wwl.nhs.uk

Mr Adam Watts
Consultant Orthopaedic Surgeon
Upper Limb Research
Wrightington Hospital
Wigan
WN6 9EP

5th February 2014

Dear Mr Watts

RE: R & D No: 744 REC REF: 13/NW/0128: Shoulder Kinematics in Patients with Recurrent Shoulder Instability Due to 'Patterning'.

This letter is confirmation that you have Research and Development approval to conduct the above titled research study within Wrightington, Wigan and Leigh NHS Foundation Trust.

I would like to draw your attention to the following Trust policies: Health and Safety at Work Act, Data Protection Act 1998, Human Tissue Act 2004: Good Clinical Practice.

It is a requirement that the Research and Development Department are informed of:

- Any Amendments arising from the research study.
- Any Serious Adverse Events (SAE's) that might arise during the course of the study.
- Any presentations or publications arising from the study.

Please note part of your condition of approval is that you notify the Research and Development Department when you consent your first patient and that you send patient recruitment updates every month to the Research and Development Manager.

Yours sincerely

Appendix A3: Kinematics and Kinetics of the Shoulder Joint Under Dynamic Conditions.

- a) After the data has been cleaned from high frequency noise, the rotation from the local coordinate system of each sensor to the global or calibration frame (G) was performed by using a quaternion rotation, described in Section 4.2.6.
- b) When all the sensors were rotated to G (X,Y and Z), the relative angular velocity between each pair of sensors (SJ_G) was calculated by subtracting the three angular velocity components of the humerus (distal part) to the three angular components of the scapula (proximal part), Eq A.1.

$$SJ_G = S_G - H_G \quad \text{Eq A1}$$

- c) The parameters for time normalization are set in this part. For time normalization the start and end point of each repetition for each participant in the humeral flexion-extension and abduction-adduction motion is set by using the angular velocity. The starting and ending parameters will be used for future time normalization (0-100%).
- d) The relative angular velocities of the GHJ joint were integrated to obtain the orientation of the joint.
- e) The angular velocity is used to calculate the joint torque. To obtain the Torque or angular momentum (M) of the joint, the inertial tensor of the joint (I) and the relative angular acceleration (α) of the GHJ components were calculated, Eq A.2.

$$M = I\alpha \quad \text{Eq A.2}$$

The inertial tensor of the GHJ components around its centre of mass (I) is calculated by using anthropometric measurements and the inertial characteristics of human body segment [165], while alpha (α) is obtained by the derivation of the angular velocity (ω) with respect to the time. The components of Eq A.2 can be described as on Eq A.3, for each axis of motion.

$$\begin{aligned}
\sum M_X &= I_X \alpha_X - (I_Y - I_Z) \omega_Y \omega_Z \\
\sum M_Y &= I_Y \alpha_Y - (I_Z - I_X) \omega_Z \omega_X \\
\sum M_Z &= I_Z \alpha_Z - (I_X - I_Y) \omega_X \omega_Y
\end{aligned}
\tag{Eq A.3}$$

I_X , α_X and ω_X represent the inertial tensor, the angular acceleration and angular velocity in the axis where the anatomical abduction-adduction occurs. The subscripts ‘Y’ and ‘Z’ represent the axes where the anatomical flexion-extension and internal/external rotation occurs.

- f) The power generated by the joint (JP) was obtained by multiplying the Torque (M) and the relative angular velocity (ω), Eq A.4.

$$JP = \begin{Bmatrix} M_X & * & \omega_X \\ M_Y & * & \omega_Y \\ M_Z & * & \omega_Z \end{Bmatrix}
\tag{Eq A.4}$$

- g) Finally all the data were normalized with respect to the time from 0 to 100% using the starting and ending parameters obtained previously. The time normalization from 0 to 100% represents one full repetition (arm up and down), being 50% of the cycle the maximum arm elevation reached by the participants.

Results for the kinematic and kinetic of the participant with shoulder instability:

The young male volunteer presents instability problems in both shoulders. The left shoulder shows symptoms of instability problems due to muscle patterning, while the right shoulder has been under different surgery procedures.

Discrepancies in scapula alignment can be observed in Fig A1.

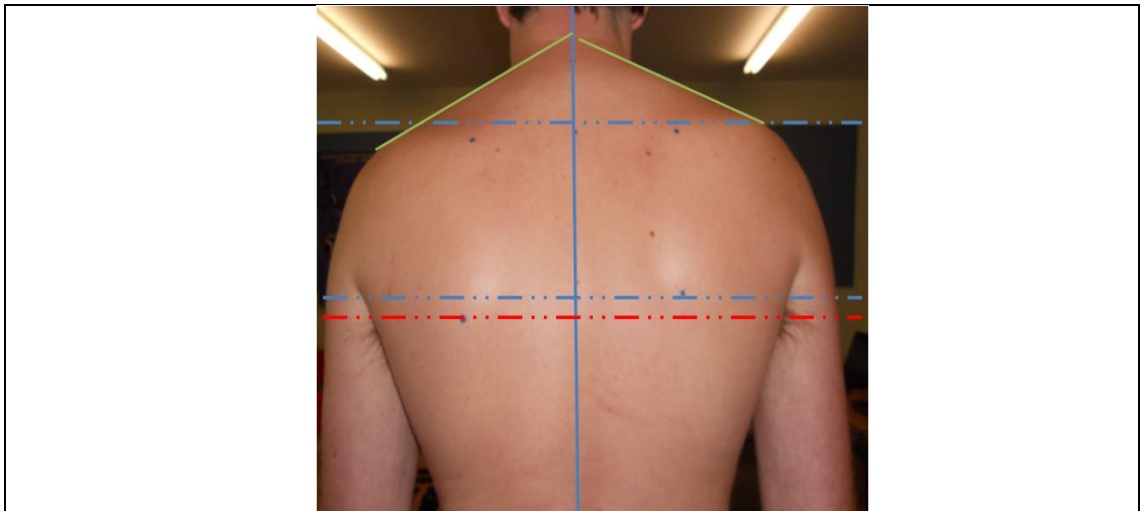


Figure A1, during landmarks identification, small differences in the alignment of the scapula were found. The left shoulder was identified as having instability due to muscle patterning, while the right shoulder had been subject to previous surgery process.

Four sensors were used to track the orientation of different parts of the upper body. Two sensors were placed in both arms, in a middle point between the elbow and the acromion process. Another two sensors were located in both left and right scapula, see Figure A2.

A total of twenty electromyography electrodes were placed in different muscles to assess the muscle activity. Two electrodes were placed in each muscle for both left and right shoulder muscles. The electrodes were located in the Sternal head of the Pectoralis Major, the middle Deltoid, Latissimus Dorsi, Upper Trapezius and in the Middle Trapezius, see Figure A2.

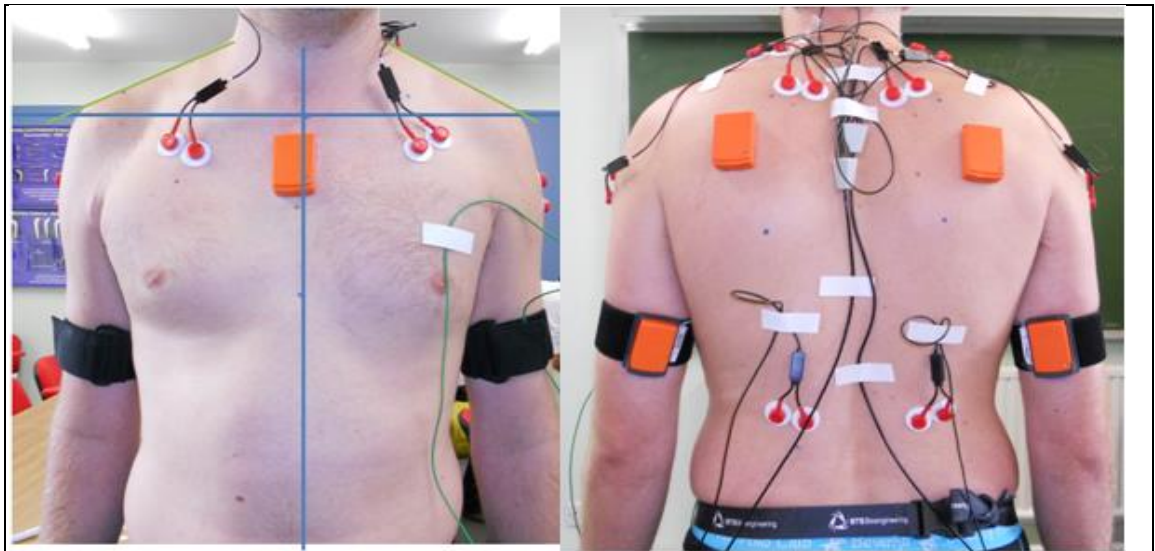


Figure A2, anterior view (frontal view) and posterior view (rear view) of the sensor and electromyography electrode placement.

Results

Note: No electromyography results were presented, because of equipment malfunction. The absence of this result will limit the utility of the report.

The anatomical flexion - extension motion is described in Figure A3.

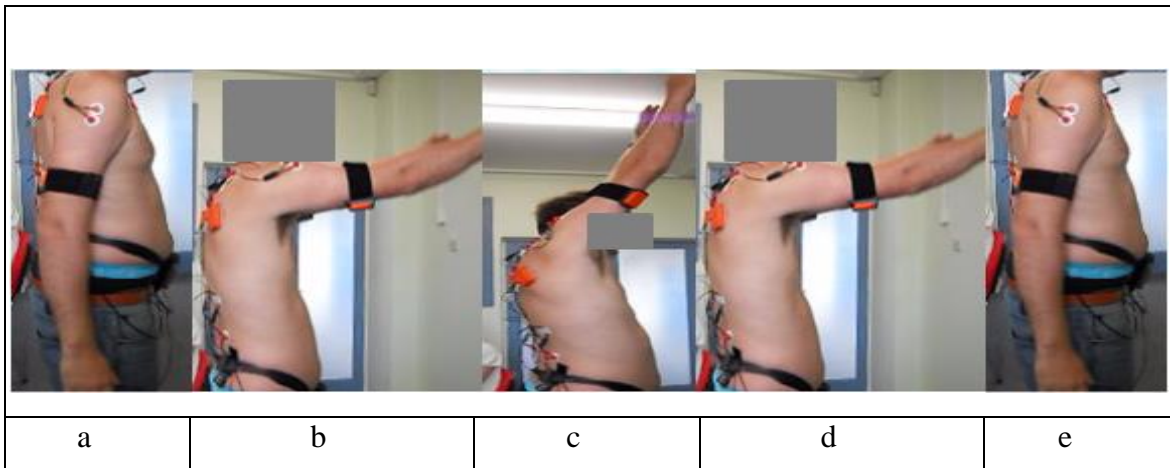


Figure A3, flexion-extension of the arm. The flexion of the arms starts at 0% of the cycle (a), approximate 90° of flexion (b), maximum elevation (c). The point 'c' represents the 50% of the cycle. The arms move downwards (extension) through 90° (d) arm in the starting position (e), 100% of the cycle.

The maximum mean amplitude reached was 149° for the left arm and 164.4° for the right arm in the flexion-extension motion axis. Shoulder movement data are shown in Figures A4 and A6.

The anatomical flexion-extension (Figure A4).

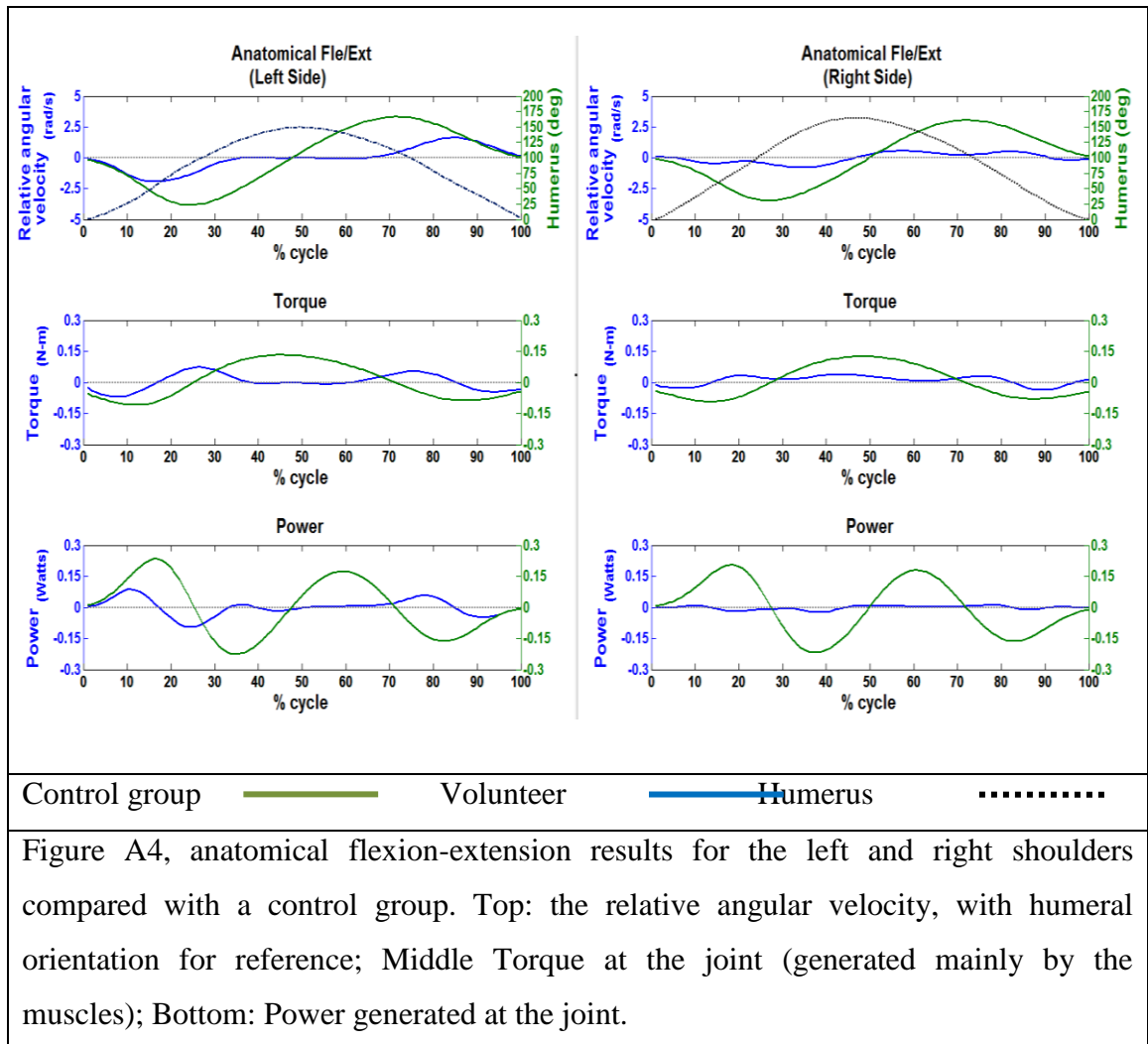


Figure A4, anatomical flexion-extension results for the left and right shoulders compared with a control group. Top: the relative angular velocity, with humeral orientation for reference; Middle Torque at the joint (generated mainly by the muscles); Bottom: Power generated at the joint.

Left shoulder see Figure A4.

0% - 18% of cycle. Dominant muscles flexors working against gravity, action concentric.

Peak torque about 50% of control peak torque and duration of extensor torque about 60% of duration in control.

Muscles do about 1/3 of the work compared with control group which indicates that peak power should be about 1/2 that of the control group.

18% - 32% of cycle. Dominant muscles extensors working with gravity, action eccentric.

When Torque is zero (about 35% of cycle) the muscle forces are balanced by gravitational forces and the arm is at maximum elevation of 149° compared with about 180° for the control group.

60%-85% of cycle. Dominant muscles extensors working with gravity, action concentric.

85%-100% of cycle. Dominant muscles flexors working against gravity, action eccentric.

Muscles do about $\frac{1}{3}$ of the work compared with control group which indicates that peak power should be about $\frac{1}{2}$ that of the control group.

Right shoulder see Figure A4.

0%-12% of cycle. Dominant muscles flexors working against the gravity, action concentric.

12%-27% of cycle. Dominant muscles extensors working with the gravity, action eccentric.

27%-50% of cycle small amount of Torque generated by the dominant extensor muscles working with gravity, generating almost none work at the joint. However small eccentric action of the extensor muscles acting eccentric between the 36% and 45% of the cycle. After the 45% of the cycle the joint Power is virtually zero until the 81% of the cycle.

50% of cycle. The arm is at its maximum elevation 164.4° compared with about 180° for the control group.

50%-70% of cycle. Torque is zero, which means that the muscle forces are in balance with the gravitational forces.

70%-81% of cycle. Dominant muscle extensors working against the gravity, with low concentric action generated at the joint.

81% to 100% of cycle. Small amount of torque is generated by the dominant flexors muscle working against the gravity, action eccentric between the 81% and 91% of the cycle. After 95% the Power generated at the joint is almost zero.

Muscle function very much reduced in both shoulders resulting in a much smaller torque and therefore reduced range of motion in both shoulder.

The anatomical abduction-adduction (Figure A5)

The anatomical abduction-adduction is described in Figure A5.

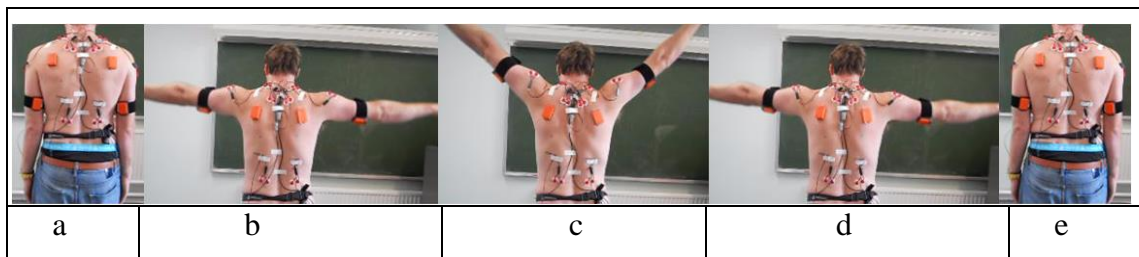


Figure A5, abduction-adduction of the arm. The abduction of the arms starts at 0% of the cycle (a), approx 90° abduction (b), maximum elevation (c). The maximum elevation of the arms represents the 50% of the cycle (c). The arms moves downward (adduction) through 90° (d) arm in the starting position (e), 100% of the cycle.

The relative angular velocity of the right and left shoulders will be of opposite sign (Figure A6). The maximum mean amplitude reached was 131.9° for the left arm and 129.2° for the right arm.

Left shoulder, Figure A6.

0%-24% of cycle. Muscles do about 1/4 of the work compared with control group which indicates that peak power should be about 1/4 that of the control group.

0%-9% of cycle. Small adductor Torque to kick off the arm abduction generated by the dominant adductor muscles working with the gravity with almost none Power generated at the joint.

9%-24% of cycle. Dominant muscles abductors working against the gravity, action concentric.

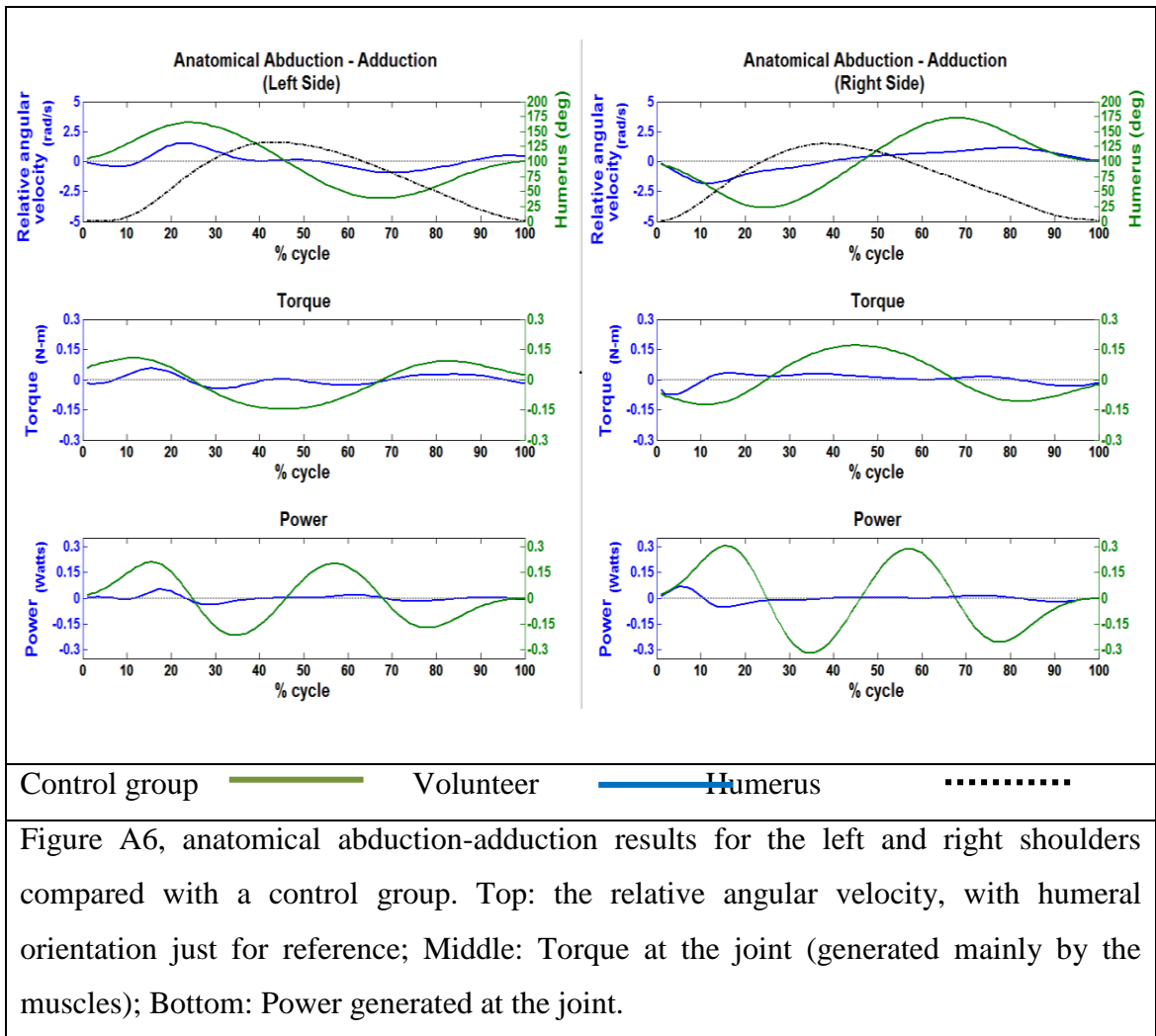


Figure A6, anatomical abduction-adduction results for the left and right shoulders compared with a control group. Top: the relative angular velocity, with humeral orientation just for reference; Middle: Torque at the joint (generated mainly by the muscles); Bottom: Power generated at the joint.

24%-38% of cycle. Dominant muscles adductors working with the gravity, action eccentric.

38%-50% of cycle. Torque is zero which means that the muscle forces are in balance with gravitational forces and no Power is generated at the joint. The arm is at maximum elevation of 132° compared with about 180 degrees for the control group.

50%-69% of cycle. Dominant muscles adductors working with gravity, action concentric.

69%-100% of cycle. Dominant muscles abductors working against gravity, action eccentric between 69% and 85% of the cycle. After the 85% of the cycle there is almost none Power generated at the joint.

Right shoulder, Figure A6.

24%-50% of cycle. Muscles do about 1/4 of the work compared with control group which indicates that peak power should be about 1/4 that of the control group.

0%-10% of cycle. Dominant muscles abductors working against the gravity, action concentric.

10%-50% of cycle. Dominant muscles adductors working with the gravity, action eccentric between 10%-24% of the cycle. After 50% of the cycle none Power is generated at the joint.

50%-66% of the cycle. Torque is zero, which means that the muscle forces are balanced by gravitational forces and no Power is generated at the joint. The arm is at maximum elevation of 129° compared with about 180° for the control group.

66%-84% of cycle. Small amount of adductor Torque is generated at the joint working with the gravity, action concentric.

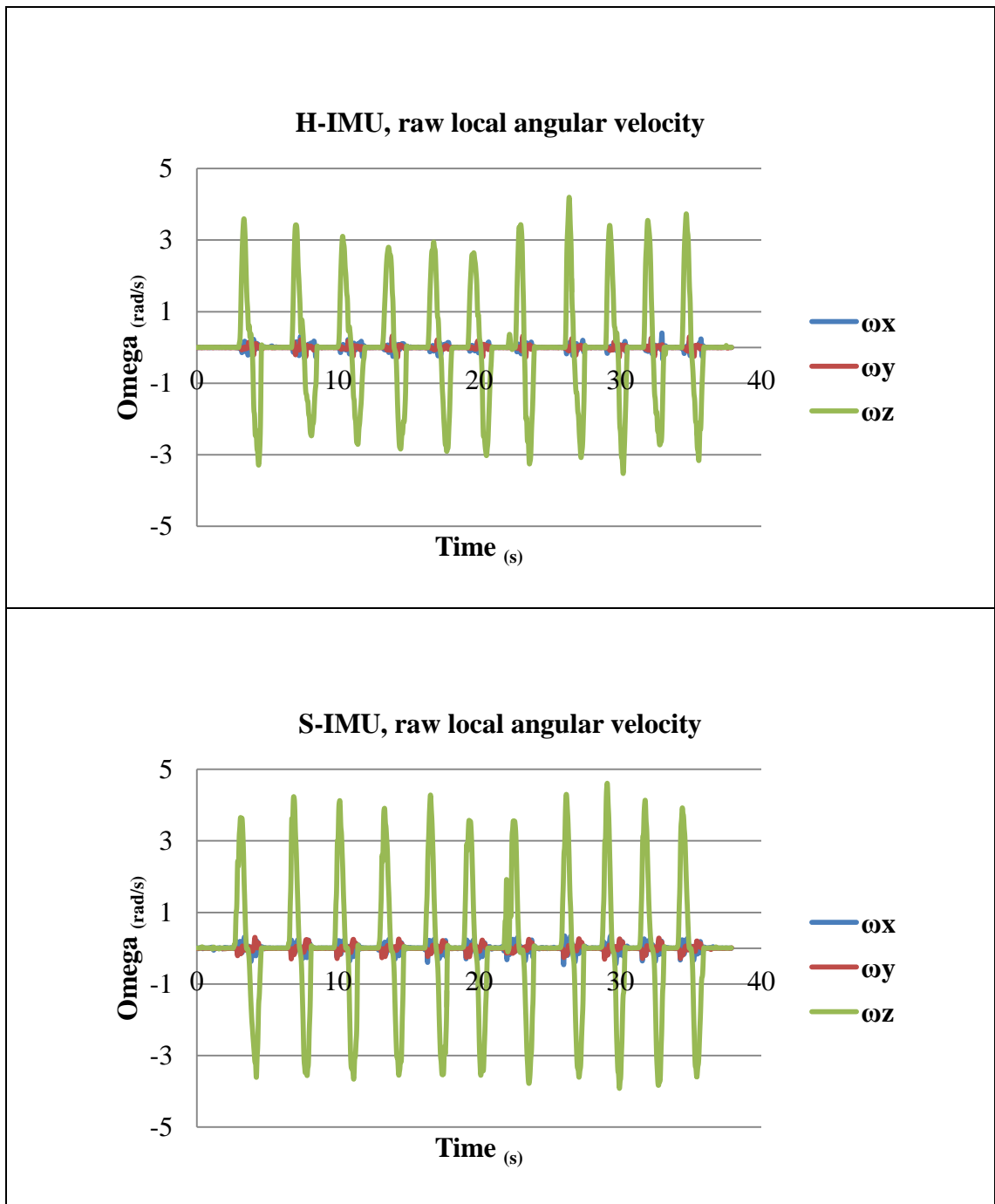
84%-100% of cycle. Dominant muscles abductors working against the gravity, action eccentric.

Conclusions

- The results suggest that the volunteer has shoulder muscles function that is very much reduced compared with the control group. Lack of EMG means that the causes cannot be identified. Could the general muscle weakness or altered activation patterns that change the way the muscles work together (ie. Working against each other rather than with each other).
- Physiotherapy and range of motion training might be useful, especially when the shoulder muscles are working against gravity.

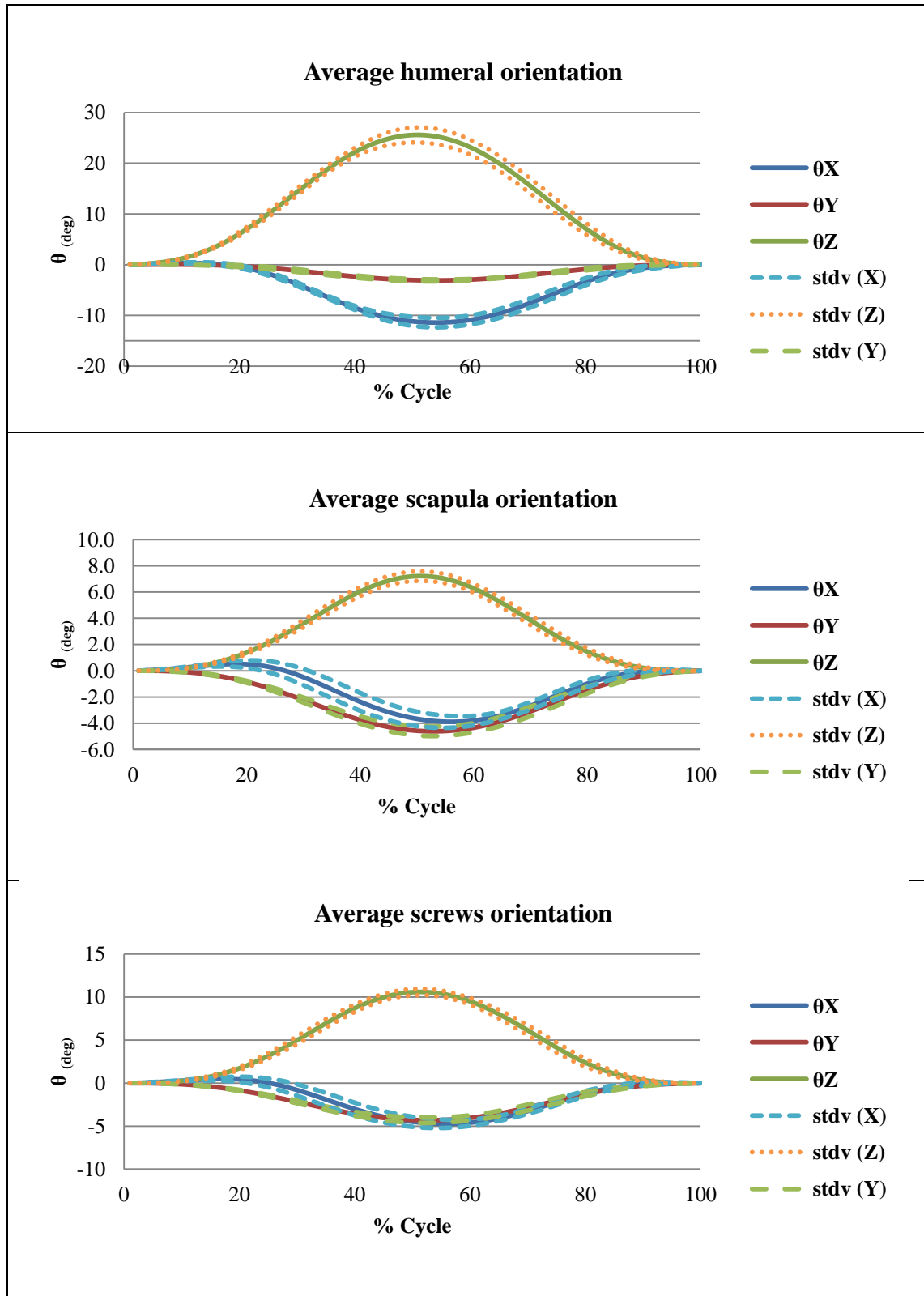
Appendix A4: Structure Test Data

Raw angular velocity recorded from the drawer structure test.

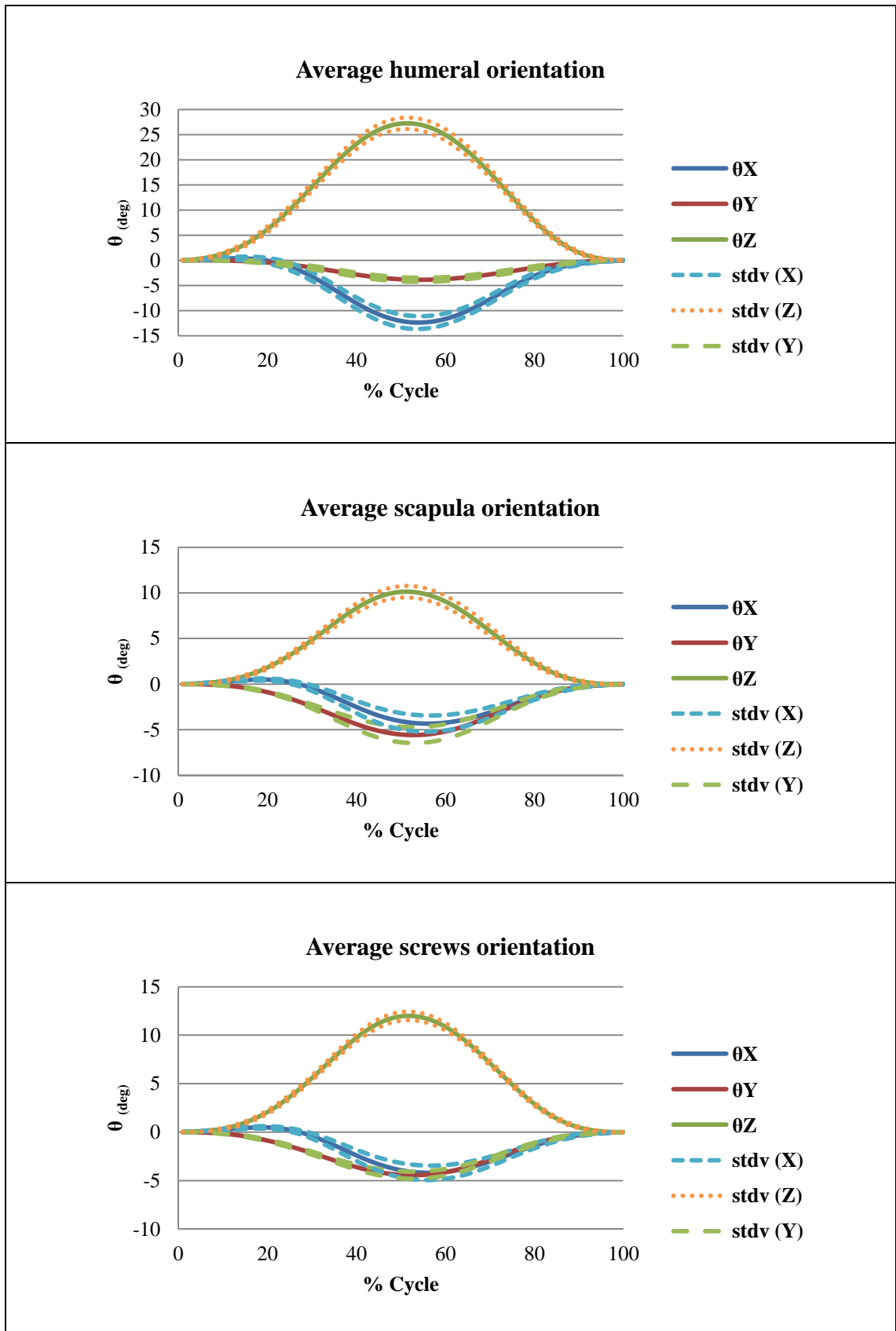


Appendix A5: Pig Test Data

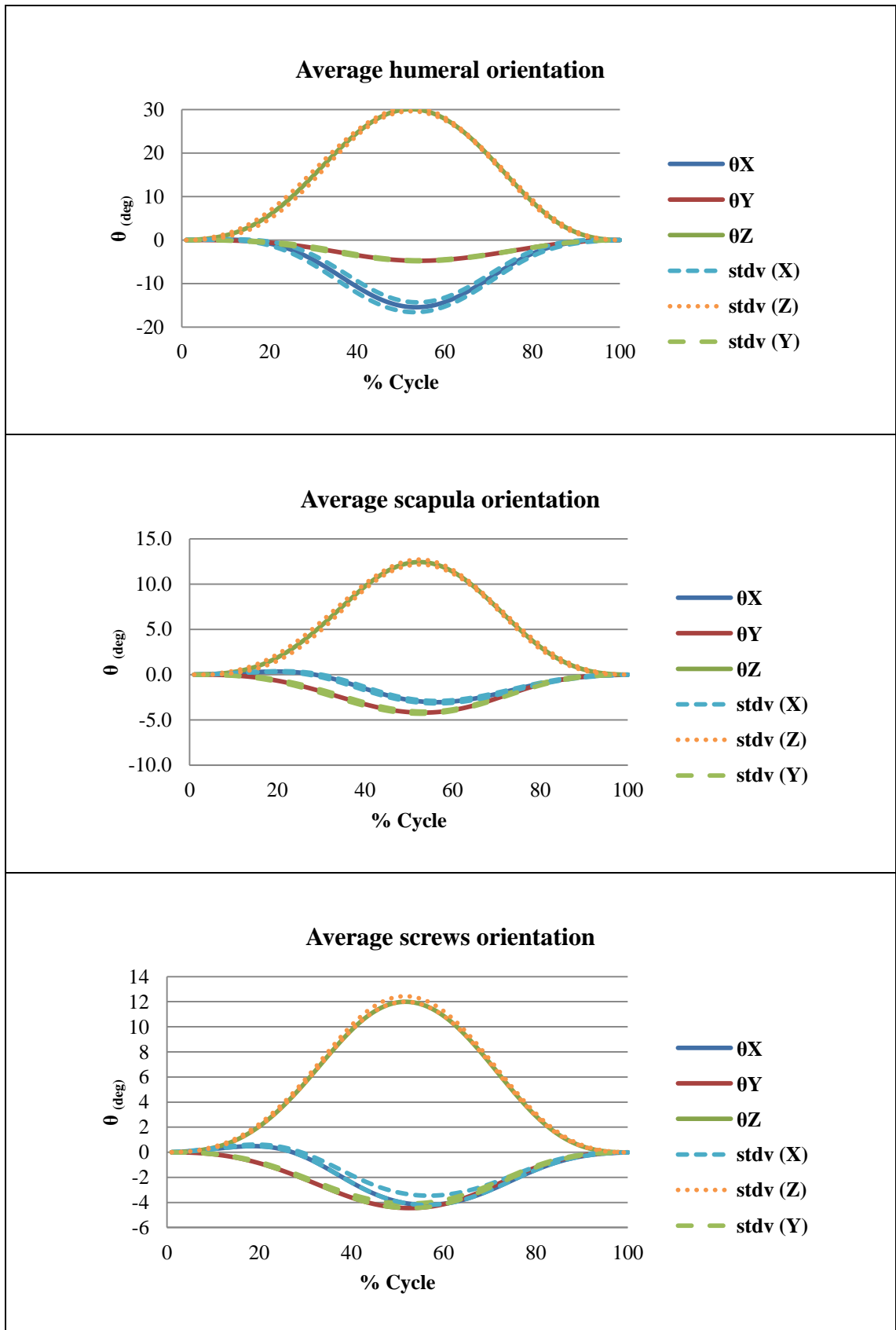
Average and standard deviation from the Humerus ($H\theta$), scapula ($S\theta$) and screws ($SC\theta$) orientations, over three global axes. Animal assessment with all the tissues intact.



Average and standard deviation from the Humerus ($H\theta$), scapula ($S\theta$) and screws ($SC\theta$) orientations, over three global axes. Animal assessment with the muscular tissue only.

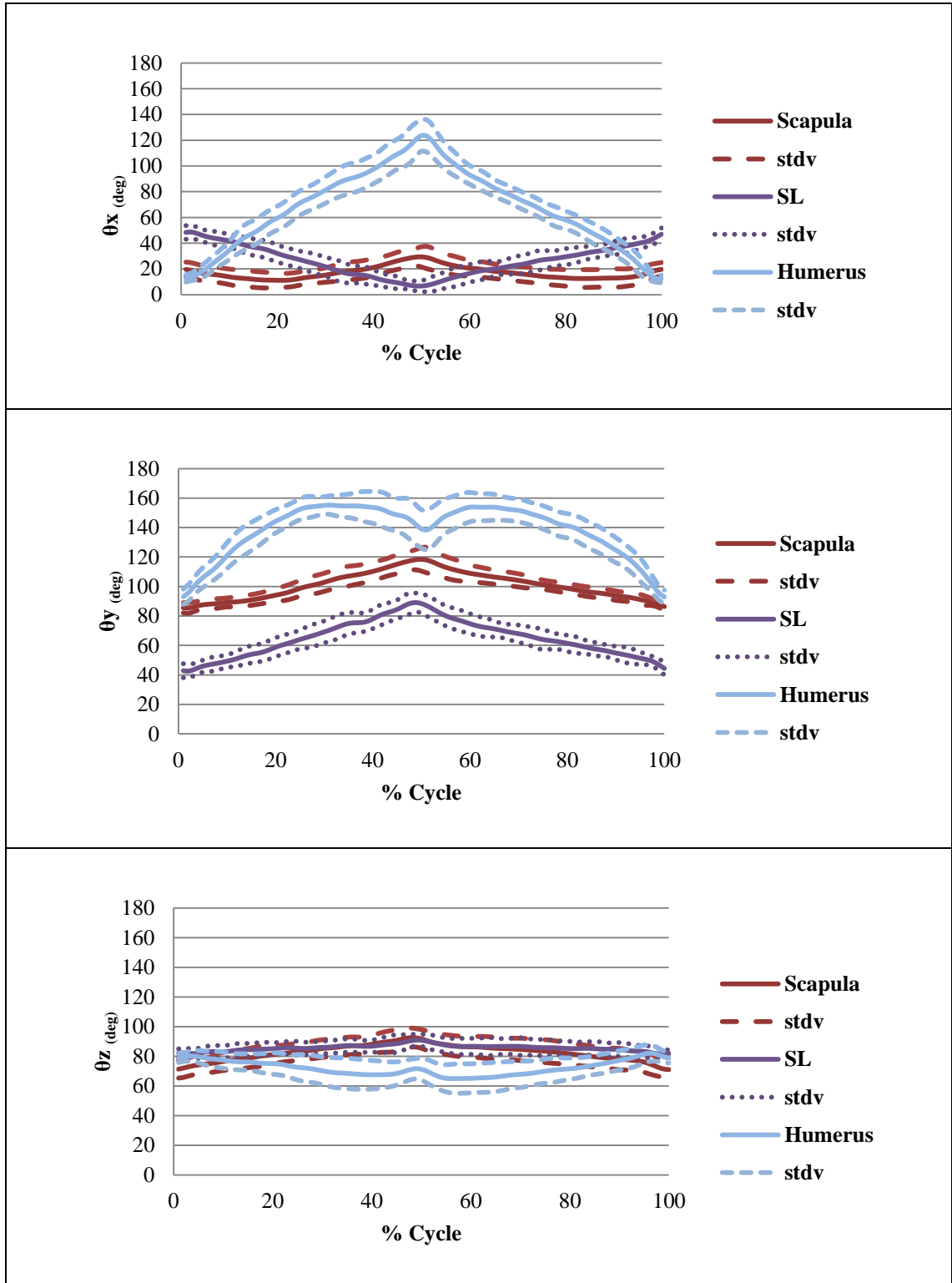


Average and standard deviation from the Humerus ($H\theta$), scapula ($S\theta$) and screws ($SC\theta$) orientations, over three global axes. Animal assessment bare bone.

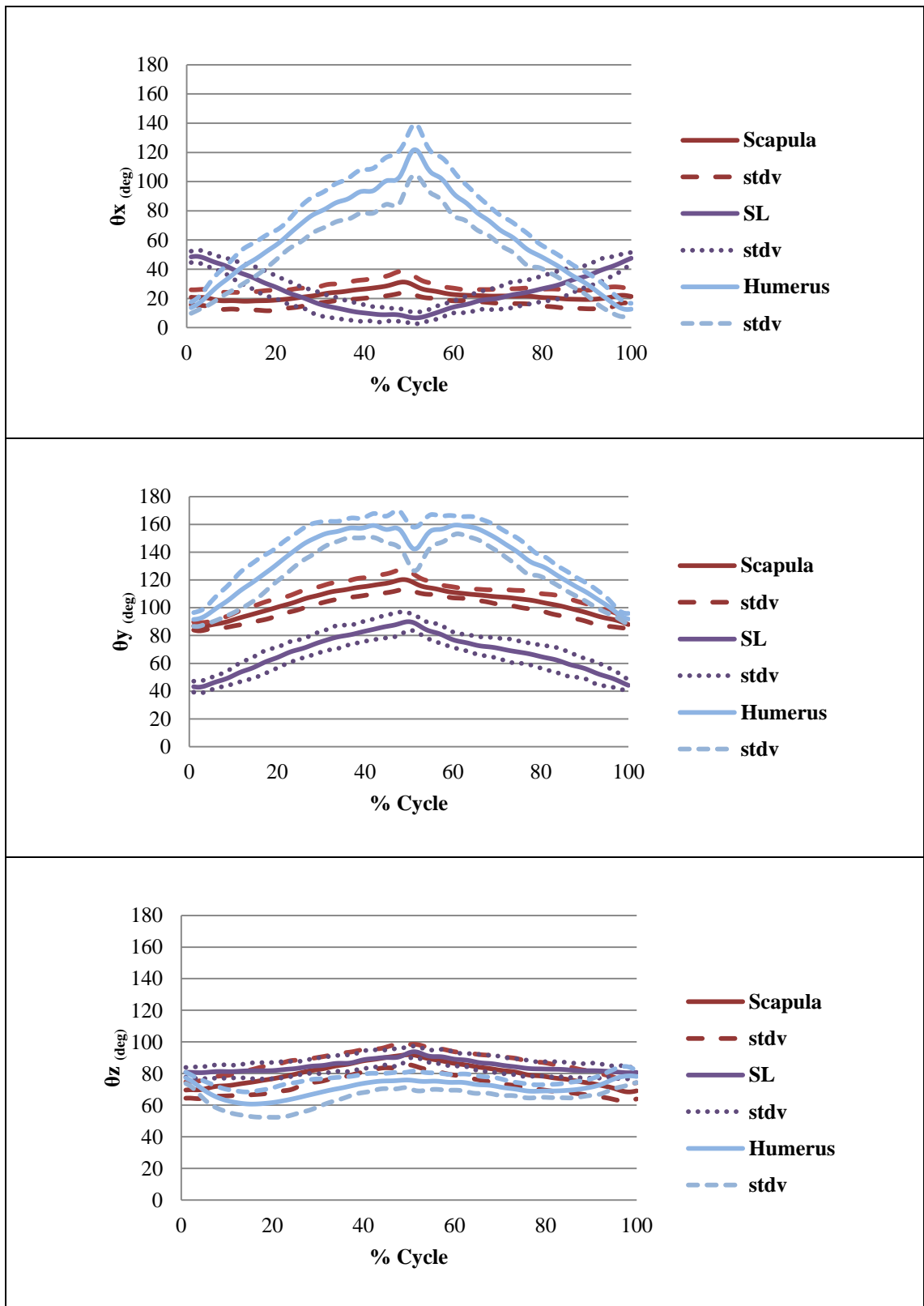


Appendix A6: Quasi-static Human Data

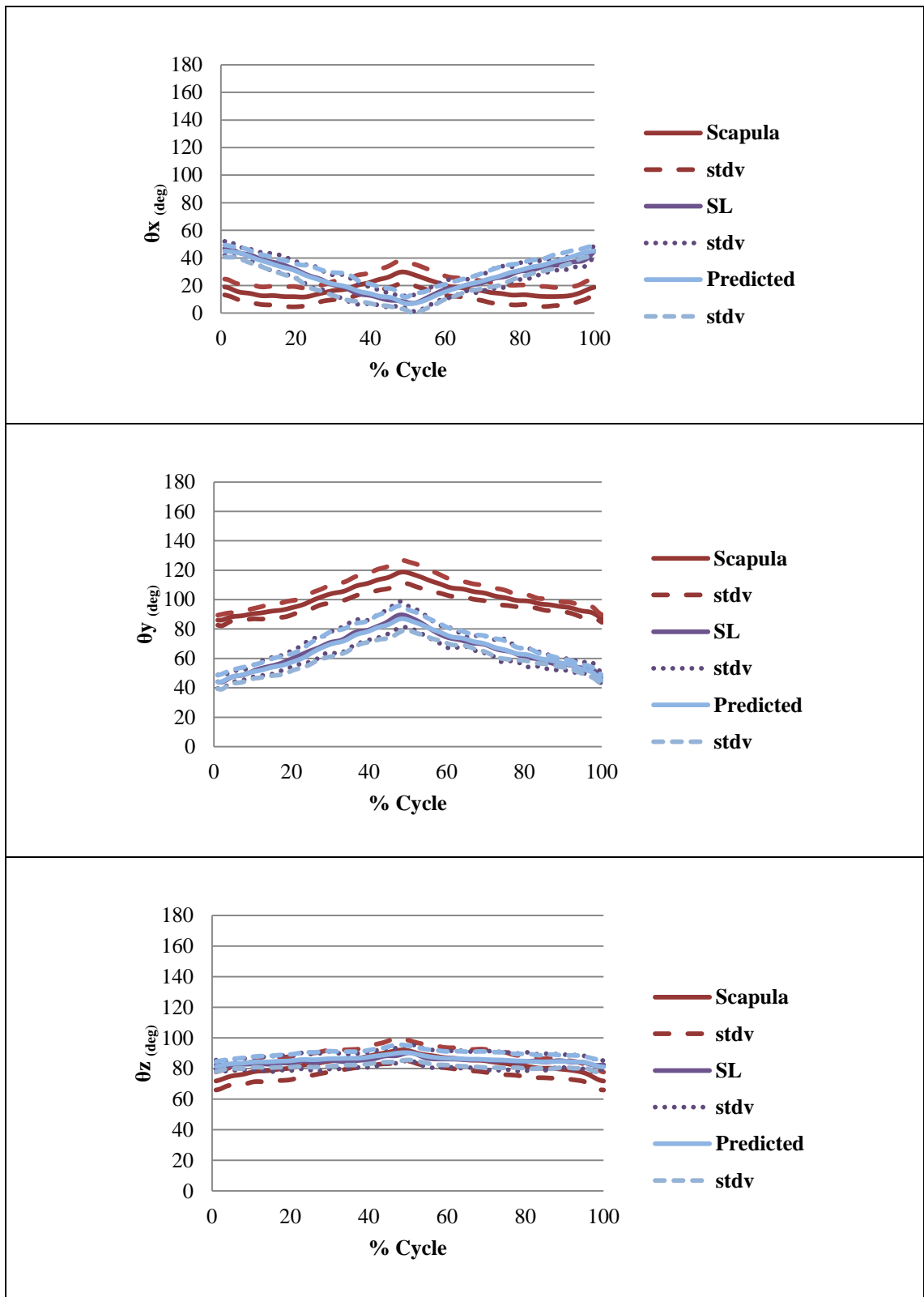
Mean and standard deviation data for nine participants (Chapter VI) under quasi-static conditions. The data presented is in respect with the vertical in three axes, in humeral flexion-extension, for the first two trials performed by the participants.



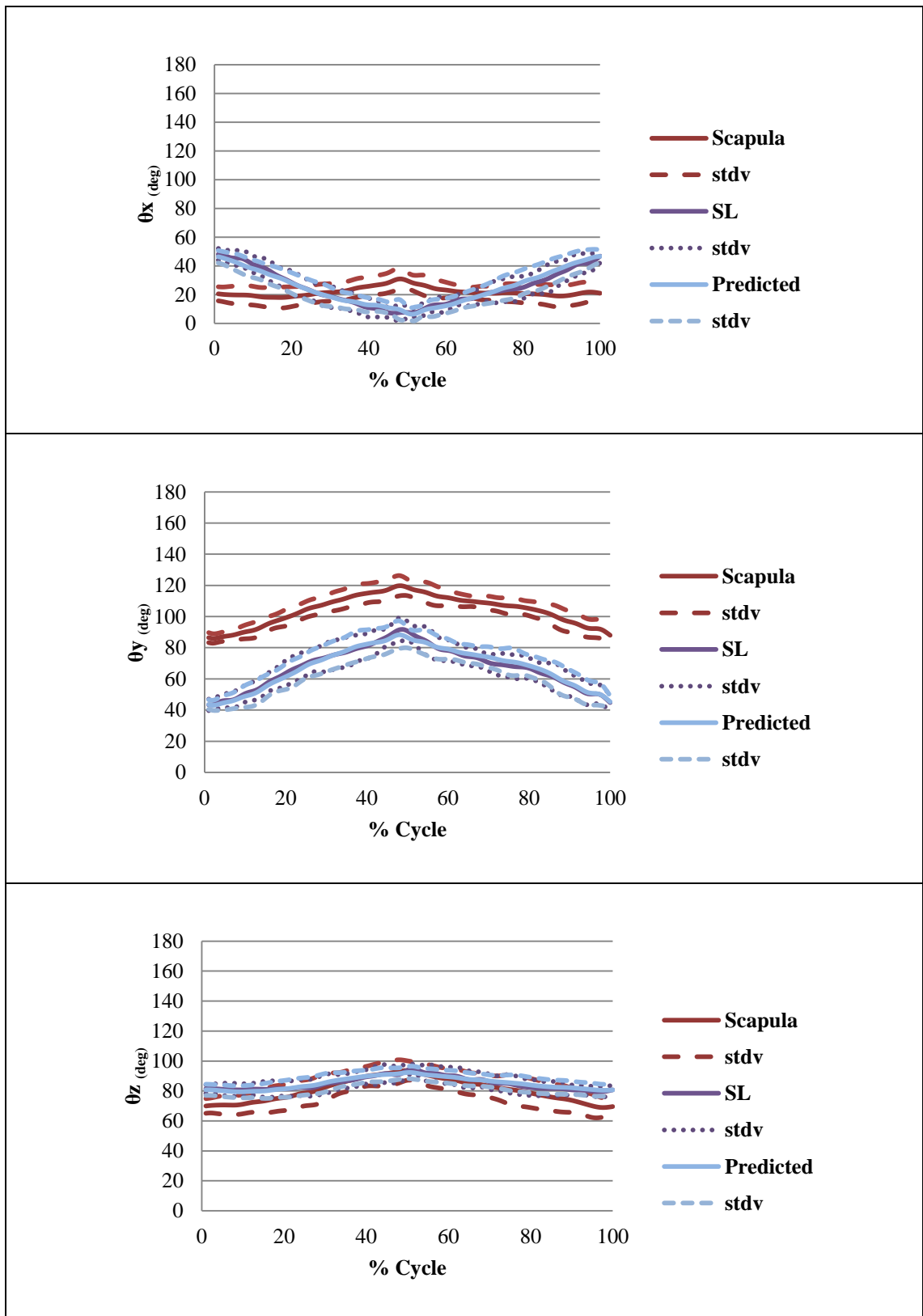
Mean and standard deviation data for nine participants (Chapter VI) under quasi-static conditions. The data presented is in respect with the vertical in three axes, in humeral abduction-adduction, for the first two trials performed by the participants.



Mean and standard deviation data for nine participants (Chapter VI) under quasi-static conditions. The data presented is in respect with the vertical in three axes, in humeral flexion-extension, for the third trial performed by the participants.

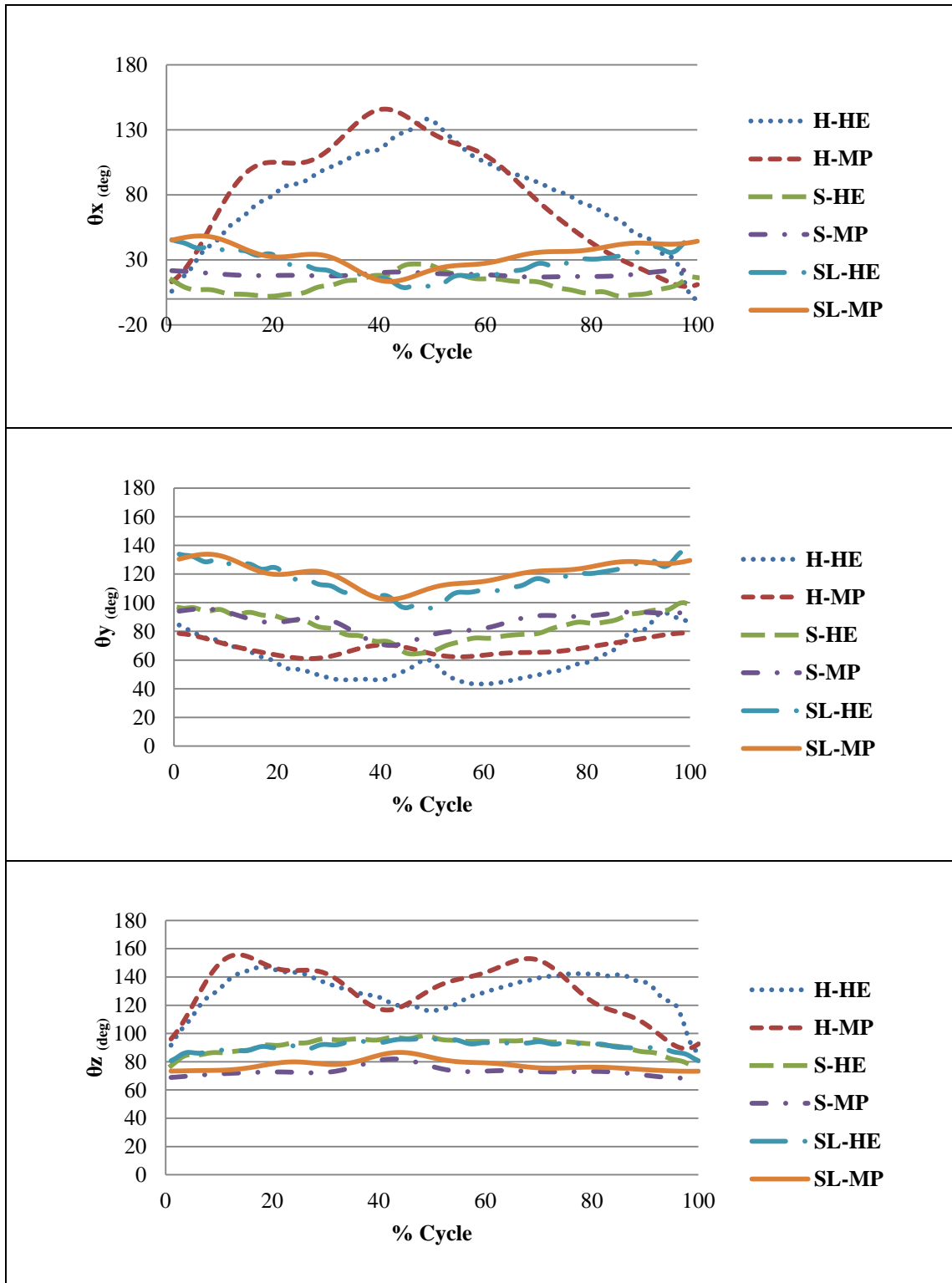


Mean and standard deviation data for nine participants (Chapter VI) under quasi-static conditions. The data presented is in respect with the vertical in three axes, in humeral abduction-adduction, for the third trial performed by the participants.

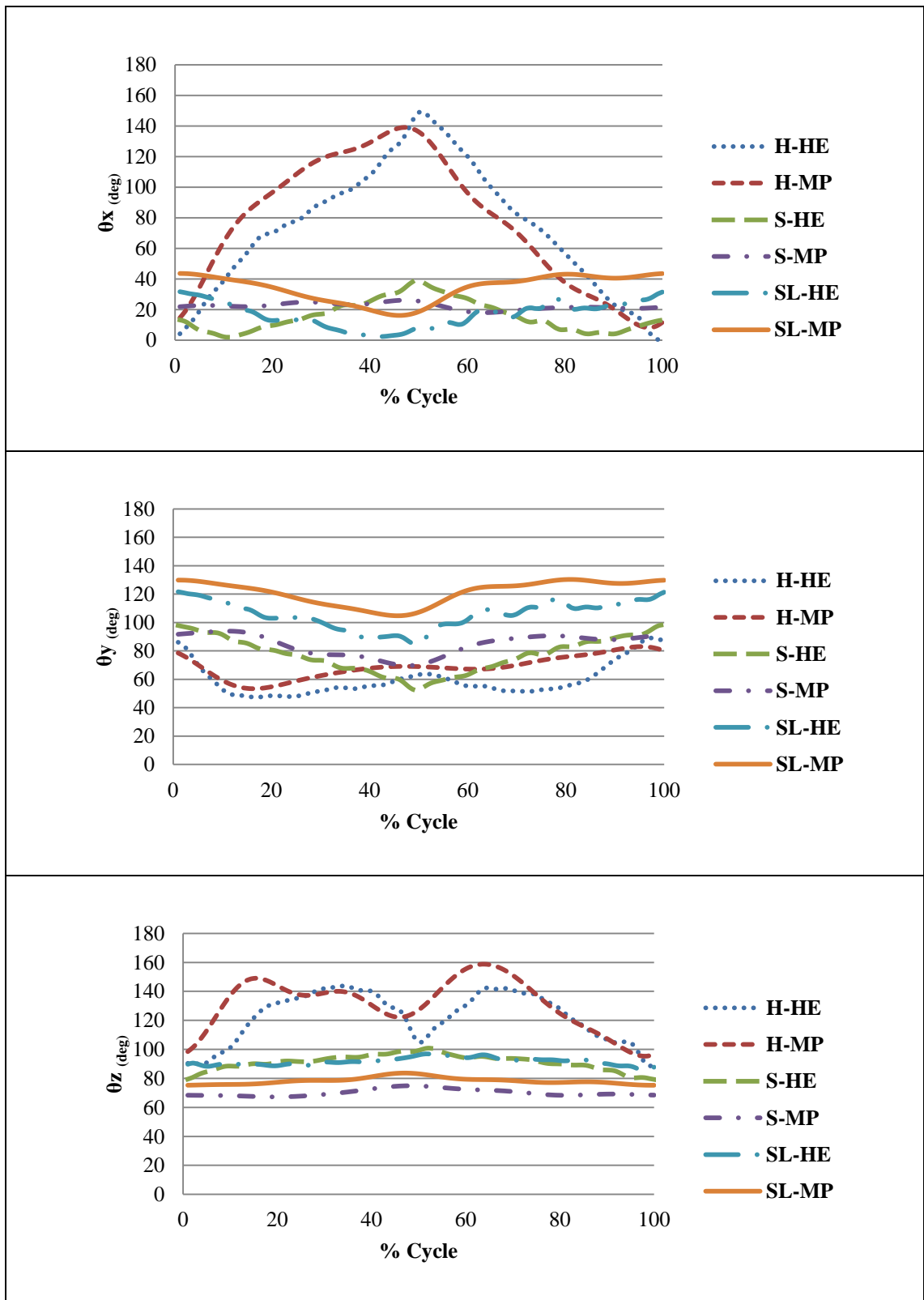


Appendix A7: Case study data

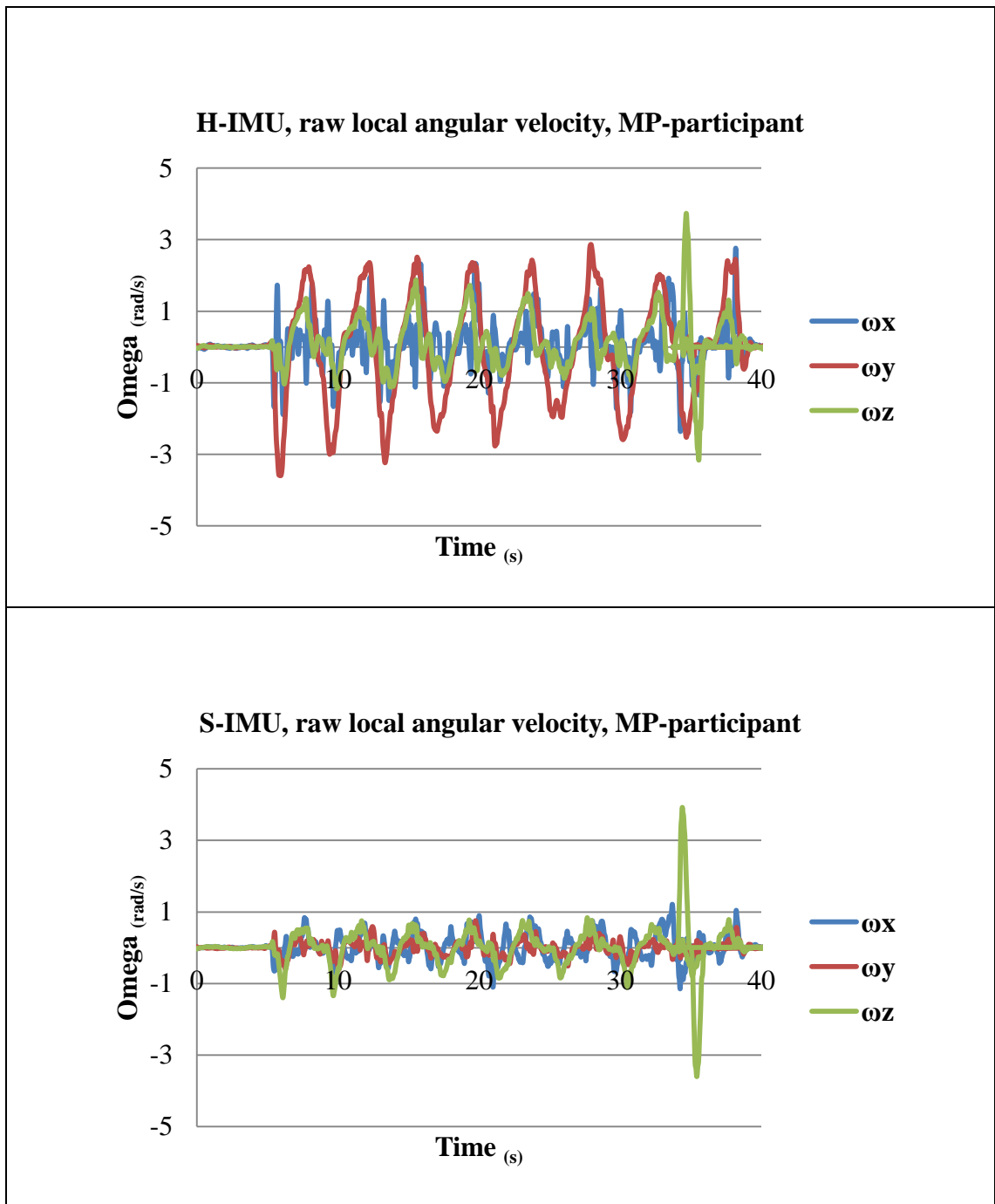
Raw mean data for the Hyper Elastic (HE) and Muscle Patterning (MP) participants (Chapter VII) under quasi-static conditions. The data presented is in respect with the vertical in three axes, in humeral flexion-extension, for the first two trials.



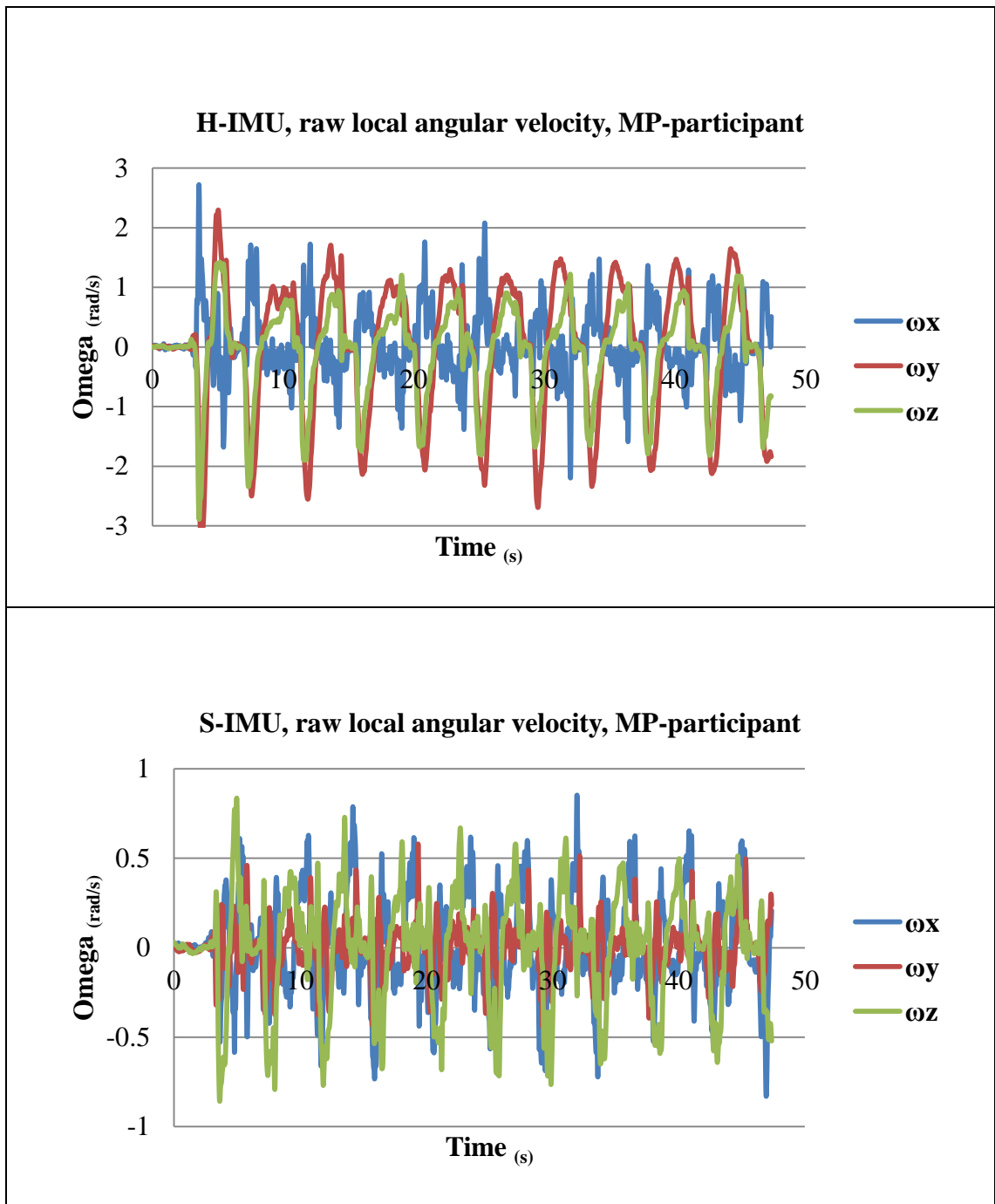
Raw mean data for the Hyper Elastic (HE) and Muscle Patterning (MP) participants (Chapter VII) under quasi-static conditions. The data presented is in respect with the vertical in three axes, in humeral flexion-extension, for the first two trials.



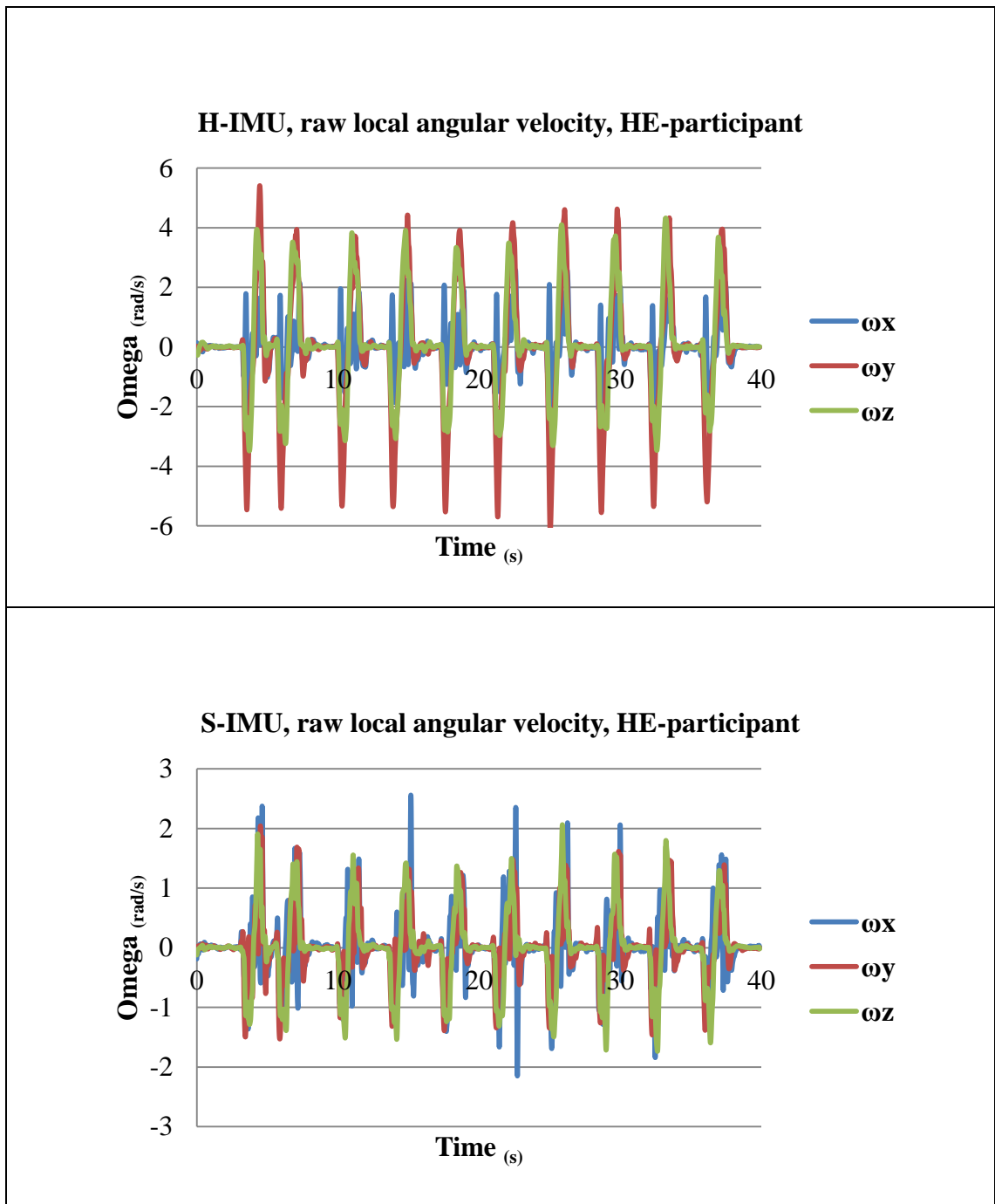
Raw local angular velocity recorded in humeral flexion-extension, MP-Participant.



Raw local angular velocity recorded in humeral abduction-adduction, MP-Participant.



Raw local angular velocity recorded in humeral flexion-extension, HE-Participant.



Raw local angular velocity recorded in humeral abduction-adduction, HE-Participant.

